EXOTIC HIGGS DECAYS

by

Felix Kling

A Dissertation Submitted to the Faculty of the

DEPARTMENT OF PHYSICS

In Partial Fulfillment of the Requirements
For the Degree of

DOCTOR OF PHILOSOPHY

In the Graduate College

THE UNIVERSITY OF ARIZONA

2016

THE UNIVERSITY OF ARIZONA
GRADUATE COLLEGE

As members of the Dissertation Committee, we certify that we have read the dissertation prepared by Felix Kling entitled Exotic Higgs Decays and recommend that it be accepted as fulfilling the dissertation requirement for the Degree of Doctor of Philosophy.

Shufang Su — Date: 05/05/2016

William D. Toussaint — Date: 05/05/2016

Kenneth A. Johns — Date: 05/05/2016

Srinivas Manne — Date: 05/05/2016

Sean P. Fleming — Date: 05/05/2016

Final approval and acceptance of this dissertation is contingent upon the candidate's submission of the final copies of the dissertation to the Graduate College.

I hereby certify that I have read this dissertation prepared under my direction and recommend that it be accepted as fulfilling the dissertation requirement.

Dissertation Director: Shufang Su — Date: 05/05/2016

STATEMENT BY AUTHOR

This dissertation has been submitted in partial fulfillment of the requirements for an advanced degree at the University of Arizona and is deposited in the University Library to be made available to borrowers under rules of the Library

Brief quotations from this dissertation are allowable without special permission, provided that an accurate acknowledgement of the source is made. Requests for permission for extended quotation from or reproduction of this manuscript in whole or in part may be granted by the head of the major department or the Dean of the Graduate College when in his or her judgment the proposed use of the material is in the interests of scholarship. In all other instances, however, permission must be obtained from the author.

SIGNED: Felix Kling

ACKNOWLEDGMENTS

At first I want to thank Shufang Su for giving me the opportunity to work with her on these very interesting projects and for his advice and support over the last four years. I would also like to thank Tilman Plehn and Tao Han for all the support that I received. In addition, I want to thank Fermilab for providing me the opportunity to work in this great environment during my last year of grad school through the Fermilab Graduate Student Research Program in Theoretical Physics. In particular I want to thank Olivia, Gardie and Shane for helping me with all the paperwork. Moreover, I want to thank Barath, Jeff, Atri, Peter, Jose, Gopi, Anthony, Malte, Peter, Aaron, Zhen, Seyda, Kiel, Gordon, Jack, Pilar, Aarti, Paddy, Roni and all my other colleagues in Tucson, at Fermilab and in other parts of the world for their advice, help and the good time we had. Furthermore, I would like to thank the GPSC, the APS, PittPACC, the Theoretical Astrophysics Program, Fermilab, MIAPP and the Fan Family for their travel support as well as the Galileo Circle and Vesto Slipher Foundation for their scholarship. I also want to thank my former roommates Jens and Sarah who let me stay at their place during all the times I visited Heidelberg. Moreover I want to thank the US Department of Energy, which supported my work both in Arizona and at Fermilab. In addition, I want to thank my roommates Tyler, Jagan, Jiawei and Ethan for being amazing roommates as well as my friends Angelica, Andres, Tobi, Henning, Lydia, Musa, Anna, Marcia, Athila, Matthieu, Adrian, Aishwarya, Jayati, Chris, Julia and Maria for making graduate school such an amazing and enjoyable time for me. Furthermore, I want to thank my parents and grand parents for all the support and interest in my academic work. Finally, I want to thank nature for being such an interesting subject to study.

Contents

ABSTRACT

Many models of physics beyond the Standard Model include an extended Higgs sector, responsible for electroweak symmetry breaking, and predict the existence of additional Higgs bosons. The Type II Two-Higgs-Doublet Model (2HDM) is a particularly well motivated scenario and a suitable framework for phenomenological studies of extended Higgs sectors. Its low energy spectrum includes two CP-even Higgses h and H, one CP-odd Higgs A, and a pair of charged Higgses $H^{\pm}$. We study the implication of the LHC Higgs search results on the Type II 2HDM and identify regions of parameter space which are consistent with all experimental and theoretical constraints and can accommodate the observed 125 GeV Higgs signal. This includes parameter space with a distinctive mass hierarchy which permit a sizable mass splitting between the undiscovered non-Standard Model Higgs states. If this mass splitting is large enough, exotic Higgs decay channels into either a Higgs plus a Standard Model gauge boson or two lighter Higgses open up. This can significantly weaken the reach of the conventional Higgs decay channels into Standard Model particles but also provide the additional opportunity to search for exotic Higgs decay channels. We provide benchmark planes to explore exotic Higgs decay scenarios and perform detailed collider analyses to study the exotic decay channels $H/A \to AZ/HZ$ and $H^{\pm} \to AW/HW$. We find that these exotic decays offer complementary discovery channels to the conventional modes for both neutral and charged Higgs searches and permit exclusion and discovery in large regions of parameter space.

Chapter 1

Introduction

In Goethes most influential play, Faust, the medieval scholar Heinrich Faust states the objectives of his work with the famous words: "So that I may perceive whatever holds, the world together in its inmost folds." Today, more than 200 years after Goethes play has been performed for the first time, this question is still not entirely understood and became subject to extensive fundamental research in physics. The field of physics that addresses this question is elementary particle physics, which analyzes the physics at the smallest observable scales.

The current model to describe the physics at such small scales is the Standard Model (SM) of particle physics. It describes the smallest constituents of matter as well as three out of four fundamental interactions between them. Indeed, from a particle physics point of view, we could see elementary particles as the "inmost folds" and their interactions as "whatever holds the world together". The SM accurately describes almost all observations in particle physics. Furthermore, after the discovery of the Higgs boson by the Large Hadron Collider (LHC) in 2012 [1, 2], all SM particles have been observed directly.

However, there is evidence for new physics beyond the Standard Model (BSM). Within the last decades, we have observed several phenomena that cannot be explained within the framework of the SM. Galactic rotation curves [3] and gravitational lensing [4] require the existence of a new form of matter, dark matter, which abundance is more than five times larger than those of baryonic matter described by the SM. Neutrino oscillation experiments [5, 6] indicate that neutrinos must have a small mass, while the SM predicts them to be massless. Furthermore, the SM is unable to explain the asymmetry between matter and anti-matter that we observe in the universe [7]. Besides the experimental evidence for new physics, there are theoretical considerations which point towards the existence of a more fundamental theory such as the hierarchy problem and the strong CP problem.

This evidence made us believe, that SM is just the low energy limit of a more fundamental theory of nature. Many theories of physics beyond the SM have been proposed to address one or more of these problems. Well known examples are supersymmetric Models [8], Composite Higgs Models [9], Peccei-Quinn Models [10] or Twin Higgs Models [11].

If any of these models are indeed the the right description of nature, we expect to directly observe new dynamics predicted at the LHC within the next years. However, no significant deviations from the SM predictions have been seen in the first run of the LHC. Therefore it is timely to expand our search strategies and consider a broader spectrum of search channels for new physics. In this work we will consider the possibility of an enlarged Higgs sector which is described using the framework of the Two-Higgs-Doublet Model (2HDM) as

predicted by many new physics models.

The 2HDM is one of the simplest extensions of the SM Higgs sector. Compared to the SM, the 2HDM contains an additional Higgs doublet which is charged under the electroweak symmetry group $SU(2)_L \times U(1)_Y$. After electroweak symmetry breaking, its low energy spectrum contains two neutral CP-even Higgs bosons h and H, a CP-odd Higgs boson A as well as a pair of charged Higgs bosons $H^\pm$. We will mainly concentrate on the Type II 2HDM in which the Higgs doublets couple to the fermionic sector in the same way as in the MSSM.

The discovery of extra Higgses would be an unambiguous evidence for new physics beyond the SM. A number of searches have been performed at the LEP [12], Tevatron and the LHC [13–20], mainly focusing on *conventional* decay channels of Higgses into a SM gauge boson and fermion pair. The absence of an observed signal in these searches already highly constrains the 2HDM parameter space.

If the mass splitting between the Higgs bosons are large enough, additional *exotic* Higgs decay channels into either two lighter Higgses, or a Higgs plus an SM gauge boson, open up and can even dominate. Therefore, in regions of parameter space in which such exotic decay channels are kinematically allowed, the branching fractions into the conventional final states are suppressed and the exclusion bounds can be significantly weakened. On the other hand, the exotic decays provide additional search channels and therefore offer a complementary opportunity for the observation of additional Higgs bosons.

In this thesis, we address two particular questions related to the 2HDM Higgs sector: First, we analyze how the Type II 2HDM is constrained by theoretical considerations and experimental results, in particular LHC searches. Second, we discuss the possibility of using exotic Higgs decays for BSM Higgs searches.

This thesis is organized as follows. In chapter 2.1, we summarize basic concepts of the SM, discuss its limitations, introduce the Two-Higgs-Doublet Model and carefully derive important properties of the model. Important aspects of collider phenomenology are reviewed. Chapter 3 introduces and summarizes the main work which has been published in journals and is attached to this thesis as appendix. In [21] (appendix A) we identify regions of 2HDM parameter space consistent with both theoretical and experimental constraints, by scanning over the entire parameter space. In [22] (appendix B) we discuss the restrictions imposed by these constraints on the allowed 2HDM mass hierarchies and provide a set benchmark planes to study exotic Higgs decays. To illustrate the discovery potential, we perform a detailed collider analysis for the exotic decay channels $A/H \to HZ/AZ$ [23] (appendix C) and $H^\pm \to HW/AW$ [24, 25] (appendix D and E). The prospects of Higgs searches both using conventional and exotic search channels at a future 100 TeV hadron collider are discussed in [26] (appendix F). We conclude in chapter 4.

The work presented in this thesis and the corresponding publications emerged from collaboration with colleagues at the University of Arizona and other institutions. Most of the work was done together with my advisor Shufang Su and our postdoctoral researcher Barath Coleppa. Additional authors will be mentioned in chapter 3 and the appendices. For most parts it is not possible to clearly separate the contributions from different authors since the work emerged from combined efforts. Whenever possible, I will try to point out my contribution when discussing each publication in chapter 3.

Chapter 2

Theory

2.1 The Standard Model of Particle Physics

Our current theory describing the physics at small scales is the Standard Model of particle physics. It describes the smallest constituents of matter, the elementary particles, and their interactions using the framework of Quantum Field Theory* (QFT). In this section, I will introduce concepts and summarize important results of the SM. This discussion partially follows the line of argument presented in [28].

2.1.1 Matter and Gauge Fields

Fermion Fields

The constituents of matter, quarks and leptons, are described by spin-$\frac{1}{2}$ Dirac fermion fields, which are summarized in Tab. 2.1. They are grouped into three generation, each consisting of an up-type quark with charge $+\frac{2}{3}$, a down-type quark with charge $-\frac{1}{3}$, a charged lepton with charge -1 and an electrically neutral neutrino. Each quark and lepton has an anti-particle with the same mass but opposite quantum numbers.

generation	up-type quark	down-type quark	charged lepton	neutrino
I	up u	down d	electron e	e-neutrino ν_e
II	charm c	strange s	muon μ	μ-neutrino ν_μ
III	top t	bottom b	tau τ	τ-neutrino ν_τ

Table 2.1: Summary of quarks and leptons.

A free Dirac fermion ψ is described by the general Lorentz invariant and renormalizable Lagrangian

$$\mathcal{L}_{Dirac} = i\overline{\psi}\gamma^\mu\partial_\mu\psi - m_\psi\overline{\psi}\psi, \tag{2.1}$$

where m_ψ is the mass of the particle.

Gauge Fields

In the Standard Model, the fermion fields respect additional local gauge symmetries, which correspond to the fundamental interactions of the theory. This implies that the Lagrangian

*A good reference to learn QFT is M. Schwartz book *Quantum Field Theory and the Standard Model* [27].

has to be invariant under the corresponding symmetry transformations. A symmetry transformation for the gauge group $SU(N)$ is represented by an unitary operator U acting on the fields ψ and transforming them into $\psi \to U\psi$. The operator U can be expressed as linear combination of N^2-1 group generators T^a with real coefficients θ_a:

$$U(\theta) = \exp(i\theta_a T^a) \tag{2.2}$$

Since the gauge symmetries are local, the coefficients $\theta_a = \theta_a(x)$ depend on the space time position x. The algebra of the generators is fully defined by their commutation relation $[T^a, T^b] = if^{abc}T^c$, where f^{abc} are the structure coefficients of the group. Since the symmetry transformation is unitary, it will leave the Dirac fermion mass term $-m_\psi\overline{\psi}\psi$ invariant under a gauge transformation acting on Dirac fermions[†]. However, the kinetic term $i\overline{\psi}\gamma^\mu\partial_\mu\psi$ will change under gauge transformations, if the symmetry is local. To construct a gauge invariant kinetic term for fermions, we have to replace the partial derivative ∂^μ by a covariant derivative

$$D^\mu = \partial^\mu - igA_a^\mu T^a. \tag{2.3}$$

Here we have introduced N^2-1 gauge fields A_a^μ. Under a gauge transformation the covariant derivative transforms into $D^\mu \to UD^\mu U^\dagger$. This implies that the covariant derivative acting on a field ψ transforms like the field itself $D^\mu\psi \to UD^\mu\psi$ and therefore the kinetic term of the Lagrangian $i\overline{\psi}\gamma^\mu D_\mu\psi$ is gauge invariant.

To construct a kinetic term for the gauge fields, we introduce the field strength tensor $F^{\mu\nu}$ as $igF^{\mu\nu} = [D^\mu, D^\nu]$ which transforms as $F^{\mu\nu} \to UF^{\mu\nu}U^\dagger$ under gauge transformation. Using the field strength tensor $F^{\mu\nu}$, we can write down kinetic term for the gauge fields[‡] as

$$\mathcal{L}_{gauge} = -\frac{1}{2}\mathrm{Tr}\big[F_{\mu\nu}F^{\mu\nu}\big]. \tag{2.4}$$

Here, the trace sums over the group indices. The Lagrangian for a Dirac fermion charged under a gauge group now reads

$$\mathcal{L} = \mathcal{L}_{Dirac} + \mathcal{L}_{gauge} = \overline{\psi}(i\gamma^\mu D_\mu - m_\psi)\psi - \frac{1}{2}\mathrm{Tr}\big[F_{\mu\nu}F^{\mu\nu}\big]. \tag{2.5}$$

The full symmetry group of the Standard Model is $SU(3)_C \times SU(2)_L \times U(1)_Y$. The group $SU(3)_C$ act on quarks only and described the strong interaction. The corresponding gauge fields are called gluons. The $SU(2)_L \times U(1)_Y$ group describes the weak and electromagnetic interactions. The fourth fundamental force, gravity, is currently not incorporated into the Standard Model and its effects can be ignored in the context of particle physics.

Chiral Gauge Theories

In 1956, the Wu experiment [29] established the parity violating nature of the weak interaction, implying that the weak gauge fields couple differently to left- and right-handed fermions. Using the projection operator $P_{L,R} = \frac{1}{2}(1 \mp \gamma_5)$ with $\gamma_5 = i\gamma_0\gamma_1\gamma_2\gamma_3$, we can

[†]Note that in the Standard Model the gauge transformation acts differently on left- and right-handed fermion fields and therefore this statement is not true anymore.

[‡]Note that in principle we could also include a Θ-term $\mathcal{L}_\Theta = \Theta\mathrm{Tr}\big[F_{\mu\nu}\tilde{F}^{\mu\nu}\big]$ where $\tilde{F}^{\mu\nu} = \frac{1}{2}\epsilon^{\mu\nu\rho\sigma}F_{\rho\sigma}$ is the dual field strength tensor. However, it turns out that this term is unphysical for the SM gauge groups $U(1)_Y$ and $SU(2)_L$. The QCD Θ-term is restricted to be very small by measurements of the neutron electric dipole moment and set to $\Theta_{QCD} = 0$ in the Standard Model. The smallness of the QCD Θ-term is related to strong-CP problem which remains unsolved in the Standard Model.

introduce the left- and right-handed fermion fields $\psi_{L,R} = P_{L,R}\psi$. In a chiral gauge theory, like the Standard Model $U(1)_Y$ hypercharge group, these fields will transform differently under gauge transformation: $\psi_{L,R} \to U_{L,R}\psi_{L,R}$ with corresponding covariant derivatives $D_{L,R}$. The kinetic term of the Dirac Lagrangian can be decomposed into

$$\mathcal{L}_{kin} = \overline{\psi}_L i\gamma^\mu D_{L,\mu}\psi_L + \overline{\psi}_R i\gamma^\mu D_{R,\mu}\psi_R \tag{2.6}$$

which stays invariant under gauge transformation. However, the mass term of the Dirac Lagrangian mixed left- and right-handed fields

$$\mathcal{L}_{mass} = m(\overline{\psi}_L i\psi_R + \overline{\psi}_R\psi_L) \tag{2.7}$$

and therefore is not gauge invariant if $U_L \neq U_R$. Therefore we cannot write gauge invariant mass terms in the chiral Lagrangian. Furthermore, in the Standard Model the left-handed fermion fields are doublets under the weak gauge group $SU(2)_L$ while the right-handed fermions are singlets and we cannot even write down a fermion mass term. This is a problem since the observed constituents of matter are massive.

An additional problem arises when trying to write down a mass term for the gauge fields. We have observed the massive W and Z boson with mass $m_W = 80.4$ GeV and $m_Z = 91.2$ GeV. However, we cannot write down a mass term $\frac{1}{2}Z_\mu Z^\mu$ since it would not be invariant under the corresponding gauge transformation. Since we cannot directly write down mass terms for the SM fields, some mechanism is needed to generate those dynamically.

2.1.2 Electroweak Symmetry Breaking

In the Standard Model the electroweak interactions are described by the gauge group $SU(2)_L \times U(1)_Y$. The problem of generating fermion and gauge boson masses is solved by introducing the mechanism of electroweak symmetry breaking (EWSB) [30–33] and has been incorporated into the Standard model by Glashow, Weinberg and Salam [34,35]. The left-handed fermions are grouped into $SU(2)_L$ doublets while the right-handed fermions are $SU(2)_L$ singlets[§].

$$Q = \begin{pmatrix} u_L \\ d_L \end{pmatrix},\ L = \begin{pmatrix} \nu_L \\ e_L \end{pmatrix},\ \left(u_R\right),\ \left(d_R\right),\ \left(e_R\right). \tag{2.8}$$

Note that there is no right-handed neutrino in the Standard Model. The covariant derivates acting on the (left-handed) doublets and (right-handed) singlets are

$$D_{L\mu} = \partial_\mu - igW_\mu^a\tau^a - ig'YB_\mu \quad \text{and} \quad D_{R\mu} = \partial_\mu - ig'YB_\mu. \tag{2.9}$$

Here we have introduced the gauge fields W_μ and B_μ corresponding to the gauge groups $SU(2)_L$ and $U(1)_Y$. Since the generators of the groups commute, we can assign different coupling constants g and g' to the $SU(2)_L$ and $U(1)_Y$ group. The generators of the $SU(2)$ group are $\tau_a = \frac{1}{2}\sigma_a$ where σ_a are the Pauli matrices. Furthermore, each field is assigned a charge Y under the $U(1)_Y$ which is called hypercharge.

To break the $SU(2)_L \times U(1)_Y$ Standard Model symmetry group, a scalar $SU(2)$ doublet Φ with hypercharge $Y = \frac{1}{2}$ is introduced. The general renormalizable and gauge invariant Lagrangian for the scalar doublet Φ is

$$\mathcal{L}_\Phi = \mathcal{L}_{\Phi,kin} - V = D_\mu\Phi^\dagger D^\mu\Phi + \mu^2\Phi^\dagger\Phi - \lambda(\Phi^\dagger\Phi)^2 \tag{2.10}$$

[§]For simplification, we only consider the first generation quarks and leptons.

If $\mu^2 > 0$, the potential V will obtain a minimum at

$$\langle \Phi \rangle = \begin{pmatrix} 0 \\ \frac{1}{\sqrt{2}} v \end{pmatrix} \quad \text{with} \quad v = \sqrt{\frac{\mu^2}{\lambda}}, \tag{2.11}$$

where v is the vacuum expectation value.

Gauge Boson Masses

To see how the appearance of the vacuum expectation value breaks the Standard Model symmetry group, let us expand the kinetic term of the scalar field around its vacuum expectation value

$$\begin{aligned}
\mathcal{L}_\Phi &= \frac{1}{2} \begin{pmatrix} 0 & v \end{pmatrix} \left(\tfrac{1}{2} g W_\mu^a \sigma^a + \tfrac{1}{2} g' B_\mu \right) \left(\tfrac{1}{2} g W_\mu^a \sigma^a + \tfrac{1}{2} g' B_\mu \right) \begin{pmatrix} 0 \\ v \end{pmatrix} \\
&= \frac{1}{8} \begin{pmatrix} 0 & v \end{pmatrix} \begin{pmatrix} g W_\mu^3 + g' B_\mu & g(W_\mu^1 - i W_\mu^2) \\ g(W_\mu^1 + i W_\mu^2) & -g W_\mu^3 + g' B_\mu \end{pmatrix} \begin{pmatrix} g W_\mu^3 + g' B_\mu & g(W_\mu^1 - i W_\mu^2) \\ g(W_\mu^1 + i W_\mu^2) & -g W_\mu^3 + g' B_\mu \end{pmatrix} \begin{pmatrix} 0 \\ v \end{pmatrix} \\
&= \frac{v^2}{8} \left[g^2 (W_\mu^2 - i W_\mu^3)(W_\mu^2 + i W_\mu^3) + (-g W_\mu^3 + g' B_\mu)^2 \right] \\
&= \frac{g^2 v^2}{4} W_\mu^+ W^{\mu -} + \frac{1}{2} \frac{(g^2 + g'^2) v^2}{4} Z_\mu Z^\mu = m_W^2 W_\mu^+ W^{\mu -} + \frac{1}{2} m_Z^2 Z_\mu Z^\mu
\end{aligned} \tag{2.12}$$

We see that close to the vacuum expectation value, the gauge boson fields obtain a mass. Here we have identified the fields and masses of the massive weak gauge bosons

$$\begin{aligned}
W_\mu^\pm &= \frac{1}{\sqrt{2}} \left(W_\mu^1 \mp i W_\mu^2 \right) && \text{with mass} \quad m_W = \frac{g v}{2} \\
Z_\mu &= \frac{1}{\sqrt{g^2 + g'^2}} \left(g W_\mu^3 - g' B_\mu \right) && \text{with mass} \quad m_Z = \sqrt{g^2 + g'^2} \frac{v}{2}.
\end{aligned} \tag{2.13}$$

There is a fourth massless gauge boson, which is orthogonal to Z_μ, the photon:

$$A_\mu = \frac{1}{\sqrt{g^2 + g'^2}} \left(g' W_\mu^3 + g B_\mu \right) \quad \text{with mass} \quad m_A = 0. \tag{2.14}$$

The mechanism of EWSB spontaneously breaks the $SU(L) \times U(1)_Y$ symmetry. The photon however stays massless and we identify it with the gauge boson corresponding to the $U(1)_{EM}$ group of electromagnetism.

According to Goldstone's theorem, a massless particle must appear for every spontaneously broken continuous symmetry of the theory: a Goldstone Boson. After EWSB three such Goldstone Bosons should appear. They have been absorbed into the fields of the W and Z boson as longitudinal components allowing them to obtain a mass term. Since a scalar doublet has four degrees of freedom, we are left with one additional degree of freedom,which we will identify later as the Higgs boson.

Electroweak Interactions

Using the physical gauge boson field that we have introduced above, we can rewrite the covariant derivative as

$$\begin{aligned} D_\mu &= \partial_\mu - \frac{ig}{\sqrt{2}}\left(W_\mu^+ T^+ + W_\mu^- T^-\right) - \frac{i(g^2 T^3 - g'^2 Y)}{\sqrt{g^2+g'^2}} Z_\mu - \frac{igg'}{\sqrt{g^2+g'^2}}(T^3+Y)A_\mu \\ &= \partial_\mu - \frac{ig}{\sqrt{2}}\left(W_\mu^+ T^+ + W_\mu^- T^-\right) - \frac{ig}{\cos\theta_w}(T^3 - \sin^2\theta_w Q)Z_\mu - ieQA_\mu, \end{aligned} \tag{2.15}$$

where $T^\pm = (T^1 \pm iT^2)$. Here we have introduced the electron charge e and the Weinberg angle θ_w as

$$e = \frac{gg'}{\sqrt{g^2+g'^2}} \quad \text{and} \quad \cos\theta_w = \frac{g}{\sqrt{g^2+g'^2}}. \tag{2.16}$$

Note that the gauge boson masses are connected by the relation $m_W = m_Z \cos\theta_W$ in the Standard Model. Furthermore we can see that the electric charge Q is given in term of the hypercharge Y and the T^3 charge of $SU(2)_L$: $Q = T^3 + Y$. This relation allows us to assign the T^3 and Y charges to the fermion fields, which are given in Tab. 2.2. The weak

	Quark	T^3	Y	Q	Lepton	T^3	Y	Q
Left-handed	$\begin{pmatrix} u_L \\ d_L \end{pmatrix}$	$\begin{matrix} +\frac{1}{2} \\ -\frac{1}{2} \end{matrix}$	$+\frac{1}{6}$	$\begin{matrix} +\frac{2}{3} \\ -\frac{1}{3} \end{matrix}$	$\begin{pmatrix} \nu_L \\ e_L \end{pmatrix}$	$\begin{matrix} +\frac{1}{2} \\ -\frac{1}{2} \end{matrix}$	$-\frac{1}{2}$	$\begin{matrix} 0 \\ -1 \end{matrix}$
Right-handed	(u_R)	0	$+\frac{2}{3}$	$+\frac{2}{3}$				
	(d_R)	0	$-\frac{1}{3}$	$-\frac{1}{3}$	(e_R)	0	-1	-1

Table 2.2: Quantum numbers of quarks and leptons.

interaction of the fermion fields directly follows from the fermion kinetic term

$$\mathcal{L}_{f,kin} = \sum i\overline{\psi}\gamma^\mu D_\mu \psi = \sum i\overline{\psi}\gamma^\mu \partial_\mu \psi + g\left(W_\mu^+ J_W^{\mu+} + W_\mu^- J_W^{\mu-} + Z_\mu J_Z^\mu\right) + eA_\mu J_{EM}^\mu \tag{2.17}$$

where we sum over the fermion field $\psi = Q, L, u_R, d_R, e_R$. The charged currents

$$J_W^{\mu+} = \frac{1}{\sqrt{2}}\left(\overline{\nu}_L \gamma^\mu e_L + \overline{u}_L \gamma^\mu d_L\right) \quad \text{and} \quad J_W^{\mu-} = \frac{1}{\sqrt{2}}\left(\overline{e}_L \gamma^\mu \nu_L + \overline{d}_L \gamma^\mu u_L\right) \tag{2.18}$$

change the fermion flavor while the neutral currents

$$J_Z^\mu = \frac{1}{\cos\theta_w}\sum \overline{\psi}\gamma^\mu\left(T^3 - \sin^2\theta_w Q\right)\psi \quad \text{and} \quad J_{EM}^\mu = Q\overline{\psi}\gamma^\mu\psi \tag{2.19}$$

are fermion flavor conserving. Here we sum over the fields $\psi = u_L, u_R, d_L, d_R, e_L, e_R, \nu_L$.

Fermion Masses

A general renormalizable Lorentz invariant Lagrangian contains Yukawa terms, which couple the left- and right handed fermions fields with the scalar doublet. Using the first generation quark fields for illustration, we can write the Yukawa term as

$$\mathcal{L}_{Yukawa} = -\lambda_d \overline{Q}_L \Phi d_R - \lambda_u \epsilon^{ab} \overline{Q}_{La} \Phi_b^\dagger u_R + h.c. \tag{2.20}$$

Note that the hypercharges sum to zero implying that the Yukawa term is gauge invariant[¶]. Here λ is the dimensionless Yukawa coupling. After EWSB, we can replace Φ by its vacuum expectation value introduced in Eq. 2.11 and obtain

$$\mathcal{L}_{Yukawa} = -\frac{v\lambda_d}{\sqrt{2}}(\overline{d}_L d_R + \overline{d}_R d_L) - \frac{v\lambda_u}{\sqrt{2}}(\overline{u}_L u_R + \overline{u}_R u_L) = -m_d\overline{d}d - m_u\overline{u}u \tag{2.21}$$

These are the fermion mass terms with mass parameter $m = \frac{1}{\sqrt{2}}\lambda v$. Additional problems appear when multiple generations of fermions are included. There is no reason to prohibit flavor mixing in the Yukawa term $\lambda_{ij}\overline{Q}^i_L \Phi d^j_R$, where λ_{ij} is a matrix that does not have to be diagonal. The Yukawa term can be diagonalized by choosing a basis of mass eigenstates. To do this, we can transform the fields by

$$u^i_L \to U^{ij}_u u^j_L,\ d^i_L \to U^{ij}_d d^j_L,\ u^i_R \to W^{ij}_u u^j_R \ \text{ and } \ d^i_R \to W^{ij}_d d^j_R \tag{2.22}$$

where we choose these matrices such that they diagonalize the Yukawa coupling $\lambda_u = U_u \lambda_u^{diag} W_u^\dagger$ and $\lambda_d = U_d \lambda_d^{diag} W_d^\dagger$. Such a field transformation leaves the neutral currents J^μ_Z and J^μ_{EM} unchanged while the charged current for the quark fields changes to

$$J^{\mu+}_W = \frac{1}{\sqrt{2}}\left(\overline{u}^i_L \gamma^\mu (U_u^\dagger U_d)_{ij} d^j_L\right) = \frac{1}{\sqrt{2}}\left(\overline{u}^i_L \gamma^\mu V_{ij} d^j_L\right). \tag{2.23}$$

Here we have introduced the CKM matrix $V = U_u^\dagger U_d$. We conclude that the weak current does mixes the quark flavors. The current best fit values of the CKM matrix can be found in [36].

2.1.3 The Higgs Boson

The Goldstone Bosons

The scalar doublet Φ, which we have introduced to spontaneously break the electroweak symmetry group $SU(2) \times U(1)_Y$, consists of four degrees of freedom. We can make this explicit by expanding Φ around its vacuum expectation value,

$$\Phi = \begin{pmatrix} \phi^+ \\ \frac{1}{\sqrt{2}}(v + h + i\varphi) \end{pmatrix}. \tag{2.24}$$

Here ϕ and φ CP-even and CP-odd neutral scalar fields and $\phi^\pm$ are charged scalar fields. After EWSB, the three fields φ, ϕ^+ and ϕ^- become massless Goldstone bosons. Let us illustrate this using the Z boson field and omit terms involving charged scalar and gauge field:

$$\begin{aligned} \mathcal{L}_Z &= \frac{1}{2}|(\partial_\mu + \frac{ig}{2}W^3_\mu - \frac{ig'}{2}B_\mu)(v + h + i\varphi)|^2 = \frac{1}{2}|(\partial_\mu + \frac{im_Z}{v}Z_\mu)(v + h + i\varphi)|^2 \\ &= \frac{1}{2}(\partial_\mu h)^2 + \frac{1}{2}(\partial_\mu \varphi)^2 + \frac{1}{2}m_Z^2 Z_\mu Z^\mu + \frac{1}{2}m_Z(\partial_\mu\varphi)Z_\mu + \cdots. \end{aligned} \tag{2.25}$$

In the last line we omitted terms that are not quadratic in h, φ and Z_μ. The last term mixes the gauge boson Z_μ with the scalar field φ with a coupling $m_Z p_\mu$, where p_μ is the momentum.

[¶]In principle we can also write down a Yukawa term including a hypothetical right handed neutrino, $\lambda_\nu \epsilon^{ab}\overline{L}_{La}\Phi^\dagger_b \nu_R$. However, the SM does not contain a right-handed neutrino since we have not observed such fields yet.

In leading order perturbation theory, the Z boson vacuum polarization amplitude $\Pi^Z_{\mu\nu}$ is then not only given by the mass term but also includes the mixing into the Goldstone boson:

$$\Pi^Z_{\mu\nu} = im_Z^2 g_{\mu\nu} + (im_Z p_\mu)\frac{i}{p^2}(im_Z p_\nu) = im_Z^2\left(g_{\mu\nu} - \frac{p_\mu p_\nu}{p^2}\right). \tag{2.26}$$

The Goldstone boson ensures that the unphysical longitudinal polarization of the Z boson vanishes. This illustrates a deep connection between the longitudinal gauge boson polarizations and the Goldstone bosons.

For our later discussion, it turns out to be convenient to choose a particular gauge, the unitary gauge, in which the Goldstone bosons vanish. Let us write the scalar doublet Φ in the form

$$\Phi = U\begin{pmatrix} 0 \\ \frac{1}{\sqrt{2}}(v+h)\end{pmatrix}, \tag{2.27}$$

where U is a gauge transformation matrix corresponding to the $SU(2)_L$ group. We can make use of our freedom to choose a particular gauge and fix the gauge by requiring $U = \mathbb{1}$. The Goldstone bosons vanish from our theory. However, in the absence of the Goldstone bosons, the gauge bosons will obtain a longitudinal polarization: the corresponding degree of freedom of the Goldstone bosons has been absorbed into the gauge bosons.

Higgs Couplings

Using the unitary gauge, the scalar doublet Φ still contains one scalar degree of freedom h. The excitation of that field is called the Higgs boson. Expanding the scalar Lagrangian from Eq. 2.10 in terms of the Higgs boson gives

$$\mathcal{L}_\Phi = m_W^2\left(1+\frac{h}{v}\right)^2 W^+_\mu W^{\mu-} + \frac{1}{2}\left(1+\frac{h}{v}\right)^2 m_Z^2 Z_\mu Z^\mu + \frac{1}{2}(\partial_\mu h)^2 - \mu^2 h^2 - \lambda v h^2 - \frac{1}{4}\lambda h^4. \tag{2.28}$$

We can see that the Higgs is massive, $m_h = \sqrt{2}\mu = \sqrt{2\lambda}v$. Furthermore it has cubic and quartic self couplings

$$g_{hhh} = -6i\lambda v \quad \text{and} \quad g_{hhhh} = -6i\lambda. \tag{2.29}$$

When expanding the kinetic term $|D_\mu\Phi|^2$ we again obtain the gauge boson mass terms as well as couplings between the Higgs and the gauge bosons

$$g_{hWW} = 2i\frac{m_W^2}{v}g^{\mu\nu} = igm_W g^{\mu\nu} \quad \text{and} \quad g_{hZZ} = 2i\frac{m_Z^2}{v}g^{\mu\nu} = ig\frac{m_Z}{\cos\theta_w}g^{\mu\nu}. \tag{2.30}$$

The Higgs boson also couples to the fermion fields f. To see that we can expand the Yukawa terms in Eq. 2.20 in terms of the Higgs and obtain

$$\mathcal{L}_{Yukawa} = -\frac{\lambda_f v}{\sqrt{2}}\left(1+\frac{h}{v}\right)\overline{f}f = -m_f\left(1+\frac{h}{v}\right)\overline{f}f. \tag{2.31}$$

The Higgs fermion coupling is proportional to the Yukawa coupling y_f and therefore also proportional to the fermion mass m_f:

$$g_{hff} = -i\frac{\lambda_f}{\sqrt{2}} = -i\frac{m_f}{v}. \tag{2.32}$$

Higgs Decays

The coupling of the Higgs to the fermion and gauge bosons is proportional to the particles mass. This implies that the Higgs will predominantly decay into heavy particles. We can write down the Higgs decay rates Γ into fermions f and vector boson V[‖]:

$$\begin{aligned}\Gamma(h \to ff) &= \frac{N_c g^2 m_f^2}{32\pi m_W^2}\left(1-\frac{4m_f^2}{m_h^2}\right)^{\frac{3}{2}} \\ \Gamma(h \to VV) &= \frac{N_V g^2 m_h^3}{64\pi m_W^2}\left(1-\frac{4m_V^2}{m_h^2}\right)^{\frac{1}{2}}\left(1-4\frac{m_V^2}{m_h^2}+12\frac{m_V^4}{m_h^4}\right).\end{aligned} \tag{2.33}$$

Here $N_c = 1$ (3) denotes the number of colors leptons (quarks) and $N_V = 2$ (1) for the W (Z) boson.

Since the Higgs boson in color- and electrically neutral, it does not decay to photons and gluons on tree level. However, such decays are possible at one-loop level via fermion and gauge boson loops [37][**].

$$\Gamma(h \to \gamma\gamma) = \frac{\alpha^2 g^2 m_h^3}{512\pi^3 m_W^2}\left|\sum_i N_{ci} Q_i^2 F_i\right| \quad \text{and} \quad \Gamma(h \to gg) = \frac{\alpha_s^2 g^2 m_h^3}{256\pi^3 m_W^2}\left|\sum_i F_i\right|. \tag{2.34}$$

Here we sum over the particles appearing the loop. The function F depends on the spin of the particle in the loop and is given by

$$F_1 = 2+3\tau+3\tau(2-\tau)f(\tau) \quad \text{and} \quad F_{\frac{1}{2}} = -2\tau[1+(1-\tau)f(\tau)] \tag{2.35}$$

where $\tau = \frac{4m^2}{m_h^2}$ and

$$f(\tau) = \begin{cases} \left[\sin^{-1}\left(\tau^{-\frac{1}{2}}\right)\right]^2, & \text{if } \tau \geq 1 \\ -\frac{1}{4}\left[\log\left(\frac{1+\sqrt{1-\tau}}{1-\sqrt{1-\tau}}\right)-i\pi\right]^2, & \text{if } \tau < 1 \end{cases} \tag{2.36}$$

In Fig. 2.1 (left) we show the branching fraction for the main decay channels of a SM-like Higgs as a function of its mass. Since a priori, the Higgs mass is a free parameter within the Standard Model, people considered a large range of Higgs masses when designing their search strategies. However, after the Higgs discovery we know that the Higgs mass is $m_h = 125$ GeV as indicated by a vertical dashed line. Note that the discoved Higgs signal lies in the interesting mass window between $m_h = 100$ GeV and 150 GeV in which multiple channels contribute significantly to the total decay width: nature provides us various complementary opportunities to test the properties of the Higgs boson.

- **Bottom Quarks** bb**:** The SM-Higgs boson decays predominately into pairs of bottom quarks, which are the heaviest fermions below the Higgs mass. The branching fraction is $\text{BR}(h \to bb) = 57.7\%$. This decay channel is challenging at LHC due to the large QCD backgrounds at a hadron collider. However, it has been shown that this channel can be observed using jet-substructure techniques [39] in the boosted Higgs regime.

[‖] See [37] or [38] for more details of the calculation.

[**] Note that the decay rate $\Gamma(H \to \gamma\gamma)$ stated in the Higgs Hunter's Guide [37] misses a factor of 2.

- **Tau Leptons $\tau\tau$:** The decay into the next lightest fermion, the τ, has a branching fraction $\mathrm{BR}(h \to \tau\tau) = 6.32\%$. Although this branching fraction is reduced by one order of magnitude compared to the decay into bottom pairs, at the LHC we can easily overcome this reduction with a significantly better background suppression using leptonic τ decays[††].

- **Light Fermions:** The decays into lighter fermions are further suppressed by their mass. Although the decay into pairs of charm quarks is still considerable, $\mathrm{BR}(h \to cc) = 2.9\%$, its prospects are limited due to the overwhelming QCD background at the LHC and the low efficienies for charm tagging. The decay into muons is highly suppressed, $\mathrm{BR}(h \to \mu\mu) = 0.022\%$, but provides a very clean signal and will be observable at high luminosities.

- W **Bosons:** Since the W boson is heavy, $2m_W > m_h$, the Higgs cannot decay into two onshell W bosons. However, such decay is possible if one of the W bosons is offshell resulting in a suppressed decay rate. It turns out that the coupling of the Higgs boson to W bosons is strong enough to overcome this suppression such that the decay $h \to WW^*$ is the subdominant Higgs decay channel with branching fraction $\mathrm{BR}(h \to WW^*) = 21.5\%$. Using the fully leptonic W decay mode, this channel provides a clean signature in the collider but suffers from a poor mass resolution due to the missing neutrino momentum.

- Z **Bosons:** The Higgs boson can decay into a pair of Z bosons in which one of the Z is offshell. Compared to the decay into W bosons, this decay suffers more strongly from the offshell suppression resulting in a branching fraction $\mathrm{BR}(h \to ZZ^*) = 2.6\%$. In particular the fully leptonic decay $h \to ZZ^* \to 4l$ channel is very clean and provides excellent mass resolution. However, it suffers from a further suppression due to the Z decay branching fraction $\mathrm{BR}(Z \to ll) = 6.73\%$.

- **Photons $\gamma\gamma$:** The Higgs boson can decay into pairs of photons via a loop of fermions or W bosons. This decay mode is loop suppressed and has a branching fraction of $\mathrm{BR}(h \to \gamma\gamma) = 0.23\%$. However, due to the clean signal and low backgrounds, this channel is one of the most promising Higgs search channels.

- **Loop Induced Decays $Z\gamma$ and gg:** Similar to the decay channel into photons, the decay modes $h \to Z\gamma$ and $h \to gg$ are loop induced. The $Z\gamma$ mode has a branching fraction $\mathrm{BR}(h \to Z\gamma) = 0.15\%$, which is comparable to the $h \to \gamma\gamma$ mode. The promising decays involving a leptonically decaying Z boson are further suppressed by the Z branching fraction and will be observable at high luminosities. The mode into gluons has a large branching fraction $\mathrm{BR}(h \to gg) = 8.6\%$, but suffers from an irreducible QCD background at hadron collliders. However, it can be observed at a lepton collider.

If the SM-Higgs boson would have a higher mass, the decay modes into the weak bosons W and Z would quickly dominate when approaching the mass threshold $2m_W$. According to the Goldstone Boson Equivalence Theorem, the branching fraction would be approximately $BR(h \to WW) = \frac{2}{3}$ and $BR(h \to ZZ) = \frac{1}{3}$. At even higher masses $m_H > 2m_t$, the additional decay channel into top pairs would open up.

[††]The leptonic τ branching fractions into muons and electrons are $\mathrm{BR}(\tau \to \mu\nu_\mu\nu_\tau) = 17.8\%$ and $\mathrm{BR}(\tau \to e\nu_e\nu_\tau) = 17.4\%$.

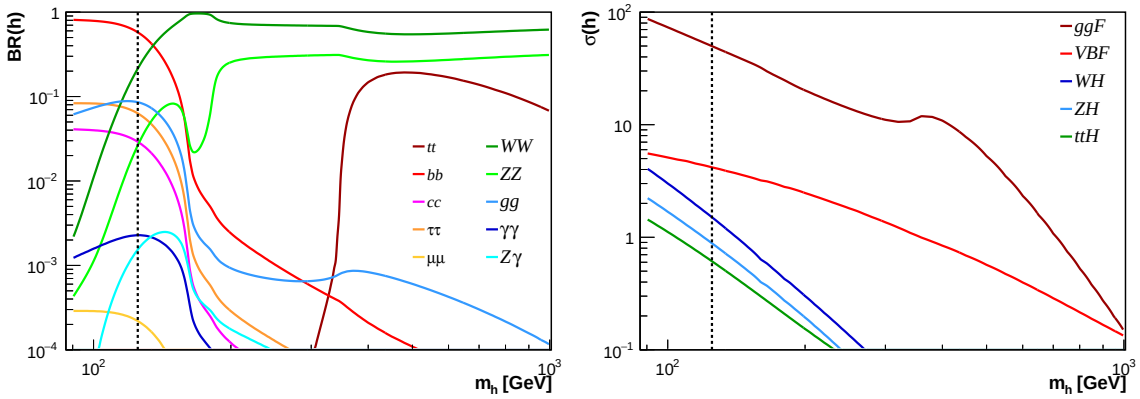

Figure 2.1: Decay branching fraction (left) and production cross section at 14 TeV LHC (right) of a Standard Model like Higgs boson with mass m_h. The vertical dashed line indicated the SM Higgs mass $m_h = 125$ GeV. Here we use the numbers provided by the LHC Higgs Cross Section Working Group [40–42]

Higgs Production at LHC

There are several Higgs production modes which have a sufficient production rate to be observable at LHC. In Fig. 2.1 (right) we show the production cross section at 14 TeV LHC of a SM-like Higgs as function of the Higgs mass.

- **Gluon-Gluon-Fusion:** The dominating Higgs production mode at LHC is gluon-gluon fusion (ggF). This process is loop induced with dominant contributions coming from top- and subleading contributions coming from bottom loops. Both the large top Yukawa coupling and the large gluon parton distribution function (pdf) enhance the cross section enough to overcome the suppression associated with the loop. The cross section at 14TeV LHC is $\sigma(\text{ggF}) = 49.8$ pb. In ggF, the Higgs is produced almost at rest, causing the decay productions to appear back-to-back in the detector. No additional activity is associated with this production channel.

- **Vector-Boson-Fusion:** The subdominant Higgs production mode is vector-boson-fusion (VBF). Both initial state quarks emit a vector boson W or Z which then fuse into a Higgs boson. This process is suppressed by the weak coupling g^4, resulting in a lower production rate compared to ggF. The cross section at 14TeV LHC is $\sigma(\text{VBF}) = 4.18$ pb. Unlike the ggF channel, a Higgs produced in VBF is associated with two jets which allow for a moderate transverse momentum of the Higgs. These jets are typically emitted in the forward direction, providing a unique feature of VBF which can be used for background suppression.

- **Vector-Boson-Associate Production:** In Higgs-W/Z boson associate production (WH/ZH), the Higgs boson is radiated of an intermediate offshell vector boson. This process is suppressed due to the offshell intermediate state. This suppression increases for higher Higgs masses resulting in small production rates. The cross section at 14TeV LHC are $\sigma(\text{WH}) = 1.5$ pb and $\sigma(\text{ZH}) = 0.88$ pb. The additional vector boson in the final state both allows for a moderate transverse momentum of the Higgs and can help suppressing the background significantly when decaying leptonically. This allows us to observe even difficult decay modes like $h \to bb$.

- **Top-Pair-Associate Production:** Furthermore, the Higgs can be produced in association with a top quark pair (ttH). The cross section at 14TeV LHC is $\sigma(\text{ttH}) = 0.61$ pb. Considering the possible combinations of different top quark and Higgs decays, this channel provides a variety of interesting collider signatures.

If the SM-Higgs boson would have a higher mass, the production cross section decreases due phase space suppression. Note the increase in the ggF production cross section around $m_H = 2m_t$, where the top quarks in the loop become onshell. The cross sections for the WH, ZH and ttH channel rapidly decrease with larger Higgs mass since the intermediate state becomes increasingly offshell.

Higgs Boson Searches at LHC

A number of searches have been performed at LEP [43], Tevatron [44, 45][‡‡] and LHC to find the Higgs. Finally, in July 2012, the ATLAS [1] and CMS [2] collaboration announced the discovery of a SM-like Higgs boson. The most significant searches look for a Higgs produced in gluon-gluon fusion decaying to $h \to ZZ^* \to 4l$ and $h \to \gamma\gamma$. The invariant mass distributions are shown in Fig. 2.2. These two decay channels only contribute a branching fractions of $\text{BR}(h \to \gamma\gamma) = 0.23\%$ and $\text{BR}(h \to ZZ^* \to 4l) = 0.011\%$ to the total Higgs decay rate. However, due to very small SM backgrounds, they provide a clean signal with large significance. Combined with the $h \to WW^* \to l\nu l\nu$ channel, both ATLAS and CMS reported a global significance of 5.1σ.

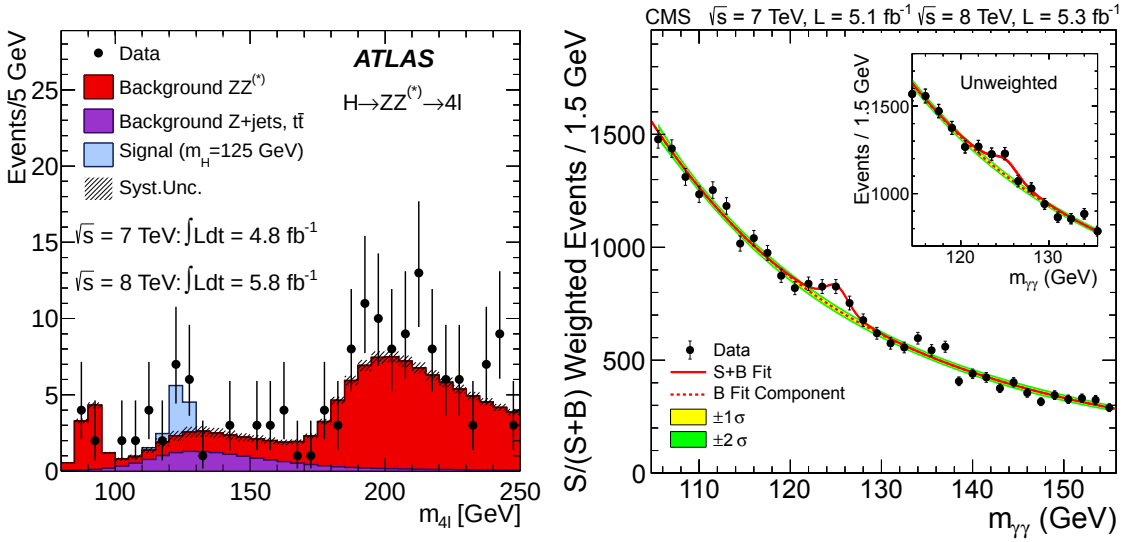

Figure 2.2: Distributions for the invariant mass of four leptons, m_{4l}, by ATLAS and two photons, $m_{\gamma\gamma}$, by CMS. These figures are taken from the original Higgs discovery publications [1] and [2].

Using the entire LHC Run 1 data, the mass of the Higgs boson is measured to be [46]

$$m_H = 125.09 \pm 0.21 \text{ (stat.)} \pm 0.11 \text{ (syst.) GeV}. \tag{2.37}$$

Furthermore, the LHC experiments were able to determine the the Higgs boson to be a CP-even scalar [47, 48], as predicted by the Standard Model.

[‡‡]Note that [45] appeared after the discovery of the Higgs boson by the LHC.

As we have seen in the previous discussion, there are a variety of decay modes that contribute significantly to the overall decay width of a $m_H = 125$ GeV Higgs boson. This allows us to measure the properties of the Higgs boson independently for different production and decay channels. Deviations from the SM expectation would be a clear indicator for new physics. To quantify the deviation, we introduce the coupling modification κ the ratio between the observed coupling g^{obs} and the expected Standard Model coupling g^{exp}

$$\kappa = \frac{g^{obs}}{g^{exp}}. \tag{2.38}$$

However, we cannot measure the modification of the coupling directly. In experiment, we measure the signal strength μ which is defined as the ratio between observed and expected cross section for a given search channel:

$$\mu = \frac{(\sigma \times BR)^{obs}}{(\sigma \times BR)^{exp}}. \tag{2.39}$$

Typically μ depends on multiple coupling modification parameters κ since production and decay contain different couplings. In particular the branching fraction is sensitive to multiple couplings since it depends on the decay width of all Higgs decay channels. Furthermore, it is not always possible to have a clear signal that only contains events from one production mechanism. Typically searches focusing on VBF production contain significant contamination from gluon-gluon fusion production with two additional jets produced in initial state radiation. A careful treatment is needed to relate the experimentally measured signal strength μ to the theoretically interesting coupling modifications κ. This has been done by ATLAS and CMS [49]. The results of a combined fit of ATLAS and CMS using the Run 1 data is shown in the left panel of Fig. 2.3. This fit assumes the absence

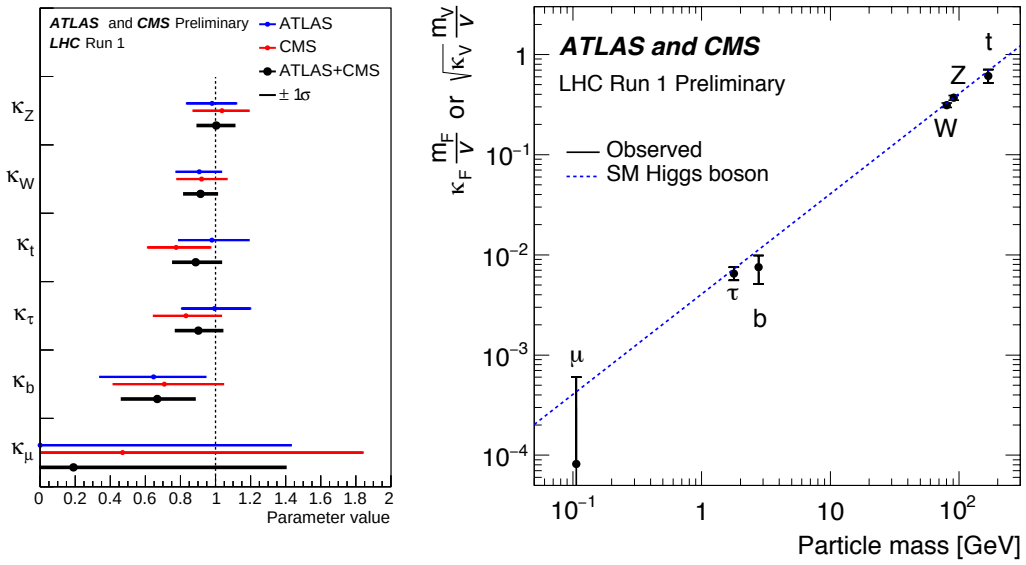

Figure 2.3: Left: Best fit values of the coupling modification κ using the run 1 data from ATLAS, CMS and their combination. Right: Reduced coupling modification $\kappa\frac{m_f}{v}$ (fermions) and $\sqrt{\kappa}\frac{m_V}{v}$ (vector bosons) as function of the particle mass. These figures are taken from the the combined analysis [49].

of additional new particle contributing to the Higgs decay width and or the loop induced couplings. We can see that the all measurements are consistent with the Standard Model prediction $\kappa = 1$. The right panel of Fig. 2.3 shows the reduced coupling modification λ appearing in the Lagrangian: $\mathcal{L} = \sum_f \lambda_f \, h\bar{f}f + \sum_V \frac{1}{2}\lambda_V \, hV^{\dagger\mu}V_\mu$. This illustrates the linear relationship between the Higgs coupling and the particle mass.

Current measurements still have large uncertainties at the order of 10 - 30% allowing for sizable deviations from the SM prediction. Although we have discovered the Higgs boson, more data is needed to verify its SM nature or to uncover deviations which would lead to the discovery of new physics.

2.2 Limitations of the Standard Model

During the last 50 years, the Standard Model of Particle Physics, has been established as the model to describe the fundamental physics at the smallest scales. It is able to describe three out of four fundamental forces of nature: the electromagnetic, the weak and the strong force. It's predictions are in excellent agreement with precision observation in atomic and nuclear physics as well as high energy collider experiments. Furthermore, after the Higgs discovery, all Standard Model particles have been observed directly.

However, there is evidence for new physics beyond the Standard Model. Within the last decades, we have observed several phenomena that cannot be explained within the framework of the Standard Model.

- **Dark Matter:** We know from astronomical observations that baryonic matter, which is the matter described by the Standard Model, only constitutes about 16% of the total mass in the universe [50]. The remaining 84% are made of dark matter.

  There are multiple independent indication for the existence of dark. We know from rotation curves of galaxies that a significant amount of the galaxy's mass have to be located outside of its visible image [3]. This predicts the existence of a new invisible form of matter: dark matter. To be consistent with observation, dark matter has to be stable on cosmological timescales, electrically neutral and in a kinematic regime that allows for structure formation. Further evidence for dark matter has been obtained by gravitational lensing, in particular the observation of a cluster merger* as described in [4]. Finally, the existence of dark matter has cosmological influences and can be seen in the angular spectrum of the Cosmic Microwave Background [50, 51].

  There is no dark matter candidate within the Standard Model particle content. The only stable neutral particle, the neutrino, is ultra-relativistic and therefore would not allow for structure formation.

- **Baryogenesis:** The universe we see mainly consists of matter, no accumulations of anti-matter have been observed so far. This is rather surprising considering the symmetry between matter and anti-matter ensured by the CPT theorem. Although the Standard Model is able to generate a small amount of baryon-asymmetry, it is unable

*The interaction between the gas molecules cause the gas contained in both colliding galaxy clusters to concentrate at the point of impact as observed through X-rays. The dark matter and galaxies however are do not interact and therefore continue to move unaltered. Gravitational lensing shows that total mass is located around the galaxies, as expected in the presence of dark matter, and not at around the gas, as expected in the absence of dark matter.

to account for the observed amount [7]. An additional mechanism for baryogenesis is needed.

- **Neutrino Masses:** We know from observation of neutrino oscillations [5, 6] that neutrinos must have a small mass splitting. This implies that at least two neutrinos must be massive. The Standard Model does not account for a neutrino mass. New dynamics have to be introduced to explain the generation of neutrino masses as well as their smallness compared to the other fermions.

- **Experimental Anomalies:** There are a number of experimental results that observe a significant deviation from from the Standard Model predictions. Two of the most significant ones are the measurement of the anomalous magnetic dipole moment of muon, $g_\mu - 2$, showing a 3.6σ deviation [36, 52], and an excess in the rare B-meson decay $\bar{B}_0 \to D^{(*)} tau^- \bar{\nu}_\tau$ at BaBar, showing a 3.4σ deviation [53]. However, it is unclear at this point if these anomalies are a hint towards new physics or correspond to statistical fluctuations[†].

Besides the experimental evidence for new physics, there are theoretical considerations which point towards the existence of a more fundamental theory. The Standard Model in its current form suffers from several theoretical inconsistencies.

- **Hierarchy Problem:** When comparing the scale associated with the weak force, the electroweak scale $\Lambda_{EW} = 100$ GeV, with the scale associated with the gravitational force, the Planck scale $\Lambda_{Pl} = 10^19$ GeV, we observe a strong hierarchy. The electroweak scale is many orders of magnitude smaller than the Planck scale. The *hierarchy problem* addresses this question: Why is the electroweak scale so much smaller than the Planck scale?

  When looking at the Lagrangian, this hierarchy is related to the Higgs potential parameter μ. This parameter has dimension of mass. The only natural mass scale is the Planck scale Λ_{Pl}. We would therefore expect the Higgs potential to contain a term of the form $\mathcal{L} = c\Lambda_{Pl}^2 \Phi^\dagger \Phi$ with an dimensionless constant c. In a natural theory, we would expect c to be order one. When comparing $c\Lambda_{Pl}^2$ with the observed value of μ, we see that dimensionless constant has to be very small $c = 10^{-34}$, which seems very unnatural. This is called the *naturalness problem*.

  Taking into account the quantum nature of QFT, this hierarchy has severe implications. The measured Higgs mass parameter m_H^2 is the sum of the bare Higgs mass parameter $\bar{m}_H^2$ and a quantum correction δm_H^2. The main quantum corrections comes from a top loop diagram [8]

$$\delta m_H^2 = -\frac{|\lambda_t|^2}{8\pi^2} \Lambda_{UV}^2, \tag{2.40}$$

  where Λ_{UV} is the ultra-violet cut off scale at which the current framework is expected to lose validity. We certainly expect such new physics at the Planck scale Λ_{Pl} at which gravity need to be included into the theory. However, if $\Lambda_{UV} = \Lambda_{Pl}$, the corrections both δm_H^2 and $\bar{m}_H^2$ have to be about 10^{34} times larger than the measured value of the Higgs mass parameter m_H^2. Furthermore, a precise cancelation between δm_H^2 and $\bar{m}_H^2$ need to be present for the measured Higgs mass parameter m_H^2 to be at the

[†]New measurements from Belle only show a less significant 1.6 - 1.8σ deviation in the leptonic channel and hadronic channel and are therefore compatible with the SM prediction [54, 55].

electroweak scale. Such a cancelation requires an incredible fine-tuning, which seems very unnatural. This problem is addressed as *fine-tuning problem*.

The hierarchy problem, the naturalness problem and the fine-tuning problem address the same fundamental problem of the theory. Many solutions have been proposed to solve this problem in a natural way, for example Supersymmetry [8], Twin Higgs Models [11] or Composite Higgs Models [9]. Solutions to the hierarchy problem typically postulate the existence of an additional symmetry as well as top partner fields, which together exactly cancel the quadratic divergence in δm_H^2.

- **Strong CP Problem** Unlike the theory of electroweak interaction, QCD has been observed to be CP-preserving. However, it would be possible to account for CP-violation in QCD. This could be done through a Θ-term[‡] in the Lagrangian

$$\mathcal{L}_\theta = \Theta \mathrm{Tr}\left[G^{\mu\nu}\tilde{G}_{\mu\nu}\right], \tag{2.41}$$

where $G^{\mu\nu}$ is the QCD field strength tensor and $\tilde{G}_{\mu\nu}$ is its dual. Searches for an electric dipole moment of the neutron constrain the CP-violation to be very small and restrict Θ to be very small: $\Theta < 10^{-10}$ [56]. Such a small value of Θ seem quite unnatural. The question why there is no CP-violation in the QCD sector is addressed as the *strong CP problem*. A possible solution has been proposed by imposing a $U(1)$ symmetry which is spontaneously broken, generating an additional Goldstone boson: the axion [10].

- **Quantum Gravity** The Standard Model describes the physics at energy scales much below the Planck scale in which gravity can be neglected. Gravity becomes important on large scales and is described by the theory of General Relativity. Currently, Quantum Field Theory and General Relativity are not compatible. However, a full theory of nature would necessarily need to describe all forces of nature. Although such a theory is beyond reach for collider experiments, it might play a role in cosmological problems like inflation or dark energy.

To explain the puzzles particle physics is facing today, the Standard Model has to be supplemented with new dynamics. Many theories [8–11] have been proposed to address one or multiple of these problems. No clear evidence has been found that could support any of those theories. Therefore it is necessary to further investigate such models and propose new possible methods and search channels to experimentally uncover new physics.

2.3 The Two-Higgs-Doublet Model

As we have seen in the previous section, theories describing physics beyond the Standard Model are well motivated. Many of such models contain an extended Higgs sector. In the following discussion let us discuss one of the simplest extensions of the SM Higgs sector, the 2HDM. Such an extended Higgs sector is well-motivated since it appears in many extensions of the SM such as the MSSM [8], Twin Higgs Models [11] or Composite Higgs Models [9].

In this work, we will neglect possible new fields in other sectors, which are typically introduced to address the limitations of the SM introduced in the last section. If we are

[‡]Note that an additional CP violating chiral phase θ in the fermion mass term $\bar{\Psi} m e^{i\theta\gamma_5}\Psi$ can be absorbed into the Θ-term by a chiral transformation of the quarks [27].

only interested in the physics of the extended Higgs sector, we can use the 2HDM as analysis framework. The 2HDM can also be seen as a low-energy effective model of a more complicated new physics model, for the case that the fields in the other sectors are heavy. More information can be found in the 2HDM review [57], which was used as the main source for the following discussion.

In my opinion the name Two-Higgs-Doublet Model is misleading since the 2HDM is just an extension of the SM but does not solve any of the problems of particle physics. A name that would describe the its purpose better would be Two-Higgs-Doublet Framework.

2.3.1 Physical Higgs Fields

Basis of the Two Higgs Doublet Model

In the SM we introduced one scalar $SU(2)$ doublet with hypercharge $Y = \frac{1}{2}$* which will then spontaneously break the $SU(2) \times U(1)$ symmetry and obtain a vacuum expectation value v. We can parameterize it in terms of the massless Goldstone bosons $G^{\pm}$ and G^0 which will be absorbed as longitudinal modes of the gauge bosons, and the SM Higgs field h_{SM}. Let us denote this doublet as Φ_v.

Let us now introduce a second scalar $SU(2)$ doublet with hypercharge $Y = \frac{1}{2}$, Φ_H, which does not contribute to electroweak symmetry breaking and does not obtain a vacuum expectation value. It will contain four new massive physical Higgs fields, a neutral CP-even scalar h_{BSM}, a neutral CP-odd scalar A and two charged scalars $H^{\pm}$. We can write

$$\Phi_v = \begin{pmatrix} G^+ \\ \frac{1}{\sqrt{2}}\left(v + h_{SM} + iG^0\right) \end{pmatrix} \qquad \text{and} \qquad \Phi_H = \begin{pmatrix} H^+ \\ \frac{1}{\sqrt{2}}\left(h_{BSM} + iA\right) \end{pmatrix}. \tag{2.42}$$

This basis, in which only one doublet obtains a vacuum expectation value, is called the *Higgs basis*.

Since h_{SM} and h_{BSM} have the same quantum numbers, they do not need to be eigenstates of the Hamiltonian. In general, the CP-even mass eigenstates h and H will be a linear combination of both field h_{SM} and h_{BSM}. Let us parameterize the mixing by an angle γ and write

$$H = h_{SM}c_\gamma - h_{BSM}s_\gamma \qquad \text{and} \qquad h = h_{SM}s_\gamma + h_{BSM}c_\gamma \tag{2.43}$$

In general, the fermion fields will couple to both doublets, Φ_v and Φ_H. For many application, it will turn out to be more convenient to change to a different basis, the *generic basis*, in which each fermion type only couple to one scalar doublet. Let us therefore perform a basis transformation $\{\Phi_v, \Phi_H\} \to \{\Phi_1, \Phi_2\}$ such that the up-type fermion fields only couple to one doublet, which we chose to be Φ_2. This transformation is just a rotation of the basis by an angle β. We can write

$$\Phi_1 = \Phi_v c_\beta - \Phi_H s_\beta \qquad \text{and} \qquad \Phi_2 = \Phi_v s_\beta + \Phi_H c_\beta, \tag{2.44}$$

where the doublets are given by

$$\Phi_i = \begin{pmatrix} \phi_i^+ \\ \frac{1}{\sqrt{2}}\left(v_i + \phi_i + i\varphi_i\right) \end{pmatrix} \tag{2.45}$$

*Note that many references, for example [57], change there hypercharge definition such that the Higgs doublet has $Y = 1$ and $Q = T_3 + \frac{1}{2}Y$.

In particular this implies that both doublets Φ_1 and Φ_2 will obtain a vacuum expectation value $v_1 = vc_\beta$ and $v_2 = vs_\beta$. Later we will often use the parameter t_β which is the ratio of the vacuum expectation values: $t_\beta = \frac{v_2}{v_1}$. This basis transformation will also mix the Goldstone and Higgs boson fields of the two doublets. We can express them in terms of the components of the doublets in the generic basis

$$\begin{aligned} G^+ &= \phi_1^+ c_\beta + \phi_2^+ s_\beta & G^0 &= \varphi_1 c_\beta + \varphi_2 s_\beta \\ H^+ &= -\phi_1^+ s_\beta + \phi_2^+ c_\beta & A &= -\varphi_1 s_\beta + \varphi_2 c_\beta. \end{aligned} \tag{2.46}$$

For the CP-even neutral fields, using Eq. 2.43 and 2.44, we get

$$\begin{aligned} H &= \phi_1 c_{\beta-\gamma} + \phi_2 s_{\beta-\gamma} = \phi_1 c_\alpha + \phi_2 s_\alpha \\ h &= -\phi_1 s_{\beta-\gamma} + \phi_2 c\beta - \gamma = -\phi_1 s_\alpha + \phi_2 c_\alpha. \end{aligned} \tag{2.47}$$

Here we introduced the angle $\alpha = \beta - \gamma$ which is conventionally used in 2HDM phenomenology. In all later discussion we will use $\beta - \alpha$ instead of γ.

Types of 2HDM

We have introduced the generic basis of the 2HDM to simplify the up-type quark Yukawa couplings to the Higgs sector such that they only couple to one Higgs doublet Φ_2. In general the down-type quarks can still couple to both Higgs doublets and we can write a general Yukawa term for the quark fields

$$\mathcal{L}_{Yuk.} = -\lambda_u \epsilon^{ab} \bar{Q}_{La} \Phi_{2b}^\dagger u_R + h.c. - \lambda_{d1} \bar{Q}_L \Phi_1 d_R - \lambda_{d2} \bar{Q}_L \Phi_2 d_R \tag{2.48}$$

Note that there are three generation of quarks and therefore λ will be a 3×3 matrix. As in the Standard Model, we are able to diagonalize λ_u and one of the λ_d. However, it will in general not be possible to simultaneously diagonalize both λ_{d1} and λ_{d2}. One of the Yukawa couplings will therefore contribute mixing terms between different down quark generations, $\mathcal{L} = h\bar{d}_i d_j$ with $i \neq j$. Such couplings are called flavor-changing neutral currents (FCNC) and are highly constrained by experimental data.

We can avoid FCNC by requiring that each fermion type obtains its mass from only Higgs doublet. In the absence of right-handed neutrino fields, there are four possibilities to couple the right-handed fermion fields to the Higgs doublets. We typically call this the *type* of the 2HDM. The definition of the different types are shown in Tab. 2.3.

Lepton	Type I	Type II	Lepton Specific	Flipped
up-type quarks	Φ_2	Φ_2	Φ_2	Φ_2
down-type quarks	Φ_2	Φ_1	Φ_2	Φ_1
charged leptons	Φ_2	Φ_1	Φ_1	Φ_2

Table 2.3: Types of 2HDM as defined in [57]. We show the Higgs doublet Φ_i which is responsible for mass generation for each fermion type.

In this work we will only consider the Type II 2HDMs. This type naturally appear in supersymmetric scenarios like the MSSM [8]. We can force the 2HDM to be Type II by imposing an additional $\mathcal{Z}_2$ symmetry on the theory. Under this $\mathcal{Z}_2$ symmetry the fields transform as

$$\Phi_1 \to -\Phi_1 \quad , \quad d_R \to -d_R \quad \text{and} \quad e_R \to -e_R \tag{2.49}$$

while all other fields stay unchanged.

2.3.2 The 2HDM Higgs Potential

Potential Term and Minima

The 2HDM Lagrangian can be written as

$$\mathcal{L} = \sum_i |D_\mu \Phi_i|^2 + V(\Phi_i, \Phi_2) + \mathcal{L}_{Yuk} \tag{2.50}$$

where the first term denotes the kinetic term for the two Higgs doublets, $V(\Phi_1, \Phi_2)$ is the Higgs potential and the last term denotes the Yukawa interactions between Φ_i and the SM fermions. Assuming CP conservation and a soft $\mathbb{Z}_2$ symmetry breaking, the 2HDM Higgs potential can be written down as[†]:

$$\begin{aligned} V(\Phi_1, \Phi_2) = {} & m_{11}^2 \Phi_1^\dagger \Phi_1 + m_{22}^2 \Phi_2^\dagger \Phi_2 - m_{12}^2 (\Phi_1^\dagger \Phi_2 + h.c.) + \frac{\lambda_1}{2} (\Phi_1^\dagger \Phi_1)^2 + \frac{\lambda_2}{2} (\Phi_2^\dagger \Phi_2)^2 \\ & + \lambda_3 (\Phi_1^\dagger \Phi_1)(\Phi_2^\dagger \Phi_2) + \lambda_4 (\Phi_1^\dagger \Phi_2)(\Phi_2^\dagger \Phi_1) + \frac{1}{2} \left[\lambda_5 (\Phi_1^\dagger \Phi_2)^2 + h.c. \right]. \end{aligned} \tag{2.51}$$

The m^2 terms are a generalization of the μ^2 term in the SM Higgs potential and have mass dimension two. The m_{12}^2 term breaks the $\mathcal{Z}_2$ symmetry softly.

This potential has a minimum at $\langle \Phi_i \rangle = \frac{1}{\sqrt{2}} \begin{pmatrix} 0 & v_i \end{pmatrix}^T$, where v_i are the vacuum expectation values that we introduced in the previous section. At its minimum the potential must be flat, $\langle \partial_{\Phi_1} V(\Phi_1, \Phi_2) \rangle$ what implies the following two conditions

$$\begin{aligned} 0 = \langle \partial_{\Phi_1} V(\Phi) \rangle = {} & m_{11}^2 \langle \Phi_1^\dagger \rangle - m_{12}^2 \langle \Phi_2^\dagger \rangle + \lambda_1 \langle (\Phi_1^\dagger \Phi_1) \Phi_1^\dagger \rangle \\ & + \lambda_3 \langle (\Phi_2^\dagger \Phi_2) \Phi_1^\dagger \rangle + \lambda_4 \langle (\Phi_1^\dagger \Phi_2) \Phi_2^\dagger \rangle + \lambda_5 \langle (\Phi_2^\dagger \Phi_1) \Phi_2^\dagger \rangle \\ 0 = \langle \partial_{\Phi_2} V(\Phi) \rangle = {} & m_{22}^2 \langle \Phi_2^\dagger \rangle - m_{12}^2 \langle \Phi_1^\dagger \rangle + \lambda_2 \langle (\Phi_2^\dagger \Phi_2) \Phi_2^\dagger \rangle \\ & + \lambda_3 \langle (\Phi_1^\dagger \Phi_1) \Phi_2^\dagger \rangle + \lambda_4 \langle (\Phi_2^\dagger \Phi_1) \Phi_1^\dagger \rangle + \lambda_5 \langle (\Phi_1^\dagger \Phi_2) \Phi_1^\dagger \rangle, \end{aligned} \tag{2.52}$$

which can be rewritten as

$$\begin{aligned} m_{11}^2 &= m_{12}^2 \frac{v_2}{v_1} - \frac{1}{2} (\lambda_1 v_1^2 + \lambda_{345} v_2^2) = m_{12}^2 t_\beta \ - \frac{1}{2} v^2 (c_\beta^2 \lambda_1 + s_\beta^2 \lambda_{345}) \\ m_{22}^2 &= m_{12}^2 \frac{v_1}{v_2} - \frac{1}{2} (\lambda_2 v_2^2 + \lambda_{345} v_1^2) = m_{12}^2 t_\beta^{-1} - \frac{1}{2} v^2 (s_\beta^2 \lambda_2 + c_\beta^2 \lambda_{345}). \end{aligned} \tag{2.53}$$

where $\lambda_{345} = \lambda_3 + \lambda_4 + \lambda_5$. We were therefore able to express the Lagrangian parameters m_{ii}^2 in terms of the vacuum expectation value v and the mixing angle β.

Physical Higgs Masses

Let us now analyze the 2HDM mass spectrum. To do so, let us expand the potential in terms of the physical Higgs fields that we have obtained above. Since this process is mathematically involved and not very illuminating, we will skip the details of the calculation[‡].

[†] The most general scalar potential also contains the term $\left[\lambda_6 (\Phi_1^\dagger \Phi_1) + \lambda_7 (\Phi_2^\dagger \Phi_2) \right] (\Phi_1^\dagger \Phi_2) + h.c.$ and potentially leads to FCNC. In the following we will neglect this term by imposing the $\mathcal{Z}_2$ which we introduced in the previous section.

[‡] [57] shows a simpler derivation in which the Higgs masses and fields are obtained as solution of an eigenvalue problem of the Higgs potential.

The Higgs masses expressed in terms of the Lagrangian parameters are

$$\begin{aligned} m_A^2 &= \frac{m_{12}^2}{s_\beta c_\beta} - \lambda_5 v^2 \\ m_{H^+}^2 &= \frac{m_{12}^2}{s_\beta c_\beta} - \frac{1}{2}(\lambda_4 + \lambda_5) v^2 \\ m_{H,h}^2 &= \frac{1}{2}\left(\left[v^2(\lambda_1 c_\beta^2 + \lambda_2 s_\beta^2) + \frac{m_{12}^2}{s_\beta c_\beta} \right] \pm \frac{1}{s_\alpha c_\alpha} \left[\lambda_{345} s_\beta c_\beta v^2 - m_{12}^2 \right] \right), \end{aligned} \tag{2.54}$$

where mixing angle between the CP-even neutral Higgs bosons α is

$$t_{2\alpha} = 2 \frac{v^2 \lambda_{345} s_\beta c_\beta - m_{12}^2}{v^2(\lambda_1 c_\beta^2 - \lambda_2 s_\beta^2) - \frac{m_{12}^2}{s_\beta c_\beta}(c_\beta^2 - s_\beta^2)}. \tag{2.55}$$

We were able to express the physical Higgs masses and the mixing angle α in terms of the Lagrangian parameters. These relationships can be inverted. We obtain[§]

$$\begin{aligned} \lambda_1 &= \frac{m_H^2 c_\alpha^2 + m_h^2 s_\alpha^2 - m_{12}^2 t_\beta}{v^2 c_\beta^2} \\ \lambda_2 &= \frac{m_H^2 s_\alpha^2 + m_h^2 c_\alpha^2 - m_{12}^2 t_\beta^{-1}}{v^2 s_\beta^2} \\ \lambda_3 &= \frac{(m_H^2 - m_h^2) s_\alpha c_\alpha + 2 m_{H^+}^2 s_\beta c_\beta - m_{12}^2}{v^2 s_\beta c_\beta} \\ \lambda_4 &= \frac{(m_A^2 - 2 m_{H^+}^2) s_\beta c_\beta + m_{12}^2}{v^2 s_\beta c_\beta} \\ \lambda_5 &= \frac{-m_A^2 s_\beta c_\beta + m_{12}^2}{v^2 s_\beta c_\beta}. \end{aligned} \tag{2.56}$$

For out later discussion we will chose the the physical Higgs masses m_{h,H,A,H^+}, the mixing angles α, β, the soft $\mathcal{Z}_2$ breaking parameter m_{12}^2 and the vacuum expectation value v as our basis to describe the 2HDM. After the discovery of the Higgs boson we already know two of them: one neutral CP-even Higgs mass $m_h = 125$ GeV and the vacuum expectation value $v = 246$ GeV. The relations in Eq. 2.56 will turn out to be useful when translating bounds on the Lagrangian parameters, for example from unitarity and vacuum stability, into bounds on the masses and mixing angles.

2.3.3 Couplings in 2HDM

Higgs Couplings to Gauge Bosons in 2HDM

Let us first investigate how the 2HDM Higgs bosons couple to the vector bosons. These coupling come from the kinetic term for the Higgs. To obtain the couplings, it is easier to change back into Higgs basis in which only one doublet obtains a vacuum expectation value. Let us write the kinetic Higgs term[¶] as

$$\mathcal{L}_{kin} = |D_\mu \Phi_1|^2 + |D_\mu \Phi_2|^2 = |D_\mu \Phi_v|^2 + |D_\mu \Phi_H|^2. \tag{2.57}$$

[§]See [58] for the details of this derivation.

[¶]Note that the kinetic Higgs term in the generic basis does not contain a mixing term $D_\mu \Phi_1 D^\mu \Phi_2$ since such a mixing would violate the imposed Z_2 symmetry and would lead to FCNC.

We see that the kinetic term is diagonal in both basis. As already discussed in the context of the Standard Model, the first term will lead to cubic couplings of the SM-like Higgs to the gauge bosons

$$\begin{aligned}|D_\mu \Phi_v|^2 &= g m_W h_{SM} W_\mu^+ W^{\mu-} + \frac{g m_Z}{2\cos\theta_w} h_{SM} Z_\mu Z^\mu + \cdots \\ &= 2\frac{m_W^2}{v}(H c_{\beta-\alpha} + h s_{\beta-\alpha}) W_\mu^+ W^{\mu-} + \frac{m_Z^2}{v}(H c_{\beta-\alpha} + h s_{\beta-\alpha}) Z_\mu Z^\mu + \cdots\end{aligned} \tag{2.58}$$

Here we have omitted all terms that do not contain three fields. We can directly read of the couplings

$$\begin{aligned}g_{hVV} &= 2 i s_{\beta-\alpha} \frac{m_V^2}{v}\, g^{\mu\nu} = s_{\beta-\alpha}\, g_{hVV}^{SM} \\ g_{HVV} &= 2 i c_{\beta-\alpha} \frac{m_V^2}{v}\, g^{\mu\nu} = c_{\beta-\alpha}\, g_{hVV}^{SM}.\end{aligned} \tag{2.59}$$

The couplings of the 2HDM Higgs bosons $h(H)$ to vector bosons are scaled with respect to the SM vector boson coupling h_{hVV}^{SM} by a factor $s_{\beta-\alpha}$ ($c_{\beta-\alpha}$). Note that there is no coupling of the Higgs bosons to photon pairs, since $U(1)_{EM}$ remains unbroken and therefore photons are massless. Furthermore, the heavy Higgs bosons A and $H^\pm$ do not have a cubic couplings to vector bosons at tree level, $g_{AVV} = g_{H^+VV} = 0$, since the doublet they are contained in does not obtain a vacuum expectation value.

Let us now turn to the second doublet Φ_H. The covariant derivative acting on Φ_H reads

$$D_\mu \Phi_H = \begin{pmatrix} \left(\partial_\mu - i\left[\frac{g}{2\cos\theta_w}\left(1 - 2\sin^2\theta_w\right) Z_\mu + e A_\mu\right]\right) H^+ - i\frac{g}{2} W_\mu^+ (h_{BSM} + iA) \\ \left(\partial_\mu + \frac{ig}{2\cos\theta_w} Z_\mu\right) \frac{1}{\sqrt{2}}(h_{BSM} + iA) - i\frac{g}{\sqrt{2}} W_\mu^- H^+ \end{pmatrix}. \tag{2.60}$$

We can now expand the kinetic term $|D_\mu \Phi_H|^2$ and obtain

$$\begin{aligned}|D_\mu \Phi_H|^2 = &\frac{g}{2\cos\theta_w} Z_\mu \left[h_{BSM} \partial^\mu A - A \partial^\mu h_{BSM}\right] \\ &+ \frac{ig}{2}\left[h_{BSM} W_\mu^- (\partial^\mu H^+) - (\partial_\mu h_{BSM}) W^{\mu-} H^+ - h.c.\right] \\ &+ \frac{g}{2}\left[(\partial_\mu A) W_\mu^- H^+ - A W_\mu^- (\partial^\mu H^+) + h.c.\right] \\ &+ i\left[\frac{m_Z}{v}(1 - 2\sin^2\theta_w) Z_\mu + e A_\mu\right]\left[H^- (\partial^\mu H^+) - h.c.\right] + \cdots .\end{aligned} \tag{2.61}$$

Note again that this term does not contain a vacuum expectation value. This implies that all cubic terms contain a derivative ∂_μ. This means that the coupling will be proportional to the particle momenta. We can extract the couplings

$$\begin{aligned}g_{H^+H^-\gamma} &= -ie(p_{H^+} - p_{H^-})^\mu \\ g_{H^+H^-Z} &= -i\frac{g\cos 2\theta_w}{2\cos\theta_w}(p_{H^+} - p_{H^-})^\mu \\ g_{AH^+W} &= \frac{g}{2}(p_{H^+} - p_A)^\mu\end{aligned} \tag{2.62}$$

and

$$\begin{aligned}g_{hAZ} &= i s_{\beta-\alpha}\frac{g}{2\cos\theta_w}(p_A - p_h)^\mu \qquad & g_{hH^+W} &= -i s_{\beta-\alpha}\frac{g}{2}(p_{H^+} - p_h)^\mu \\ g_{HAZ} &= i c_{\beta-\alpha}\frac{g}{2\cos\theta_w}(p_A - p_H)^\mu \qquad & g_{HH^+W} &= -i c_{\beta-\alpha}\frac{g}{2}(p_{H^+} - p_H)^\mu\end{aligned} \tag{2.63}$$

Note that there are no couplings of a two CP-even or CP-odd Higgs to the Z boson vanishes, $g_{HhZ} = g_{hhZ} = g_{HHZ} = g_{AAZ} = 0$, since such a coupling would violate the CP-invariance.

Higgs Coupling to Fermions in 2HDM

Let us now investigate the coupling of the Higgs bosons to the fermionic sector. As we argued above, to avoid FCNC, each fermion type is only allowed to couple to one Higgs doublet. In Type II 2HDM, the up-type quarks couple to Φ_2 while the down-type quarks couple to Φ_1. Let us for simplicity concentrate on the quark sector and only consider one generation. Then we can write the Yukawa term

$$\begin{aligned}\mathcal{L}_{Yuk} &= -Y_u \epsilon^{ab} \bar{Q}_{La} \Phi^\dagger_{2b} u_R - Y_d \bar{Q}_L \Phi_1 d_R + h.c. \\ &= -\frac{Y_u}{\sqrt{2}} \bar{u}_L (v_2 + \phi_2 + i\varphi_2) u_R - \frac{Y_d}{\sqrt{2}} \bar{d}_L (v_1 + \phi_1 + i\varphi_1) d_R - Y_u \bar{d}_L \phi_2^- u_R - Y_d \bar{u}_L \phi_1^+ d_R + h.c.\end{aligned} \tag{2.64}$$

We can read out the fermion masses $m_u = \frac{Y_u}{\sqrt{2}} v_2 = \frac{Y_u}{\sqrt{2}} v s_\beta$ and $m_d = \frac{Y_d}{\sqrt{2}} v_1 = \frac{Y_d}{\sqrt{2}} v c_\beta$ We can then rewrite the coupling of the physical Higgs fields to the fermions as

$$\begin{aligned}\mathcal{L}_{Yuk} = &-\frac{m_u}{v s_\beta} (H s_\alpha + h c_\alpha + i A c_\beta) \bar{u}_L u_R - \frac{m_d}{v c_\beta} (H c_\alpha - h s_\alpha - i A s_\beta) \bar{d}_L d_R \\ &- \frac{\sqrt{2} m_u}{v s_\beta} c_\beta H^- \bar{d}_L u_R + \frac{\sqrt{2} m_d}{v c_\beta} s_\beta H^+ \bar{u}_L d_R + h.c.\end{aligned} \tag{2.65}$$

If we introduce multiple generations of fermions, we have to take into account that the Yukawa coupling matrices Y_u and Y_d will in general not be diagonal in the flavor basis. However, we can change into the mass basis in which the Yukawa matrices are diagonal. As in the case of weak interactions, this introduces the appearance of the CKM matrix V in the charged current interaction. We can perform an analog calculation for the leptonic sector.

We can now extract the couplings of the Higgs fields to the fermions. Let us express the result in terms of the SM-Higgs couplings $g^{SM}_{hff} = -i\frac{m_f}{v}$. We obtain for the neutral Higgs bosons

$$\begin{aligned} g_{huu} &= \frac{c_\alpha}{s_\beta} g^{SM}_{huu} & g_{Huu} &= \frac{s_\alpha}{s_\beta} g^{SM}_{huu} & g_{Auu} &= i\gamma_5 \frac{c_\beta}{s_\beta} g^{SM}_{huu} \\ g_{hdd} &= \frac{c_\alpha}{c_\beta} g^{SM}_{hdd} & g_{Hdd} &= \frac{s_\alpha}{c_\beta} g^{SM}_{hdd} & g_{Add} &= i\gamma_5 \frac{c_\beta}{c_\beta} g^{SM}_{hdd} \\ g_{hll} &= \frac{c_\alpha}{c_\beta} g^{SM}_{hll} & g_{Hll} &= \frac{s_\alpha}{c_\beta} g^{SM}_{hll} & g_{All} &= i\gamma_5 \frac{c_\beta}{c_\beta} g^{SM}_{hll}. \end{aligned} \tag{2.66}$$

Note that the CP-odd Higgs A couples to the axial current, as expected from it's CP properties. Furthermore, we obtain couplings of the charged Higgs boson to the fermions

$$\begin{aligned} g_{H^+ u_i d_j} &= \frac{1}{\sqrt{2}v} V_{ij} \left((t_\beta m_d + t_\beta^{-1} m_u) + (t_\beta m_d - t_\beta^{-1} m_u) \gamma_5 \right) \\ g_{H^+ l \nu} &= \frac{1}{\sqrt{2}v} t_\beta m_l (1 + \gamma_5) \end{aligned} \tag{2.67}$$

Note that the projection operator $1 + \gamma_5$ in the charged Higgs coupling ensures that the charged Higgs will only couple to left-handed neutrinos and not to hypothetical right-handed neutrinos.

Cubic Higgs Couplings in 2HDM

Furthermore, there are cubic and quartic couplings between the 2HDM Higgs bosons arising from the Higgs potential introduced in Eq. 2.51. Since a derivation would be both mathematically involved and not very illuminating, we will just state the results for the most important couplings[‖]:

$$
\begin{aligned}
g_{hhh} &= -\frac{3}{4s_{2\beta}v}\Big(\frac{4m_{12}^2}{s_\beta c_\beta}(c_{\beta-\alpha}^2 c_{\beta+\alpha} - m_h^2(c_{3\alpha-\beta}+3c_{\alpha+\beta})\Big)\\
g_{HHH} &= -\frac{3}{4s_{2\beta}v}\Big(\frac{4m_{12}^2}{s_\beta c_\beta}(s_{\beta-\alpha}^2 s_{\beta+\alpha} + m_H^2(s_{3\alpha-\beta}+3s_{\alpha+\beta})\Big)\\
g_{Hhh} &= -\frac{1}{4s_{2\beta}v}\Big(\frac{4m_{12}^2}{s_\beta c_\beta}(c_{\beta-\alpha}^2 s_{\beta+\alpha} - 2s_{\beta-\alpha}c_{\beta-\alpha}c_{\beta+\alpha}) - (2m_h^2+m_H^2)(s_{3\alpha-\beta}+s_{\alpha+\beta})\Big)\\
g_{hHH} &= -\frac{1}{4s_{2\beta}v}\Big(\frac{4m_{12}^2}{s_\beta c_\beta}(s_{\beta-\alpha}^2 c_{\beta+\alpha} - 2s_{\beta-\alpha}c_{\beta-\alpha}s_{\beta+\alpha}) + (2m_H^2+m_h^2)(c_{3\alpha-\beta}-c_{\alpha+\beta})\Big)\\
g_{hAA} &= -\frac{1}{4s_{2\beta}v}\Big(\frac{4m_{12}^2}{s_\beta c_\beta}c_{\beta+\alpha} - 8m_A^2 s_{\beta-\alpha}s_\beta c_\beta - m_h^2(c_{\alpha-3\beta}+3c_{\alpha+\beta})\Big)\\
g_{HAA} &= -\frac{1}{4s_{2\beta}v}\Big(\frac{4m_{12}^2}{s_\beta c_\beta}s_{\beta+\alpha} - 8m_A^2 c_{\beta-\alpha}s_\beta c_\beta - m_H^2(s_{\alpha-3\beta}+3s_{\alpha+\beta})\Big)\\
g_{hH^+H^-} &= -\frac{1}{4c_{2\beta}v}\Big(\frac{4m_{12}^2}{c_\beta c_\beta}c_{\beta+\alpha} - 8m_{H^\pm}^2 s_{\beta-\alpha}s_\beta c_\beta - m_h^2(c_{\alpha-3\beta}+3c_{\alpha+\beta})\Big)\\
g_{HH^+H^-} &= -\frac{1}{4s_{2\beta}v}\Big(\frac{4m_{12}^2}{s_\beta c_\beta}s_{\beta+\alpha} - 8m_{H^\pm}^2 c_{\beta-\alpha}s_\beta c_\beta - m_H^2(s_{\alpha-3\beta}+3s_{\alpha+\beta})\Big)
\end{aligned}
\tag{2.68}
$$

Note that a single CP-odd Higgs A cannot couple to CP-even or charged Higgs due to CP-conservation and therefore $g_{Ahh} = g_{AHH} = g_{AH^+H^-} = 0$.

These couplings not only depend on the Higgs masses but also on the soft $\mathcal{Z}_2$ symmetry breaking term m_{12}^2. Therefore this otherwise experimentally unobservable parameter has a significant impact on the cubic Higgs couplings. As we will see later, some of these couplings can even vanish depending on the choice of m_{12}^2. We also want to point out that the couplings stated in Eq. 2.68 differ from those reported in the Higgs Hunter Guide [37]. The Higgs Hunter Guide states the couplings for MSSM which implies a relationship $m_{12}^2 = m_A^2 s_\beta c_\beta$.

2.3.4 Connection to MSSM

One of the main motivations to consider a Type II 2HDM is that is has the same structure has the Higgs sector in the Minimal Supersymmetric Extension of the Standard Model (MSSM)[**]. Since the superpotential has to be a holomorphic function of the fields, we are not allowed to write down the Yukawa term for the up-types quarks $Y_u \epsilon^{ab} \bar{Q}_{La} \Phi_b^\dagger u_R$ anymore, as we have done in the Standard Model. Instead, we introduce a second Higgs doublet

$$
\Phi_u = \begin{pmatrix} \frac{1}{\sqrt{2}}(v_u + \phi_u - i\varphi_u) \\ -\phi_u^- \end{pmatrix} \tag{2.69}
$$

[‖] I derived these results by expanding the Lagrangian and collecting the right coefficients using Mathematica. If there is a reference providing these couplings which I have overseen, I want to apologize.

[**] A phenomenological introduction to Supersymmetry and the MSSM can be found in [8]

which couples to the up-type fermion instead of $\epsilon^{ab}\Phi_b^\dagger$.We can now write a up-type quark Yukawa term $Y_u\bar{Q}\Phi_u u_R$. Note that we defined the doublet $\Phi_u = \epsilon^{ab}\Phi_{2b}^\dagger$ such that it contains the complex conjugate fields to avoid complex conjugation in the Lagrangian. Therefore Φ_u has the opposite hypercharge $Y = -\frac{1}{2}$ compared to Φ_2. This is just a redefinition of the field, $\Phi_2 \to \Phi_u$, and will not change the results we have obtained above. The appearance of a $Y = -\frac{1}{2}$ hypercharge doublet also ensures that $\mathrm{Tr}[T_3^2 Y]$ =$\mathrm{Tr}[Y^3] = 0$ and therefore cancellation of gauge anomalies.

Supersymmetry imposes special relationships between the Lagrangian parameters of the 2HDM. The quartic couplings are fixed by electroweak couplings g and g'[††]:

$$\begin{aligned} \lambda_1 = \lambda_2 = \frac{1}{4}(g^2 + g'^2) = \frac{m_Z^2}{v^2} \qquad & \lambda_3 = \frac{1}{4}(g^2 - g'^2) = \frac{2m_W^2 - m_Z^2}{v^2} \\ \lambda_4 = -\frac{1}{2}g^2 = -\frac{2m_W^2}{v^2} \qquad & \lambda_5 = 0. \end{aligned} \tag{2.70}$$

The mass spectrum of the MSSM therefore reads

$$\begin{aligned} m_A^2 = \frac{m_{12}^2}{s_\beta c_\beta} \qquad & m_{H^+}^2 = m_A^2 + m_W^2 \\ m_{H,h}^2 = \frac{1}{2}(m_A^2 + m_Z^2 \pm \sqrt{(m_A^2 + m_Z^2)^2 - 4m_Z^2 m_Z^2 c_{2\beta}}) & \end{aligned} \tag{2.71}$$

and the mixing angel α is fixed by

$$t_{2\alpha} = t_{2\beta}\frac{m_A^2 + m_Z^2}{m_A^2 - m_Z^2}. \tag{2.72}$$

We can see that the parameter space is describes by only two free parameters which are conventionally chosen to be m_A and t_β. Notice that the soft $\mathcal{Z}_2$ breaking term m_{12}^2 is also fixed by $m_{12}^2 = m_A^2 s_\beta c_\beta$.

Often people consider the alignment case in which the $m_A \gg m_Z$. In this case $m_A \approx m_H \approx m_{H^+}$ and $c_{\beta-\alpha} \approx 0$.

2.4 Collider Phenomenology

2.4.1 Detectors at LHC

The Large Hadron Collider

As discussed above, many theories of physics beyond the Standard Model have been proposed to explain the puzzles particle physics is facing today. Many of these models predict new physics at or not far above the weak scale. This is particularly true for solutions of the hierarchy problem which address the smallness of the weak scale compared to the Planck scale.

The currently most powerful experiment to test such scenarios is the LHC, which is located at CERN. This synchrotron has a circumference of 27 km and is designed to accelerate protons and lead nuclei. During its first operational run between 2010 and 2012 it was operating with a proton-proton center-of-mass energy of 7 TeV (2010 and 2011) and 8 TeV (2012). After the first major upgrade, LHC restarted in 2015 with a center-of-mass

[††]See [58] for details of the calculation.

energy of 13 TeV. The second run is expected to collect data corresponding to an integrated luminosity* of 100 fb^{-1} until its end in 2018. After another major upgrade, which might also increase the center-of-mass energy to 14 TeV, LHC is expected to collect 300 fb^{-1} of data during run 3. Proposals for a further upgrade to High-Luminosity LHC aim for a total integrated luminosity of 3000 fb^{-1} until 2037 [59].

The LHC contains four major experiments. ATLAS (A Toroidal LHC ApparatuS) and CMS (Compact Muon Solenoid) are general purpose detectors and designed for SM measurements and BSM physics searches. Furthermore the LHC accommodate the LHCb (Large Hadron Collider beauty), which is a b-physics experiment, and ALICE (A Large Ion Collider Experiment), which is designed to study the quark-gluon plasma created in heavy-ion collisions. In our further discussion we will mainly discuss ATLAS and CMS.

The Detector Composition

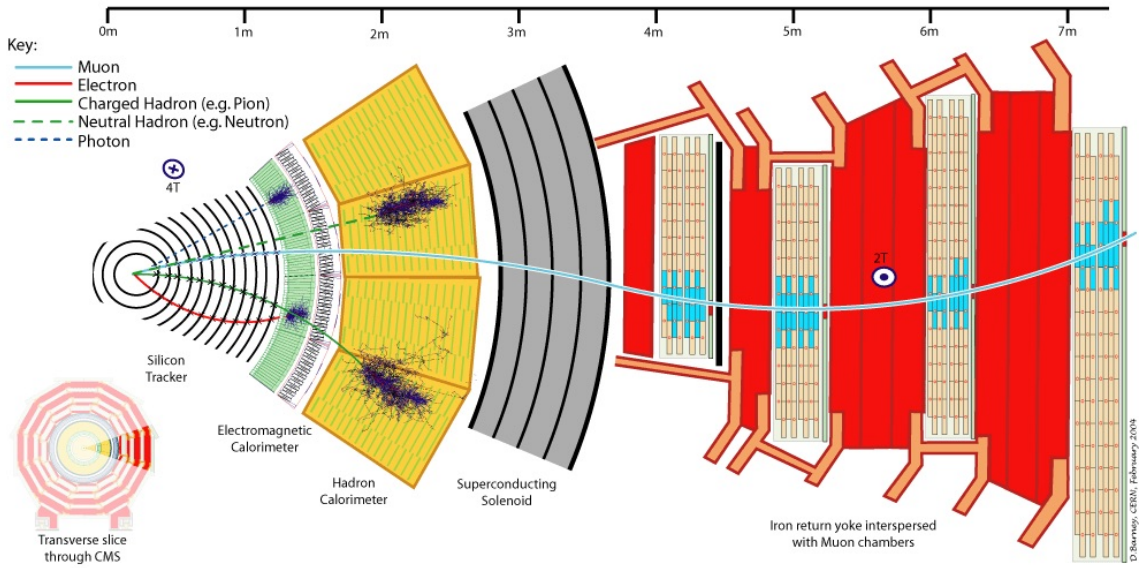

Figure 2.4: Transverse slice of the CMS detector. This figure has been taken from [60].

To observe new physics at the LHC, the LHC detectors need to be able to detect all Standard Model particles which can be produced in association with or in the decay of new, so far undiscovered, states. This includes a good energy and momentum resolution of these particles and the identification of electrons, muons and photons. Furthermore, a good vertex resolution is needed to distinguish b-initiated jets from light-quark and gluon jets. The principle structure of the general purpose detectors is shown in Fig. 2.4, using the example of the CMS detector. The ATLAS detector has a similar structure.

Let us briefly discuss the main components of the detector, as shown in Fig. 2.4, starting with its innermost part†:

*The integrated luminosity $\mathcal{L}$ is a collider specific number describing the number of particles crossing a unit area and relates the number of measured events N with the cross section σ via $N = \sigma\mathcal{L}$.

†My knowledge about the physics of the detector is mainly based on Peter Lochs lecture on jet physics [61].

- **The Tracking System:** Through it's interaction with matter, we are able to track the path of charged particles in the region close to the detector, called the tracking system. This region is put into a strong magnetic field, produced by a solenoid, which bends the path of the charged particles. We are therefore able to measure the direction, the transverse momentum as well as the charge to mass ratio of these particles.

  The most precise part of the tracking system is the pixel detector, which is located a few centimeters apart from the beam axis and has a resolution better than 100 μm. This is precise enough to allow for the reconstruction of displaced vertices. Such displaced vertices occur when a long living particle, such as B mesons, decay a short distance away from the interaction point and can be used to distinguish b-quark initiated jets from light-quark jets.

  The ATLAS and CMS experiment use silicon sensors in their tracking system. An energetic charged particle passing through the semiconductor material creates electron-hole pairs which are accelerated by the applied voltage and result in a measurable current. The ATLAS tracking system additionally includes a transition radiation tracker as its outer layer.

- **The Electromagnetic Calorimeter (ECAL):** The electromagnetic calorimeter is designed to detect electrons, positrons and photons. When entering a material, high energetic electrons and positrons will emit photons via bremsstrahlung while high energetic photons will produce electron-positron pairs. In the calorimeter, this process is repeated producing an electromagnetic shower. The shower ends when the energy loss through ionization of the calorimeter material dominates. Some atoms were excited during this process and emitted light with an intensity proportional to the energy of the incoming particle.

- **The Hadronic Calorimeter (HCAL):** Unlike electrons and photons, hadrons will mainly interact with the detector material via QCD interactions. These inelastic hadron-nucleon interactions happen in layers of passive material with large density and result in a shower of lighter hadrons and mesons which then further interact with the detector or decay. There are over 200 different processes involved in the hadronic shower, including electromagnetic showers e.g. from pion decays $\pi^0 \to \gamma\gamma$. The particles produced in the shower then pass through a layer of scintillators, measuring the energy deposit of the shower, before entering the next layer of passive material. The hadronic shower is typically much bigger than the electromagnetic shower.

- **The Muon Spectrometer:** Due to the high mass of the muon, the energy loss due to Bremstrahlung is suppressed compared to the electron[‡]. Therefore the muon is able to pass all parts of the calorimeter without losing much energy. The muon spectrometer itself is a large tracking system: the muons pass though the spectrometer, consisting of a large number of chambers used to determine the trajectory of the muon. Since the muon system is located in a magnetic field, this trajectory is curved and therefore a precise measurement of the muon track allows a precise determination of the muon momentum.

[‡]The power radiated off a particle with mass m via bremsstrahlung is proportional to m^{-4} [62].

Detector Geometry

At LHC, two protons with same energy but opposite momentum collider at the interaction point in the center of the LHC detectors. Therefore the center-of-mass frame of the colliding protons coincides with laboratory frame of the experiments. The protons themselves are composite particles, consisting of partons: the quarks and gluons. During this collision, these partons interact in a hard process. Each parton only carries a fraction of the proton momentum which, due to the quantum mechanical nature, can only be described by the probabilistic by parton distribution function (pdf). Therefore the center-of-mass frame of the partonic interaction is typically boosted along the proton-beam axis, which is typically chosen to be the z-axis. The cross section itself is symmetric with respect to rotations around this axis. The ATLAS and CMS detectors have been designed accordingly and therefore exhibit a cylindrical shape. To describe the kinematics of the interaction, it is most convenient to work in a coordinate system that respects the cylindrical symmetry of both the cross section and the detector[§].

The momentum transverse to the beam axis, $\vec{p_T}$, can be parameterized using polar coordinates: the magnitude of the transverse momentum p_T and the azimuthal angle ϕ. Since the transverse momentum of the initial state partons is negligible, conservation of momentum requires that the final state partons transverse momentum also vanishes: $\sum \vec{p_T} = 0$. This feature does not change under boosts along the beam axis and therefore holds in both the laboratory frame as well as the partonic center-of-mass frame. This allows us to determine the transverse momentum carried by particles that are not measured by the detector, for example neutrinos or possibly dark matter particles, which is called missing transverse energy (MET).

The momentum longitudinal to the beam axis p_L and the energy transform under boost along the z-axis. It is therefore convenient to parameterize these components of the four-momentum p^μ in terms of the rapidity y and invariant mass m, which is boost invariant by construction. In the context of collider physics, the rapidity y parameterizes the longitudinal boost of particle relative to the frame in which the particles longitudinal momentum vanishes $p_{L,0} = 0$. Let us write the particles energy in this frame as E_0. Then we can write for the longitudinal momentum p_L and energy E in the boosted frame

$$\begin{pmatrix} E \\ p_L \end{pmatrix} = \exp\left[y \begin{pmatrix} 0 & 1 \\ 1 & 0 \end{pmatrix} \right] \begin{pmatrix} E_0 \\ 0 \end{pmatrix} = E_0 \begin{pmatrix} \cosh y \\ \sinh y \end{pmatrix} \tag{2.73}$$

This definition implies that the rapidities of multiple successive boosts simply add up. We can solve the previous expression for the rapidity and obtain[¶]

$$y = \frac{1}{2} \log\left(\frac{E + p_L}{E - p_L} \right). \tag{2.74}$$

At ATLAS and CMS, the detector geometry allows us to observe rapidities of $|y| < 2.5$ in the tracking system, ECAL and muon system. For the HCAL, a forward calorimeter extends the observable rapidity range up to $|\eta| < 5$.

[§]More details about LHC physics and collider phenomenology can be found in [63], which has been used as guideline for this section.

[¶]Often people also use the pseudorapidity $\eta = \frac{1}{2} \log\left(\frac{|\vec{p}| + p_L}{|\vec{p}| - p_L} \right)$ which coincides with the rapidity y only for massless particles.

Since both the azimuthal angle ϕ and the rapidity y have the same order of magnitude, it turns out to be useful to define a distance measure[‖]

$$(\delta R)^2 = (\delta y)^2 + (\delta \phi)^2. \tag{2.75}$$

This distance measure will be used both for the definition of objects like jets and isolated leptons as well as for analysis cuts.

2.4.2 The Methodology of Collider Studies

To estimate the reach of a given search channel at the LHC, we perform phenomenological collider studies. The goal is to extract events corresponding to a new physics signal from a large number of Standard Model background events. These studies use Monte Carlo tools to simulate the detector output and study the performance of different analysis strategies. In the following we discuss the steps performed during such a collider study as well as the tools used in the collider studies presented in this thesis.

Monte Carlo Event Generation: MadGraph

In LHC physics[**], an *event* describes the result of the crossing of two bunches of protons within the detector. Let us for simplicity assume that this involves exactly one collision between two protons, and discuss the effect of multiple collisions at a later stage. In most cases this collision is dominated by the interaction between two partons and we refer to this as the *hard process*. Since the momentum transfer during such a hard processes is typically much larger than the confinement scale of QCD, at which non-perturbative effects become important, the matrix element $\mathcal{M}_{ij\to X}$ for the partonic reaction can be calculated using perturbation theory. The matrix elements are evaluated using the matrix element creator MadGraph [66]. It generated the Feynman diagrams for all relevant subprocesses $ij \to X$ and calculated the corresponding amplitudes $|\mathcal{M}_{ij\to X}|^2$. While MadGraph5 [67], which is mainly used in this thesis, only calculated amplitudes at tree level, a newer version of the code, MG5_aMC@NLO [68], is able to calculate the matrix elements at next-to-leading order.

To correctly simulate a process at LHC, we need to calculate the hadronic cross section $\sigma_{pp\to X}$. According to the QCD factorization theorem, we can write for this cross section

$$\sigma_{pp\to X} = \sum_{i,j} \int dx_i \int dx_j \int \frac{d\Pi}{2x_i x_j S} f_i(x_i,\mu) f_j(x_j,\mu) \left|\mathcal{M}_{ij\to X}\right|^2 . \tag{2.76}$$

Here S denotes the center of mass energy of the hadronic system. The functions $f_i(x_i,\mu)$ are called parton distribution function (pdf). They describe the probability of finding a parton i ($i = g, u\bar{u}, d, \bar{d}, ...$) carrying a fraction x_i of the protons momentum, evaluated a factorization scale μ. There are several different sets of pdf, which are typically expressed by numerical fits. To obtain a total hadronic cross section we integrate the partonic cross section, weighted by the initial state pdfs, over the initial state phase space, described by x_i and x_j, and final state phase space, denoted by Π and sum over all possible initial states.

[‖] Note that many references define this measure using the pseudorapidity instead of the rapidity. However, the jet algorithms as implemented in FastJet [64] use the rapidity.

[**] This section is based on the discussion presented in [65], which is also a good reference about general purpose detectors.

This phase space integral can not be solved analytically and therefore numerical tools are needed. Madgraph5 [67] uses the event generator MadEvent [69] which uses Monte-Carlo techniques to perform the integration. The idea is to approximate an n-dimensional integral over a function $F(p)$ by a finite sum phase space volumes Δp_i around a phase space point p_i weighted by $F(p_i)$:

$$\int F(p) d^n p \approx \sum_{i=1}^{N} F(p_i) \Delta p_i. \tag{2.77}$$

The phase space points p_i, at which the integrant is evaluated, are chosen randomly according to some prior distribution $f(p)$. There is no need to demand the phase space volumes Δp_i to have the same size. Indeed, we can optimize the convergence by applying a so called importance sampling: regions of parameter space in which $F(p)$ is large, will be sampled by a larger density of points. Ideally, we want to choose the sampling, described by the prior distribution $f(p)$, such that each term $F(p_i)\Delta p_i$ in the sum above has about equal size. In this case, each generated phase space point has equal weight. We can also use the events corresponding to each generated phase space point to simulate the detector signal. If the phase space points have equal weight, the corresponding events are called unweighted events.

Parton Shower and Hadronization: Pythia

Both initial and final state partons are able to radiate off quarks and gluons. Let us consider a matrix element $\mathcal{M}_{q\to qg}$ in which a quark q with momentum p_q radiates of a gluon g with momentum p_g and leaving the quark with momentum $p'_q = p_q - p_g$. This matrix element is proportional to quark propagator,

$$\mathcal{M}_{q\to qg} \sim \frac{1}{p_q^2} = \frac{1}{(p'_q + p_g)^2} = \frac{1}{2p'_q p_g} = \frac{1}{2E_q E_g (1 - \cos\theta_{qg})}. \tag{2.78}$$

Here E_q and E_g are the final quark and gluon energies and θ_{qg} is the angel between the final state momenta. We can see that the amplitude for this process diverges when $\theta_{qg} \to 0$ and $E_g \to 0$ corresponding to a collinear and soft divergency of the theory. Therefore the partons tend to radiate producing a cascade of partons, called a *parton shower*.

It is not practical to calculate the matrix elements for such soft and collinear radiation due to the high dimensionality of the final state. Instead this is simulated using the parton shower model [††]. To avoid the double counting between hard radiation (included in the matrix element) and soft radiation (simulated using the parton shower), a matching procedure is needed [‡‡].

Furthermore, a realistic description of a collision at LHC, need to take into account the following features:

- **Initial and Final State Radiation:** As discussed above, the partons in both the initial and final state will emit soft and collinear radiation.
- **Hadronization:** Quickly after production, the partons charged under QCD will form color neutral bound states. This process is called *hadronization*.

[††] An introduction to parton showers can be found in [70]

[‡‡] A pedagogical introduction to matching an be found in [63].

- **Underlying Event:** Not only the partons involved in the hard process will contribute to the event. The remaining partons are also able to interact, although this interaction is typically much less energetic compared to the hard interaction. Furthermore, the remnants of the initial state protons will also hadronize.

- **Ordinary Decays:** Many particles produced both in the hard interaction, such as τs, and during hadronization, such as heavy mesons and hadrons, are not stable. They will further decay into lighter particles, possibly leading to long decay chains.

There are multiple programs to include these effects into the event generation. In our analysis we use Pythia6 [71].

Detector Simulation: Delphes

To simulate the effects of the detector, we use the fast detector simulation Delphes [72, 73]. Unlike a full detector simulation used at ATLAS or CMS, it does not include transport of particles through the detector material, various detector inefficiencies, dead material or geometrical details.

For photons, electrons, muons and tracks of long living charged hadrons, Delphes includes a finite identification or tracking efficiency as well as an energy smearing. A simulation of the calorimeter takes into account both its granularity as well as the energy smearing in each calorimeter cell. The missing transverse energy is calculated as the negative sum of all observable smeared transverse momenta. Furthermore, jets are reconstructed using jet algorithms implemented in FastJet [64]. In our work we mainly use anti-k_T jets with $R = 0.4$. b and τ tagging are implemented using a purely probabilistic approach: a reconstructed jet overlapping with a parton level b (τ) are labeled as b-tagged jet with a probability of ϵ_b while jets not containing a b (τ) are mistagged with a probability of ϵ_{miss} (which can depend on the flavor of the initiating parton). These tagging/mistagging efficiencies can depend on both the jet transverse momentum and rapidity. Most parameters can be modified in a detector card to match the properties of the detector. In our work we mainly use the combined Snowmass detector card [74] which designed to reflects the performance expected from the LHC experiments in the future.

In principle, Delphes is also able to take into account contributions from additional collisions within one bunch crossing, called *pile up*. However, we decide to not take this into account in this thesis due to the high computation time associated with pile-up simulations.

Collider Study

In our collider study, we develope an analysis strategy to distinguish events coming from a signal process from Standard Model background events. Using the programs discussed above, we generate events both for the signal as well as all backgrounds that are able to mimic the signal.

At LHC, the Standard Model background coming from multi-jet production is so overwhelming, that it is impossible to record and analyze all events. Therefore the experiments use a *trigger* system to select potentially interesting events containing leptons, photons, missing energy, displaced tracks or highly energetic jets. Our collider study takes this into account, by selecting events which pass these trigger requirements.

To suppress the fraction of background events in the event sample, further analysis cuts need to be applied. These select regions of phase space in which the signal rate is high and

typically includes cuts on the invariant mass, transverse momentum, angular correlations of objects in the final state. A detailed description of the analysis strategy used for the processes discussed in this thesis can be found in the publications in the appendix.

The experimental collaborations often use multivariate analysis techniques to further increase the efficiency of the analysis. Machine learning approaches, such as boosted decision trees or neural networks, have shown a good performance in LHC searches and have been implemented in the data analysis framework ROOT [75].

Statistical Analysis

After performing the collider analysis, we obtain the predicted number of signal and background events, N_S and N_B passing all cuts[§§]. The number of signal events N_S typically depends on the parameters of the new physics model. In the following, we will use this result to identify regions of parameter space of the theory which can allow for the observation of a excess of events as well as regions of parameter space which can be excluded by the absence of such an excess. This is a purely statistical problem: is the predicted excess (or it's absence) significant enough to discover (exclude) a model.

There are two hypothesis relevant for this discussion: the *background only hypothesis* with a predicted number of events N_B, and the *signal plus background hypothesis* with predicted number of events $N_S + N_B$. We can ask two questions:

- **Discovery:** Let us assume that we observe a number of events consistent with the signal plus background hypothesis with event number $N_S + N_B$. What is the minimal number of signal events N_S^{Disc} needed to exclude the background only hypothesis at 5σ? This number is called discovery reach.

- **Exclusion:** Let us assume that we observe a number of events consistent with the background only hypothesis $N_{obs} = N_B$. What is the minimal number of signal events N_S^{Excl} needed to exclude the corresponding signal plus background hypothesis at 95% CL? This number is called exclusion reach.

This problem is further complicated, if we want to take into account a systematic uncertainty for the number of background events, parameterized by ϵ. The simplest approach to this problem is a gaussian approximation. Let us assume, that we have a given number of background events N_B. Now we want to predict the number of signal events N_S needed to claim discovery or exclusion.

- **Discovery:** If we want to exclude the background only hypothesis, the number of events in the signal plus background hypothesis $N_{S+B} = N_S + N_B$ needs to be larger than the number of events in the background only hypothesis N_B plus five times the uncertainty for this number $\sigma(N_B)$. The uncertainty is the sum of the statistical uncertainty $\sigma_{stat}(NB) = \sqrt{N_B}$ and a systematic uncertainty $\sigma_{syst}(NB) = \epsilon N_B$. We obtain the discovery reach

$$N_S + N_B > N_B + 5 \cdot \sigma(N_B) \quad \longrightarrow \quad N_S > 5 \cdot (\sqrt{N_B} + \epsilon N_B) \tag{2.79}$$

[§§]In a more sophisticated analysis we could consider multiple independent channels. These channels might correspond to different bins of a kinematic distribution (for example invariant mass) or different final states (for example including different additional jet multiplicities). In this case each channel would have a separate number of signal and background events N_S and N_B.

- **Exclusion:** If we want to exclude the signal plus background hypothesis, the number of events in the background only hypothesis N_B needs to be smaller than the number of events in the signal plus background hypothesis $N_S + N_B$ minus 1.645[¶¶] times the uncertainty for this number $\sigma(N_{S+B})$. The uncertainty is the sum of the statistical uncertainty $\sigma_{stat}(N_{S+B}) = \sqrt{N_S + N_B}$ and a systematic uncertainty $\sigma_{syst}(N_{S+B}) = \epsilon N_B$:

$$N_B < N_S + N_B - 1.645 \cdot \sigma(N_{S+B}) \quad \longrightarrow \quad N_S > 1.645 \cdot (\sqrt{N_S + N_B} + \epsilon N_B) \quad (2.80)$$

  The last equation can be solved for N_S to obtain the exclusion reach.

The discovery and exclusion reach on N_S are a function of the number of background events N_B. For the gaussian approach this is shown in the black line of Fig. 2.5. There are more sophisticated programs to obtain the discovery and exclusion reach. In this work we use the framework Theta [76], which is based on a bayesian approach, and routines from RooStats [77] based on a frequentist approach. The discovery and exclusion reach obtained using these programs is also shown in Fig. 2.5. We see that the gaussian approximation can reproduce these results reasonably well for large number of events. However, when the number of events becomes small ($N_S, N_B < 10$), the gaussian approximation overestimates the discovery reach.

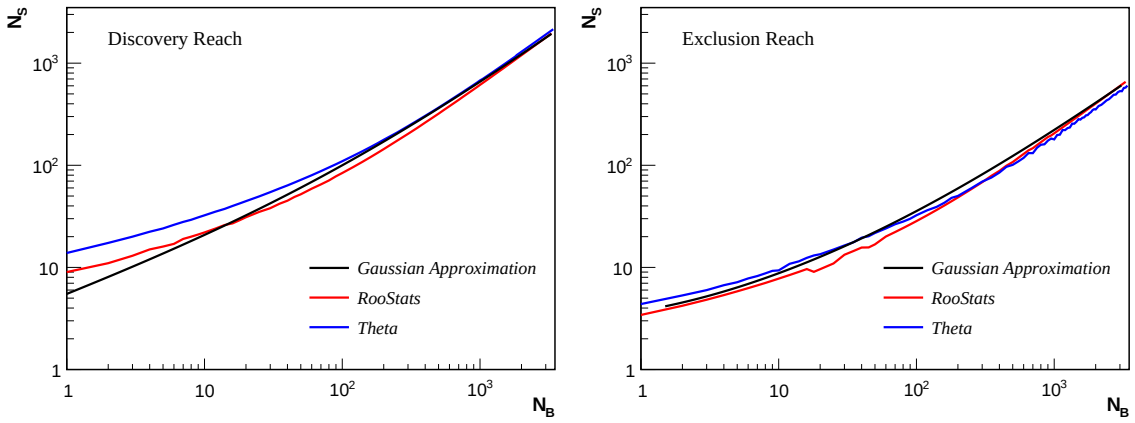

Figure 2.5: Discovery (left) and exclusion (right) reach for the number of signal events N_S as a function of the number of background events N_B. We show the results from RooStats (red), Theta (blue) and the gaussian approximation (black).

[¶¶] This is a one sided hypothesis test.

Chapter 3

Exotic Higgs Decays in Two-Higgs Doublet Models

The main work done in the context of this thesis has already been presented in the form of published articles to the scientific community [21–26]. These publications are attached to this thesis as appendix. In this chapter, we will present the motivation for the work presented in each publication and discuss the main results we obtained*.

3.1 Constraining Type II 2HDM in Light of LHC Higgs Searches

Before its discovery in 2012 by the ATLAS and CMS collaboration [1, 2], the Higgs boson has been the last missing particle predicted by the Standard Model of particle physics. Its discovery completes our knowledge about the structure of the Standard Model. However, we have seen that the Standard Model has to be supplemented with additional dynamics to explain the puzzles particle physics is facing today. Therefore it is possible that the scalar sector responsible for electroweak symmetry breaking itself has a richer structure. In this case, the discovery of a SM-like Higgs boson will constrain the parameter space of an extended Higgs sector.

In [21], we study the implication of the LHC Higgs search results on the Type II 2HDM†. In the context of a 2HDM, the observed 125 Higgs signal‡ can be interpreted as either the light CP-even Higgs h or heavy CP-even Higgs H, while the other one remains undiscovered. The 2HDM parameter space is further constrained by experimental results coming from LEP, Tevatron and the LHC Higgs searches, precision observables and flavor physics as well as theoretical considerations concerning perturbativity, unitarity and vacuum stability. We identify regions of parameter space which are consistent with all constraints and can accommodate the observed 125 GeV Higgs signal, considering that this signal corresponds to either h or H, by scanning over the remaining parameter space, described by the undiscovered Higgs masses $m_{H(h)}$, m_A, $m_{H^\pm}$ and the mixing angles t_β and $s_{\beta-\alpha}$. Note that this works assumes that the soft $\mathcal{Z}_2$ breaking term vanishes, $m_{12}^2 = 0$. This results in an upper bound on the Higgs masses as well as the $\tan\beta$ due to unitarity. In later publications, in

*Note that this chapter will have significant text overlap with the publications that it is referring to.

†Note that this paper was published in may 2013 and therefore only considers parts of the results obtained from the LHC run 1 data set.

‡Note that in [21] we assume $m_h = 126$ GeV while more recent measurements suggest a value of m_h close to 125 GeV [46].

particular [22] we relax this constraint.

We find that in the $m_h = 125$ GeV case, we are restricted to a narrow SM-like regions of $s_{\beta-\alpha} \approx \pm 1$ with t_β up to 4, or an extended non-SM-like region with $0.55 < s_{\beta-\alpha} < 0.9$ and $1.5 < t_\beta < 4$. The values of m_H, m_A and $m_{H^\pm}$, however, are relatively unconstrained. In the $m_H = 125$ GeV case, we are restricted to a narrow SM-like region of $s_{\beta-\alpha} \approx 0$ with t_β up to about 8, or an extended non-SM-like region of $s_{\beta-\alpha}$ between 0.8 to 0.05, with t_β extended to 30 or higher. m_A and $m_{H^\pm}$ are nearly degenerate due to electroweak precision constraints. The SM-like region corresponds to the alignment limit in which the couplings to SM particles are not modified while the non-SM-like region permits deviations from SM couplings.

This work, which has been done in collaboration with Shufang Su and Barath Coleppa, has been published in JHEP [21] and can be found in appendix A. Most results have been obtained, and in particular all figures have been produced by, the author of this thesis.

3.2 Anatomy of Exotic Higgs Decays in 2HDM

In the previous section, we saw that there are regions of 2HDM parameter space consistent with all constraints that can have sizable mass splitting between the undiscovered heavy Higgs states. If the mass splitting is large enough, exotic Higgs decay channels into either a Higgs plus an SM gauge boson or two lighter Higgses open up.

In [22], we discuss scenarios which permit such exotic decays in the context of a Type II 2HDM. In particular we analyze how theoretical and experimental constraints restrict possible mass hierarchies and therefore constrain the parameter space which allows for exotic Higgs decays. We mostly focus on the experimentally preferred alignment limit but also discuss deviations from the alignment limit.

We find that the value of the the soft $\mathcal{Z}_\in$ breaking term m_{12} is strongly constrained by requiring the model to be unitary. At high $t_\beta > 5$, unitarity requires $m_{12}^2 = m_H^2 s_\beta c_\beta$ while smaller values of m_{12}^2 are possible for low t_β. In the former case, vacuum stability further constraints H to be the slightest non-SM Higgs. Therefore, at high t_β, the 2HDM cannot accommodate exotic decays of the Type $H \to AZ$, H^+W, AA or H^+H^-. Electroweak precision measurement further require the charged Higgs mass to be close to one of the heavy neutral scalar masses: $m_{H^\pm} \approx m_A$ or $m_{H^\pm} \approx m_H$. Based on these requirements, we provide benchmark planes to explore exotic Higgs decay scenarios and discuss their potential to probe the hierarchical 2HDM parameter space during LHC Run 2. Higgs cross sections and branching fractions are presented. Further constraints coming from unitarity, LEP and LHC Higgs searches and flavor physics are discussed for each benchmark plane.

This work started as a contribution for the LHC Higgs Cross Section Working Group for BSM Higgs Yearly Report 4 and developed into an independent project. This work, which has been done in collaboration with Shufang Su and Jose No, has been published in JHEP [22] and can be found in appendix B. Most results have been obtained, and in particular all figures have been produced, by the author of this thesis.

3.3 Exotic Decays of a Heavy Neutral Higgs through HZ/AZ Channel

In the previous section we systematically analyzed the possibility of exotic Higgs decays in the context of a Type II 2HDM. We have seen that if such decay channels are kinemati-

cally accessible, they have a sizable branching fraction and can even dominate. The most promising exotic Higgs decay channel at LHC is the decay in which a heavy neutral Higgs decays, H or A, into a lighter neutral Higgs, H, A or h, and a Z boson. If the Z boson decays leptonically, this channel provides a clean collider signature.

In [23], we study the decays $A \to HZ$ and $H \to AZ$, where A refers to the neutral CP-odd Higgs and H refers to one of the CP-even Higgs bosons. With detailed collider analysis, we obtain model independent exclusion bounds as well as discovery reach at the 14TeV LHC for the process: $gg \to A/H \to HZ/AZ$. We consider leptonic decays of the Z, with the A/H in the final states decaying to either a pair of fermions (bb or $\tau\tau$) or a pair of Z bosons (ZZ) and explore the exclusion bounds as well as discovery reach at LHC for various combinations of m_A and m_H. We further interpret these bounds in the context of the Type II Two Higgs Doublet Model, considering three different classes of processes: $A \to hZ$, $A \to HZ$, and $H \to AZ$, in which h and H are the light and heavy neutral CP-even Higgses respectively. We conclude that a study of exotic decays of extra Higgses as appearing in extensions of the Standard Model would extend the reach at 14 TeV LHC and provides nice complementarity to conventional Higgs search channels.

This work is part of the Snowmass Community Summer Study 2013 and resulted in a white paper [78] and a contribution to the Community Summer Study New Particles Working Group Report [79]. This work, which has been done in collaboration with Shufang Su and Barath Coleppa, has been published in JHEP [23] and can be found in appendix C. While the results in section 4 on the collider analysis have mainly been obtained by the author of this thesis, the results of section 5 on the implications for 2HDM have mainly been worked out by Barath Coleppa.

3.4 Charged Higgs Search via $AW^{\pm}/HW^{\pm}$ Channel

The discovery of charged Higgs bosons at a hadron collider is expected to be very difficult. If the mass of the charged Higgs $m_{H^{\pm}}$ is larger than the top mass $m_t = 173$ GeV, the dominant production mechanism is the top quark associated production $H^{\pm}tb$. At LHC, the corresponding charged Higgs production rate is typically about one order of magnitude smaller compared to the production rate of a heavy neutral Higgs of the same mass.

In the absence of exotic decay channels, the charged Higgs is assumed to either decay leptonically ($H^{\pm} \to \tau\nu$), or hadronically ($H^{\pm} \to tb$). Together with the top and bottom quark, which are produced in association with the charged Higgs, the leptonic and hadronic decay channel results in a $tb\tau\nu$ and $ttbb$ final state, respectively. These are very similar to the overwhelming top pair background and therefore further complicate attempt to discover a charged Higgs boson. If the exotic decays of the charged Higgs are kinematically allowed, the rates of the conventional search channels for charged Higgs bosons are even further suppressed. However, this provides an additional opportunity to search for a charged Higgs boson.

In [24], we study the $H^{\pm}tb$ associated production of the charged Higgs with the subsequent exotic decay $H^{\pm} \to AW/HW$. We consider leptonic decay of one of the W bosons either coming from charged Higgs or top decay, with the A/H in the final state decaying into a pair of fermions (bb or $\tau\tau$). With detailed collider analysis, we obtain the model independent exclusion bounds as well as discovery reach at the 14 TeV LHC. We find that $\tau_{lep}\tau_{had}$ case is particularly promising since we can utilize the same sign di-lepton signal with the leptons from W decay and from τ decay. We further interpret these bounds in the

context of the Type II Two Higgs Doublet Model and conclude that the exotic decay mode $H^\pm \to AW^\pm/HW^\pm$ offers a complementary channel to the conventional modes for charged Higgs searches.

This work, which has been done in collaboration with Shufang Su and Barath Coleppa, has been published in JHEP [24] and can be found in appendix D. While the results in section 4 on the collider analysis have mainly been obtained by the author of this thesis, the results of section 5 on the implications for 2HDM have mainly been worked out by Barath Coleppa.

3.5 Light Charged Higgs Bosons to AW/HW via Top Decay

In the previous section we focused on a heavy charged Higgs boson, which suffers from a small production rate at LHC. However, a light charged Higgs boson with $m_{H^+} < m_t$ can be produced in top decays $t \to H^+ b$ and therefore its production rate can benefit from the large top production cross section at LHC.

Conventional search strategies assume that the charged Higgs decays either leptonically $H^\pm \to \tau\nu$) or hadronically ($H^\pm \to cs$). The null search results at both the ATLAS and CMS exclude a light charged Higgs below a mass of about 160 GeV for most of the parameter space. However, if there exists a neutral Higgs A or H light enough such that the exotic decay channel $H^\pm \to AW/HW$ is kinematically open, the branching fractions into the conventional final states $\tau\nu$ and cs are suppressed and the exclusion bounds can be significantly weakened. Due to experimental challenges at low energies, such a light neutral Higgs has not been fully excluded yet. Therefore in an hierarchical 2HDM, a relatively large region of parameter space with $m_{H^\pm} > 150$ GeV and $t_\beta < 20$ is still allowed, while no limits exist for $m_{H^\pm} > 160$ GeV.

In [25], we investigate the possibility of the exotic decay $H^\pm \to AW/hW$ of a light charged Higgs[§] produced in top decay via single top or top pair production. A charged Higgs produced in top pair production $pp \to tt \to tH^\pm b$ has the same final state as a heavy charged Higgs produced in top quark associate production. We therefore extend the previous analysis to lower charged Higgs masses and furthermore include a discussion of the single top channel. While the top pair channel benefits from a large production cross section, the single top channel permits a cleaner signal due to its unique kinematic features. With a detailed collider analysis, we obtain model independent exclusion and discovery bounds for the 14TeV LHC assuming the existence of a 70 GeV neutral scalar. Assuming $\mathrm{BR}(H^\pm \to AW/hW) = 100\%$ and $\mathrm{BR}(A/h \to \tau\tau) = 8.6\%$, the exclusion limits on $\mathrm{BR}(t \to H^\pm b)$ are about 0.2% and 0.03% for single top and top pair production, respectively, with an integrated luminosity of 300 fb^1. A significantly worse reach is obtained in the $A/h \to bb$ channel. We further discuss the implications of the obtained exclusion and discovery bounds in the context of the Type II 2HDM. We conclude that an exotic decay search channel will be able to discover a light charged Higgs in the region which remains unconstrained by searches in $\tau\nu$ channel.

This work, which has been done in collaboration with Shufang Su and Adarsh Pyarelal, has been published in JHEP [25] and can be found in appendix E. While the results in

[§]We want to note that a light charged Higgs is already in strong tension with flavor physics bounds, in particular the measurement of the branching fraction of the rare decay $b \to s\gamma$. However, these bounds are highly model independent and can be significantly weakened in the presence of additional dynamics coupling to the fermion sector.

section 4.1 on the single top collider analysis have mainly been worked out by Adarsh Pyarelal, the results on the top pair production case and limits (section 4.2 and 4.3) as well as the implications for 2HDM (section 3 and 5) have been mainly obtained the author of this thesis.

3.6 Searches for non-SM Heavy Higgses at a 100 TeV *pp* Collider

In the previous sections we discussed exotic Higgs decays in the context of LHC. However, the high energy physics community is already discussing the next generation of particle accelerators. Concrete proposals include the International Linear Collider (ILC) in Japan, the Circular Electron Positron Collider (CEPC) and Super Proton-Proton Collider (SPPC) in China or Future Circular Collider (FCC) at Cern. The future hadron collider are intended to operate at a center of mass energy of about 100 TeV. It is just timely to study the physics potential of such future colliders to motivate the investment in such a machine. Furthermore these studies allow us to formulate requirements on detectors needed at these colliders which are needed when designing the detector.

In [26] we discuss the physics potential of a 100 TeV collider for searches of an extended Higgs sector. In particular we concentrate on the Type II 2HDM and discuss conventional and exotic decay channels of additional heavy Higgs bosons at such a collider. We present the production cross section for the heavy Higgses. Comparing to the 14 TeV LHC, the production rates can be enhanced by about a factor of 3050 for gluon-gluon fusion and bb associated production, and about a factor of 90 for the top-quark associated charged Higgs production, $H^{\pm}tb$, for Higgs mass of about 500 GeV, and even more for heavier Higgses. This makes a 100 TeV collider the right experiment to study the charged Higgs, which production rate is then comparable to those of the neutral Higgses. We present the reach for the conventional decay channels $H/A \to tt, \tau\tau$ and $H^{\pm} \to tb, \tau\nu$ and outline the possible search channels via Higgs exotic decays.

This work started as a contribution to the CEPC-SPPC Study Group and has been published as part of the CEPC-SPPC Preliminary Conceptual Design Report (Volume I - Physics and Detector) [80]. Furthermore, parts of this work also contribute to the FCC study: Physics at a 100 TeV pp collider: Higgs and EW symmetry breaking studies [81]. This work, which has been done in collaboration with Jan Hajer, Ahmed Ismail, Ying-Ying Li, Tao Liu and Shufang Su, has been published in the International Journal of Modern Physics A [26] and can be found in appendix F. While the results on the Higgs cross section (section 3) have been mainly obtained by Ahmed Ismail, the collider analysis for the conventional channels (section 5) has been done by the Hong Kong group and been published in a separate article [82]. The results of section 4 (including Fig. 2) and section 6 have been obtained by the author of this thesis and Shufang Su.

Chapter 4

Conclusion

In 2012, the ATLAS and CMS collaboration discovered a new fundamental scalar particle which properties have been measured to consistent with those of a Standard Model Higgs boson. The Higgs boson has been the last missing particle predicted by the Standard Model and its discovery completes our knowledge about the structure of the Standard Model. Although the predictions of the Standard Model are in excellent agreement with observation in many areas of physics, we except the existence of physics beyond the Standard Model. Such physics is motivated by phenomena that cannot be explained within the framework of the Standard Model, such as dark matter, baryogenesis and neutrino masses, as well as theoretical considerations such as the hierarchy problem and strong CP-problem. Many theories have been proposed to address one or multiple of these problems. No clear evidence has been found that could support any of those theories. Therefore it is necessary to further investigate such models and propose new possible methods and search channels to experimentally uncover new physics.

Many models of physics beyond the Standard Model include an extended Higgs sector, responsible for electroweak symmetry breaking, and predict the existence of additional Higgs bosons. The Type II Two-Higgs-Doublet Model (2HDM) is particularly well motivated scenario and a suitable framework for phenomenological studies of extended Higgs sectors. Its low energy spectrum includes two CP-even Higgses h and H, one CP-odd Higgs A, and a pair of charged Higgses $H^{\pm}$. The properties of this model have been carefully derived in chapter .

In [21], we study the implication of the observation of the SM-like Higgs signal on the Type II 2HDM. The 2HDM parameter space is further constrained by experimental results coming from LEP, Tevatron and LHC Higgs searches, precision observables and flavor physics as well as theoretical considerations concerning perturbativity, unitarity and vacuum stability. We identify regions of parameter space which are consistent with all constraints and can accommodate the observed 125 GeV Higgs signal corresponding to either h or H. This is done by scanning over the remaining parameter space, described by the undiscovered Higgs masses and the mixing angles. We find that there are both SM-like, corresponding to the alignment limit, and non-SM like regions of parameter space which are consistent will all constraints.

In particular, parameter space with a distinctive mass hierarchy, and therefore permitting a sizable mass splitting between the undiscovered heavy Higgs states, can be consistent LHC Higgs search results. Most LHC Higgs searches focus on the conventional Higgs decay channels into SM fermions and gauge bosons. However, if the mass splitting between the

additional Higgs bosons is large enough, exotic Higgs decay channels into either a Higgs plus an SM gauge boson or two lighter Higgses open up. If these exotic decay channels are kinematically open, the branching fractions into the conventional final states are suppressed and the exclusion bounds can be significantly weakened.

In [22], we discuss scenarios which permit such exotic decays in the context of a Type II 2HDM. We find that requiring the 2HDM to be unitary and in agreement with electroweak precision measurements as well as it's vacuum to be stable restricts the hierarchical 2HDM to particular mass hierarchies. Based on these results, we provide benchmark planes to explore exotic Higgs decay scenarios and discuss their potential to probe the hierarchical 2HDM parameter space during LHC Run 2.

The discovery of one or more of these new scalar particles would be a clear indication of an extended Higgs sector as the source of electroweak symmetry breaking. In the presence of exotic Higgs decays, the reach of the conventional Higgs search channels is weakened. However, exotic decay channels provide an additional opportunity to search for these particles.

We therefore further investigate these exotic decay channels and obtain the reach of these decay modes at the LHC. In [23] we analyze the particularly promising channel $H/A \to AZ/HZ$ where the heavy Higgs is produced in gluon-gluon Fusion. This final state has clean collider signature. Furthermore, we also consider the exotic decay of a heavy and light charged Higgs boson [24, 25] via the decay channel $H^\pm \to AW/HW$. The heavy charged Higgs is mainly produced in top-quark associate production, which suffers from a small rate at LHC. A light charged can be produced in top decay $t \to H^\pm b$ and therefore benefits from the large top pair production rate at LHC. With detailed collider analysis, we obtain the model independent exclusion bounds, as well as discovery reach and interpret them in the context of Type II 2HDM. We find that these exotic decays offer complementary discovery channels to the conventional modes for both neutral and charged Higgs searches and permit exclusion and discovery in large regions of parameter space.

Currently, the high energy physics community is already discussing the next generation of particle accelerators. Concrete proposals include the Super Proton-Proton Collider (SPPC) in China and Future Circular Collider (FCC) at Cern. These future hadron colliders are intended to operate at a center of mass energy of 100 TeV. In [26] we discuss the physics potential of a 100 TeV collider for searches of an extended Higgs sector. In particular we concentrate on the Type II 2HDM and discuss conventional and exotic decay channels of additional heavy Higgs bosons at such a collider.

While most of the recent searches for additional Higgs bosons have focused on conventional decay channels, searches using exotic decay channels have just started [83, 84]. Studying all of the possibilities for the non-SM Higgs decays will allow us to explore the full potential of the LHC and future colliders in understanding the nature of electroweak symmetry breaking.

Bibliography

[1] **ATLAS** Collaboration, G. Aad et al., *Observation of a new particle in the search for the Standard Model Higgs boson with the ATLAS detector at the LHC*, *Phys. Lett.* **B716** (2012) 1–29, [arXiv:1207.7214].

[2] **CMS** Collaboration, S. Chatrchyan et al., *Observation of a new boson at a mass of 125 GeV with the CMS experiment at the LHC*, *Phys. Lett.* **B716** (2012) 30–61, [arXiv:1207.7235].

[3] V. C. Rubin, N. Thonnard, and W. K. Ford, Jr., *Rotational properties of 21 SC galaxies with a large range of luminosities and radii, from NGC 4605 /R = 4kpc/ to UGC 2885 /R = 122 kpc/*, *Astrophys. J.* **238** (1980) 471.

[4] D. Clowe, M. Bradac, A. H. Gonzalez, M. Markevitch, S. W. Randall, C. Jones, and D. Zaritsky, *A direct empirical proof of the existence of dark matter*, *Astrophys. J.* **648** (2006) L109–L113, [astro-ph/0608407].

[5] **Super-Kamiokande** Collaboration, Y. Fukuda et al., *Evidence for oscillation of atmospheric neutrinos*, *Phys. Rev. Lett.* **81** (1998) 1562–1567, [hep-ex/9807003].

[6] **SNO** Collaboration, Q. R. Ahmad et al., *Measurement of the rate of $\nu_e + d \to p + p + e^-$ interactions produced by ^8B solar neutrinos at the Sudbury Neutrino Observatory*, *Phys. Rev. Lett.* **87** (2001) 071301, [nucl-ex/0106015].

[7] A. Riotto, *Theories of baryogenesis*, in *High energy physics and cosmology. Proceedings, Summer School, Trieste, Italy, June 29-July 17, 1998*, pp. 326–436, 1998. hep-ph/9807454.

[8] S. P. Martin, *A Supersymmetry primer*, hep-ph/9709356. [Adv. Ser. Direct. High Energy Phys.18,1(1998)].

[9] G. Panico and A. Wulzer, *The Composite Nambu-Goldstone Higgs*, *Lect. Notes Phys.* **913** (2016) pp.1–316, [arXiv:1506.01961].

[10] R. D. Peccei and H. R. Quinn, *CP Conservation in the Presence of Instantons*, *Phys. Rev. Lett.* **38** (1977) 1440–1443.

[11] Z. Chacko, H.-S. Goh, and R. Harnik, *The Twin Higgs: Natural electroweak breaking from mirror symmetry*, *Phys. Rev. Lett.* **96** (2006) 231802, [hep-ph/0506256].

[12] **DELPHI, OPAL, ALEPH, LEP Working Group for Higgs Boson Searches, L3** Collaboration, S. Schael et al., *Search for neutral MSSM Higgs bosons at LEP*, *Eur. Phys. J.* **C47** (2006) 547–587, [hep-ex/0602042].

[13] **ATLAS** Collaboration, G. Aad et al., *Search for neutral Higgs bosons of the minimal supersymmetric standard model in pp collisions at $\sqrt{s} = 8$ TeV with the ATLAS detector*, *JHEP* **11** (2014) 056, [arXiv:1409.6064].

[14] **CMS** Collaboration, V. Khachatryan et al., *Search for neutral MSSM Higgs bosons decaying to a pair of tau leptons in pp collisions*, *JHEP* **10** (2014) 160, [arXiv:1408.3316].

[15] **CMS** Collaboration, V. Khachatryan et al., *Search for a Higgs Boson in the Mass Range from 145 to 1000 GeV Decaying to a Pair of W or Z Bosons*, *JHEP* **10** (2015) 144, [arXiv:1504.00936].

[16] **ATLAS** Collaboration, T. A. collaboration, *Search for charged Higgs bosons in the τ+jets final state with pp collision data recorded at $\sqrt{s} = 8$ TeV with the ATLAS experiment*, .

[17] **CMS** Collaboration, S. Chatrchyan et al., *Search for a light charged Higgs boson in top quark decays in pp collisions at $\sqrt{s} = 7$ TeV*, *JHEP* **07** (2012) 143, [arXiv:1205.5736].

[18] **ATLAS** Collaboration, G. Aad et al., *Search for a light charged Higgs boson in the decay channel $H^+ \to c\bar{s}$ in $t\bar{t}$ events using pp collisions at $\sqrt{s} = 7$ TeV with the ATLAS detector*, *Eur. Phys. J.* **C73** (2013), no. 6 2465, [arXiv:1302.3694].

[19] **CMS** Collaboration, *Search for H+ to cs-bar decay*, *CMS-PAS-HIG-13-035* (2014).

[20] **ATLAS** Collaboration, M. Aaboud et al., *Search for charged Higgs bosons produced in association with a top quark and decaying via $H^\pm \to \tau\nu$ using pp collision data recorded at $\sqrt{s} = 13$ TeV by the ATLAS detector*, arXiv:1603.09203.

[21] B. Coleppa, F. Kling, and S. Su, *Constraining Type II 2HDM in Light of LHC Higgs Searches*, *JHEP* **01** (2014) 161, [arXiv:1305.0002].

[22] F. Kling, J. M. No, and S. Su, *Anatomy of Exotic Higgs Decays in 2HDM*, arXiv:1604.01406.

[23] B. Coleppa, F. Kling, and S. Su, *Exotic Decays Of A Heavy Neutral Higgs Through HZ/AZ Channel*, *JHEP* **09** (2014) 161, [arXiv:1404.1922].

[24] B. Coleppa, F. Kling, and S. Su, *Charged Higgs search via $AW^\pm/HW^\pm$ channel*, *JHEP* **12** (2014) 148, [arXiv:1408.4119].

[25] F. Kling, A. Pyarelal, and S. Su, *Light Charged Higgs Bosons to AW/HW via Top Decay*, *JHEP* **11** (2015) 051, [arXiv:1504.06624].

[26] J. Hajer, A. Ismail, F. Kling, Y.-Y. Li, T. Liu, and S. Su, *Searches for non-SM heavy Higgses at a 100 TeV pp collider*, *Int. J. Mod. Phys.* **A30** (2015), no. 23 1544005.

[27] M. D. Schwartz, *Quantum Field Theory and the Standard Model*. Cambridge University Press, 2014.

[28] M. E. Peskin and D. V. Schroeder, *An Introduction to quantum field theory*. 1995.

[29] C. S. Wu, E. Ambler, R. W. Hayward, D. D. Hoppes, and R. P. Hudson, *Experimental Test of Parity Conservation in Beta Decay*, *Phys. Rev.* **105** (1957) 1413–1414.

[30] P. W. Anderson, *Plasmons, Gauge Invariance, and Mass*, *Phys. Rev.* **130** (1963) 439–442.

[31] P. W. Higgs, *Broken Symmetries and the Masses of Gauge Bosons*, *Phys. Rev. Lett.* **13** (1964) 508–509.

[32] F. Englert and R. Brout, *Broken Symmetry and the Mass of Gauge Vector Mesons*, *Phys. Rev. Lett.* **13** (1964) 321–323.

[33] G. S. Guralnik, C. R. Hagen, and T. W. B. Kibble, *Global Conservation Laws and Massless Particles*, *Phys. Rev. Lett.* **13** (1964) 585–587.

[34] S. L. Glashow, *Partial Symmetries of Weak Interactions*, *Nucl. Phys.* **22** (1961) 579–588.

[35] S. Weinberg, *A Model of Leptons*, *Phys. Rev. Lett.* **19** (1967) 1264–1266.

[36] **Particle Data Group** Collaboration, K. A. Olive et al., *Review of Particle Physics*, *Chin. Phys.* **C38** (2014) 090001.

[37] J. F. Gunion, H. E. Haber, G. L. Kane, and S. Dawson, *The Higgs Hunter's Guide*, *Front. Phys.* **80** (2000) 1–448.

[38] V. D. Barger and R. J. N. Phillips, *COLLIDER PHYSICS*. 1987.

[39] J. M. Butterworth, A. R. Davison, M. Rubin, and G. P. Salam, *Jet substructure as a new Higgs search channel at the LHC*, *Phys. Rev. Lett.* **100** (2008) 242001, [arXiv:0802.2470].

[40] **LHC Higgs Cross Section Working Group** Collaboration, S. Dittmaier et al., *Handbook of LHC Higgs Cross Sections: 1. Inclusive Observables*, arXiv:1101.0593.

[41] S. Dittmaier et al., *Handbook of LHC Higgs Cross Sections: 2. Differential Distributions*, arXiv:1201.3084.

[42] **LHC Higgs Cross Section Working Group** Collaboration, J. R. Andersen et al., *Handbook of LHC Higgs Cross Sections: 3. Higgs Properties*, arXiv:1307.1347.

[43] **OPAL, DELPHI, LEP Working Group for Higgs boson searches, ALEPH, L3** Collaboration, R. Barate et al., *Search for the standard model Higgs boson at LEP*, *Phys. Lett.* **B565** (2003) 61–75, [hep-ex/0306033].

[44] **CDF, D0** Collaboration, T. W. Group, *Combined CDF and D0 Upper Limits on Standard Model Higgs Boson Production with up to 8.6 fb^{-1} of Data*, 2011. arXiv:1107.5518.

[45] **CDF, D0** Collaboration, B. Tuchming and o. b. o. t. CDF, *Tevatron Higgs results*, *EPJ Web Conf.* **60** (2013) 02003, [arXiv:1307.4873].

[46] **ATLAS, CMS** Collaboration, G. Aad et al., *Combined Measurement of the Higgs Boson Mass in pp Collisions at $\sqrt{s} = 7$ and 8 TeV with the ATLAS and CMS Experiments*, *Phys. Rev. Lett.* **114** (2015) 191803, [arXiv:1503.07589].

[47] **ATLAS** Collaboration, G. Aad et al., *Study of the spin and parity of the Higgs boson in diboson decays with the ATLAS detector*, *Eur. Phys. J.* **C75** (2015), no. 10 476, [arXiv:1506.05669].

[48] **CMS** Collaboration, V. Khachatryan et al., *Precise determination of the mass of the Higgs boson and tests of compatibility of its couplings with the standard model predictions using proton collisions at 7 and 8 TeV*, *Eur. Phys. J.* **C75** (2015), no. 5 212, [arXiv:1412.8662].

[49] **ATLAS, CMS** Collaboration, *Measurements of the Higgs boson production and decay rates and constraints on its couplings from a combined ATLAS and CMS analysis of the LHC pp collision data at sqrt s = 7 and 8 TeV*, *ATLAS-CONF-2015-044, CMS-PAS-HIG-15-002* (2015).

[50] **Planck** Collaboration, P. A. R. Ade et al., *Planck 2013 results. I. Overview of products and scientific results*, *Astron. Astrophys.* **571** (2014) A1, [arXiv:1303.5062].

[51] **WMAP** Collaboration, G. Hinshaw et al., *Five-Year Wilkinson Microwave Anisotropy Probe (WMAP) Observations: Data Processing, Sky Maps, and Basic Results*, *Astrophys. J. Suppl.* **180** (2009) 225–245, [arXiv:0803.0732].

[52] **Muon g-2** Collaboration, G. W. Bennett et al., *Final Report of the Muon E821 Anomalous Magnetic Moment Measurement at BNL*, *Phys. Rev.* **D73** (2006) 072003, [hep-ex/0602035].

[53] **BaBar** Collaboration, J. P. Lees et al., *Evidence for an excess of $\bar{B} \to D^{(*)}\tau^-\bar{\nu}_\tau$ decays*, *Phys. Rev. Lett.* **109** (2012) 101802, [arXiv:1205.5442].

[54] **Belle** Collaboration, A. Abdesselam et al., *Measurement of the branching ratio of $\bar{B}^0 \to D^{*+}\tau^-\bar{\nu}_\tau$ relative to $\bar{B}^0 \to D^{*+}\ell^-\bar{\nu}_\ell$ decays with a semileptonic tagging method*, arXiv:1603.06711.

[55] **Belle** Collaboration, M. Huschle et al., *Measurement of the branching ratio of $\bar{B} \to D^{(*)}\tau^-\bar{\nu}_\tau$ relative to $\bar{B} \to D^{(*)}\ell^-\bar{\nu}_\ell$ decays with hadronic tagging at Belle*, *Phys. Rev.* **D92** (2015), no. 7 072014, [arXiv:1507.03233].

[56] C. A. Baker et al., *An Improved experimental limit on the electric dipole moment of the neutron*, *Phys. Rev. Lett.* **97** (2006) 131801, [hep-ex/0602020].

[57] G. C. Branco, P. M. Ferreira, L. Lavoura, M. N. Rebelo, M. Sher, and J. P. Silva, *Theory and phenomenology of two-Higgs-doublet models*, *Phys. Rept.* **516** (2012) 1–102, [arXiv:1106.0034].

[58] J. F. Gunion and H. E. Haber, *The CP conserving two Higgs doublet model: The Approach to the decoupling limit*, *Phys. Rev.* **D67** (2003) 075019, [hep-ph/0207010].

[59] G. Apollinari, I. Béjar Alonso, O. Brüning, M. Lamont, and L. Rossi, *High-Luminosity Large Hadron Collider (HL-LHC) : Preliminary Design Report*, .

[60] **CMS** Collaboration, *Interactive Slice of the CMS detector*, *CMS-doc-4172* (2010).

[61] P. Loch, *Jet Reconstruction at Hadron Colliders*, 2015.

[62] J. D. Jackson, *Classical Electrodynamics*. Wiley, 1998.

[63] T. Plehn, *Lectures on LHC Physics*, *Lect. Notes Phys.* **844** (2012) 1–193, [arXiv:0910.4182].

[64] M. Cacciari, G. P. Salam, and G. Soyez, *FastJet User Manual*, *Eur. Phys. J.* **C72** (2012) 1896, [arXiv:1111.6097].

[65] A. Buckley et al., *General-purpose event generators for LHC physics*, *Phys. Rept.* **504** (2011) 145–233, [arXiv:1101.2599].

[66] T. Stelzer and W. F. Long, *Automatic generation of tree level helicity amplitudes*, *Comput. Phys. Commun.* **81** (1994) 357–371, [hep-ph/9401258].

[67] J. Alwall, M. Herquet, F. Maltoni, O. Mattelaer, and T. Stelzer, *MadGraph 5 : Going Beyond*, *JHEP* **06** (2011) 128, [arXiv:1106.0522].

[68] J. Alwall, R. Frederix, S. Frixione, V. Hirschi, F. Maltoni, O. Mattelaer, H. S. Shao, T. Stelzer, P. Torrielli, and M. Zaro, *The automated computation of tree-level and next-to-leading order differential cross sections, and their matching to parton shower simulations*, *JHEP* **07** (2014) 079, [arXiv:1405.0301].

[69] F. Maltoni and T. Stelzer, *MadEvent: Automatic event generation with MadGraph*, *JHEP* **02** (2003) 027, [hep-ph/0208156].

[70] S. Höche, *Introduction to parton-shower event generators*, in *Theoretical Advanced Study Institute in Elementary Particle Physics: Journeys Through the Precision Frontier: Amplitudes for Colliders (TASI 2014) Boulder, Colorado, June 2-27, 2014*, 2014. arXiv:1411.4085.

[71] T. Sjostrand, S. Mrenna, and P. Z. Skands, *PYTHIA 6.4 Physics and Manual*, *JHEP* **05** (2006) 026, [hep-ph/0603175].

[72] S. Ovyn, X. Rouby, and V. Lemaitre, *DELPHES, a framework for fast simulation of a generic collider experiment*, arXiv:0903.2225.

[73] **DELPHES 3** Collaboration, J. de Favereau, C. Delaere, P. Demin, A. Giammanco, V. Lemaître, A. Mertens, and M. Selvaggi, *DELPHES 3, A modular framework for fast simulation of a generic collider experiment*, *JHEP* **02** (2014) 057, [arXiv:1307.6346].

[74] J. Anderson et al., *Snowmass Energy Frontier Simulations*, in *Community Summer Study 2013: Snowmass on the Mississippi (CSS2013) Minneapolis, MN, USA, July 29-August 6, 2013*, 2013. arXiv:1309.1057.

[75] A. Hocker et al., *TMVA - Toolkit for Multivariate Data Analysis*, *PoS* **ACAT** (2007) 040, [physics/0703039].

[76] T. Muller, J. Ott, and J. Wagner-Kuhr, *theta - a framework for template-based modeling and inference*, .

[77] L. Moneta, K. Belasco, K. S. Cranmer, S. Kreiss, A. Lazzaro, D. Piparo, G. Schott, W. Verkerke, and M. Wolf, *The RooStats Project*, *PoS* **ACAT2010** (2010) 057, [arXiv:1009.1003].

[78] B. Coleppa, F. Kling, and S. Su, *Exotic Higgs Decay via AZ/HZ Channel: a Snowmass Whitepaper*, arXiv:1308.6201.

[79] Y. Gershtein et al., *Working Group Report: New Particles, Forces, and Dimensions*, in *Community Summer Study 2013: Snowmass on the Mississippi (CSS2013) Minneapolis, MN, USA, July 29-August 6, 2013*, 2013. arXiv:1311.0299.

[80] C.-S. S. Group, *CEPC-SPPC Preliminary Conceptual Design Report. 1. Physics and Detector*, .

[81] Editors et al., *Physics at a 100 TeV pp collider: Higgs and EW symmetry breaking studies*, arXiv:1606.09408.

[82] J. Hajer, Y.-Y. Li, T. Liu, and J. F. H. Shiu, *Heavy Higgs Bosons at 14 TeV and 100 TeV*, *JHEP* **11** (2015) 124, [arXiv:1504.07617].

[83] **CMS** Collaboration, C. Collaboration, *Search for H/A decaying into Z+A/H, with Z to ll and A/H to fermion pair*, .

[84] **CMS** Collaboration, V. Khachatryan et al., *Search for neutral resonances decaying into a Z boson and a pair of b jets or tau leptons*, arXiv:1603.02991.

Appendix A

Constraining Type II 2HDM in Light of LHC Higgs Searches

The article *Constraining Type II 2HDM in Light of LHC Higgs Searches* has been submitted to arXiv and accepted for publication in the Journal of High Energy Physics [21].

Published for SISSA by Springer

Received: *May 21, 2013*
Revised: *December 2, 2013*
Accepted: *December 23, 2013*
Published: *January 29, 2014*

Constraining type II 2HDM in light of LHC Higgs searches

Baradhwaj Coleppa, Felix Kling and Shufang Su

Department of Physics, University of Arizona
1118 E. 4th st., Tucson, AZ 85721, U.S.A.

E-mail: baradhwa@email.arizona.edu, kling@email.arizona.edu, shufang@email.arizona.edu

Abstract: We study the implication of the LHC Higgs search results on the Type II Two Higgs-Doublet Model. In particular, we explore the scenarios in which the observed 126 GeV Higgs signal is interpreted as either the light CP-even Higgs h^0 or the heavy CP-even Higgs H^0. Imposing both theoretical and experimental constraints, we analyze the surviving parameter regions in m_H (m_h), m_A, $m_{H^\pm}$, $\tan\beta$ and $\sin(\beta-\alpha)$. We further identify the regions that could accommodate a 126 GeV Higgs with cross sections consistent with the observed Higgs signal. We find that in the h^0-126 case, we are restricted to narrow regions of $\sin(\beta-\alpha)\approx\pm1$ with $\tan\beta$ up to 4, or an extended region with $0.55 < \sin(\beta-\alpha) < 0.9$ and $1.5 < \tan\beta < 4$. The values of m_H, m_A and $m_{H^\pm}$, however, are relatively unconstrained. In the H^0-126 case, we are restricted to a narrow region of $\sin(\beta-\alpha)\sim 0$ with $\tan\beta$ up to about 8, or an extended region of $\sin(\beta-\alpha)$ between -0.8 to -0.05, with $\tan\beta$ extended to 30 or higher. m_A and $m_{H^\pm}$ are nearly degenerate due to $\Delta\rho$ constraints. Imposing flavor constraints shrinks the surviving parameter space significantly for the H^0-126 case, limiting $\tan\beta \lesssim 10$, but has little effect in the h^0-126 case. We also investigate the correlation between $\gamma\gamma$, VV and $bb/\tau\tau$ channels. $\gamma\gamma$ and VV channels are most likely to be highly correlated with $\gamma\gamma : VV \sim 1$ for the normalized cross sections.

Keywords: Phenomenological Models

ArXiv ePrint: 1305.0002

doi:10.1007/JHEP01(2014)161

JHEP01(2014)161

Contents

JHEP01(2014)161

1 Introduction

The discovery of a resonance at 126 GeV with properties consistent with the Standard Model (SM) Higgs boson in both the ATLAS [1, 2] and CMS experiments [3, 4] is undoubtedly the most significant experimental triumph of the Large Hadron Collider (LHC) to date. The nature of this particle, as regards its CP properties and couplings, are currently being established [4–7]. Though further data would undoubtedly point us in the right direction, at this point it is useful to explore the implication of the current Higgs search results on models beyond the SM. There are quite a few models that admit a scalar particle in their spectrum and many of them can have couplings and decays consistent with the SM Higgs boson. Thus it behooves us to constrain these models as much as possible with the Higgs search results at hand.

One of the simplest extensions of the SM involves enlarged Higgs sectors. This can be done by simply adding more scalar doublets, or considering Higgs sectors with more complicated representations. In the work, we will study the Two Higgs-Doublet Models (2HDM) that involve two scalar doublets both charged under the SM $\mathrm{SU}(2)_L \times \mathrm{U}(1)_Y$ gauge symmetries [8–11]. The neutral components of both the Higgs fields develop vacuum

expectation values (vev), breaking $SU(2)_L \times U(1)_Y$ down to $U(1)_{em}$. Assuming no CP-violation in the Higgs sector, the resulting physical spectrum for the scalars is enlarged relative to the SM and includes light and heavy neutral CP-even Higgses (h^0 and H^0), charged Higgses ($H^\pm$), and a pseudoscalar A^0. In addition to the masses, two additional parameters are introduced in the theory: the ratio of the vevs of the two Higgs fields ($\tan\beta$), and the mixing of the two neutral CP-even Higgses ($\sin\alpha$).

There are many types of 2HDMs, each differing in the way the two Higgs doublets couple to the fermions (for a comprehensive review, see [8]). In this work, we will be concentrating on the Type II case, in which one Higgs doublet couples to the up-type quarks, while the other Higgs doublet couples to the down-type quarks and leptons. This model is of particular interest as it shares many of the features of the Higgs sector of the Minimal Supersymmetric Standard Model (MSSM). This enables us to translate existing LHC MSSM results to this case. Before proceeding, we point out that over the last few months, there have been various studies on the 2HDM based on the recent discovery [12–25]. While most studies concentrated on finding regions of parameter space that admit $\sigma\times$ Br values reported by the LHC experiments in various channels, some also looked at correlations between the various decay channels. The authors of ref. [12] and ref. [13] did the initial study of looking at the $\tan\beta - \sin\alpha$ plane where the observed Higgs signal is feasible, interpreting the discovered scalar as either the light or the heavy CP-even Higgs boson. Ref. [14–19] fit the observed Higgs signals in various 2HDM scenarios, taken into account theoretical and experimental constraints. Ref. [20] also paid careful attention to various Higgs production modes. Ref. [21] focused on the CP-violating Type II 2HDM. Ref. [22] studied the case of nearly degenerate Higgs bosons. In addition, ref. [23, 24] investigated the possibility that the signal could correspond to the pseudoscalar A^0 - in this context, it is worth remarking that ref. [26] considered the pseudoscalar interpretation of the observed 126 GeV resonance and found that while it is strongly disfavored, the possibility is not yet ruled out at the 5σ level.[1]

In the present paper, we extended the above analyses by combining all the known experimental constraints (the LEP, Tevatron and the LHC Higgs search bounds, and precision observables) with the theoretical ones (perturbativity, unitarity, and vacuum stability), as well as flavor constraints. A unique aspect of the present work is that our analysis looks at combinations of all parameters of the theory to identify regions that survive all the theoretical and experimental constraints. We further focus on regions that could accommodate the observed Higgs signal as either the light or the heavy CP-even Higgs, and are thus interesting from a collider study perspective. This enables us to draw conclusions about correlations between different masses and mixing angles to help identify aspects of the model that warrant future study.

We start by briefly introducing the structure and parameters of the Type II 2HDM in section 2. In section 3, we discuss the theoretical constraints and experimental bounds, and outline our analysis methodology. In section 4, we present our results for the light CP-even Higgs being the observed 126 GeV SM-like Higgs boson, looking at surviving regions

[1] The latest experimental results indicate that the pseudoscalar interpretation of the 126 GeV excess is disfavored [4–6].

JHEP01(2014)161

in various combinations of free parameters. In section 5, we do the same for the heavy CP-even Higgs as the observed 126 GeV SM-like Higgs boson. In section 6, we explore the implications for the Vector Boson Fusion (VBF) or VH associated production, and decays of Higgs into bb and $\tau\tau$ channels. We conclude in section 7.

2 Type II 2HDM

In this section, we briefly describe the Type II 2HDM, focusing on the particle content, Higgs couplings, and model parameters. For more details about the model, see ref. [8] for a recent review of the theory and phenomenology of 2HDM.

2.1 Potential, masses and mixing angles

Labeling the two $\mathrm{SU}(2)_L$ doublet scalar fields Φ_1 and Φ_2, the most general potential for the Higgs sector can be written down in the following form:

$$\begin{aligned} V(\Phi_1,\Phi_2) = {} & m_{11}^2\Phi_1^\dagger\Phi_1 + m_{22}^2\Phi_2^\dagger\Phi_2 - m_{12}^2(\Phi_1^\dagger\Phi_2 + \text{h.c.}) \\ & + \frac{1}{2}\lambda_1(\Phi_1^\dagger\Phi_1)^2 + \frac{1}{2}\lambda_2(\Phi_2^\dagger\Phi_2)^2 + \lambda_3(\Phi_1^\dagger\Phi_1)(\Phi_2^\dagger\Phi_2) + \lambda_4(\Phi_1^\dagger\Phi_2)(\Phi_2^\dagger\Phi_1) \\ & + \frac{1}{2}\left\{\lambda_5(\Phi_1^\dagger\Phi_2)^2 + \text{h.c.}\right\} + \left\{\left[\lambda_6(\Phi_1^\dagger\Phi_1) + \lambda_7(\Phi_2^\dagger\Phi_2)\right](\Phi_1^\dagger\Phi_2) + \text{h.c.}\right\}. \end{aligned} \tag{2.1}$$

We impose a discrete Z_2 symmetry on the Lagrangian, the effect of which is to render $m_{12}, \lambda_6, \lambda_7 = 0$.[2] Note that one consequence of requiring $m_{12} = 0$ is that there is no so called decoupling limit in which only one SM-like Higgs appears at low energy while all other Higgses are heavy and decoupled from the low energy spectrum. After electroweak symmetry breaking (EWSB): $\langle\phi_1^0\rangle = v_1/\sqrt{2}$, $\langle\phi_2^0\rangle = v_2/\sqrt{2}$ with $\sqrt{v_1^2+v_2^2} = 246\,\text{GeV}$, we are left with six free parameters, which can be chosen as the four Higgs masses (m_h, m_H, m_A, $m_{H^\pm}$), a mixing angle $\sin\alpha$ between the two CP-even Higgses, and the ratio of the two vacuum expectation values, $\tan\beta = v_2/v_1$.

Writing the two Higgs fields as:

$$\Phi_i = \begin{pmatrix} \phi_i^+ \\ (v_i + \phi_i^0 + iG_i)/\sqrt{2} \end{pmatrix}, \tag{2.2}$$

the mass eigenstates of the physical scalars can be written as:

$$\begin{pmatrix} H^0 \\ h^0 \end{pmatrix} = \begin{pmatrix} \cos\alpha & \sin\alpha \\ -\sin\alpha & \cos\alpha \end{pmatrix}\begin{pmatrix} \phi_1^0 \\ \phi_2^0 \end{pmatrix}, \quad \begin{aligned} A^0 &= -G_1\sin\beta + G_2\cos\beta \\ H^\pm &= -\phi_1^\pm\sin\beta + \phi_2^\pm\cos\beta \end{aligned}. \tag{2.3}$$

For our purposes, it is useful to express the quartic couplings $\lambda_{1\ldots5}$ in terms of the physical Higgs masses, $\tan\beta$ and the mixing angle α:

$$\lambda_1 = \frac{m_H^2\cos^2\alpha + m_h^2\sin^2\alpha}{v^2\cos^2\beta}, \qquad \lambda_2 = \frac{m_H^2\sin^2\alpha + m_h^2\cos^2\alpha}{v^2\cos^2\beta} \tag{2.4}$$

$$\lambda_3 = \frac{\sin 2\alpha(m_H^2 - m_h^2) + 2\,\sin 2\beta\, m_{H^\pm}^2}{v^2\,\sin 2\beta}, \quad \lambda_4 = \frac{m_A^2 - 2m_{H^\pm}^2}{v^2}, \qquad \lambda_5 = -\frac{m_A^2}{v^2}. \tag{2.5}$$

[2] Ref. [15], which also addresses similar issues as in this paper, allowed for a soft breaking of the Z_2 symmetry with $m_{12}^2 \neq 0$. In this paper, we don't consider such soft-breaking terms.

ξ_h^{VV}	$\sin(\beta-\alpha)$	ξ_H^{VV}	$\cos(\beta-\alpha)$	ξ_A^{VV}	0
ξ_h^{u}	$\cos\alpha/\sin\beta$	ξ_H^{u}	$\sin\alpha/\sin\beta$	ξ_A^{u}	$\cot\beta$
$\xi_h^{d,l}$	$-\sin\alpha/\cos\beta$	$\xi_H^{d,l}$	$\cos\alpha/\cos\beta$	$\xi_A^{d,l}$	$\tan\beta$

Table 1. The multiplicative factor ξ by which the couplings of the CP-even Higgses and the CP-odd Higgs to the gauge bosons and fermions scale with respect to the SM value. The superscripts u, d, l and VV refer to the up-type quarks, down-type quarks, leptons, and WW/ZZ respectively.

Imposing the perturbativity and unitarity bounds, as explained below in section 3.1, typically leads to an upper bound on the masses of H^0, A^0 and $H^\pm$. The couplings of the CP-even Higgses and CP-odd Higgs to the SM gauge bosons and fermions are scaled by a factor ξ relative to the SM value — these are presented in table 1. In order to translate the ATLAS and CMS limits, we need to pay particular attention to the couplings of the light (heavy) CP-even Higgs to the SM gauge bosons (controlling the partial decay width to WW, ZZ as well as $\gamma\gamma$ channels) and to the top quark (controlling the gluon fusion production cross section), as well as to the bottom quark (controlling the bb partial decay width, which enters the total decay width as well). From table 1, we see that the relevant couplings are proportional to $\sin(\beta-\alpha)$ ($\cos(\beta-\alpha)$), $1/\sin\beta$ and $1/\cos\beta$. Thus, even though it is customary to look at the combination of parameters $(\sin\alpha, \tan\beta)$, we present our results in section 4 and 5 using $\sin(\beta-\alpha)$ and $\tan\beta$ as the independent parameters (in addition to the masses of the physical Higgses) to manifest the effects on the Higgs couplings to gauge bosons. Using $\sin(\beta-\alpha)$ instead of $\sin\alpha$ has the additional advantage of being basis-independent, as explained in ref. [27–29].

3 Constraints and analyses

3.1 Theoretical and experimental constraints

To implement the various experimental and theoretical constraints, we have employed two programs: the 2HDM Calculator (2HDMC) [30] to calculate the Higgs couplings, compute all the decay branching fractions of the Higgses, and implement all the theoretical constraints; and HiggsBounds 3.8 [31] to consistently put in all the experimental constraints on the model. Here, we briefly describe the list of theoretical and experimental bounds that are of interest.

Theoretical constraints:

- Vacuum Stability: this implies that the potential should be bounded from below, which is translated to various conditions for the quartic couplings in the Higgs potential [36–38]: $\lambda_1 > 0$, $\lambda_2 > 0$, $\lambda_3 > -\sqrt{\lambda_1\lambda_2}$, and $\lambda_3 + \lambda_4 - |\lambda_5| > -\sqrt{\lambda_1\lambda_2}$. With eqs. (2.4) and (2.5), the above requirements serve to constrain the Higgs masses and angles.

- Perturbativity: 2HDMC imposes constraints on the physical Higgs quartic couplings, specifically demanding that $\lambda_{h_i h_j h_k h_l} < 4\pi$ to stay inside the perturbative regime.

JHEP01(2014)161

Note that even though these are different from the λs in the Higgs potential in eq. (2.1), we can still use eqs. (2.4) and (2.5) as rough guides to understand the perturbative bounds, as we will do in later sections to explain the features of our results. The top yukawa coupling y_t could also become nonperturbative for very small $\tan\beta$. We require the perturbativity of y_t at scales below 1 TeV, which results in $\tan\beta \gtrsim 0.35$ [39].

- Unitarity: it is well known that in the SM, the scattering cross section for the longitudinal W modes is unitary only if the Higgs exchange diagrams are included. Since the couplings of the Higgs are modified in the 2HDM, we need to ensure unitarity by demanding that the S matrix of *all* scattering cross sections of Higgs$-$Higgs and Higgs$-V_L$ (where V_L is either W_L or Z_L) have eigenvalues bounded by 16π [40].

Experimental constraints: the LHC experiments have searched for the SM Higgs in $\gamma\gamma$, ZZ, WW, $\tau\tau$ and bb channels. Both the ATLAS and CMS collaboration have reported the observation of a new resonance at a mass of around 126 GeV with more than 5σ significance [1–7, 41–52]. The production cross sections and partial decay widths of the 2HDM Higgses to the various SM final states differ from that of the SM Higgs, which can be obtained using the coupling scaling factors ξ from table 1. Thus, we can identify the regions in parameter space where the signal cross sections are compatible with the Higgs signal observed at the ATLAS and CMS collaborations. We can also translate the exclusion bounds on the Higgs search to the ones in the 2HDM. We used HiggsBounds 3.8 to impose the exclusion limits from Higgs searches at the LEP and the Tevatron [53–57]. We also incorporated the latest Higgs search results at the LHC [2, 4, 41–52, 58–64].

Z-pole precision observables, in particular, the oblique parameters S, T (or equivalently, $\Delta\rho$, which is the deviation of $\rho \equiv \frac{m_W^2}{m_Z^2 \cos^2\theta_W}$ from the SM value), and U [65] constrain any new physics model that couples to the W and Z. In particular, T imposes a strong constraint on the amount of custodial symmetry breaking in the new physics sector. In the case of 2HDM, the mass difference between the various Higgses are therefore highly constrained [66], which leads to interesting correlations between some of the masses, as will be demonstrated in section 4 and section 5. In our analysis, we require the contribution from extra Higgses to S and T to fall within the 90% C.L. $S-T$ contour, for a SM Higgs reference mass of 126 GeV [67]. In addition, the charged Higgs contributes to Zbb coupling [68], which has been measured precisely at the LEP via the observable $R_b = \Gamma(Z \to b\bar{b})/\Gamma(Z \to \text{hadrons})$ [69]. Imposing bounds from R_b rules out small $\tan\beta$ regions for a light charged Higgs.

We also show the effect on the available parameter spaces once bounds from flavor sector are imposed in addition to the ones described. To do this, we employed the program SuperIso 3.3 [70], which incorporates, among other things, bounds from $B \to X_s\gamma$, ΔM_{B_d}, $B^- \to \tau^-\bar{\nu}_\tau$, $D_s^\pm \to \tau^\pm(\mu^\pm)\nu$, $B \to \tau^+\tau^-$ and $B_{d,s} \to \mu^+\mu^-$ [71–77]. A summary of flavor bounds can be found in ref. [78]. We have used the latest bounds either from PDG [71][3] or from individual experiment. To show the impact of the flavor constraints on the 2HDM parameter space, in figure 1, we present the regions excluded by various flavor constraints in

[3] And 2013 partial update for the 2014 edition.

JHEP01(2014)161

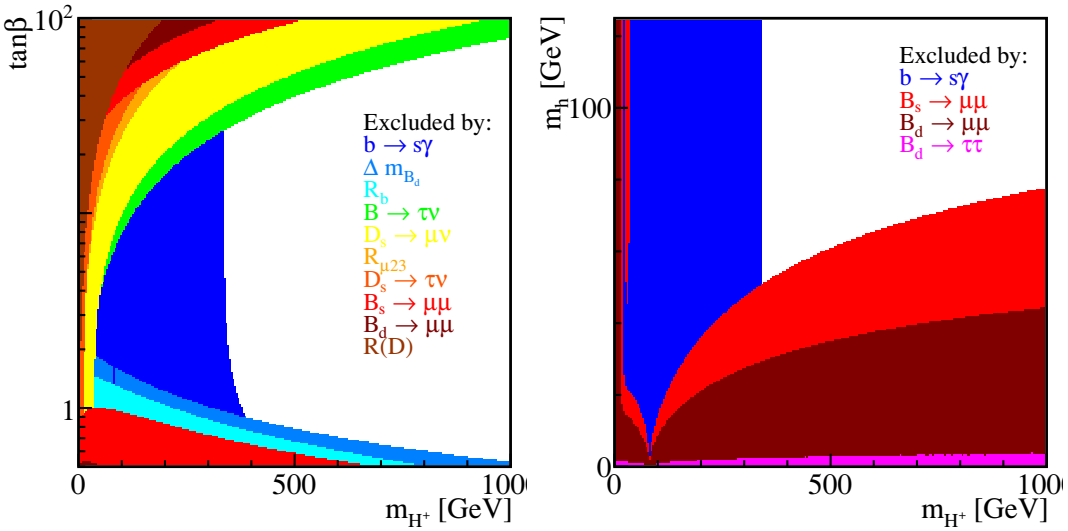

Figure 1. Regions of parameter space excluded by various flavor constraints. The left plot shows the $m_{H^\pm}$ versus $\tan\beta$ plane for fixed $m_h = 125\,\text{GeV}$, $m_H = 400\,\text{GeV}$, $m_A = 200\,\text{GeV}$ and $\sin(\beta - \alpha) = -0.1$. The right plot shows the $m_{H^\pm}$ versus m_h plane for $m_A = m_{H^\pm}$, $m_H = 125\,\text{GeV}$, $\tan\beta = 5$ and $\sin(\beta - \alpha) = -0.01$.

the $m_{H^\pm}$ versus $\tan\beta$ plane (left panel) and the $m_{H^\pm}$ versus m_h plane (right panel). While $B \to X_s\gamma$ excludes $m_{H^\pm}$ up to about 300 GeV for all $\tan\beta$, $B^- \to \tau^-\bar{\nu}_\tau$ and ΔM_{B_d} provide the strongest constraints at large and small $\tan\beta$, respectively. The strongest bound on the neutral Higgs mass comes from $B_s \to \mu^+\mu^-$, which excludes m_h at about 50 GeV or lower.

In addition, we included the latest results from BaBar on $\bar{B} \to D\tau\bar{\nu}_\tau$ and $\bar{B} \to D^*\tau\bar{\nu}_\tau$ [79], which observed excesses over the SM prediction at about 2 σ level. We treat the observed excesses as upper bounds and take the 95% C.L. range as $R(D) < 0.58$ and $R(D^*) < 0.39$. Note that as pointed out in ref. [79], the excesses in both $R(D)$ and $R(D^*)$ can not be simultaneously explained by the Type II 2HDM [80, 81]. Other new physics contributions have to enter if the excesses in both $R(D)$ and $R(D^*)$ stay in the future. Flavor constraints on the Higgs sector are, however, typically more model-dependent. Therefore, our focus in this work is mainly on the implication of the Higgs search results on the Type II 2HDM, and we only impose the flavor bounds at the last step to indicate how the surviving regions further shrink.

3.2 Analysis method

In our analysis, we considered two scenarios:

- h^0-126 case where $m_h = 126\,\text{GeV}$ with $m_H > 126\,\text{GeV}$,
- H^0-126 case where $m_H = 126\,\text{GeV}$ with $m_h < 126\,\text{GeV}$

JHEP01(2014)161

and scanned over the entire remaining parameter space varying m_H (or m_h), $m_A, m_{H^\pm}$, $\tan\beta$ and $\sin(\beta-\alpha)$:

$$
\begin{aligned}
20\ \text{GeV} \leq\ & m_A, m_{H^\pm} && \leq 900\ \text{GeV} && \text{in steps of 20 GeV}, && (3.1)\\
-1 \leq\ & \sin(\beta-\alpha) && \leq 1 && \text{in steps of 0.05}, && (3.2)\\
\mathbf{h^0-126\ case}: 0.25 \leq\ & \tan\beta && \leq 5 && \text{in steps of 0.25}, && (3.3)\\
126\ \text{GeV} \leq\ & m_H && \leq 900\ \text{GeV} && \text{in steps of 20 GeV}, && (3.4)\\
\mathbf{H^0-126\ case}: 1 \leq\ & \tan\beta && \leq 30 && \text{in steps of 1}, && (3.5)\\
6\ \text{GeV} \leq\ & m_h && < 126\ \text{GeV} && \text{in steps of 5 GeV}. && (3.6)
\end{aligned}
$$

In certain regions in which very few points are left after all the constraints are imposed, we generated more points with smaller steps. We used the 2HDMC 1.2beta [30] which tested if each parameter point fulfills the theoretical and experimental constraints implemented in HiggsBounds 3.8 [31]. New LHC results that are not included in HiggsBounds 3.8 were implemented in addition. In particular, the CMS results on MSSM Higgs search in $\tau\tau$ channel [61–64] were imposed using the cross section limits reverse-engineered from bounds in $m_A - \tan\beta$ plane for m_h^{max} scenario, as provided in HiggsBounds 4.0 [31]. We also required each parameter point to satisfy the precision constraints, in particular, S and T, as well as R_b.

We further required either h^0 or H^0 to satisfy the dominant gluon fusion cross section requirement for $\gamma\gamma$, WW and ZZ channels to accommodate the observed Higgs signal at 95% C.L. [4, 7]:

$$
0.7 < \frac{\sigma(gg \to h^0/H^0 \to \gamma\gamma)}{\sigma_{\text{SM}}} < 1.5, \quad 0.6 < \frac{\sigma(gg \to h^0/H^0 \to WW/ZZ)}{\sigma_{\text{SM}}} < 1.3, \qquad (3.7)
$$

in which we have taken the tighter limits from the ATLAS and CMS results, as well as the tighter results for the WW and ZZ channel. In the last step, we imposed the flavor bounds on all points that satisfy eq. (3.7) using the SuperIso 3.3 program to study the consequence of the flavor constraints.

4 Light Higgs at 126 GeV

4.1 Cross sections and correlations

Before presenting the results of the numerical scanning of parameter regions with all the theoretical and experimental constraints imposed, let us first study the $\tan\beta$ and $\sin(\beta-\alpha)$ dependence of the cross sections for the major search channels at the LHC: $gg \to h^0 \to \gamma\gamma, WW/ZZ$. Both production cross sections and decay branching fractions are modified relative to the SM values:

$$
\frac{\sigma \times \text{Br}(gg \to h^0 \to XX)}{\text{SM}} = \frac{\sigma(gg \to h^0)}{\sigma_{\text{SM}}} \times \frac{\text{Br}(h^0 \to XX)}{\text{Br}(h_{\text{SM}} \to XX)}, \qquad (4.1)
$$

for $XX = \gamma\gamma, VV$. Note that since the WW and ZZ couplings are modified the same way in the Type II 2HDM, we use VV to denote both WW and ZZ channels.

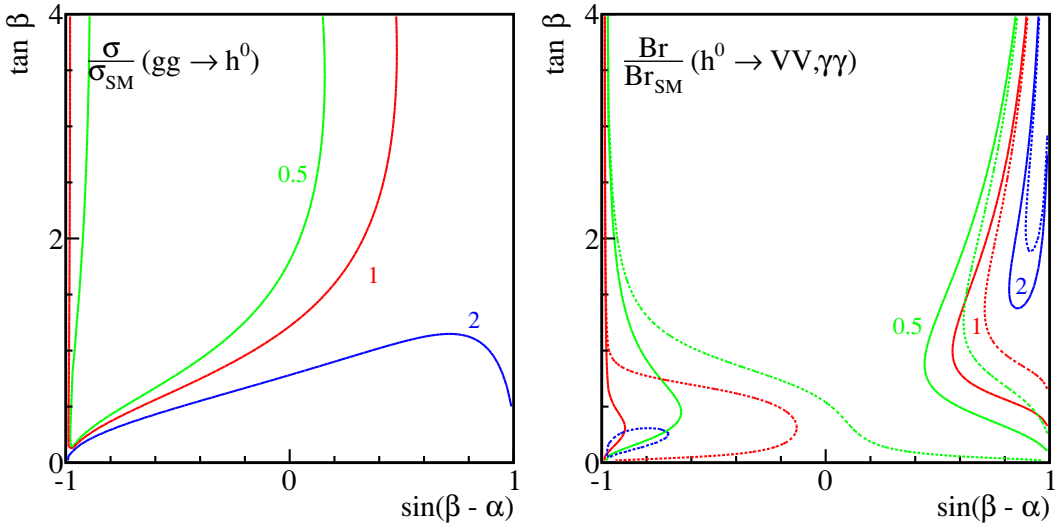

Figure 2. The normalized $gg \to h^0$ production cross section contours (left panel) and $h^0 \to VV$ (solid lines of the right panel) and $h^0 \to \gamma\gamma$ (dashed lines of the right panel) branching fractions in the h^0-126 case. The contour lines are $\sigma/\sigma_{\rm SM}$, $\mathrm{Br}/\mathrm{Br}_{\rm SM} = 0.5$ (green), 1 (red), and 2 (blue).

The ratio of the gluon fusion cross section normalized to the SM value can be written as:

$$\frac{\sigma(gg \to h^0)}{\sigma_{\rm SM}} = \frac{\cos^2\alpha}{\sin^2\beta} + \frac{\sin^2\alpha\,|A_{1/2}(\tau_b)|^2}{\cos^2\beta\,|A_{1/2}(\tau_t)|^2} \tag{4.2}$$

$$= \left[\frac{\cos(\beta-\alpha)}{\tan\beta} + \sin(\beta-\alpha)\right]^2 + [\cos(\beta-\alpha)\tan\beta - \sin(\beta-\alpha)]^2\,\frac{|A_{1/2}(\tau_b)|^2}{|A_{1/2}(\tau_t)|^2}. \tag{4.3}$$

The expression for the fermion loop functions $A_{1/2}(\tau_{t,b})$ can be found in ref. [66]. The first term in eq. (4.2) is the top-loop contribution, and the second term is the bottom-loop contribution. In the SM, the top-loop contributes dominantly to the gluon fusion diagram, while the bottom-loop contribution is negligibly small. The situation alters in type II 2HDM for large $\tan\beta$, when the bottom-loop contribution can be substantial due to the enhanced bottom Yukawa [12]. We also rewrite it in $\sin(\beta-\alpha)$, $\cos(\beta-\alpha)$ and $\tan\beta$ in eq. (4.3) to make their dependence explicit.

In the left panel of figure 2, we show contours of $\sigma/\sigma_{\rm SM}$ for the gluon fusion: $\sigma/\sigma_{\rm SM} = 0.5$ (green), 1 (red), and 2 (blue). While contours of $\sigma/\sigma_{\rm SM} \geq 1$ accumulate in $\sin(\beta-\alpha) \sim -1$ region, there is a wide spread of the contours for $\sin(\beta-\alpha) > 0$. For most regions of $\sin(\beta-\alpha) < 0$, $gg \to h^0$ is suppressed compared to the SM value due to cancellations between the $\cos(\beta-\alpha)$ and $\sin(\beta-\alpha)$ terms in the top Yukawa coupling, as shown in eq. (4.3). Note that we have shown the plots only for $\tan\beta \leq 4$ since the model is perturbatively valid only for $\tan\beta \lesssim 4$, as will be demonstrated below in the results of the full analysis.

JHEP01(2014)161

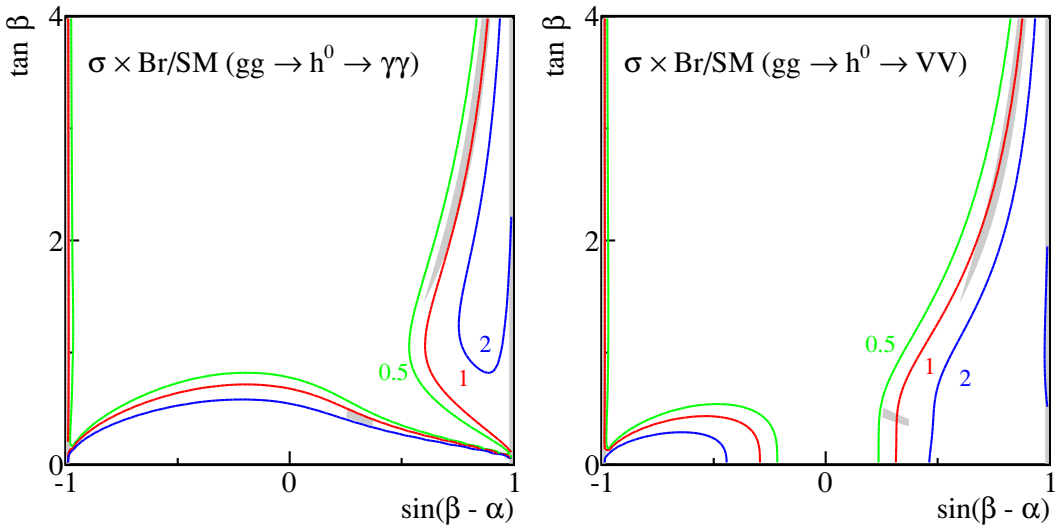

Figure 3. $\sigma \times \mathrm{Br/SM}$ for the processes $gg \to h^0 \to \gamma\gamma$ (left), and $gg \to h^0 \to WW/ZZ$ (right) in the h^0-126 case. The contour lines are $\sigma \times \mathrm{Br/SM} = 0.5$ (green), 1 (red), and 2 (blue). The shaded gray are regions where cross sections of $\gamma\gamma$ and WW/ZZ channels satisfy eq. (3.7).

The h^0 decay branching fractions $h^0 \to VV, \gamma\gamma$ can be written approximately as

$$\frac{\mathrm{Br}(h^0 \to XX)}{\mathrm{Br}(h_{\mathrm{SM}} \to XX)} = \frac{\Gamma_{XX}}{\Gamma_{total}} \times \frac{\Gamma^{\mathrm{SM}}_{total}}{\Gamma^{\mathrm{SM}}_{XX}} \approx \begin{cases} \dfrac{\sin^2(\beta-\alpha)}{\sin^2(\beta-\alpha)\mathrm{Br}(h_{\mathrm{SM}}\to VV)+\frac{\sin^2\alpha}{\cos^2\beta}\mathrm{Br}(h_{\mathrm{SM}}\to bb)+\ldots} \\ \dfrac{\Gamma(h^0\to\gamma\gamma)/\Gamma(h_{\mathrm{SM}}\to\gamma\gamma)}{\sin^2(\beta-\alpha)\mathrm{Br}(h_{\mathrm{SM}}\to VV)+\frac{\sin^2\alpha}{\cos^2\beta}\mathrm{Br}(h_{\mathrm{SM}}\to bb)+\ldots} \end{cases} , \quad (4.4)$$

where we have explicitly listed the dominant bb and WW/ZZ channels and used "$+\ldots$" to indicate other sub-dominant SM Higgs decay channels.

In the right panel of figure 2, we show contours of $\mathrm{Br/Br_{SM}}$ for VV (solid lines) and $\gamma\gamma$ (dashed lines) channels. Both VV and loop induced (dominantly W-loop) $\gamma\gamma$ channels exhibit similar parameter dependence on $\tan\beta$ and $\sin(\beta-\alpha)$ since both channels are dominantly controlled by the same h^0VV coupling. While contours of $\mathrm{Br/Br_{SM}} \gtrsim 1$ appear near $\sin(\beta-\alpha) \sim \pm 1$ for unsuppressed h^0VV couplings, $h^0 \to \gamma\gamma$ shows some spread for negative $\sin(\beta-\alpha)$ and small $\tan\beta$ due to the correction to top Yukawa in the loop-indued $h^0\gamma\gamma$ coupling.

Combining both the production and the decay branching fractions, we present the contours of $\sigma \times \mathrm{Br/SM}$ in figure 3 for $\gamma\gamma$ (left panel) and VV (right panel) for $\sigma \times \mathrm{Br/SM} =$ 0.5 (green), 1 (red), and 2 (blue). Once we demand that the cross sections for these processes be consistent with the experimental observation of a 126 GeV Higgs, as given in eq. (3.7), the allowed regions of parameter space split into four distinct regions, as indicated by the shaded gray areas. There are two narrow regions one each at $\sin(\beta-\alpha) = \pm 1$ (the gray regions at $\sin(\beta-\alpha) = \pm 1$ overlap with the picture frame boundary and are therefore hard to see), one extended region of $0.55 < \sin(\beta-\alpha) < 0.9$, and one low $\tan\beta$ region around $\sin(\beta-\alpha) \sim 0.3$ for $\tan\beta \sim 0.5$. Constraints from R_b disfavor this low $\tan\beta$ region and

JHEP01(2014)161

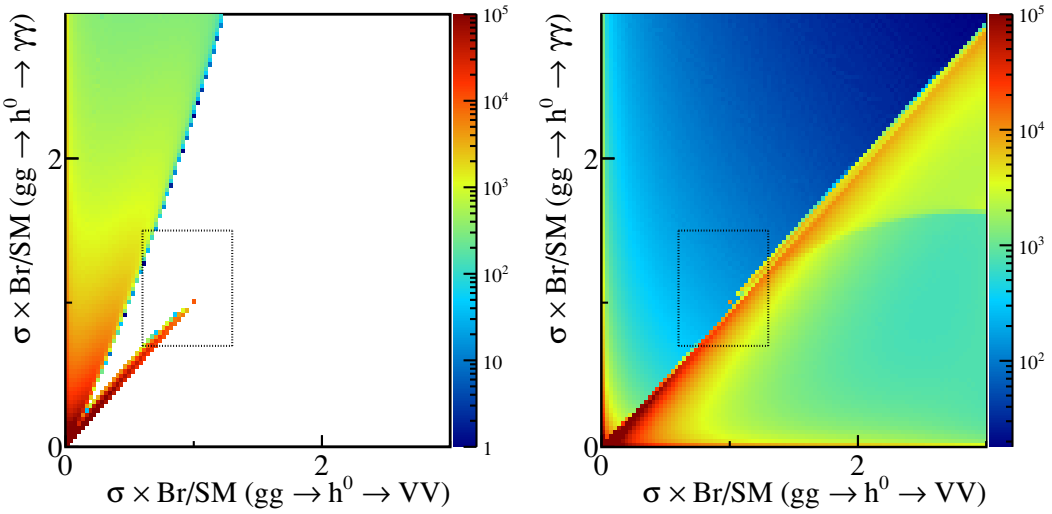

Figure 4. $\sigma \times \mathrm{Br/SM}$ for $gg \to h^0 \to \gamma\gamma$ versus $gg \to h^0 \to VV$ for negative $\sin(\beta-\alpha)$ (left panel), and positive $\sin(\beta-\alpha)$ (right panel) in the h^0-126 case. Color map indicates the density of points with red being the most dense region and blue being the least dense region. Also indicated by the small rectangular box is the normalized signal cross section range of $\gamma\gamma$ between 0.7 and 1.5, and VV channels between 0.6 and 1.3 [4, 7].

therefore we will not discuss it further. In what follows, we will display separate plots for positive and negative $\sin(\beta-\alpha)$ to show the different features that appear in these two cases.

In figure 4, we show the correlations for $\sigma \times \mathrm{Br/SM}$ for the $\gamma\gamma$ channel against VV, for negative (positive) values of $\sin(\beta-\alpha)$ in the left (right) panel as a density plot. Color coding is such that the points in red are the most dense (i.e., most likely) and points in blue are the least dense (i.e., less likely). Also indicated by the small rectangular box is the normalized signal cross section range of $\gamma\gamma$ between 0.7 and 1.5, and VV channels between 0.6 and 1.3, as given in eq. (3.7) [4, 7]. Note that the corresponding signal windows in $\tan\beta$ versus $\sin(\beta-\alpha)$ plane are also sketched in figure 3 as the shaded gray regions. For negative $\sin(\beta-\alpha)$, there are two branches: the one along the diagonal line with $\gamma\gamma : VV \sim 1$ and $\sigma_{\gamma\gamma} \lesssim 1$, which can be mapped on to the $\sin(\beta-\alpha) = -1$ branch in figure 3. The other branch in the upper-half plane where $\gamma\gamma : VV \gtrsim 2$ and $\sigma_{\gamma\gamma}$ extends to 2 or larger is strongly disfavored given the current observed Higgs signal region.

For positive values of $\sin(\beta-\alpha)$, the diagonal region is the most probable, with $\gamma\gamma : VV \lesssim 1$ and $\sigma_{\gamma\gamma}$ possibly extending over a relatively large range around 1. Branches with $\sigma_{\gamma\gamma}$ or $\sigma_{VV} \sim 0$ along the axes are strongly disfavored given the current observation of the Higgs signal.

Thus we see that for all values of $\sin(\beta-\alpha)$, the VV and $\gamma\gamma$ channels are positively correlated.[4] Most of the points falls into $\gamma\gamma : VV \sim 1$ with the cross section of both around the SM strength. This means that an excess in the $\gamma\gamma$ channel should most likely

[4]This agrees with the results of [15].

JHEP01(2014)161

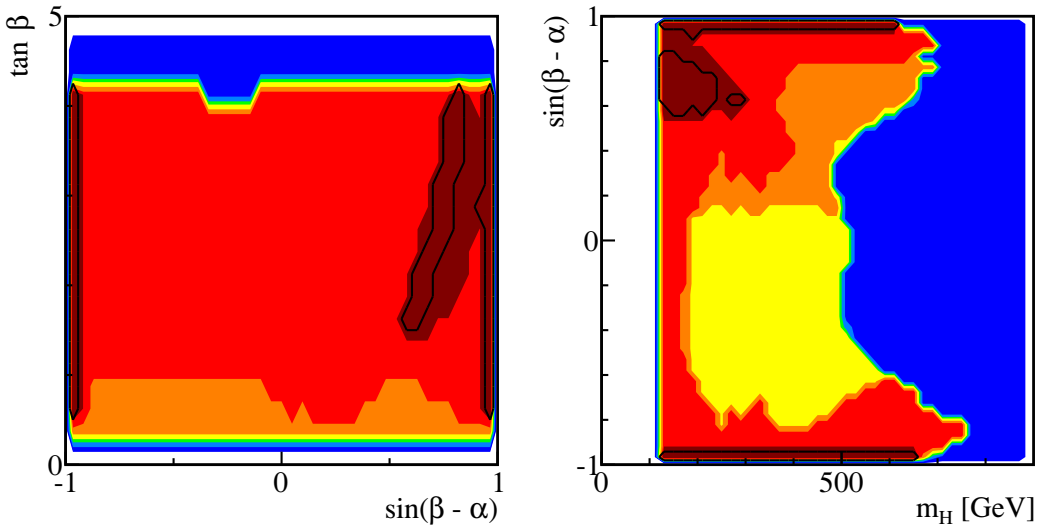

Figure 5. Parameter regions in the h^0-126 case for $\tan\beta$ versus $\sin(\beta-\alpha)$ (left panel) and $\sin(\beta-\alpha)$ versus m_H (right panel). We show regions excluded by stability, unitarity and perturbativity (dark blue), S and T (light blue), LEP results (green), Tevatron and LHC results (yellow), and R_b (orange). Regions that survive all the theoretical and experimental constraints are shown in red. Also shown in dark red are regions consistent with the light CP-even Higgs interpreted as the observed 126 GeV scalar resonance, satisfying the cross section requirement of eq. (3.7) for $gg \to h^0 \to \gamma\gamma, WW/ZZ$. Regions enclosed by the black curves are the ones that survive the flavor constraints.

be accompanied by an excess in the ZZ and WW channels, and this fact serves as an important piece of discrimination for this model as more data is accumulated.

The above analysis illustrates the cross section and decay branching fraction behavior of the light CP-even Higgs when it is interpreted as the observed 126 GeV SM-like Higgs, using the approximate formulae in eqs. (4.2)–(4.4). Note that we have only included the usual SM Higgs decay channels in Γ_{total} in eq. (4.4). While it is a valid approximation in most regions of the parameter space, it might break down when light states in the spectrum open up new decay modes or introduce large loop contributions to either $gg \to h^0$ or $h^0 \to \gamma\gamma$. In our full analysis presented below with scanning over the parameter spaces, we used the program 2HDMC, which takes into account all the decay channels of the Higgs, as well as other loop corrections to the gluon fusion production or Higgs decays to $\gamma\gamma$.

4.2 Parameter spaces

Fixing $m_h = 126$ GeV still leaves us with five parameters: three masses, $m_H, m_A, m_{H^\pm}$, and two angles $\tan\beta$ and $\sin(\beta-\alpha)$. Varying those parameters in the ranges given in eqs. (3.1)–(3.4), we now study the remaining parameter regions satisfying all the theoretical and experimental constraints as well as regions that are consistent with the observed Higgs signal.

The left panel of figure 5 shows the viable regions in $\tan\beta$ versus $\sin(\beta-\alpha)$ plane when various theoretical constraints and experimental bounds are imposed sequentially. The red regions are those that satisfy all the constraints. Also shown in dark red are regions

JHEP01(2014)161

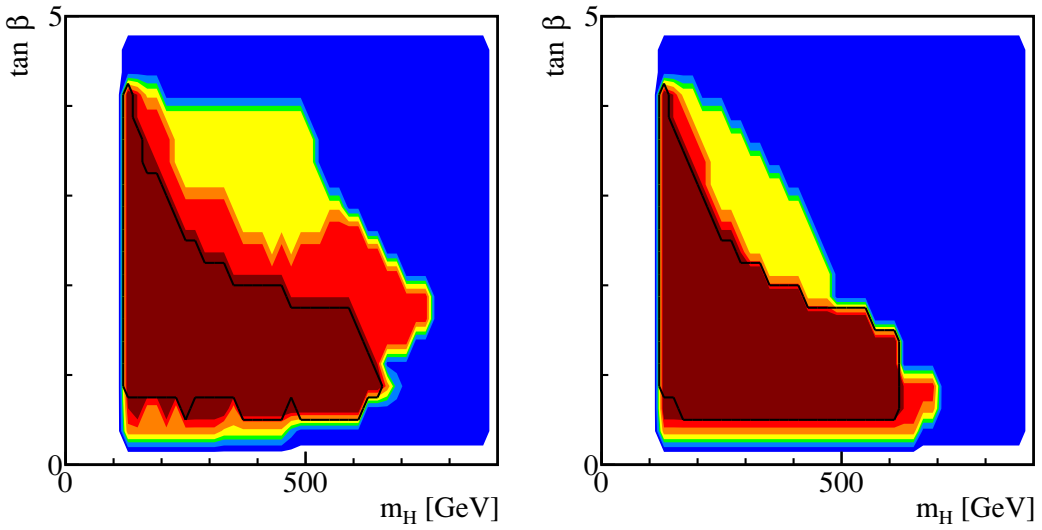

Figure 6. Parameter regions in the h^0-126 case for $\tan\beta$ versus m_H with $\sin(\beta-\alpha) < 0$ (left panel) and $\sin(\beta-\alpha) > 0$ (right panel). Color coding is the same as figure 5.

consistent with the light CP-even Higgs interpreted as the observed 126 GeV scalar particle, satisfying the cross section requirement of eq. (3.7) for $gg \to h^0 \to \gamma\gamma, WW/ZZ$. The signal regions (two narrow regions at $\sin(\beta-\alpha) = \pm 1$, and one extended region with $0.55 < \sin(\beta-\alpha) < 0.9$) agree well with the shaded region in figure 3. The small region around $\sin(\beta-\alpha) \sim 0.3$, however, disappeared, due to the R_b constraint [68]. Regions with $\tan\beta \gtrsim 4$ are excluded by perturbative bounds since one of $\lambda_{1,2}$ becomes non-perturbative for larger value of $\tan\beta$ ($\cos\beta \to 0$), as shown in eq. (2.4). Consequently, the bottom loop contribution to the gluon fusion production cross section [8] is not a major factor for the h^0-126 case.

To further explore the flavor constraints, we show in figure 5 the regions enclosed by the black curves being those that survive the flavor bounds. As can clearly be seen, flavor bounds do not significantly impact the surviving signal regions.

The right panel of figure 5 shows the allowed region in the $\sin(\beta-\alpha)-m_H$ plane. Imposing all the theoretical constraints, in particular, the perturbativity requirement, translates into an upper bound on m_H of around 750 GeV. Higgs search bounds from the LHC removes a large region in negative $\sin(\beta-\alpha)$, mostly from the stringent bounds from WW and ZZ channels for the heavy Higgs. The positive $\sin(\beta-\alpha)$ region is less constrained since $gg \to H^0 \to WW/ZZ$ are much more suppressed. R_b, in addition, excludes part of the positive $\sin(\beta-\alpha)$ region with relatively large m_H. Requiring h^0 to fit the observed Higgs signal further narrows down the favored regions, as shown in dark red. For $\sin(\beta-\alpha) = \pm 1$, m_H could be as large as 650 GeV. For $0.55 \lesssim \sin(\beta-\alpha) \lesssim 0.9$, m_H is constrained to be less than 300 GeV. The correlation between m_H and $\sin(\beta-\alpha)$ indicates that if a heavy CP-even Higgs is discovered to be between 300 and 650 GeV, $\sin(\beta-\alpha)$ is constrained to be very close to ± 1, indicating the light Higgs has SM-like couplings to the gauge sector.

JHEP01(2014)161

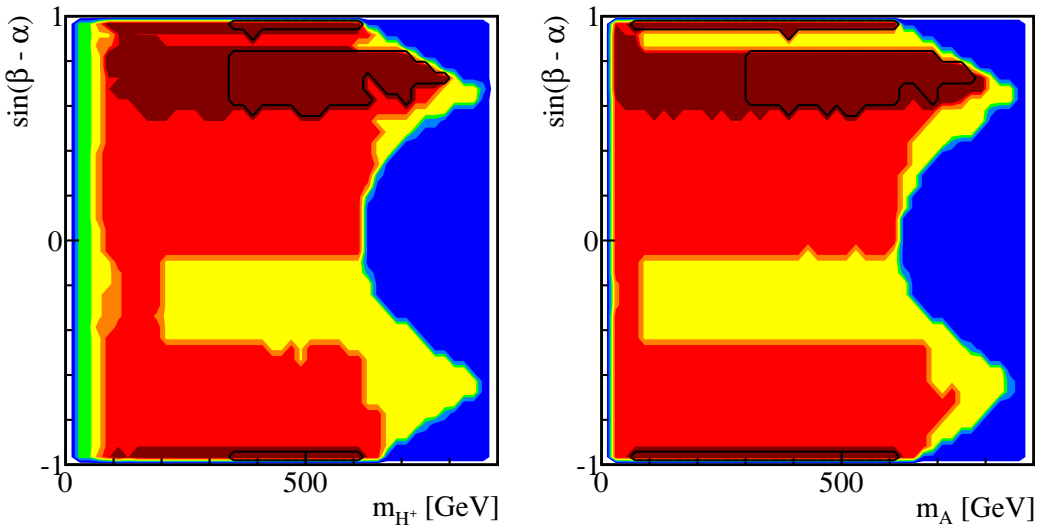

Figure 7. Parameter regions in the h^0-126 case for $\sin(\beta-\alpha)$ versus $m_{H^\pm}$ (left panel) and m_A (right panel). Color coding is the same as figure 5.

In figure 6, we present the parameter regions for $\tan\beta$ versus m_H with $\sin(\beta-\alpha)<0$ (left panel) and $\sin(\beta-\alpha)>0$ (right panel). Regions with large m_H are typically realized for small $\tan\beta$ roughly between 1 and 2. There are also noticeable difference for positive or negative $\sin(\beta-\alpha)$ for regions that survive all the experimental constraints (red regions). Negative $\sin(\beta-\alpha)$ allows larger values of $\tan\beta$ for a given mass of m_H. Small values of $\tan\beta$ is disfavored by the perturbativity of top Yukawa coupling [39], R_b [68], and the flavor constraints [78].

Figure 7 shows the parameter regions in $\sin(\beta-\alpha)$ versus $m_{H^\pm}$ (left panel) and m_A (right panel). For negative $\sin(\beta-\alpha)$ between -0.5 to -0.1, only regions with $m_A<60\,\text{GeV}$ survive the LHC Higgs search bounds. This is because $H^0\to A^0A^0$ opens up in this region, which leads to the suppression of $H^0\to WW/ZZ$ allowing it to escape the experimental constraints. The corresponding surviving region in $120\,\text{GeV}<m_{H^\pm}<200$ GeV is introduced by the correlation between m_A and $m_{H^\pm}$ due to $\Delta\rho$ constraints. Imposing the cross section requirement for h^0 to satisfy the Higgs signal region results in three bands in both m_A and $m_{H^\pm}$, with masses extending all the way to about 800 GeV. Imposing the flavor constraints leaves regions with $m_{H^\pm}\gtrsim 300\,\text{GeV}$ viable for $\sin(\beta-\alpha)=\pm1$ or $\sin(\beta-\alpha)$ between 0.55 and 0.9, while even smaller values for m_A remain viable at $\sin(\beta-\alpha)=\pm1$.

The allowed regions in the $\tan\beta-m_{H^\pm}$ and $\tan\beta-m_A$ planes share similar features before flavor constraints are taken into account, which are shown in figure 8. The top two panels show the allowed regions in the $\tan\beta-m_{H^\pm}$ plane for negative and positive $\sin(\beta-\alpha)$, while the lower two panels are for $\tan\beta-m_A$. LEP places a lower bound on the charged Higgs mass around 80 GeV [55, 56]. In the signal region for $\sin(\beta-\alpha)<0$, both $m_{H^\pm}$ and m_A are less than about 600 GeV, while their masses could be extended to 800 GeV for $\sin(\beta-\alpha)>0$ and $\tan\beta>2$. The difference between the m_A range for different

JHEP01(2014)161

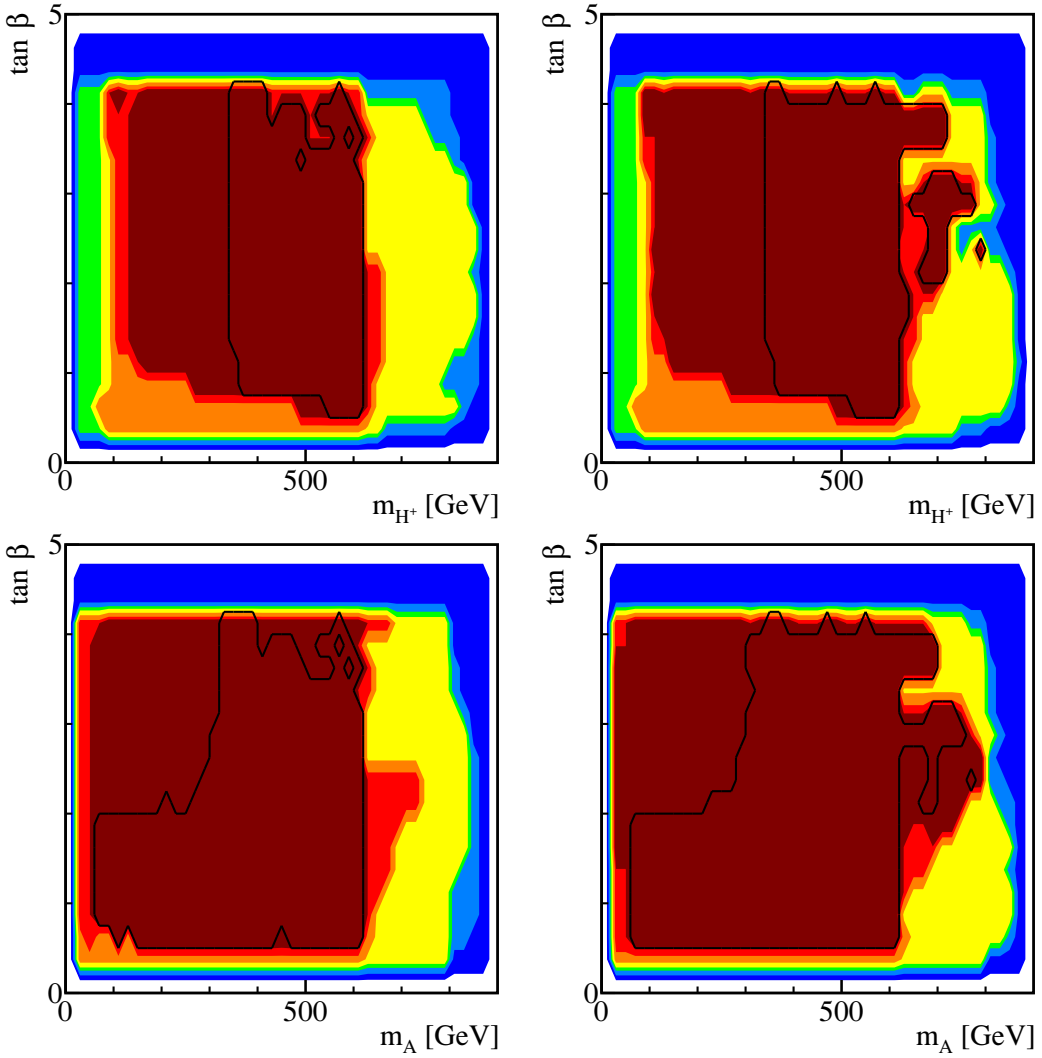

Figure 8. Parameter regions in the h^0-126 case for $\tan\beta$ versus $m_{H^\pm}$ (top panels) and m_A (lower panels) with $\sin(\beta-\alpha) < 0$ (left panels) and $\sin(\beta-\alpha) > 0$ (right panels). Color coding is the same as figure 5.

signs of $\sin(\beta-\alpha)$ can be explained as follows: regions with $m_A > 600\,\text{GeV}$ can only occur for $|\sin(\beta-\alpha)|$ between 0.4 and 0.8, as shown in the right panel of figure 7. The Higgs signal region of $\tan\beta$ versus $\sin(\beta-\alpha)$ (left panel of figure 5) shows that to simultaneously satisfy both the $\tan\beta$ range and $\sin(\beta-\alpha)$ range, only positive $\sin(\beta-\alpha)$ case survives.

Flavor bounds, as expected, have a marked effect here ruling out any value of $m_{H^\pm} \lesssim 300\,\text{GeV}$ for all values of $\tan\beta$, mainly due to the $b \to s\gamma$ constraint. For the CP-odd Higgs, only a corner of $\tan\beta > 2$ and $m_A < 300\,\text{GeV}$ is excluded, due to the combination of flavor and $\Delta\rho$ constraints. As shown in figure 6, only relatively light $m_H \lesssim 300\,\text{GeV}$ is allowed for $\tan\beta > 2$. The flavor constraints of $m_{H^\pm} \gtrsim 300\,\text{GeV}$ is then translated to $m_A \gtrsim 300\,\text{GeV}$

JHEP01(2014)161

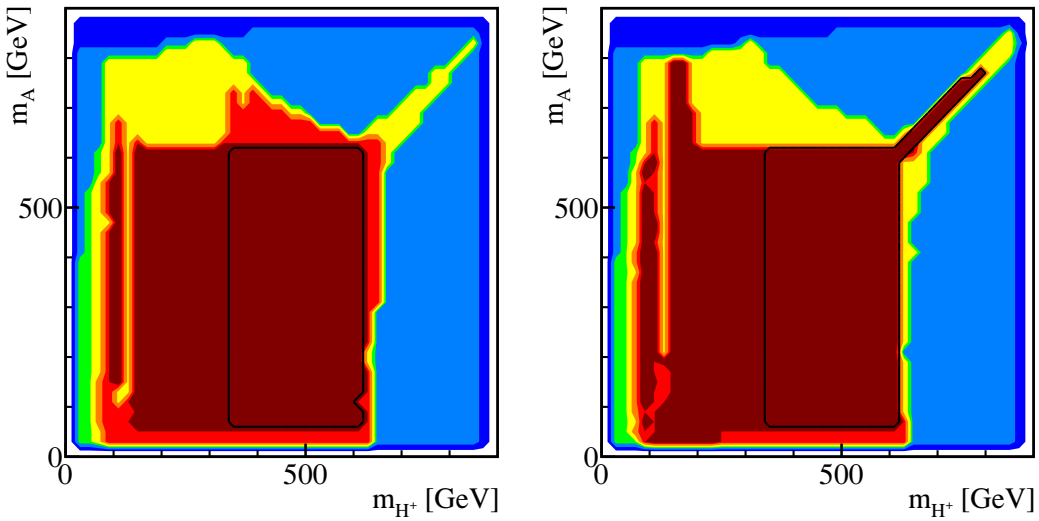

Figure 9. Parameter regions in the h^0-126 case for m_A versus $m_{H^\pm}$ with $\sin(\beta-\alpha) < 0$ (left panel) and $\sin(\beta-\alpha) > 0$ (right panel). Color coding is the same as figure 5.

since the difference between m_A and $m_{H^\pm}$ is constrained by $\Delta\rho$ considerations when both m_h and m_H are relatively small. For $\tan\beta < 2$, m_H could be relatively high, which cancels the large contribution to $\Delta\rho$ from large $m_{H^\pm}$ while allowing m_A to be light.

In figure 9, we present the parameter regions in the $m_A - m_{H^\pm}$ plane for negative and positive values of $\sin(\beta-\alpha)$. m_A and $m_{H^\pm}$ are uncorrelated for most parts of the parameter space. For $\sin(\beta-\alpha) > 0$ when $m_{A,H^\pm}$ could reach values larger than 600 GeV, $\tan\beta$ is at least 2 or larger (see figure 8). m_H is restricted to less than 300 GeV in this region, which results in a strong correlation between m_A and $m_{H^\pm}$ due to the $\Delta\rho$ constraints.

Figure 10 shows the parameter space in the $m_A - m_H$ plane for negative (left panel) and positive (right panel) $\sin(\beta-\alpha)$. These two masses are largely uncorrelated for either sign of $\sin(\beta-\alpha)$. Note that for $\sin(\beta-\alpha) > 0$, large m_A between $600-800$ GeV is only possible for small values of $m_H \lesssim 250$ GeV. This is because the corresponding $\tan\beta$ is larger than 2, which bounds m_H from above. The lower-left corners excluded by flavor constraints correspond to the upper-left corners in $m_A - \tan\beta$ plots in figure 8, since at least one of m_A or m_H would need to be relatively heavy to cancel the contribution to $\Delta\rho$ from $m_{H^\pm} > 300$ GeV.

We conclude this section with the following comments:

- If h^0 is the 126 GeV resonance, then the $\gamma\gamma$ channel is closely correlated with WW/ZZ. Specifically, a moderate excess in $\gamma\gamma$ should be accompanied by a corresponding excess in WW/ZZ.

- The combination of all theoretical constraints requires $\tan\beta \lesssim 4$. Therefore, the bottom-loop enhancement to the gluon fusion [8] is never a major factor. Regions of $\sin(\beta-\alpha)$ and $\tan\beta$ are highly restricted once we require the light CP-even Higgs to be the observed 126 GeV scalar particle: $\tan\beta$ between 0.5 to 4 for $\sin(\beta-\alpha) = \pm 1$, $\tan\beta$ between 1.5 to 4 for $0.55 < \sin(\beta-\alpha) < 0.9$. The masses of the other Higgses,

JHEP01(2014)161

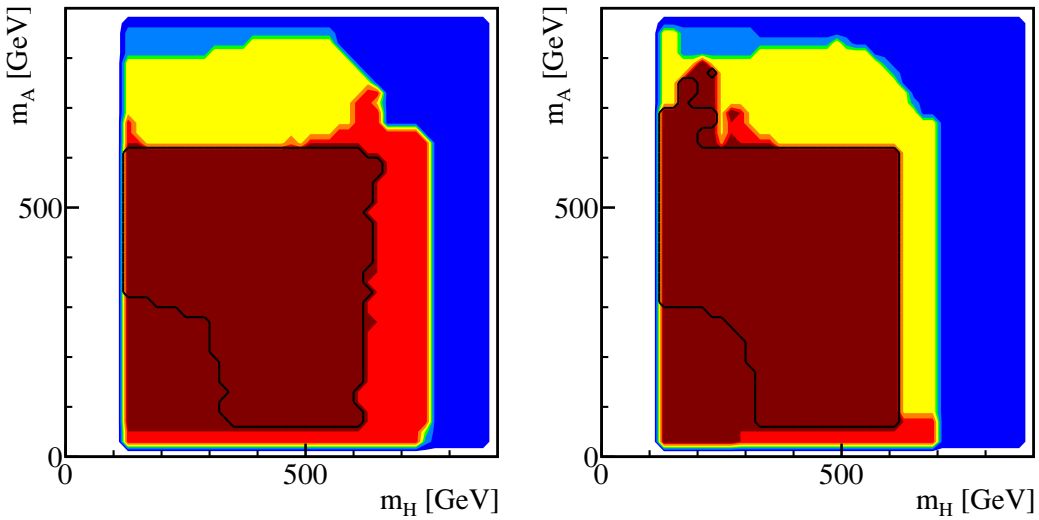

Figure 10. Parameter regions in the h^0-126 case for m_A versus m_H with $\sin(\beta-\alpha) < 0$ (left panel) and $\sin(\beta-\alpha) > 0$ (right panel). Color coding is the same as figure 5.

m_H, m_A, and $m_{H^\pm}$, however, are largely unrestricted and uncorrelated, except for the region where $\sin(\beta-\alpha) > 0$ and $m_{A,H^\pm} \gtrsim 600\,\text{GeV}$, which exhibits a strong correlation between these two masses.

- The discovery of any one of the extra scalars can largely narrow down the parameter space, in particular, if the masses of those particles are relatively high.
- Flavor bounds do not change the allowed parameter space much except for the charged Higgs mass, which is constrained to lie above 300 GeV.

5 Heavy Higgs at 126 GeV

5.1 Cross sections and correlations

It is possible that the 126 GeV resonance discovered at the LHC corresponds to the heavier of the two CP-even Higgses, H^0. There are a few noticeable changes for the heavy H^0 being the SM-like Higgs boson. First of all, since the coupling of the heavy Higgs to a gauge boson pair is scaled by a factor of $\cos(\beta-\alpha)$ as opposed to $\sin(\beta-\alpha)$, demanding SM-like cross sections for H^0 forces us to consider $\sin(\beta-\alpha) \sim 0$, as opposed to $\sin(\beta-\alpha) \sim \pm 1$ in the h^0-126 case. Secondly, as will be demonstrated below, the bottom contribution to the gluon fusion production could be significantly enhanced since the range of $\tan\beta$ could be much larger compared to the h^0-126 case.

Similar to eqs. (4.2) and (4.3) in section 4, the ratios of the gluon fusion cross sections normalized to the SM can be written approximately as:

$$\frac{\sigma(gg \to H^0)}{\sigma_{\text{SM}}} = \frac{\sin^2\alpha}{\sin^2\beta} + \frac{\cos^2\alpha}{\cos^2\beta}\frac{|A_{1/2}(\tau_b)|^2}{|A_{1/2}(\tau_t)|^2} \tag{5.1}$$

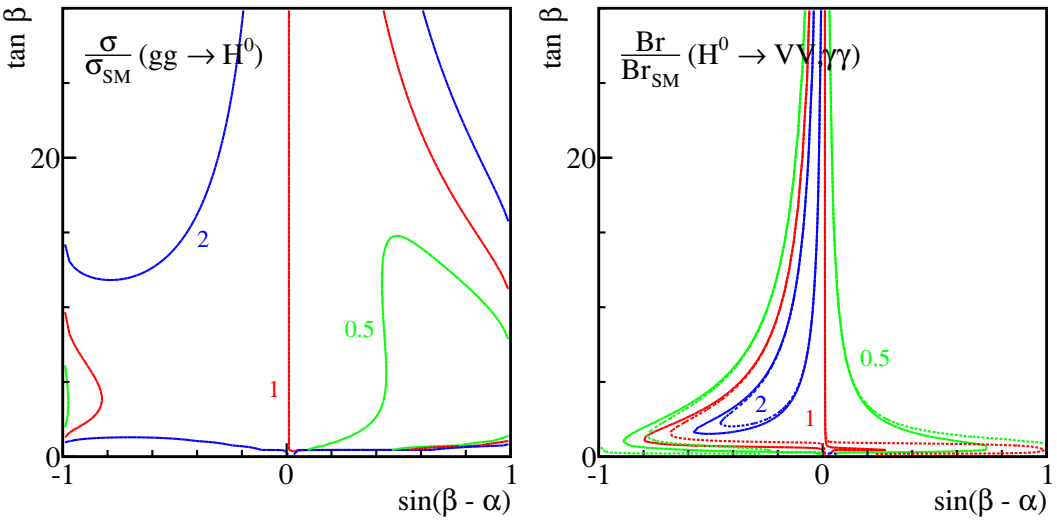

Figure 11. The normalized $gg \to H^0$ production cross section contours (left panel) and $H^0 \to VV$ (solid lines of the right panel) and $H^0 \to \gamma\gamma$ (dashed lines of the right panel) branching fractions in the H^0-126 case. The contour lines are $\sigma/\sigma_{\rm SM}$, $\mathrm{Br}/\mathrm{Br}_{\rm SM} = 0.5$ (green), 1 (red), and 2 (blue).

$$= \left[\frac{\sin(\beta-\alpha)}{\tan\beta} - \cos(\beta-\alpha)\right]^2 + [\sin(\beta-\alpha)\tan\beta + \cos(\beta-\alpha)]^2 \frac{|A_{1/2}(\tau_b)|^2}{|A_{1/2}(\tau_t)|^2}. \quad (5.2)$$

Contours of $\sigma/\sigma_{\rm SM}(gg \to H^0) = 0.5$ (green), 1 (red), and 2 (blue) are shown in the left panel of figure 11. H^0 couples exactly like the SM Higgs for $\sin(\beta-\alpha) = 0$, while deviations from the SM values occur for $\sin(\beta-\alpha)$ away from zero. For $\sin(\beta-\alpha) < 0$, $\sigma/\sigma_{\rm SM}(gg \to H^0)$ is almost always larger than 1 (except for a small region around $\sin(\beta-\alpha) \sim -1$ and $\tan\beta \lesssim 10$) while a suppression of the gluon fusion production is possible for positive values of $\sin(\beta-\alpha)$. This is due to cancellations between the $\sin(\beta-\alpha)$ and $\cos(\beta-\alpha)$ terms in the top Yukawa coupling, in particular, for low $\tan\beta$. The bottom loop contributes significantly when $\tan\beta$ is large, which enhances the gluon fusion production cross section.

$\mathrm{Br}(H^0 \to VV, \gamma\gamma)/\mathrm{Br}_{\rm SM}$ can also be expressed similar to eq. (4.4):

$$\frac{\mathrm{BR}(H^0 \to XX)}{\mathrm{BR}(h_{\rm SM} \to XX)} = \frac{\Gamma_{XX}}{\Gamma_{total}} \times \frac{\Gamma^{\rm SM}_{total}}{\Gamma^{\rm SM}_{XX}} = \begin{cases} \dfrac{\cos^2(\beta-\alpha)}{\cos^2(\beta-\alpha)\mathrm{Br}(h_{\rm SM}\to VV) + \frac{\cos^2\alpha}{\cos^2\beta}\mathrm{Br}(h_{\rm SM}\to bb)+\ldots} \\ \dfrac{\Gamma(H^0\to\gamma\gamma)/\Gamma(h_{\rm SM}\to\gamma\gamma)}{\cos^2(\beta-\alpha)\mathrm{Br}(h_{\rm SM}\to VV) + \frac{\cos^2\alpha}{\cos^2\beta}\mathrm{Br}(h_{\rm SM}\to bb)+\ldots} \end{cases}, \quad (5.3)$$

with the contour lines given in the right panel of figure 11. A relative enhancement of the branching fractions over the SM values are observed in extended region of negative $\sin(\beta-\alpha)$, while it is mostly suppressed for positive $\sin(\beta-\alpha)$.

Combining the production cross sections and the decay branching fractions, contours of $gg \to H^0 \to XX$ are given in figure 12 for $\gamma\gamma$ (left panel) and WW/ZZ channels (right panel). Requiring the cross section to be consistent with the observed Higgs signal: $0.7 - 1.5$ for the $\gamma\gamma$ channel and $0.6 - 1.3$ for the WW/ZZ channel, results in two distinct regions: a region close to $\sin(\beta-\alpha) \sim 0$, and an extended region of $-0.8 \lesssim \sin(\beta-\alpha) \lesssim -0.05$.

JHEP01(2014)161

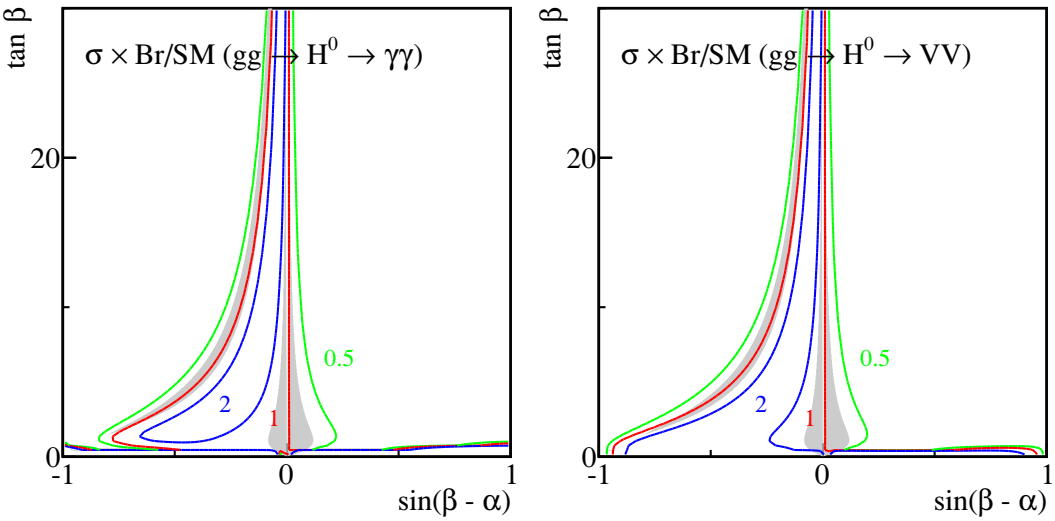

Figure 12. $\sigma \times$ Br/SM for the processes $gg \to H^0 \to \gamma\gamma$ (left), and $gg \to H^0 \to WW/ZZ$ (right) in the H^0-126 case. The contour lines are $\sigma \times$ Br/SM = 0.5 (green), 1 (red), and 2 (blue). The regions where cross sections of $\gamma\gamma$ and WW/ZZ channels satisfy eq. (3.7) are shaded gray.

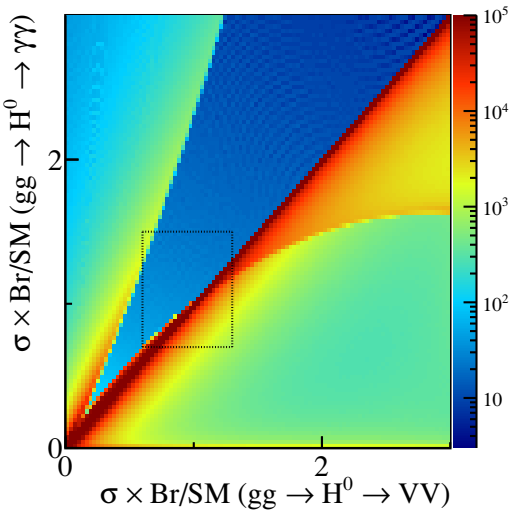

Figure 13. $\sigma \times$ Br/SM for $gg \to H^0 \to \gamma\gamma$ versus $gg \to H^0 \to VV$ in the H^0-126 case. Color coding is the same as in figure 4. Also indicated by the small rectangular box is the normalized signal cross section range of $\gamma\gamma$ between 0.7 and 1.5, and VV channels between 0.6 and 1.3 [4, 7].

Figure 13 shows the correlation between the $\gamma\gamma$ and VV channels. Most of the points lie along the diagonal: $\gamma\gamma : VV \sim 1$. A second branch of $\gamma\gamma : WW \sim 2$ also appears, which corresponds to the very low $\tan\beta < 1$ region in figure 12. This region is strongly constrained by R_b and flavor bounds, and is therefore not considered further in our study.

JHEP01(2014)161

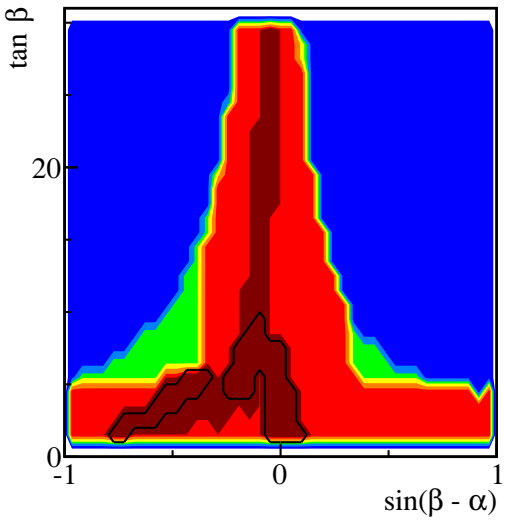

Figure 14. Parameter regions in the H^0-126 case for $\tan\beta$ versus $\sin(\beta-\alpha)$. Color coding is the same as figure 5 except that the dark red regions are the ones consistent with the heavy CP-even Higgs interpreted as the observed Higgs signal.

5.2 Parameter spaces

We now present the results for H^0-126 case with the full parameter scan, including all the theoretical and experimental constraints. Figure 14 presents the parameter regions in $\tan\beta$ versus $\sin(\beta-\alpha)$. The color coding is the same as in figure 5, except that the signal regions in dark red are those with the heavy CP-even Higgs H^0 interpreted as the observed 126 GeV scalar.

Requiring the heavy CP-even Higgs to satisfy the cross section ranges of the observed Higgs signal results in two signal regions: one region near $\sin(\beta-\alpha)\sim 0$ and an extended region of $-0.8 \lesssim \sin(\beta-\alpha) \lesssim -0.05$, consistent with figure 12. Note however that the region around $\sin(\beta-\alpha)\sim 0$ is actually reduced to $\tan\beta \lesssim 8$. This is because larger values of $\tan\beta$ leads to smaller m_h such that $m_h < m_H/2$ (see right panel of figure 15 below). The opening of $H^0 \to h^0h^0$ channel reduces the the branching fractions of $H^0 \to WW/ZZ, \gamma\gamma$ forcing it outside the signal cross section region. Regions surviving the flavor bounds are the ones enclosed by black curves. Larger values of $\tan\beta \gtrsim 10$ are disfavored.

Figure 15 shows the parameter region in $\sin(\beta-\alpha)$ versus m_h (left panel) and $\tan\beta$ versus m_h (right panel). Within the narrow region around $\sin(\beta-\alpha)\sim 0$, m_h can take all values up to 126 GeV. For $-0.8 \lesssim \sin(\beta-\alpha) \lesssim -0.35$, when the H^0WW, H^0ZZ couplings could significantly deviate from the SM value while h^0WW, h^0ZZ couplings are sizable, the light CP-even Higgs mass is constrained to be larger than about 80 GeV from LEP Higgs searches [53, 54]. This is the interesting region where the two Higgses are close to being degenerate, with both h^0 and H^0 showing significant deviation of their couplings to gauge bosons from the SM value.

JHEP01(2014)161

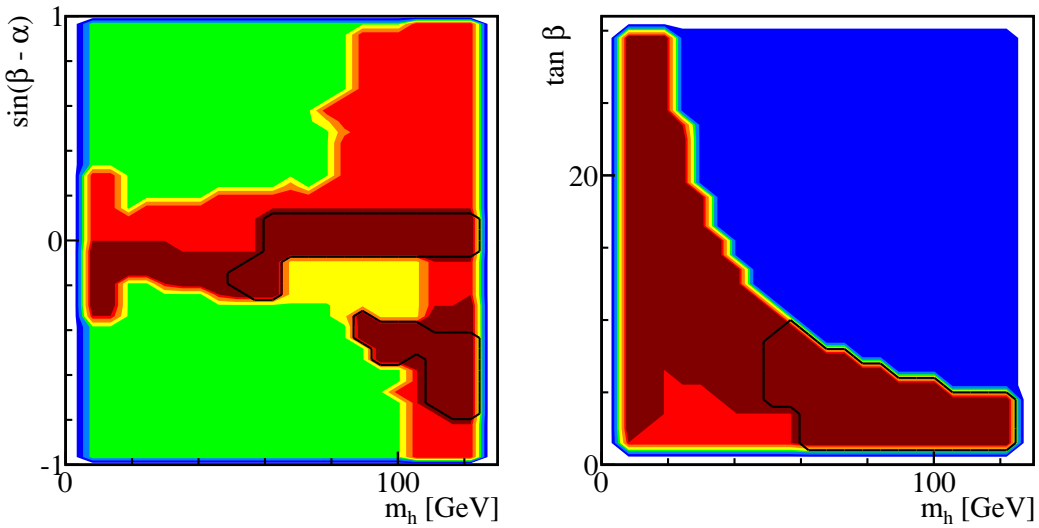

Figure 15. Parameter regions in the H^0-126 case for $\sin(\beta-\alpha)$ versus m_h (left panel) and $\tan\beta$ versus m_h (right panel). Color coding is the same as figure 14.

The right panel of figure 15 shows the parameter region of $\tan\beta$ versus m_h. Larger values of $\tan\beta$ is only allowed for small values of m_h. The red region where $m_h < 60\,\text{GeV}$ and $\tan\beta \lesssim 5$ can not satisfy the Higgs signal cross section requirement due to the opening of $H^0 \to h^0h^0$ mode, which corresponds to the $m_h < 60\,\text{GeV}$, $\sin(\beta-\alpha) \sim 0$ red region in the $\sin(\beta-\alpha)$ versus m_h plot (left panel of figure 15). Imposing the flavor bounds further rules out regions with light m_h below about 50 GeV, mainly due to the process $B_s \to \mu^+\mu^-$, as shown in the right panel of figure 1. Large values of $\tan\beta \gtrsim 10$ are excluded correspondingly.

Figure 16 shows $\sin(\beta-\alpha)$ versus $m_{A,H^\pm}$ (left panels) and $\tan\beta$ versus $m_{A,H^\pm}$ (right panels). The plots for m_A and $m_{H^\pm}$ are very similar, except for very low masses. Very large values of $m_{A,H^\pm} \gtrsim 800\,\text{GeV}$ are excluded by theoretical considerations, similar to the h^0-126 case. $m_A \lesssim 60\,\text{GeV}$ and $\tan\beta \gtrsim 5$ are excluded by the LEP Higgs search [53], while the triangle region of $130 \lesssim m_A \lesssim 400\,\text{GeV}$ and $\tan\beta \gtrsim 13$ is excluded by the LHC searches for the CP-odd Higgs in $\tau\tau$ mode [58–64]. For the charged Higgs, small values of $m_{H^\pm} \lesssim 80\,\text{GeV}$ are ruled out by LEP searches on charged Higgs [55, 56]. Tevatron and the LHC charged Higgs searches [58–64]: $t \to H^\pm b \to \tau\nu_\tau b$ further rule out regions of $m_{H^\pm} \lesssim 150\,\text{GeV}$ and $\tan\beta \gtrsim 17$. The triangle in $m_{H^\pm}$ versus $\tan\beta$ plot for $150\,\text{GeV} \lesssim m_{H^\pm} \lesssim 400\,\text{GeV}$ and $\tan\beta \gtrsim 13$ is translated from the corresponding region in $\tan\beta$ versus m_A, due to the correlation between m_A and $m_{H^\pm}$ introduced by $\Delta\rho$, as shown below in figure 17. Imposing the flavor constraints further limits $m_A \gtrsim 300\,\text{GeV}$, $m_{H^\pm} \gtrsim 300\,\text{GeV}$ and $\tan\beta \lesssim 10$.

m_A and $m_{H^\pm}$ exhibit a much stronger correlation in the H^0-126 case, mostly due to the the $\Delta\rho$ constraints, as shown in the left panel of figure 17. Comparing with the h^0-126 case, in which m_H could be large with a relaxed constraints on m_A and $m_{H^\pm}$ mass

JHEP01(2014)161

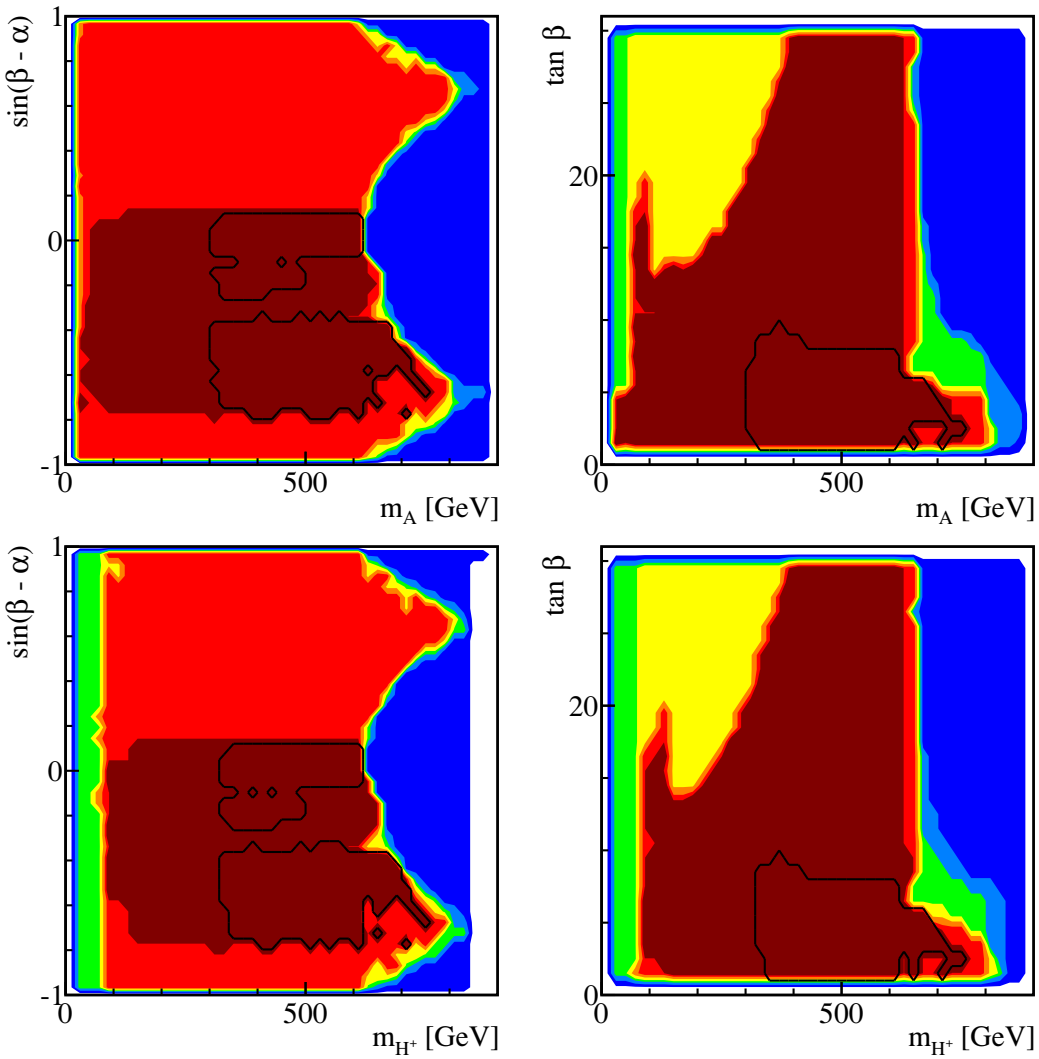

Figure 16. Parameter regions in the H^0-126 case for $\sin(\beta-\alpha)$ versus m_A (upper left panel) and $\tan\beta$ versus m_A (upper right panel), as well as similar plots for $m_H^{\pm}$ (lower panels). Color coding is the same as figure 14.

correlation, in the H^0-126 case, both m_h and m_H are relatively small. m_A and $m_{H^\pm}$ should therefore be highly correlated in order to avoid large custodial symmetry breaking in the Higgs sector. However, there is a small strip of allowed region at $m_{H^\pm} \sim 100\,\text{GeV}$ with m_A between $200 - 700\,\text{GeV}$. This region escapes the $\Delta\rho$ constraint since for $m_{H^\pm} \sim m_h \sim m_H$, the contribution to $\Delta\rho$ introduced by the large mass difference between m_A and $m_{H^\pm}$ is cancelled by the $(h^0,\ A^0)$ loop and $(H^0,\ A^0)$ loop. Imposing the flavor constraints again limits $m_{H^\pm}$ to be larger than 300 GeV. m_A is constrained to be more than 300 GeV as well due to the correlations.

The right panel of figure 17 shows the parameter region of m_A versus m_h, which does not show much correlation. For $m_h \lesssim 90\,\text{GeV}$, low values of $m_A \lesssim 100\,\text{GeV}$ is

JHEP01(2014)161

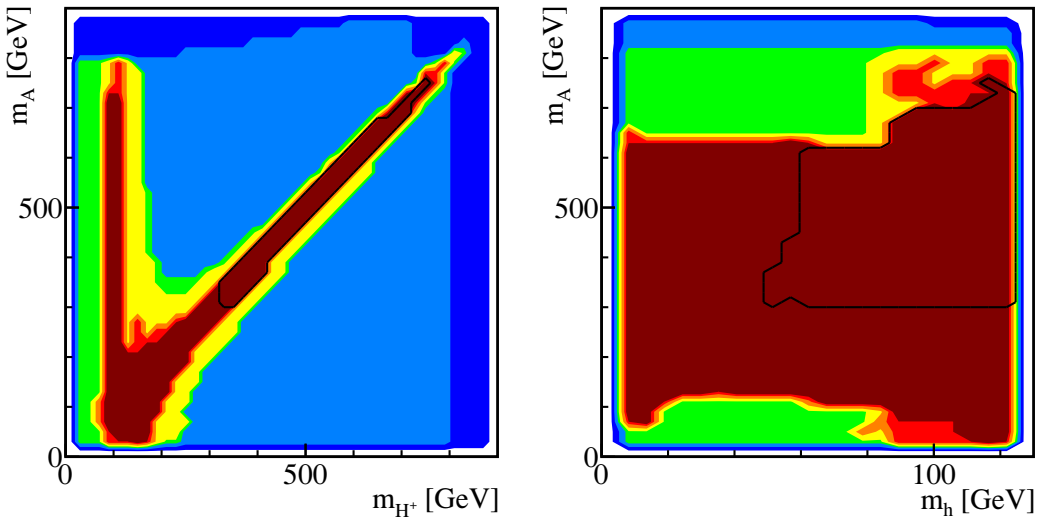

Figure 17. Parameter regions in the H^0-126 case for m_A versus $m_{H^\pm}$ (left panel) and m_h (right panel). Color coding is the same as figure 14.

excluded by LEP searches of h^0A^0 channel [53]. High values of $m_A \gtrsim 600\,\text{GeV}$ are excluded for $m_h < 90\,\text{GeV}$. This is because such a large value of m_A can only be realized for $|\sin(\beta-\alpha)| > 0.3$ (see the upper-left panel of figure 16). Such regions of $|\sin(\beta-\alpha)| > 0.3$ and $m_h < 90\,\text{GeV}$ are excluded by the LEP Higgs search of h^0Z channel [54], as shown clearly in the m_h versus $\sin(\beta-\alpha)$ plot (left panel of figure 15). Such excluded regions for large m_A (and large $m_{H^\pm}$ due to correlation) also appears in the $\tan\beta$ versus m_A ($m_{H^\pm}$) plots in figure 16.

We end the section with the following observations:

- Contrary to the h^0-126 case, fixing the heavy CP-even Higgses to be the 126 GeV resonance forces us into a small narrow region of $\sin(\alpha-\beta) \sim 0$ with $\tan\beta \lesssim 8$ or an extended region of $-0.8 \lesssim \sin(\alpha-\beta) \lesssim -0.05$ with less restrictions on $\tan\beta$.
- The light CP-even Higgs can have mass of any value up to 126 GeV, with smaller m_h only allowed for $\sin(\beta-\alpha) \sim 0$. Note that the case of nearly degenerate h^0 and H^0 is allowed, as studied in detail in ref. [22].
- m_A and $m_{H^\pm}$ exhibit a strong correlation: $m_A \simeq m_{H^\pm}$, due to $\Delta\rho$ constraints.
- Flavor bounds impose the strong constraints: $\tan\beta \lesssim 10$, $m_h > 50\,\text{GeV}$, and $m_{H^\pm} > 300\,\text{GeV}$. m_A is also constrained to be more than 300 GeV due to the correlation between m_A and $m_{H^\pm}$.

6 Other Higgs channels

Thus far, we have concentrated on the gluon fusion production mechanism and the dominant $\gamma\gamma$, ZZ and WW decay channels for the Higgs. The vector boson fusion channel is

JHEP01(2014)161

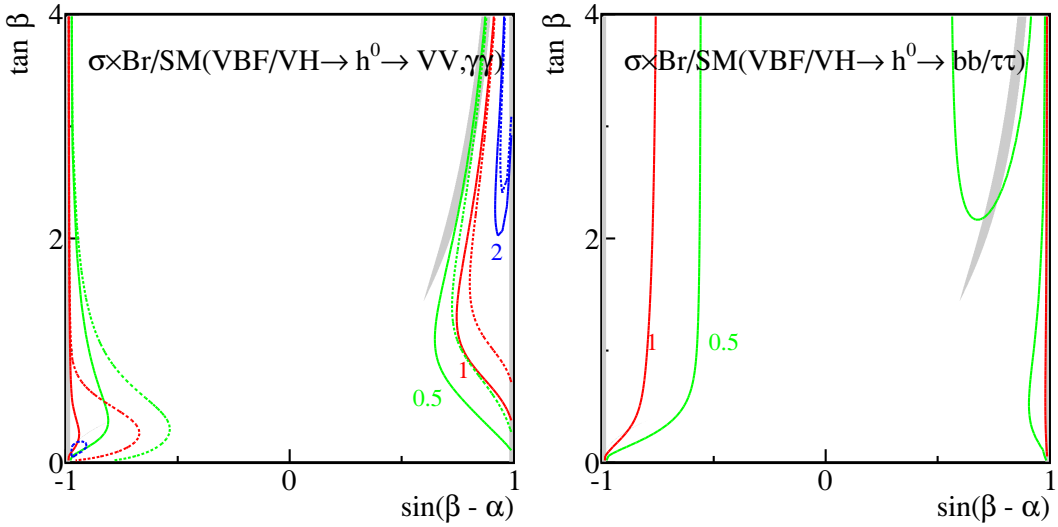

Figure 18. $\sigma \times$ Br/SM for $VBF/VH \to h^0 \to WW/ZZ$ (solid curves in left panel), $\gamma\gamma$ (dashed curves in left panel) and $VBF/VH \to h^0 \to bb/\tau\tau$ (right panel) for the h^0-126 case. The contour lines show $\sigma \times$ Br/SM = 0.5(green), 1 (red) and 2 (blue). The shaded gray regions correspond to the signal regions where cross sections of $\gamma\gamma$ and WW/ZZ channels satisfy eq. (3.7) as well as R_b.

another important production channel for the CP-even Higgses. For certain Higgs decay channels, for example, $\tau\tau$ mode, VBF production is the one that provides the dominant sensitivity due to the excellent discrimination of the backgrounds using the two forward tagging jets and the central jet-veto [82]. Other production channels, VH and ttH associated production, can also be of interest for Higgs decay to bb. In this section, we discuss the cross sections in other search channels for both h^0 and H^0 when they are interpreted as the observed 126 GeV scalar.

In figure 18, we show the normalized cross sections for the WW/ZZ, $\gamma\gamma$ (left panel) and $bb/\tau\tau$ (right panel) final states via VBF or VH associated production (both production cross sections are controlled by h^0VV coupling) in the $\tan\beta$ versus $\sin(\beta-\alpha)$ plane for the h^0-126 case. For $VBF/VH \to h^0 \to WW/ZZ$, both the production and decay are proportional to $\sin(\beta-\alpha)$, resulting in regions highly centered around $\sin(\beta-\alpha) \sim \pm 1$ for any enhancement above the SM value. For the currently preferred gray Higgs signal regions, $VBF/VH \to h^0 \to WW/ZZ$ is typically in the range of $0.5 - 1$ of the SM value.

The current observation of the Higgs signal has been fitted into the signal strength in both the gluon fusion channel and VBF channel for $\gamma\gamma$, WW and ZZ final states [4–7]. Imposing the 95% C.L. contours of the $\mu_{ggF+ttH} \times \mathrm{B/B_{SM}}$ versus $\mu_{VBF+VH} \times \mathrm{B/B_{SM}}$ on top of the one-dimensional gluon fusion signal regions as given in eq. (3.7) does not lead to additional reduction of the signal parameter space, given the VBF channel is relatively loosely constrained.

For $VBF/VH \to h^0 \to bb/\tau\tau$, the cross section is suppressed for most of the regions, except in the neighborhood of $\sin(\beta-\alpha) = \pm 1$ where SM rates can be achieved. The current preferred signal regions typically have a suppression of 0.5 or stronger for this

JHEP01(2014)161

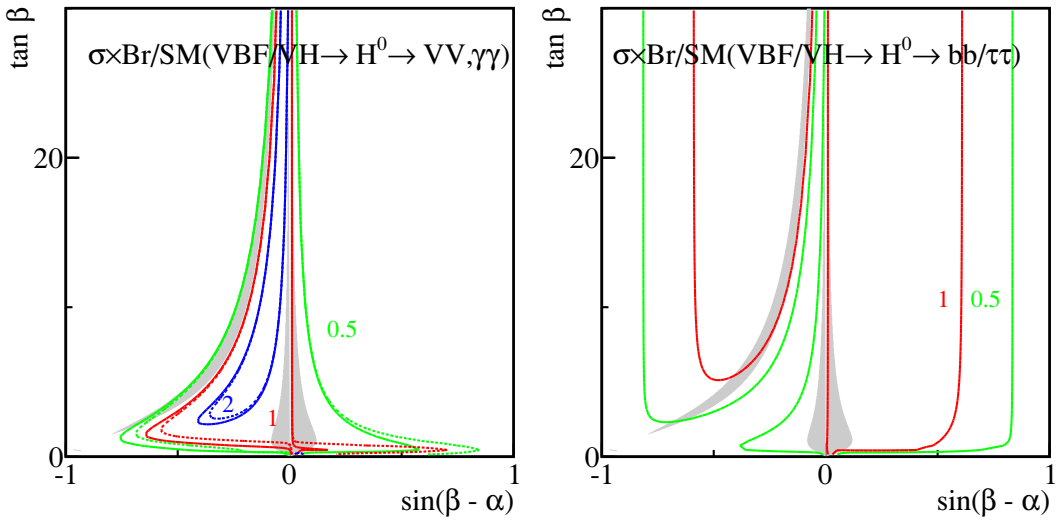

Figure 19. $\sigma \times \mathrm{Br/SM}$ for $VBF/VH \to H^0 \to WW/ZZ, \gamma\gamma$ (left) and $VBF/VH \to H^0 \to bb/\tau\tau$ (right) for the H^0-126 case. Color coding is the same as in figure 18.

$bb/\tau\tau$ channel. There is also a strong inverse correlation between the WW/ZZ and $bb/\tau\tau$ channels, since an increase in bb decay branching fraction can only occur at the expense of WW. Given the relatively loose bounds on the signal strength in the bb and $\tau\tau$ channels from the LHC and the Tevatron experiments [4, 83–86], imposing the current search results for bb and $\tau\tau$ channels does not lead to further reduction of the signal parameter space.

Figure 19 show the $\sigma \times \mathrm{Br/SM}$ plots for VV, $\gamma\gamma$, and $bb/\tau\tau$ channel via VBF/VH production for the H^0-126 case. The qualitative features of the VV, $\gamma\gamma$ plot is the same as that of figure 12. The currently favored gray signal regions typically correspond to a normalized cross section of $VBF/VH \to H^0 \to WW/ZZ$ around 1 as well.

The $bb/\tau\tau$ channel, however, exhibits a very different behavior. For two regions of $-0.6 \leq \sin(\beta - \alpha) \leq -0.1$ and $0 \leq \sin(\beta - \alpha) \leq 0.6$ (regions enclosed by the red curves in the right panel of figure 19), a normalized cross section of at least the SM signal strength can be achieved. A strong suppression, sometimes as small as 0.1, can be obtained in the other regions. The currently favored gray signal region near $\sin(\beta - \alpha) \sim 0$ corresponds to $\sigma/\sigma_{\mathrm{SM}}$ of order 1 for $VBF/VH \to H^0 \to bb/\tau\tau$ channel, while a suppression as large as 0.5 is possible for the extended regions in negative $\sin(\beta - \alpha)$. The inverse correlation between $bb/\tau\tau$ and WW channels also appears in the H^0-126 case. Similar to the h^0-126 case, imposing the 95% C.L. range for the VBF process for $\gamma\gamma$ and WW/ZZ channel, as well as the signal strength obtained from the bb and $\tau\tau$ modes does not lead to further reduction of the signal region.

We also studied $gg \to h^0, H^0 \to bb/\tau\tau$ channel for both the h^0-126 and H^0-126 cases, and noticed that for the currently favored Higgs signal regions, a factor of 2 enhancement could be realized.

JHEP01(2014)161

7 Conclusions

In this paper, we presented a detailed analysis of the Type II 2HDM (with an imposed Z_2 symmetry) parameter space, identifying either the light or the heavy CP-even Higgs as the recently discovered resonance at 126 GeV. We scanned the remaining five parameters $\sin(\beta-\alpha)$, $\tan\beta$, m_A, $m_{H^\pm}$, and m_H or m_h while fixing either m_h or m_H to be 126 GeV. We took into account all the theoretical constraints, precision measurements, as well as current experimental search limits on the Higgses. We further studied the implications on the parameter space once flavor constraints are imposed. We found unique features in each of these two cases.

In the h^0-126 case, we are forced into regions of parameter space where $\sin(\beta-\alpha)=\pm1$ with $\tan\beta$ between 0.5 to 4, or an extended region of $0.55<\sin(\beta-\alpha)<0.9$, with $\tan\beta$ constrained to be in the range of 1.5 to 4. There is, however, a wide range of values that are still allowed for the masses of the heavy CP-even, pseudo scalar and charged Higgses. The Higgs masses are typically not correlated, except when $m_{A,H^\pm}\gtrsim 600\,\text{GeV}$ and $\sin(\beta-\alpha)>0$ where there is a strong correlation between m_A and $m_{H^\pm}$ because of the $\Delta\rho$ constraint. Imposing flavor constraints further restricts $m_{H^\pm}>300\,\text{GeV}$.

In the H^0-126 case, we are forced into an orthogonal region of parameter space where $\sin(\beta-\alpha)\sim 0$, $\tan\beta\lesssim 8$ or an extended region of $-0.8\lesssim\sin(\alpha-\beta)\lesssim -0.05$ with less restricted $\tan\beta$. m_A and $m_{H^\pm}$ exhibit strong correlations: $m_A\simeq m_{H^\pm}$, due to the $\Delta\rho$ constraint. The interesting scenario of the light CP-even Higgs being close to 126 GeV still survives. Imposing flavor bounds further shrinks the parameter space considerably: $\tan\beta\lesssim 10$, $m_h>50\,\text{GeV}$, $m_{H^\pm}>300\,\text{GeV}$, and $m_A>300\,\text{GeV}$.

Note that in both cases, the extended region in $\sin(\beta-\alpha)$ is of particular interest, since a deviation of the Higgs coupling to WW and ZZ can be accommodated for the observed Higgs signal at 126 GeV.

We find that in either of these scenarios, one can identify regions of parameter space that pass all theoretical and experimental bounds and still allow a slightly higher than SM rate to diphotons. $\gamma\gamma$ and WW/ZZ rates are most likely strongly correlated: $\gamma\gamma:VV\sim 1$ for the normalized cross sections.

We further studied the implication for the Higgs production via VBF or VH process, and decays to bb, $\tau\tau$ channels. We found that in the h^0-126 case, both $VBF/VH\to h^0\to bb/\tau\tau, WW/ZZ$ could be significantly suppressed in the Higgs signal region. For the H^0-126 case, $VBF/VH\to H^0\to WW/ZZ$ channel is almost the SM strength. Possible suppression of $bb/\tau\tau$ channel up to 0.5 is possible for the extended signal regions in negative $\sin(\beta-\alpha)$. Future observation of the bb and $\tau\tau$ modes can provide valuable information for the parameter regions of the type II 2HDM.

Comparing to the MSSM, with its Higgs sector being a restricted type II 2HDM and the tree level Higgs spectrum completely determined by m_A and $\tan\beta$, the parameter regions of the general Type II 2HDM is much more relaxed. Unlike the MSSM in which the h^0-126 case corresponds to the decoupling region where $m_A\gtrsim 300\,\text{GeV}$, and the H^0-126 GeV case corresponds to the non-decoupling region where $m_A\sim 100-130\,\text{GeV}$ [87], the value of m_A in the general Type II 2HDM could vary over the entire viable region up

JHEP01(2014)161

to about 800 GeV. The MSSM relation of $m_A \sim m_{H^\pm} \sim m_H$ in the decoupling region is also much more relaxed in the Type II 2HDM. No obvious correlation is observed between m_A, $m_{H^\pm}$, and m_H for the h^0-126 case, except for the region with large $m_{A,H^\pm} \gtrsim 600$ GeV. Note also that in the Type II 2HDM with Z_2 symmetry (such that $m_{12} = 0$) that we are considering, with the additional perturbativity and unitarity constraints imposed, there is an upper limit of about 800 GeV for the mass of H^0, A^0 and $H^\pm$. The presence of an upper bound on the heavy Higgs masses reiterates our point that unlike the MSSM, there is no sensible decoupling limit in this case where only one light SM-like Higgs appears in the low energy spectrum with other Higgses heavy and decouple.

Observations of extra Higgses in the future would further pin down the Higgs sector beyond the SM. While the conventional decay channels of Higgses to SM particles continue to be important channels to search for extra Higgses, novel decay channels of a heavy Higgs into light Higgses or light Higgs plus gauge boson could also appear. Future work along the lines of collider phenomenology of multiple Higgs scenarios is definitely warranted.

Acknowledgments

We thank L. Carpenter for her participation at the beginning of this project. We would also like to thank David Lopez-Val for useful discussions and Oscar Stål for sharing the 2HDMC package. This work was supported by the Department of Energy under Grant DE-FG02-04ER-41298.

References

[1] ATLAS collaboration, *Observation of a new particle in the search for the Standard Model Higgs boson with the ATLAS detector at the LHC*, *Phys. Lett.* **B 716** (2012) 1 [arXiv:1207.7214] [INSPIRE].

[2] ATLAS collaboration, *Combined measurements of the mass and signal strength of the Higgs-like boson with the ATLAS detector using up to* 25 fb^{-1} *of proton-proton collision data*, ATLAS-CONF-2013-014, CERN, Geneva Switzerland (2013).

[3] CMS collaboration, *Observation of a new boson at a mass of* 125 *GeV with the CMS experiment at the LHC*, *Phys. Lett.* **B 716** (2012) 30 [arXiv:1207.7235] [INSPIRE].

[4] CMS collaboration, *Combination of Standard Model Higgs boson searches and measurements of the properties of the new boson with a mass near* 125 *GeV*, CMS-PAS-HIG-13-005, CERN, Geneva Switzerland (2013).

[5] ATLAS collaboration, *Study of the spin of the new boson with up to* 25 fb^{-1} *of ATLAS data*, ATLAS-CONF-2013-040, CERN, Geneva Switzerland (2013).

[6] ATLAS collaboration, *Combined coupling measurements of the Higgs-like boson with the ATLAS detector using up to* 25 fb^{-1} *of proton-proton collision data*, ATLAS-CONF-2013-034, CERN, Geneva Switzerland (2013).

JHEP01(2014)161

[7] ATLAS collaboration, *Measurements of Higgs boson production and couplings in diboson final states with the ATLAS detector at the LHC*, *Phys. Lett.* **B 726** (2013) 88 [arXiv:1307.1427] [INSPIRE].

[8] G. Branco et al., *Theory and phenomenology of two-Higgs-doublet models*, *Phys. Rept.* **516** (2012) 1 [arXiv:1106.0034] [INSPIRE].

[9] H. Haber, G.L. Kane and T. Sterling, *The Fermion mass scale and possible effects of Higgs bosons on experimental observables*, *Nucl. Phys.* **B 161** (1979) 493 [INSPIRE].

[10] L.J. Hall and M.B. Wise, *Flavor changing Higgs-boson couplings*, *Nucl. Phys.* **B 187** (1981) 397 [INSPIRE].

[11] J.F. Donoghue and L.F. Li, *Properties of charged Higgs bosons*, *Phys. Rev.* **D 19** (1979) 945 [INSPIRE].

[12] P. Ferreira, R. Santos, M. Sher and J.P. Silva, *Implications of the LHC two-photon signal for two-Higgs-doublet models*, *Phys. Rev.* **D 85** (2012) 077703 [arXiv:1112.3277] [INSPIRE].

[13] P. Ferreira, R. Santos, M. Sher and J.P. Silva, *Could the LHC two-photon signal correspond to the heavier scalar in two-Higgs-doublet models?*, *Phys. Rev.* **D 85** (2012) 035020 [arXiv:1201.0019] [INSPIRE].

[14] H. Cheon and S.K. Kang, *Constraining parameter space in type-II two-Higgs doublet model in light of a* 126 *GeV Higgs boson*, *JHEP* **09** (2013) 085 [arXiv:1207.1083] [INSPIRE].

[15] A. Drozd, B. Grzadkowski, J.F. Gunion and Y. Jiang, *Two-Higgs-doublet models and enhanced rates for a* 125 *GeV Higgs*, *JHEP* **05** (2013) 072 [arXiv:1211.3580] [INSPIRE].

[16] S. Chang et al., *Comprehensive study of two Higgs doublet model in light of the new boson with mass around* 125 *GeV*, *JHEP* **05** (2013) 075 [arXiv:1210.3439] [INSPIRE].

[17] C.-Y. Chen and S. Dawson, *Exploring two Higgs doublet models through Higgs production*, *Phys. Rev.* **D 87** (2013) 055016 [arXiv:1301.0309] [INSPIRE].

[18] B. Grinstein and P. Uttayarat, *Carving out parameter space in type-II two Higgs doublets model*, *JHEP* **06** (2013) 094 [*Erratum ibid.* **09** (2013) 110] [arXiv:1304.0028] [INSPIRE].

[19] C.-W. Chiang and K. Yagyu, *Implications of Higgs boson search data on the two-Higgs doublet models with a softly broken Z_2 symmetry*, *JHEP* **07** (2013) 160 [arXiv:1303.0168] [INSPIRE].

[20] N. Craig and S. Thomas, *Exclusive signals of an extended Higgs sector*, *JHEP* **11** (2012) 083 [arXiv:1207.4835] [INSPIRE].

[21] L. Basso et al., *Probing the charged Higgs boson at the LHC in the CP-violating type-II* 2*HDM*, *JHEP* **11** (2012) 011 [arXiv:1205.6569] [INSPIRE].

[22] P. Ferreira, R. Santos, H.E. Haber and J.P. Silva, *Mass-degenerate Higgs bosons at* 125 *GeV in the two-Higgs-doublet model*, *Phys. Rev.* **D 87** (2013) 055009 [arXiv:1211.3131] [INSPIRE].

[23] G. Burdman, C.E. Haluch and R.D. Matheus, *Is the LHC observing the pseudo-scalar state of a two-Higgs doublet model?*, *Phys. Rev.* **D 85** (2012) 095016 [arXiv:1112.3961] [INSPIRE].

[24] E. Cervero and J.-M. Gerard, *Minimal violation of flavour and custodial symmetries in a vectophobic two-Higgs-doublet-model*, *Phys. Lett.* **B 712** (2012) 255 [arXiv:1202.1973] [INSPIRE].

JHEP01(2014)161

[25] J. Shu and Y. Zhang, *Impact of a CP-violating Higgs: from LHC to baryogenesis*, *Phys. Rev. Lett.* **111** (2013) 091801 [arXiv:1304.0773] [INSPIRE].

[26] B. Coleppa, K. Kumar and H.E. Logan, *Can the* 126 *GeV boson be a pseudoscalar?*, *Phys. Rev.* **D 86** (2012) 075022 [arXiv:1208.2692] [INSPIRE].

[27] S. Davidson and H.E. Haber, *Basis-independent methods for the two-Higgs-doublet model*, *Phys. Rev.* **D 72** (2005) 035004 [*Erratum ibid.* **D 72** (2005) 099902] [hep-ph/0504050] [INSPIRE].

[28] H.E. Haber and D. O'Neil, *Basis-independent methods for the two-Higgs-doublet model. II. The significance of* $\tan\beta$, *Phys. Rev.* **D 74** (2006) 015018 [hep-ph/0602242] [INSPIRE].

[29] I.F. Ginzburg and M. Krawczyk, *Symmetries of two Higgs doublet model and CP-violation*, *Phys. Rev.* **D 72** (2005) 115013 [hep-ph/0408011] [INSPIRE].

[30] D. Eriksson, J. Rathsman and O. Stal, 2*HDMC: two-Higgs-doublet model calculator physics and manual*, *Comput. Phys. Commun.* **181** (2010) 189 [arXiv:0902.0851] [INSPIRE].

[31] P. Bechtle, O. Brein, S. Heinemeyer, G. Weiglein and K. Williams, *New HiggsBounds from LEP and the Tevatron*, *AIP Conf. Proc.* **1200** (2010) 510 [arXiv:0909.4664] [INSPIRE].

[32] P. Bechtle, O. Brein, S. Heinemeyer, G. Weiglein and K.E. Williams, *Introducing HiggsBounds* 2.0.0, PoS(CHARGED 2010)027 [arXiv:1012.5170] [INSPIRE].

[33] P. Bechtle, O. Brein, S. Heinemeyer, G. Weiglein and K.E. Williams, *HiggsBounds: confronting arbitrary Higgs sectors with exclusion bounds from LEP and the Tevatron*, *Comput. Phys. Commun.* **181** (2010) 138 [arXiv:0811.4169] [INSPIRE].

[34] P. Bechtle, O. Brein, S. Heinemeyer, G. Weiglein and K.E. Williams, *HiggsBounds* 2.0.0*: confronting neutral and charged Higgs sector predictions with exclusion bounds from LEP and the Tevatron*, *Comput. Phys. Commun.* **182** (2011) 2605 [arXiv:1102.1898] [INSPIRE].

[35] P. Bechtle et al., *Recent developments in HiggsBounds and a preview of HiggsSignals*, PoS(CHARGED 2012)024 [arXiv:1301.2345] [INSPIRE].

[36] N.G. Deshpande and E. Ma, *Pattern of symmetry breaking with two Higgs doublets*, *Phys. Rev.* **D 18** (1978) 2574 [INSPIRE].

[37] M. Sher, *Electroweak Higgs potentials and vacuum stability*, *Phys. Rept.* **179** (1989) 273 [INSPIRE].

[38] A.W. El Kaffas, W. Khater, O.M. Ogreid and P. Osland, *Consistency of the two Higgs doublet model and CP-violation in top production at the LHC*, *Nucl. Phys.* **B 775** (2007) 45 [hep-ph/0605142] [INSPIRE].

[39] J. Bijnens, J. Lu and J. Rathsman, *Constraining general two Higgs doublet models by the evolution of Yukawa couplings*, *JHEP* **05** (2012) 118 [arXiv:1111.5760] [INSPIRE].

[40] I. Ginzburg and I. Ivanov, *Tree-level unitarity constraints in the most general* 2*HDM*, *Phys. Rev.* **D 72** (2005) 115010 [hep-ph/0508020] [INSPIRE].

[41] ATLAS collaboration, *Measurements of the properties of the Higgs-like boson in the* $WW^{(*)} \to \ell\nu\ell\nu$ *decay channel with the ATLAS detector using* $25\,\text{fb}^{-1}$ *of proton-proton collision data*, ATLAS-CONF-2013-030, CERN, Geneva Switzerland (2013).

[42] ATLAS collaboration, *Measurements of the properties of the Higgs-like boson in the two photon decay channel with the ATLAS detector using* $25\,\text{fb}^{-1}$ *of proton-proton collision data*, ATLAS-CONF-2013-012, CERN, Geneva Switzerland (2013).

JHEP01(2014)161

[43] ATLAS collaboration, *Measurements of the properties of the Higgs-like boson in the four lepton decay channel with the ATLAS detector using* $25\,\text{fb}^{-1}$ *of proton-proton collision data*, ATLAS-CONF-2013-013, CERN, Geneva Switzerland (2013).

[44] ATLAS collaboration, *Search for the Standard Model Higgs boson produced in association with top quarks in proton-proton collisions at* $\sqrt{s} = 7$ *TeV using the ATLAS detector*, ATLAS-CONF-2012-135, CERN, Geneva Switzerland (2012).

[45] ATLAS collaboration, *Search for the Standard Model Higgs boson produced in association with a vector boson and decaying to a b-quark pair with the ATLAS detector*, *Phys. Lett.* **B 718** (2012) 369 [arXiv:1207.0210] [INSPIRE].

[46] ATLAS collaboration, *Search for the Standard Model Higgs boson in the* $H \to \tau^+\tau^-$ *decay mode in* $\sqrt{s} = 7$ *TeV pp collisions with ATLAS*, *JHEP* **09** (2012) 070 [arXiv:1206.5971] [INSPIRE].

[47] CMS collaboration, *Updated measurements of the Higgs boson at* 125 *GeV in the two photon decay channel*, CMS-PAS-HIG-13-001, CERN, Geneva Switzerland (2013).

[48] CMS collaboration, *Properties of the Higgs-like boson in the decay* $H \to ZZ \to 4\ell$ *in pp collisions at* $\sqrt{s} = 7$ *and* 8 *TeV*, CMS-PAS-HIG-13-002, CERN, Geneva Switzerland (2013).

[49] CMS collaboration, *Evidence for a particle decaying to* W^+W^- *in the fully leptonic final state in a Standard Model Higgs boson search in pp collisions at the LHC*, CMS-PAS-HIG-13-003, CERN, Geneva Switzerland (2013).

[50] CMS collaboration, *Search for the Standard Model Higgs boson decaying to* τ *pairs in proton-proton collisions at* $\sqrt{s} = 7$ *and* 8 *TeV*, CMS-PAS-HIG-13-004, CERN, Geneva Switzerland (2013).

[51] CMS collaboration, *Search for Higgs boson production in association with top quark pairs in pp collisions*, CMS-PAS-HIG-12-025, CERN, Geneva Switzerland (2012).

[52] CMS collaboration, *Search for the Standard Model Higgs boson produced in association with W or Z bosons, and decaying to bottom quarks for HCP* 2012, CMS-PAS-HIG-12-044, CERN, Geneva Switzerland (2012).

[53] ALEPH, DELPHI, L3, OPAL and LEP Working Group for Higgs Boson Searches collaborations, S. Schael et al., *Search for neutral MSSM Higgs bosons at LEP*, *Eur. Phys. J.* **C 47** (2006) 547 [hep-ex/0602042] [INSPIRE].

[54] LEP Working Group for Higgs boson searches, ALEPH, DELPHI, L3 and OPAL collaborations, R. Barate et al., *Search for the Standard Model Higgs boson at LEP*, *Phys. Lett.* **B 565** (2003) 61 [hep-ex/0306033] [INSPIRE].

[55] LEP Higgs Working Group for Higgs boson searches, ALEPH, DELPHI, L3 and OPAL collaborations, *Search for charged Higgs bosons: preliminary combined results using LEP data collected at energies up to* 209 *GeV*, hep-ex/0107031 [INSPIRE].

[56] ALEPH collaboration, A. Heister et al., *Search for charged Higgs bosons in* e^+e^- *collisions at energies up to* $\sqrt{s} = 209$ *GeV*, *Phys. Lett.* **B 543** (2002) 1 [hep-ex/0207054] [INSPIRE].

[57] Tevatron New Physics Higgs Working Group, CDF and D0 collaborations, *Updated combination of CDF and D0 searches for Standard Model Higgs boson production with up to* $10.0\,\text{fb}^{-1}$ *of data*, arXiv:1207.0449 [INSPIRE].

[58] ATLAS collaboration, *Search for neutral MSSM Higgs bosons in* $\sqrt{s} = 7$ *TeV pp collisions at ATLAS*, ATLAS-CONF-2012-094, CERN, Geneva Switzerland (2012).

JHEP01(2014)161

[59] ATLAS collaboration, *Search for charged Higgs bosons decaying via $H^+ \to \tau\nu$ in top quark pair events using pp collision data at $\sqrt{s} = 7$ TeV with the ATLAS detector*, *JHEP* **06** (2012) 039 [arXiv:1204.2760] [INSPIRE].

[60] ATLAS collaboration, *Search for a light charged Higgs boson in the decay channel $H^+ \to c\bar{s}$ in $t\bar{t}$ events using pp collisions at $\sqrt{s} = 7$ TeV with the ATLAS detector*, *Eur. Phys. J.* **C 73** (2013) 2465 [arXiv:1302.3694] [INSPIRE].

[61] CMS collaboration, *Search for neutral Higgs bosons decaying to τ pairs in pp collisions at $\sqrt{s} = 7$ TeV*, *Phys. Lett.* **B 713** (2012) 68 [arXiv:1202.4083] [INSPIRE].

[62] CMS collaboration, *Search for MSSM neutral Higgs bosons decaying to τ pairs in pp collisions*, CMS-PAS-HIG-12-050, CERN, Geneva Switzerland (2012).

[63] CMS collaboration, *Search for a Higgs boson decaying into a b-quark pair and produced in association with b-quarks in proton-proton collisions at 7 TeV*, *Phys. Lett.* **B 722** (2013) 207 [arXiv:1302.2892] [INSPIRE].

[64] CMS collaboration, *Search for a light charged Higgs boson in top quark decays in pp collisions at $\sqrt{s} = 7$ TeV*, *JHEP* **07** (2012) 143 [arXiv:1205.5736] [INSPIRE].

[65] M.E. Peskin and T. Takeuchi, *A new constraint on a strongly interacting Higgs sector*, *Phys. Rev. Lett.* **65** (1990) 964 [INSPIRE].

[66] J.F. Gunion, H.E. Haber, G. Kane and S. Dawson, *The Higgs hunter's guide*, Addison-Wesley Publishing Company, U.S.A. (1990) [INSPIRE].

[67] Particle Data Group collaboration, K. Nakamura et al., *Review of particle physics*, *J. Phys.* **G 37** (2010) 075021 [INSPIRE].

[68] H.E. Logan, *Radiative corrections to the $Zb\bar{b}$ vertex and constraints on extended Higgs sectors*, hep-ph/9906332 [INSPIRE].

[69] ALEPH, CDF, D0, DELPHI, L3, OPAL, SLD, LEP Electroweak Working Group, Tevatron Electroweak Working Group and SLD Electroweak and Heavy Flavour Groups collaborations, *Precision electroweak measurements and constraints on the Standard Model*, arXiv:1012.2367 [INSPIRE].

[70] F. Mahmoudi, *SuperIso v2.3: a program for calculating flavor physics observables in supersymmetry*, *Comput. Phys. Commun.* **180** (2009) 1579 [arXiv:0808.3144] [INSPIRE].

[71] Particle Data Group collaboration, J. Beringer et al., *Review of particle physics (RPP)*, *Phys. Rev.* **D 86** (2012) 010001 [INSPIRE].

[72] Heavy Flavor Averaging Group collaboration, Y. Amhis et al., *Averages of B-hadron, C-hadron and τ-lepton properties as of early* 2012, arXiv:1207.1158 [INSPIRE].

[73] *Heavy Flavor Averaging Group online updates webpage*, http://www.slac.stanford.edu/xorg/hfag.

[74] Belle collaboration, I. Adachi et al., *Measurement of $B^- \to \tau^- \bar{\nu}_\tau$ with a hadronic tagging method using the full data sample of Belle*, *Phys. Rev. Lett.* **110** (2013) 131801 [arXiv:1208.4678] [INSPIRE].

[75] BaBar collaboration, P. del Amo Sanchez et al., *Measurement of the absolute branching fractions for $D_s^- \to \ell^- \bar{\nu}_\ell$ and extraction of the decay constant f_{D_s}*, *Phys. Rev.* **D 82** (2010) 091103 [arXiv:1008.4080] [INSPIRE].

JHEP01(2014)161

[76] LHCb collaboration, *Measurement of the $B_s^0 \to \mu^+\mu^-$ branching fraction and search for $B^0 \to \mu^+\mu^-$ decays at the LHCb experiment*, *Phys. Rev. Lett.* **111** (2013) 101805 [arXiv:1307.5024] [INSPIRE].

[77] BABAR collaboration, B. Aubert et al., *A search for the rare decay $B^0 \to \tau^+\tau^-$ at BABAR*, *Phys. Rev. Lett.* **96** (2006) 241802 [hep-ex/0511015] [INSPIRE].

[78] F. Mahmoudi and O. Stal, *Flavor constraints on the two-Higgs-doublet model with general Yukawa couplings*, *Phys. Rev.* **D 81** (2010) 035016 [arXiv:0907.1791] [INSPIRE].

[79] BABAR collaboration, J. Lees et al., *Evidence for an excess of $\bar{B} \to D^{(*)}\tau^-\bar{\nu}_\tau$ decays*, *Phys. Rev. Lett.* **109** (2012) 101802 [arXiv:1205.5442] [INSPIRE].

[80] M. Tanaka and R. Watanabe, *Tau longitudinal polarization in $B \to D\tau\nu$ and its role in the search for charged Higgs boson*, *Phys. Rev.* **D 82** (2010) 034027 [arXiv:1005.4306] [INSPIRE].

[81] V.D. Barger, J. Hewett and R. Phillips, *New constraints on the charged Higgs sector in two Higgs doublet models*, *Phys. Rev.* **D 41** (1990) 3421 [INSPIRE].

[82] D.L. Rainwater, D. Zeppenfeld and K. Hagiwara, *Searching for $H \to \tau^+\tau^-$ in weak boson fusion at the CERN LHC*, *Phys. Rev.* **D 59** (1998) 014037 [hep-ph/9808468] [INSPIRE].

[83] CMS collaboration, *Search for Higgs boson production in association with a top-quark pair and decaying to bottom quarks or tau leptons*, CMS-PAS-HIG-13-019, CERN, Geneva Switzerland (2013).

[84] ATLAS collaboration, *Search for the bb decay of the Standard Model Higgs boson in associated W/ZH production with the ATLAS detector*, ATLAS-CONF-2013-079, CERN, Geneva Switzerland (2013).

[85] ATLAS collaboration, *Search for the Standard Model Higgs boson produced in association with top quarks in proton-proton collisions at $\sqrt{s} = 7$ TeV using the ATLAS detector*, ATLAS-CONF-2012-135, CERN, Geneva Switzerland (2012).

[86] CDF and D0 collaboration, T. Aaltonen et al., *Higgs boson studies at the Tevatron*, *Phys. Rev.* **D 88** (2013) 052014 [arXiv:1303.6346] [INSPIRE].

[87] N.D. Christensen, T. Han and S. Su, *MSSM Higgs bosons at the LHC*, *Phys. Rev.* **D 85** (2012) 115018 [arXiv:1203.3207] [INSPIRE].

JHEP01(2014)161

Appendix B

Anatomy of Exotic Higgs Decays in 2HDM

The article *Anatomy of Exotic Higgs Decays in 2HDM* has been submitted to aXiv [22] and is currently under review in the Journal of High Energy Physics.

Prepared for submission to JHEP

FERMILAB-PUB-16-093-T

Anatomy of Exotic Higgs Decays in 2HDM

Felix Kling,[a,b] **Jose Miguel No,**[c] **Shufang Su**[a]

[a] *Department of Physics, University of Arizona, Tucson, Arizona 85721, USA*
[b] *Fermilab, P.O. Box 500, Batavia, IL 60510, USA*
[c] *Department of Physics and Astronomy, University of Sussex, Brington, BN1 9QH, UK*
E-mail: kling@email.arizona.edu, J.M.No@sussex.ac.uk, shufang@email.arizona.edu

Abstract: Large mass splittings between new scalars in two-Higgs-doublet models (2HDM) open a key avenue to search for these new states via exotic heavy Higgs decays. We discuss in detail the different search channels for these new scalars at the LHC in the presence of a sizable mass splitting, *i.e.* a hierarchical 2HDM scenario, taking into account the theoretical and experimental constraints. We provide benchmark planes to exploit the complementarity among these searches, analyzing their potential to probe the hierarchical 2HDM parameter space during LHC Run 2.

Contents

1 Introduction

Analyses of the results from the LHC 7-8 TeV run by both ATLAS and CMS show that the properties of the Higgs particle at $m_h \sim 125$ GeV are close to those expected for the Standard Model (SM) Higgs boson $h_{\rm SM}$ [1, 2]. The complete nature of the scalar sector responsible for electroweak (EW) symmetry-breaking, however, remains to be determined, and it is particularly interesting to ascertain whether the Higgs sector consists of only one $\mathrm{SU}(2)_L$ scalar doublet or has a richer structure containing additional states. Addressing this question is a key task for present and future studies at the Large Hadron Collider (LHC).

Two Higgs doublet models (2HDM) constitute the prime example of a well-motivated extended Higgs sector, appearing in many extensions of the SM such as the MSSM [3], composite Higgs models [4] and viable EW baryogenesis scenarios [5]. In addition to the SM-like CP-even Higgs boson, the 2HDM spectrum contains one more CP-even Higgs, a CP-odd Higgs and a pair of charged ones*. In recent years, its allowed parameter space has been scrutinized in light of ATLAS/CMS Higgs coupling measurements and searches for extra Higgses at the LHC [6–15].

A key avenue to probe the 2HDM heavy Higgs bosons at the LHC which has started to attract attention recently is the search for exotic decays of the heavy Higgses in the presence of a sizable mass splitting among them [16–21] (see also [15])†. While the conventional decay channels of a heavy Higgs into two SM quarks, leptons or gauge bosons have been the focus of most of the existing searches, the exotic (non-SM) modes of a heavy Higgs decaying into two light Higgses, or one light Higgs with one SM gauge boson quickly dominate once they are kinematically open. The current exclusion bounds on extra Higgses based on their conventional decays only will be therefore significantly relaxed. On the other hand, the exotic decay modes offer new discovery channels, which have already shown exclusion power during the 8 TeV LHC run [22, 23], and yield very promising prospects for the 13 TeV LHC run. In this work, we aim to provide a comprehensive categorization and analysis of the exotic search channels for the new 2HDM scalars, highlighting the complementarity among them, and provide guiding benchmark planes for Run 2 of the LHC at 13 TeV.

After a review of the 2HDM in Section 2, we present the constraints on the 2HDM parameter space coming from theoretical considerations (stability of the EW minimum, perturbativity and tree-level unitarity) and experimental measurements in Section 3, where we also introduce the salient features of our benchmark scenarios for exotic 2HDM Higgs decays (Section 3.6) motivated by the theoretical and experimental constraints. In Section 4 we discuss the production and decay of non-SM Higgses at the LHC, and then analyze in depth our different benchmark scenarios in Section 5, before concluding in Section 6.

*Here we take the assumption of a CP-conserving 2HDM. In the case of CP-violation, the three neutral Higgses are mixed together to form three mass eigenstates without definite CP properties.

†Incidentally, it has been shown in [18] that sizable mass splittings between the 2HDM new scalars favour a strong EW phase transition that could lead to baryogenesis.

2 Two Higgs Doublet Models: A Review

2.1 2HDM Lagrangian and Higgs Potential

In the 2HDM, we introduce two $\mathrm{SU}(2)_L$ doublets Φ_i $(i = 1, 2)$:

$$\Phi_i = \begin{pmatrix} \phi_i^+ \\ (v_i + \phi_i^0 + i\varphi_i)/\sqrt{2} \end{pmatrix}, \tag{2.1}$$

where v_i are the vacuum expectation values (vev) of the neutral components, satisfying $v_1^2 + v_2^2 = v^2$, with $v = 246$ GeV. The ratio of vevs is defined as $\tan\beta \equiv v_2/v_1$. The 2HDM Lagrangian for Φ_i can be written as

$$\mathcal{L} = \sum_i |D_\mu \Phi_i|^2 - V(\Phi_1, \Phi_2) + \mathcal{L}_{\mathrm{Yuk}}, \tag{2.2}$$

where the first term denotes the kinetic term for the two Higgs doublets, $V(\Phi_1, \Phi_2)$ is the Higgs potential and the last term denotes the Yukawa interactions between Φ_i and the SM fermions. Assuming CP conservation and a soft $\mathbb{Z}_2$ symmetry breaking, the 2HDM Higgs potential can be written down as[‡]:

$$\begin{aligned} V(\Phi_1, \Phi_2) = {} & m_{11}^2 \Phi_1^\dagger \Phi_1 + m_{22}^2 \Phi_2^\dagger \Phi_2 - m_{12}^2 (\Phi_1^\dagger \Phi_2 + \mathrm{h.c.}) + \frac{\lambda_1}{2} (\Phi_1^\dagger \Phi_1)^2 + \frac{\lambda_2}{2} (\Phi_2^\dagger \Phi_2)^2 \\ & + \lambda_3 (\Phi_1^\dagger \Phi_1)(\Phi_2^\dagger \Phi_2) + \lambda_4 (\Phi_1^\dagger \Phi_2)(\Phi_2^\dagger \Phi_1) + \frac{1}{2} \left[\lambda_5 (\Phi_1^\dagger \Phi_2)^2 + \mathrm{h.c.} \right]. \end{aligned} \tag{2.3}$$

After EW symmetry breaking, the physical 2HDM scalar spectrum consists of five states: two CP-even Higgses h, H with $m_h < m_H$, a CP-odd scalar A and a charged scalar pair $H^\pm$ [24], which may be written as

$$\begin{aligned} \begin{pmatrix} H \\ h \end{pmatrix} &= \begin{pmatrix} c_\alpha & s_\alpha \\ -s_\alpha & c_\alpha \end{pmatrix} \begin{pmatrix} \phi_1^0 \\ \phi_2^0 \end{pmatrix}, \\ \begin{pmatrix} G \\ A \end{pmatrix} = \begin{pmatrix} c_\beta & s_\beta \\ -s_\beta & c_\beta \end{pmatrix} \begin{pmatrix} \varphi_1 \\ \varphi_2 \end{pmatrix}, \quad & \begin{pmatrix} G^\pm \\ H^\pm \end{pmatrix} = \begin{pmatrix} c_\beta & s_\beta \\ -s_\beta & c_\beta \end{pmatrix} \begin{pmatrix} \phi_1^\pm \\ \phi_2^\pm \end{pmatrix}, \end{aligned} \tag{2.4}$$

with the angle α parametrizing the mixing between the neutral CP-even components (we use the shorthand notation $s_x \equiv \sin x$, $c_x \equiv \cos x$, $t_x \equiv \tan x$). The Goldstone bosons G and $G^\pm$ are absorbed as longitudinal components of the Z and $W^\pm$ bosons. In the limit $c_{\beta-\alpha} = 0$ (the *alignment limit* for h), the state h can be identified with the SM Higgs, its couplings to fermions and gauge bosons being precisely those predicted by the SM[§]. It is thus convenient to describe the model in terms of t_β, $c_{\beta-\alpha}$, the physical scalar masses

[‡]The most general scalar potential also contains the terms $\left[\lambda_6 (\Phi_1^\dagger \Phi_1) + \lambda_7 (\Phi_2^\dagger \Phi_2)\right] (\Phi_1^\dagger \Phi_2)$+h.c. (leading to potentially dangerous flavour changing neutral currents), which can however be forbidden by imposing a $\mathbb{Z}_2$ symmetry, softly broken by the m_{12}^2 term.

[§]We note that if the heavier neutral CP even Higgs H is identified with the observed 125 GeV SM-like Higgs, the alignment limit is instead described by $s_{\beta-\alpha} = 0$ [25].

$m_h, m_H, m_A, m_{H^\pm}$, the soft $\mathbb{Z}_2$ symmetry breaking parameter m_{12}^2 and the vev v. The quartic couplings in Eq. (2.3) can be expressed in terms of the physical masses and mixing angles as (see e.g. [26])

$$
\begin{aligned}
v^2\lambda_1 &= \frac{m_H^2 c_\alpha^2 + m_h^2 s_\alpha^2 - m_{12}^2 t_\beta}{c_\beta^2}, \quad v^2\lambda_2 = \frac{m_H^2 s_\alpha^2 + m_h^2 c_\alpha^2 - m_{12}^2 t_\beta^{-1}}{s_\beta^2}, \\
v^2\lambda_3 &= \frac{(m_H^2 - m_h^2) s_\alpha c_\alpha + 2m_{H^\pm}^2 s_\beta c_\beta - m_{12}^2}{s_\beta c_\beta}, \quad v^2\lambda_4 = \frac{(m_A^2 - 2m_{H^\pm}^2) s_\beta c_\beta + m_{12}^2}{s_\beta c_\beta}, \\
v^2\lambda_5 &= \frac{-m_A^2 s_\beta c_\beta + m_{12}^2}{s_\beta c_\beta}\,.
\end{aligned}
\tag{2.5}
$$

2.2 Interactions in the 2HDM

The couplings of the CP-even scalars to a pair of gauge bosons, arising from the Higgs kinetic term in Eq. (2.2), are [24]

$$
g_{hZZ} = \frac{2im_Z^2}{v} s_{\beta-\alpha}, \quad g_{HZZ} = \frac{2im_Z^2}{v} c_{\beta-\alpha}, \quad g_{hWW} = \frac{2im_W^2}{v} s_{\beta-\alpha}, \quad g_{HWW} = \frac{2im_W^2}{v} c_{\beta-\alpha}. \tag{2.6}
$$

The CP-odd scalar A does not couple to pairs of vector bosons, while the charged scalar $H^\pm$ only couples to pair of vector bosons at loop level. In addition, the couplings of two scalars and one vector boson read

$$
\begin{aligned}
g_{hAZ} &= \frac{m_Z}{v} c_{\beta-\alpha}(p_A^\mu - p_h^\mu), & g_{HAZ} &= -\frac{m_Z}{v} s_{\beta-\alpha}(p_A^\mu - p_H^\mu), \\
g_{hH^\pm W^\mp} &= \pm\frac{im_W}{v} c_{\beta-\alpha}(p_{H^+}^\mu - p_h^\mu), & g_{HH^\pm W^\mp} &= \mp\frac{im_W}{v} s_{\beta-\alpha}(p_{H^+}^\mu - p_H^\mu), \\
g_{AH^\pm W^\mp} &= \frac{m_W}{v}(p_{H^+}^\mu - p_A^\mu),
\end{aligned}
\tag{2.7}
$$

in which p^μ are the outgoing momentum for the corresponding particle. The hHZ-coupling is absent due to CP conservation. We note that, considering h (H) to be the SM-like 125 GeV Higgs with $c_{\beta-\alpha} = 0$ ($s_{\beta-\alpha} = 0$), gauge boson couplings to two non-SM like Higgses are unsuppressed, while the gauge boson couplings to h (H) and one non-SM like Higgs are suppressed by $c_{\beta-\alpha}$ ($s_{\beta-\alpha}$).

Regarding the cubic couplings among scalars arising from the 2HDM scalar potential Eq. (2.3), the relevant ones for our analysis are

$$
\begin{aligned}
g_{Hhh} &= -\frac{1}{4\, s_{2\beta}\, v}\Big(\frac{4m_{12}^2}{s_\beta c_\beta}(c_{\beta-\alpha}^2 s_{\beta+\alpha} - 2s_{\beta-\alpha}c_{\beta-\alpha}c_{\beta+\alpha}) - (2m_h^2 + m_H^2)(s_{3\alpha-\beta} + s_{\alpha+\beta})\Big), \\
g_{HAA} &= -\frac{1}{4\, s_{2\beta}\, v}\Big(\frac{4m_{12}^2}{s_\beta c_\beta} s_{\beta+\alpha} - 8m_A^2 c_{\beta-\alpha} s_\beta c_\beta - m_H^2(s_{\alpha-3\beta} + 3s_{\alpha+\beta})\Big), \\
g_{HH^+H^-} &= -\frac{1}{4\, s_{2\beta}\, v}\Big(\frac{4m_{12}^2}{s_\beta c_\beta} s_{\beta+\alpha} - 8m_{H^\pm}^2 c_{\beta-\alpha} s_\beta c_\beta - m_H^2(s_{\alpha-3\beta} + 3s_{\alpha+\beta})\Big),
\end{aligned}
\tag{2.8}
$$

which could mediate decays with H being the parent scalar: $H \to hh$, $H \to AA$ and $H \to H^+H^-$. As seen directly from Eq. (2.8), these couplings depend not only on the

mass spectrum, but also on the soft $\mathbb{Z}_2$ symmetry breaking term m_{12}^2 (we note here that the couplings shown in [24] assume the MSSM relation $m_{12}^2 = m_A^2 s_\beta c_\beta$). We also stress that for a light CP-odd scalar A with $m_A < m_h/2$, the decay channel $h \to AA$ could be open, being however very constrained experimentally[¶] (see [28] for a discussion of this region of the 2HDM parameter space).

State	Up-type fermions	Down-type fermions
h	$c_\alpha/s_\beta = s_{\beta-\alpha} + c_{\beta-\alpha}/t_\beta$	$-s_\alpha/c_\beta = s_{\beta-\alpha} - c_{\beta-\alpha}\, t_\beta$
H	$s_\alpha/s_\beta = c_{\beta-\alpha} - s_{\beta-\alpha}/t_\beta$	$c_\alpha/c_\beta = c_{\beta-\alpha} + s_{\beta-\alpha}\, t_\beta$
A	$1/t_\beta$	t_β

Table 1. Tree-level couplings to up-type fermions and down-type fermions normalized to their SM values for h, H and A in the Type II 2HDM.

Finally, as is well-known the couplings of the 2HDM scalars to SM fermions, contained in $\mathcal{L}_{\rm Yuk}$ in Eq. (2.2) are not univocally determined by the gauge structure of the model. In the presence of a $\mathbb{Z}_2$ symmetry guaranteeing the absence of tree-level flavour changing neutral currents [29], four possible 2HDM types exist (see [30] for a discussion). The couplings of the neutral scalar states to SM fermions, normalized to their SM values, can be expressed in terms of functions of α and β, shown in Table 1 for the particular case of a Type II 2HDM (one Higgs doublet Φ_2 couples to the up-type quarks, while the other Higgs doublet Φ_1 couples to the down-type quarks and leptons).

2.3 The Alignment Limit and the Role of m_{12}^2

It is useful to cast the relations between the quartic couplings and the physical masses Eq. (2.5) in terms of $c_{\beta-\alpha}$, which characterizes the departure from the alignment limit for h

$$
\begin{aligned}
v^2\lambda_1 &= m_h^2 - \frac{t_\beta\,(m_{12}^2 - m_H^2 s_\beta c_\beta)}{c_\beta^2} + (m_h^2 - m_H^2)\left[c_{\beta-\alpha}^2(t_\beta^2 - 1) - 2t_\beta s_{\beta-\alpha}c_{\beta-\alpha}\right], \\
v^2\lambda_2 &= m_h^2 - \frac{(m_{12}^2 - m_H^2 s_\beta c_\beta)}{t_\beta s_\beta^2} + (m_h^2 - m_H^2)\left[c_{\beta-\alpha}^2(t_\beta^{-2} - 1) + 2t_\beta^{-1} s_{\beta-\alpha}c_{\beta-\alpha}\right], \\
v^2\lambda_3 &= m_h^2 + 2m_{H^\pm}^2 - 2m_H^2 - \frac{(m_{12}^2 - m_H^2 s_\beta c_\beta)}{s_\beta c_\beta} - (m_h^2 - m_H^2)\left[2c_{\beta-\alpha}^2 + s_{\beta-\alpha}c_{\beta-\alpha}(t_\beta - t_\beta^{-1})\right], \\
v^2\lambda_4 &= m_A^2 - 2m_{H^\pm}^2 + m_H^2 + \frac{(m_{12}^2 - m_H^2 s_\beta c_\beta)}{s_\beta c_\beta}, \\
v^2\lambda_5 &= m_H^2 - m_A^2 + \frac{(m_{12}^2 - m_H^2 s_\beta c_\beta)}{s_\beta c_\beta}.
\end{aligned}
\tag{2.9}
$$

Current data from LHC Run 1 favour the alignment limit $c_{\beta-\alpha} = 0$ [31] (see also [6–8, 10–12, 14]). For a Type II 2HDM the only other allowed possibility is the *wrong-sign*

[¶]The possibility of a light charged scalar with $m_{H^\pm} < m_h/2$ has been ruled out experimentally by LEP, which puts a lower bound $m_{H^\pm} > 80$ GeV for Type II ($m_{H^\pm} > 72$ GeV for Type I) 2HDM [27], thus forbidding the decay $h \to H^+H^-$.

scenario [32] $s_{\beta+\alpha} \simeq 1$ (compatible with measurements of Higgs signal strengths for $t_\beta > 3$). For $c_{\beta-\alpha} = 0$, the relations Eq. (2.9) simply become

$$\begin{aligned}
v^2\lambda_1 &= m_h^2 - \frac{t_\beta\,(m_{12}^2 - m_H^2 s_\beta c_\beta)}{c_\beta^2}\,,\\
v^2\lambda_2 &= m_h^2 - \frac{(m_{12}^2 - m_H^2 s_\beta c_\beta)}{t_\beta s_\beta^2}\,,\\
v^2\lambda_3 &= m_h^2 + 2m_{H^\pm}^2 - 2m_H^2 - \frac{(m_{12}^2 - m_H^2 s_\beta c_\beta)}{s_\beta c_\beta}\,,\\
v^2\lambda_4 &= m_A^2 - 2m_{H^\pm}^2 + m_H^2 + \frac{(m_{12}^2 - m_H^2 s_\beta c_\beta)}{s_\beta c_\beta}\,,\\
v^2\lambda_5 &= m_H^2 - m_A^2 + \frac{(m_{12}^2 - m_H^2 s_\beta c_\beta)}{s_\beta c_\beta}\,.
\end{aligned} \tag{2.10}$$

The combination $m_{12}^2 - m_H^2 s_\beta c_\beta$ in Eq. (2.10) will play a key role in the following discussion: the value of m_{12}^2 is not fixed by the mass spectrum or the scalar couplings to gauge bosons and fermions, only entering the trilinear scalar couplings Eq. (2.8). Its possible allowed values are dictated by theoretical constraints on the 2HDM parameter space, namely the boundedness from below of the scalar potential Eq. (2.3) and the stability of the EW minimum, and the requirements of perturbativity and tree-level unitarity on the quartic couplings λ_i, as shown in the next section. These have a large impact on the allowed values of masses m_H, m_A, $m_{H^\pm}$, m_{12}^2 and t_β (and $c_{\beta-\alpha}$ away from alignment), as the absence of a value of m_{12}^2 satisfying the theoretical constraints for a given set of values for m_H, m_A, $m_{H^\pm}$ and t_β, indicates that such set of values is not physically viable (see e.g. [15]).

3 2HDM Theoretical and Experimental Constraints

3.1 Vacuum Stability

In order to have a stable vacuum, the following conditions need to be fulfilled [26]

$$\lambda_1 > 0\,, \quad \lambda_2 > 0\,, \quad \lambda_3 > -\sqrt{\lambda_1\lambda_2}\,, \quad \lambda_3 + \lambda_4 + |\lambda_5| > -\sqrt{\lambda_1\lambda_2}\,. \tag{3.1}$$

For $c_{\beta-\alpha} = 0$, satisfying the first two conditions requires $m_{12}^2 - m_H^2 s_\beta c_\beta \lesssim 0$ for either $t_\beta > 1$ or $t_\beta < 1$, as seen from Eq. (2.10). Moreover, Eq. (2.9) shows that a departure from alignment generically has a negative impact on the first two stability conditions. Focusing on the alignment limit, the first two requirements are automatically satisfied for $m_{12}^2 - m_H^2 s_\beta c_\beta = 0$, with the last two given by

$$m_h^2 + m_{H^\pm}^2 - m_H^2 > 0 \quad , \qquad m_h^2 + m_A^2 - m_H^2 > 0\,. \tag{3.2}$$

This implies that for $m_H > m_A, m_{H^\pm}$, the mass splittings between the heavy CP-even Higgs H and the other heavy scalars A and $H^\pm$ have to be small, such that the decays of H into AZ, AA, H^+H^- or $H^\pm W^\mp$ are not kinematically allowed. For $m_{12}^2 = 0$ all four stability conditions of Eq. (3.1) are automatically fulfilled. The allowed region in

the m_{12} vs. t_β plane is shown in the left panel of Figure 1 for $m_A = m_{H^\pm} = 400$ GeV and $m_H = 200,\ 300,\ 400$ GeV as an illustration. As seen from Figure 1, the regions $m_{12}^2 < m_H^2 s_\beta c_\beta$ are generically allowed by the vacuum stability requirement.

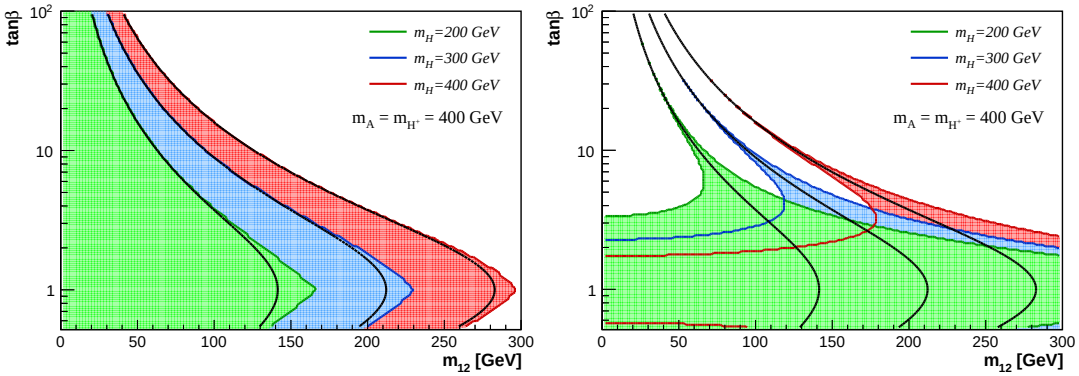

Figure 1. Allowed region in the $(m_{12},\ t_\beta)$ plane from vacuum stability (left panel) and unitarity $|\Lambda_i| < 8\pi$ (right panel) for $m_H = 400$ GeV (red), 300 GeV (blue) and 200 GeV (green), assuming $c_{\beta-\alpha} = 0$ and $m_A = m_{H^\pm} = 400$ GeV. The black lines denote the relation $m_{12}^2 = m_H^2 s_\beta c_\beta$.

3.2 Perturbativity and Unitarity

Upon imposing the perturbativity condition $|\lambda_i| \leq 4\pi$, the strongest constraints in the alignment limit come respectively from $v^2\lambda_1 \sim t_\beta^3(m_{12}^2 - m_H^2 s_\beta c_\beta)$ for $t_\beta \gg 1$ and $v^2\lambda_2 \sim t_\beta^{-3}(m_{12}^2 - m_H^2 s_\beta c_\beta)$ for $t_\beta \ll 1$. Thus, perturbativity requires $\left|m_{12}^2 - m_H^2 s_\beta c_\beta\right| \lesssim v^2$ unless $t_\beta \sim 1$. Moreover, even for $m_{12}^2 = m_H^2 s_\beta c_\beta$, perturbativity of λ_{3-5} imposes constraints on the size of the mass splittings among the new scalars.

Even stronger constraints are found when requiring tree-level unitarity of the scattering matrix in the 2HDM scalar sector [33]. The eigenvalues of the scattering matrix read

$$\begin{aligned}
\Lambda_{1,2} &= \lambda_3 \pm \lambda_4, \\
\Lambda_{3,4} &= \lambda_3 \pm \lambda_5, \\
\Lambda_{5,6} &= \lambda_3 + 2\lambda_4 \pm 3\lambda_5, \\
\Lambda_{7,8} &= \frac{1}{2}\left(\lambda_1 + \lambda_2 \pm \sqrt{(\lambda_1 - \lambda_2)^2 + 4\lambda_4^2}\right), \\
\Lambda_{9,10} &= \frac{1}{2}\left(\lambda_1 + \lambda_2 \pm \sqrt{(\lambda_1 - \lambda_2)^2 + 4|\lambda_5|^2}\right), \\
\Lambda_{11,12} &= \frac{1}{2}\left(3(\lambda_1 + \lambda_2) \pm \sqrt{9(\lambda_1 - \lambda_2)^2 + 4(2\lambda_3 + \lambda_4)^2}\right),
\end{aligned} \tag{3.3}$$

and for the S-matrix to be unitary (at tree-level), it is necessary that $|\Lambda_i| < 8\pi$[‖] [33]. A quick inspection of Eq. (3.3) shows that for $t_\beta \gg 1$ the scattering matrix eigenvalues scale as $\Lambda_{7,9,11} \sim \lambda_1$ (particularly $\Lambda_{11} \simeq 3\,\lambda_1$), which again imposes $\left|m_{12}^2 - m_H^2 s_\beta c_\beta\right| \lesssim v^2$ (and yields an even stronger constraint than the perturbativity one). A similar argument follows

[‖] We note that the 2HDMC Code [34] uses $|\Lambda_i| < 16\pi$ as tree-level unitarity condition, which results in the perturbativity constraint being more important.

for $t_\beta \ll 1$, this time with $\Lambda_{7,9,11} \sim \lambda_2$. As a result, $m_{12}^2 \approx m_H^2 s_\beta c_\beta$ is strongly preferred unless $t_\beta \sim 1$, as shown explicitly in the right panel of Figure 1 (for $m_A = m_{H^\pm}$). In the limit $m_{12}^2 = m_H^2 s_\beta c_\beta$, the scattering matrix eigenvalues from Eq. (3.3) become independent of t_β (in alignment $c_{\beta-\alpha} = 0$) and read

$$\begin{aligned}
&\Lambda_{1(9),10} v^2 = m_h^2 \mp m_H^2 \pm m_A^2, && \Lambda_2 v^2 = m_h^2 - 3m_H^2 - m_A^2 + 4m_{H^\pm}^2, \\
&\Lambda_3 v^2 = m_h^2 - m_H^2 - m_A^2 + 2m_{H^\pm}^2, && \Lambda_{4,5} v^2 = m_h^2 \mp 3m_H^2 \pm m_A^2 \pm 2m_{H^\pm}^2, \\
&\Lambda_6 v^2 = m_h^2 - 3m_H^2 + 5m_A^2 - 2m_{H^\pm}^2, && \Lambda_{7,8} v^2 = m_h^2 \pm m_H^2 \pm m_A^2 \mp 2m_{H^\pm}^2, \\
&\Lambda_{11} v^2 = 5m_h^2 - 3\, m_H^2 + m_A^2 + 2m_{H^\pm}^2, && \Lambda_{12} v^2 = m_h^2 + 3m_H^2 - m_A^2 - 2m_{H^\pm}^2,
\end{aligned} \tag{3.4}$$

such that $|\Lambda_i| < 8\pi$ impose upper limits on the mass splittings (although not on the masses themselves). We also note that for $m_{12}^2 = 0$, Λ_{1-6} are independent of t_β (depending only on the scalar masses) while Λ_{7-12} do depend on t_β, which once again results in $t_\beta \approx 1$ being the only accessible region for large mass splittings in this case.

3.3 Electroweak Precision Measurements

Measurements of EW precision observables (EWPO) impose strong constraints on the 2HDM mass spectrum. Adopting the current 95% C.L. constraints on the S and T oblique parameters (with $U = 0$) [35], the allowed region of parameter space in the (m_A, $m_{H^\pm}$) plane is shown, for $c_{\beta-\alpha} = 0$ (neither t_β nor m_{12}^2 affect S and T), in the left panel of Figure 2 respectively for $m_H = 400$ GeV (red), $m_H = 300$ GeV (blue) and $m_H = 200$ GeV (green). Satisfying EWPO constraints requires the charged scalar mass to be close to one of the heavy neutral scalar masses: $m_{H^\pm} \approx m_H$ or $m_{H^\pm} \approx m_A$.

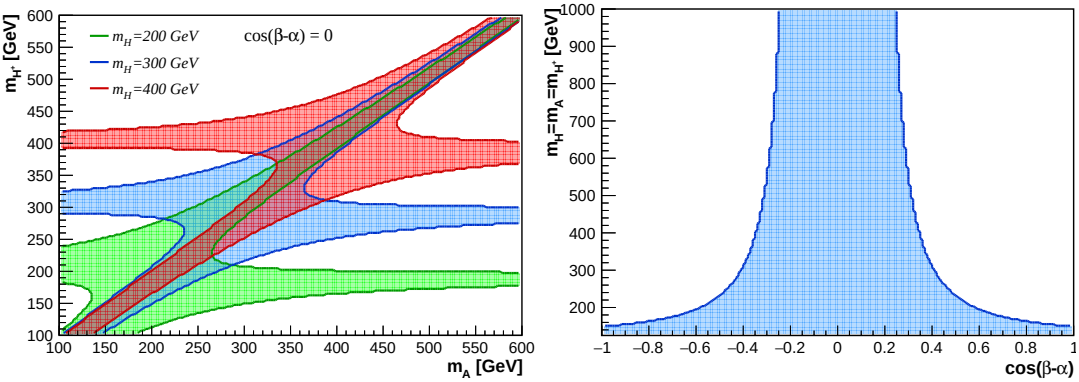

Figure 2. Left: 2HDM parameter space in the (m_A, $m_{H^\pm}$) plane allowed at 95% C.L. by S and T measurements [35], for $m_H = 400$ GeV (red), $m_H = 300$ GeV (blue) and $m_H = 200$ GeV (green), assuming $c_{\beta-\alpha} = 0$. Right: $S - T$ constraints in the ($c_{\beta-\alpha}$, m_H) plane for $m_H = m_A = m_{H^\pm}$.

Away from the alignment limit, additional contributions to S and T proportional to $c_{\beta-\alpha}$ appear [24] (see also [36]), such that the scenario $m_H = m_A = m_{H^\pm}$ is only allowed for small $|c_{\beta-\alpha}|$ once $m_H \gg v$ is realized, as shown in the right panel of Figure 2. The departure from alignment also allows for mild mass splittings among all the new scalars (e.g. $m_A > m_H + m_Z$ and $m_H \gtrsim m_{H^\pm} + m_W$), which however does not significantly alter the phenomenology of exotic Higgs decays at the LHC, discussed in detail in Section 5.

3.4 Flavour Constraints

Various flavour measurements [37] provide indirect constraints on the charged scalar mass $m_{H^\pm}$ as a function of t_β. The different limits are computed for the case of a Type II 2HDM with SuperIso [38, 39], and shown in the left panel of Figure 3. The most stringent of these[**] comes from the measurement of the branching fraction (BR) of $b \to s\gamma$ ($B_d^0 \to X_s\gamma$), which sets a limit $m_{H^\pm} > 480$ GeV at 95 % C.L. [43] (we note that the limit is even stronger for $t_\beta < 2$). For large $t_\beta \gtrsim 20$, the lower limit on $m_{H^\pm}$ set by the measurement of the branching fraction $B_d^+ \to \tau^+\nu$ is significantly stronger, with $m_{H^\pm} \gtrsim 700$ GeV for $t_\beta = 30$. Similarly, the region $t_\beta \lesssim 1$ is very strongly constrained by $B_s^0 \to \mu\mu$ and Δm_{B_d}.

For $m_H = 125$ GeV and $s_{\beta-\alpha} = 0$, when the heavy CP-even scalar H is the SM-like Higgs, the mass of the light CP-even Higgs h is constrained by flavour measurements as well, as shown in the right panel of Figure 3 for Type II 2HDM. The strongest constraint in this case comes from $B_s^0 \to \mu^+\mu^-$, which can exclude up to $m_h < 100$ GeV (the precise bound depending on m_{12}^2 and t_β) for masses $m_{H^\pm}$ satisfying the $b \to s\gamma$ constraint.

Note that flavour constraints are typically very model dependent. Contributions from additional sectors in the model could relax the constraints, as has e.g. been studied in the MSSM framework for $b \to s\gamma$ [44]. Being mostly focused on the collider aspects of 2HDM Higgses, we will not consider flavour as a hard constraint in the following, however indicating its effect on the parameter space under consideration.

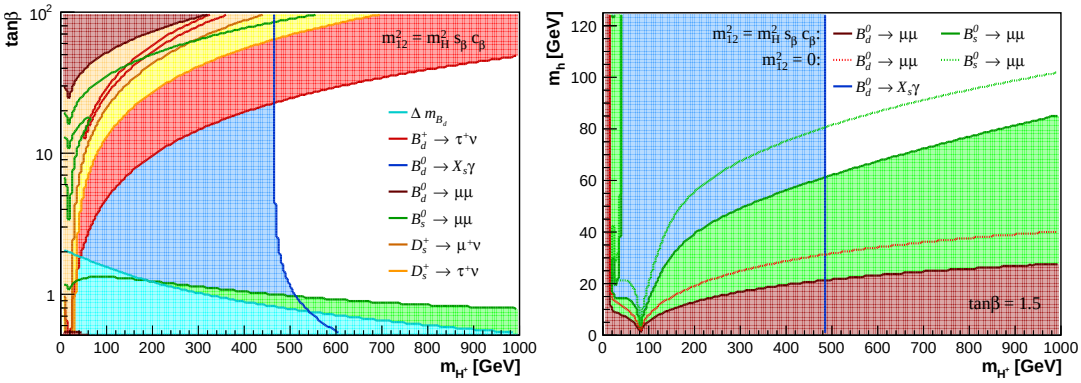

Figure 3. Type II 2HDM parameter space excluded by flavour constraints (see text for details).

3.5 LHC and LEP Constraints

We now review the constraints from direct searches of the new scalars. Besides the LEP bound $m_{H^\pm} > 80$ GeV (72 GeV) for Type II (I) 2HDM [27], LEP searches for $e^+e^- \to A\,H$ ($H \to bb/\tau\tau$, $A \to bb/\tau\tau$) constrain the sum of the masses $m_A + m_H \gtrsim 209$ GeV [45]. At the LHC, the searches for A/H in bb-associated production and decaying to $\tau\tau$ by

[**]We note here that the recent measurement from the BaBar Collaboration of the ratios of $B \to D^*\tau\nu$ to $B \to D^*\ell\nu$ decays and $B \to D\tau\nu$ to $B \to D\ell\nu$ decays cannot be accommodated within the Type II 2HDM [40]. However, a new measurement of the former ratio by the Belle Collaboration [41, 42] is in tension with this conclusion. Since this matter is not settled yet, we choose not to include these flavour measurements in our discussion.

ATLAS/CMS [46, 47] constrain the high t_β region in the Type II 2HDM. Away from alignment, searches by ATLAS/CMS for $H \to W^+W^-, ZZ$ [48–50], $A \to hZ\,(h \to bb)$ [51, 52] and $H \to hh \to bb\gamma\gamma, bbbb$ [53–55] yield strong constraints on the $(c_{\beta-\alpha}, t_\beta)$ plane as a function of the respective mass m_H/m_A (see e.g. [13, 15]). We however stress that the limits summarized above can be significantly weakened once exotic Higgs decay channels are open [15–17, 19, 21]). Searches for these new channels, e.g. via $A/H \to HZ/AZ$ are then crucial for probing 2HDM scenarios with large mass splittings among the new states (i.e. hierarchical 2HDM scenarios), and there is already ongoing effort by CMS in this direction [22, 23].

Finally, ATLAS/CMS searches impose constraints on the charged scalar [56, 57] beyond those of LEP. A light charged scalar $m_{H^\pm} \lesssim m_t$ is mostly excluded by the non-observation of the decay $t \to H^+b \to \tau\nu b$ where the top is produced in top pair production. For $m_{H^\pm} > m_t$, the current limit is very weak and only constrains the high t_β region for $m_{H^\pm}$ not much above the top mass (see [19] for a detailed discussion).

3.6 From Constraints to 2HDM Benchmarks

The combination of previous constraints provides a key guideline to the design of simplified 2HDM benchmark scenarios for LHC Run 2 searches at 13 TeV. EWPO measurements require the mass of the charged scalar to be close to the mass of one of the neutral scalars, and so we fix $m_{H^\pm} = m_H$ or $m_{H^\pm} = m_A$ in the following. In addition, measurements of Higgs signal strengths at the LHC favour the alignment limit ($c_{\beta-\alpha} = 0$ if h is the 125 GeV SM-like Higgs), particularly for Type II 2HDM. We then focus our analysis mostly on the alignment limit, and only consider deviations from alignment when discussing possible decays of the new scalars into the SM-like Higgs h.

Regarding the impact of theoretical constraints on the 2HDM parameter space, the previous discussion shows that satisfying unitarity/perturbativity and vacuum stability bounds (close to the alignment limit) for arbitrary values of t_β requires $m_{12}^2 = m_H^2 s_\beta c_\beta$ and $m_H \lesssim m_A, m_{H^\pm}$. Alternatively, stability is satisfied for any mass ordering if $m_{12}^2 = 0$, while unitarity requires in this case a low value of t_β. We thus consider these two scenarios as benchmark cases for our analysis:

- **Case 1:** $m_{12}^2 = m_H^2 s_\beta c_\beta$
  - From Eq. (3.2), vacuum stability requires $m_H \lesssim m_A$ and $m_H \lesssim m_{H^+}$, and thus the exotic decays $H \to A\,Z$ and $H \to H^\pm\,W^\mp$ are not kinematically allowed.
  - Unitarity requires $|\Lambda_i| < 8\pi$, constraining the mass differences among the new scalar states (but not the absolute mass values). In particular, using Eq. (3.4) we obtain the bound $\left|5(m_A^2 - m_H^2) + m_h^2\right| < 8\pi v^2$ if $m_{H^\pm} = m_H$, and the bound $\left|3(m_A^2 - m_H^2) + 5\,m_h^2\right| < 8\pi v^2$ if $m_{H^\pm} = m_A$.

– The cubic scalar couplings Eq. (2.8) now read

$$\begin{aligned} g_{Hhh} &= -\frac{c_{\beta-\alpha}}{s_{2\beta}\, v}\left[2\,(m_H^2 + m_h^2)\, s_{2\alpha} - m_H^2\, s_{2\beta}\right] \\ g_{HAA} &= -\frac{c_{\beta-\alpha}}{2\, v}(m_H^2 - 2\, m_A^2) \\ g_{HH^+H^-} &= -\frac{c_{\beta-\alpha}}{2\, v}(m_H^2 - 2\, m_{H^\pm}^2) \end{aligned} \tag{3.5}$$

In the alignment limit $c_{\beta-\alpha} = 0$ all these couplings vanish, and therefore the decays $H \to AA$, $H \to H^+H^-$ and $H \to h\,h$ are absent ($H \to A\,A$ and $H \to H^+H^-$ are also not kinematically allowed for $m_{12}^2 = m_H^2 s_\beta c_\beta$).

- **Case 2:** $m_{12}^2 = 0$ and $t_\beta \sim 1$

  – Vacuum stability does not constrain the parameter space. In particular $m_H > m_A$, m_{H^+} is now possible, allowing the decays $H \to A\,Z$ and $H \to H^\pm\, W^\mp$ (and potentially also $H \to AA$ and $H \to H^+H^-$).

  – Unitarity imposes an upper bound on the scalar masses (not only on the mass splittings). This bound scales as t_β^{-2} for $t_\beta > 1$ and as t_β^2 for $t_\beta < 1$, such that only the region $t_\beta \sim 1$ is allowed (we recall that in Type II 2HDM, at least one of the neutral scalars needs to be heavy due to the combination of EWPO and flavour constraints).

  – The cubic scalar couplings Eq. (2.8) now read

$$\begin{aligned} g_{Hhh} &= \frac{c_{\beta-\alpha}}{2\, s_{2\beta}\, v}(2m_h^2 + m_H^2)\left[(c_{\beta-\alpha}^2 - s_{\beta-\alpha}^2)\, s_{2\beta} - 2\, s_{\beta-\alpha}\, c_{\beta-\alpha}\, c_{2\beta}\right] \\ g_{HAA} &= -\frac{1}{2\, s_{2\beta}\, v}\left[(m_H^2 - 2m_A^2)\, c_{\beta-\alpha}\, s_{2\beta} + 2\, m_H^2\, s_{\beta-\alpha}\, c_{2\beta}\right] \\ g_{HH^+H^-} &= -\frac{1}{2\, s_{2\beta}\, v}\left[(m_H^2 - 2m_{H^\pm}^2)\, c_{\beta-\alpha}\, s_{2\beta} + 2\, m_H^2\, s_{\beta-\alpha}\, c_{2\beta}\right] \end{aligned} \tag{3.6}$$

  In the alignment limit the coupling g_{Hhh} vanishes and thus the decay $H \to hh$ is absent. However, the couplings g_{HAA} and $g_{HH^+H^-}$ are non-vanishing as long as $t_\beta \neq 1$.

For our analysis of benchmark scenarios away from alignment, which focus on the decays of A, H, $H^\pm$ into the SM-like Higgs h, we consider the same two cases above for consistency (even though these cases are motivated by theoretical constraints for $c_{\beta-\alpha} = 0$).

4 LHC Production and Decay of 2HDM Higgses

We now discuss the salient features of the production and decay of the new 2HDM scalars at the LHC. The production of the CP-even and CP-odd neutral scalars H, A at the 13 TeV LHC occurs via gluon fusion ($gg \to H/A$) and bb-associated production. Gluon fusion is the dominant production mechanism for small and moderate values of t_β, while for Type II 2HDM, bb-associated production dominates at large t_β. In both cases, we

compute the production cross section for H and A at NNLO in QCD via SusHi [58] (for H, the cross section does depend on $c_{\beta-\alpha}$, and in that case we consider the alignment limit $c_{\beta-\alpha} = 0$). For the charged scalar $H^\pm$, the dominant production mode for $m_{H^\pm} > m_t$ is in association with a tb pair, and we use the NLO cross section values provided by the Higgs Cross Section Working Group (HXSWG) for $m_{H^\pm} > 200$ GeV [59]. A light charged scalar ($m_{H^\pm} < m_t$) is mainly produced through top quark decays $t \to H^+ b$, and we use Top++2.0 [60] to compute the top pair production to NNLO in QCD, assuming a top-quark mass $m_t = 172.5$ GeV. The LHC production cross sections for H, A and H^+ at 13 TeV are shown in Appendix A.

Regarding the decays of the new scalars, in the alignment limit $c_{\beta-\alpha} = 0$ the conventional (SM-like) decays of A and H are into tt (if kinematically accessible), bb, cc, $\tau\tau$, and with a highly suppressed branching fraction into gg, $\gamma\gamma$ and $\mu\mu$. When open, the decay into tt is dominant for low and moderate t_β, followed by the decay into bb. At high t_β, for Type II 2HDM, the decay into $\tau\tau$ becomes important, where the decay into bb can dominate even above the tt threshold. For the CP-even Higgs H, the decay into massive gauge bosons W^+W^- and ZZ is present away from the alignment limit, and dominates as soon as the departure from alignment is sizeable. For the charged scalar, the decay $H^\pm \to tb$ dominates once it is kinematically open, followed by $H^\pm \to \tau\nu$, cs and cb. In the following, we compute all 2HDM branching fractions using 2HDMC [34].

Parent Scalar	Decay	Possible Final States	Channels in 2HDM
Neutral H, A	H_iH_i	$(bb/\tau\tau/WW/ZZ/\gamma\gamma)\,(bb/\tau\tau/WW/ZZ/\gamma\gamma)$	$H \to AA$, hh
	H_iZ	$(bb/\tau\tau/WW/ZZ/\gamma\gamma)\,(\ell\ell/qq/\nu\nu)$	$H \to AZ, A \to HZ, hZ$
	H^+H^-	$(tb/\tau\nu/cs)\,(tb/\tau\nu/cs)$	$H \to H^+H^-$
	$H^\pm W^\mp$	$(tb/\tau\nu/cs)\,(\ell\nu/qq')$	$H/A \to H^\pm W^\mp$
Charged $H^\pm$	$H_iW^\pm$	$(bb/\tau\tau/WW/ZZ/\gamma\gamma)\,(\ell\nu/qq')$	$H^\pm \to hW^\pm, HW^\pm, AW^\pm$

Table 2. Summary of exotic decay modes for non-SM Higgs bosons. For each type of exotic decays (second column), we present possible final states (third column) and relevant channels in 2HDM (fourth column). In the second column, $H_i = h$, H, A.

We here stress that the above conventional decays of the new 2HDM scalars become suppressed once exotic (non SM-like) decay modes open up. These can be decays involving several states among H, A, $H^\pm$, in the presence of a large mass splitting among the new scalars (see e.g. [16–21] for existing studies on individual channels), and/or decays into the SM-like Higgs boson h, namely $H \to hh$, $A \to hZ$, $H^\pm \to hW^\pm$, which are possible for $c_{\beta-\alpha} \neq 0$ and are also considered in the following as exotic (despite involving SM decay products) as they don't occur in the SM. In the former case, we can further distinguish between the decay of a new scalar into another one and a gauge boson, and the potential decays of H into either AA or H^+H^-. The different types of exotic decay modes for the 2HDM are summarized in Table 2.

The impact of the presence of exotic Higgs decay modes on the branching ratios is shown in Figure 4 for $c_{\beta-\alpha} = 0$. The top two panels show the relevant branching fractions of A with $m_H = m_{H^\pm} < m_A$ (left), and $m_H < m_A = m_{H^\pm}$ (right) for $m_A = 500$ GeV and $m_H = 200$ GeV, with $m_{12}^2 = m_H^2 s_\beta c_\beta$. In the former case, the decays $A \to H^\pm W^\mp$ (solid

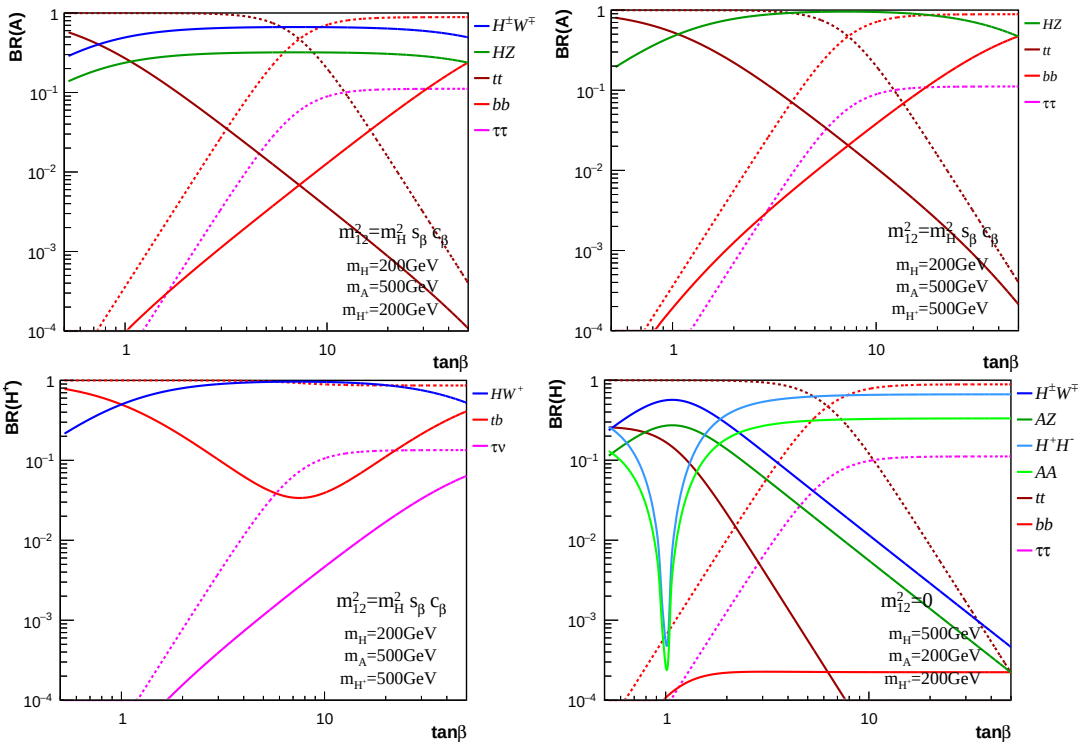

Figure 4. Branching fractions in Type II 2HDM as a function of t_β for $c_{\beta-\alpha}=0$, with parent and daughter scalar masses fixed to 500 GeV and 200 GeV, respectively. Top: Branching fractions for A with $m_H=m_{H^\pm}<m_A$ (left) and with $m_H<m_A=m_{H^\pm}$ (right), in both cases for $m_{12}^2=m_H^2 s_\beta c_\beta$. Bottom: Branching fractions for $H^\pm$ with $m_H<m_{H^\pm}=m_A$ and $m_{12}^2=m_H^2 s_\beta c_\beta$ (left) and for H with $m_H>m_{H^\pm}=m_A$ and $m_{12}^2=0$ (right). In all cases, dashed lines indicate the branching fractions to SM fermion pairs when exotic decay modes are absent.

blue) and $A\to HZ$ (solid green) completely dominate over the SM decays $A\to tt$, bb, $\tau\tau$ for most values of t_β, with $\mathrm{BR}(A\to H^\pm W^\mp)\sim 50{-}60\%$ and $\mathrm{BR}(A\to HZ)\sim 20{-}30\%$, while in the latter with $A\to H^\pm W^\mp$ being absent, the branching fraction of $A\to HZ$ is more than 50%. Decays of $A\to tt$, bb are only important for very small or very large t_β. The dashed lines show for comparison the branching fractions into the conventional SM states when the exotic decays are absent, which highlights the suppression the SM channels suffer in the presence of the exotic decays. The bottom left panel in Figure 4 shows the branching fractions of $H^\pm$ for $m_H<m_A=m_{H^\pm}$ (with $m_A=500$ GeV and $m_H=200$ GeV) and $m_{12}^2=m_H^2 s_\beta c_\beta$. The decay $H^\pm\to HW^\pm$ (solid blue) dominates with $\mathrm{BR}(H^\pm\to HW^\pm)\gtrsim 50\%$, particularly for a not too heavy state $H^\pm$. In that case, $H^\pm\to tb$ is suppressed to be about few percent for intermediate t_β, and only reaches about 50% in the very small and very large t_β region. Finally, the bottom right panel in Figure 4 shows the branching fractions of H for $m_H>m_{H^\pm}=m_A$ (with $m_H=500$ GeV and $m_A=200$ GeV) and $m_{12}^2=0$. In this case the decays $H\to AA$ and $H\to H^+H^-$ are allowed and dominate over most of the t_β region, except for $t_\beta\sim 1$, where $H\to AZ$

and $H \to H^\pm W^\mp$ become dominant due to the accidental suppression of the HH^+H^- and HAA couplings at $t_\beta \sim 1$. Note however that for $m_{12}^2 = 0$ the theoretical constraints do not allow a significant departure from $t_\beta \sim 1$, such that a large branching fraction for $H \to AZ$ and $H \to H^\pm W^\mp$ is expected. Decays to SM fermions are highly suppressed in this scenario.

5 2HDM Planes for Exotic Higgs Decays

Our analysis of exotic Higgs decays in the 2HDM focuses on a few key benchmark planes which show the complementarity among different LHC search channels for the new scalars. We first focus on the alignment limit: $c_{\beta-\alpha} = 0$ for $m_H > m_h = 125$ GeV and $s_{\beta-\alpha} = 0$ for $m_h < m_H = 125$ GeV. In this context, we consider two possible mass planes: m_A vs. $m_H = m_{H^\pm}$ (Plane I) and m_H vs. $m_A = m_{H^\pm}$ (Plane II). These two choices are motivated by EWPO constraints (recall the discussion in Section 3.3). This is in contrast to a potential $m_{H^\pm}$ vs. $m_H = m_A$ plane, highly constrained by EWPO to a small mass splitting $m_{H^\pm} - m_{H/A}$ which closes the phase space needed for on-shell exotic Higgs decays[††], so that we don't consider such benchmark plane in our current study. Finally let us remark that, while we do not impose the flavour bounds as hard constraints on our 2HDM benchmark planes (recall the discussion in Section 3.4), we do show them as indicative in the following. Our 2HDM benchmark plane (BP) scenarios in alignment are then:

Plane I: m_A vs. $m_H = m_{H^\pm}$

- BP IA: $m_A > m_H = m_{H^\pm}$.

  As discussed in Section 3.6, this mass ordering is allowed for Case 1 ($m_{12}^2 = m_H^2 s_\beta c_\beta$ and all t_β values) and Case 2 ($m_{12}^2 = 0$ and $t_\beta \sim 1$). We thus consider four scenarios: Case 1 with $t_\beta = 1.5$, 7, 30 and Case 2 with $t_\beta = 1.5$.

- BP IB: $m_A < m_H = m_{H^\pm}$.

  This mass ordering is not compatible with Case 1 due to vacuum stability (see Sections 3.1 and 3.6). Thus, we only consider Case 2 with $t_\beta = 1.5$[‡‡].

Plane II: m_H vs. $m_A = m_{H^\pm}$

- BP IIA: $m_H > m_A = m_{H^\pm}$.

  As for BP IB, this mass ordering is not compatible with Case 1, and so we only consider Case 2 with $t_\beta = 1.5$.

- BP IIB: $m_H < m_A = m_{H^\pm}$.

  As for BP IA, we consider Case 1 with $t_\beta = 1.5$, 7, 30 and Case 2 with $t_\beta = 1.5$.

[††] As discussed in Section 3.3, a sizable departure from alignment could allow for a mass hierarchy $m_A > m_H + m_Z$ (such that $A \to HZ$ is kinematically allowed) and $m_H \gtrsim m_{H^\pm} + m_W$ (such that $H \to H^\pm W^\mp$ is kinematically allowed, but nevertheless phase space suppressed). The phenomenology of this kind of scenario is however largely contained in Planes I-II, and so we do not consider it separately.

[‡‡] $t_\beta \neq 1$ is chosen for the exotic decays into two lighter new scalars ($H \to AA$ in this case) not to vanish.

In order to study the decays of the new scalars into the SM-like Higgs, we also consider a plane in which the departure from alignment is explored, assuming h is the 125 GeV SM-like Higgs (Plane III). We set $m_H = m_A = m_{H^\pm}$ for simplicity, and define the plane as $m_H = m_A = m_{H^\pm}$ vs. $c_{\beta-\alpha}$:

Plane III: $m_A = m_H = m_{H^\pm}$ **vs.** $c_{\beta-\alpha}$

- BP III:

  We consider Case 1 with $t_\beta = 1.5$, 7, 30 and Case 2 with $t_\beta = 1.5$.

A summary of the different benchmark planes considered and the relevant exotic decay modes is shown in Table 3. In all cases, we present the $\sigma\times$ BR of each characteristic decay channel at the 13 TeV LHC, together with a detailed analysis of the regions disfavoured by theoretical and experimental constraints (including flavour constraints, shown for reference only). The results for Planes I and II ($c_{\beta-\alpha} = 0$) are presented in Section 5.1, while the results for decays to SM-like Higgs away from alignment, corresponding to Plane III, are presented in Section 5.2. Further details on the cross sections and decay branching fractions for the non-SM like Higgses can be found in Appendix A.

	Mass Planes	decays	m_{12}^2	$\tan\beta$	Figures
BP IA	$m_A > m_H = m_{H^\pm}$	$A \to H^\pm W^\mp$	$m_H^2 s_\beta c_\beta$	1.5, 7, 30	5, 6
		$A \to HZ$	0	1.5	
BP IB	$m_A < m_H = m_{H^\pm}$	$H \to AZ$, $H \to AA$	0	1.5	9
		$H^\pm \to AW^\pm$			
BP IIA	$m_H > m_A = m_{H^\pm}$	$H \to AZ$, $H \to AA$	0	1.5	10
		$H \to H^+H^-$, $H \to H^\pm W^\mp$			
BP IIB	$m_H < m_A = m_{H^\pm}$	$A \to HZ$	$m_H^2 s_\beta c_\beta$	1.5, 7, 30	7, 8
		$H^\pm \to HW^\pm$	0	1.5	
BP III	$m_A = m_H = m_{H^\pm}$	$A \to hZ$, $H^\pm \to hW^\pm$	$m_H^2 s_\beta c_\beta$	1.5, 7, 30	11, 12, 13
	vs. $c_{\beta-\alpha}$	$H \to hh$	0	1.5	

Table 3. Summary Table of the different 2HDM benchmark planes.

Before we move on to discuss in detail our different 2HDM planes for LHC searches at 13 TeV, let us comment on the comparison of these benchmark scenarios with others proposed in the literature. In particular, our Planes I and II have a substantial overlap with the 2HDM "*short cascade*" scenario D from [61], while our specific BP IA and BP IIB have similarities with the $A \to HZ$ benchmarks for $c_{\beta-\alpha} = 0$ in [15] (see also [18]). As compared to [61], the present analysis explores the full mass plane, not restricted to specific benchmark lines with fixed relations[§§] among m_H, m_A and $m_{H^\pm}$. We also explore the dependence on t_β, which has a significant impact on the allowed 2HDM parameter space

[§§]In particular, we note that the fixed relations in [61] result in the exotic Higgs decays being largely subdominant above the $t\bar{t}$ threshold, which may not be the case in general (see e.g. Figure 4).

for Planes I and II. Moreover, our analysis includes the 8 TeV experimental constraint from the CMS $H \to AZ/A \to HZ$ search [22, 23], precisely tailored to probe these 2HDM scenarios and thus a key ingredient in a study of 2HDM exotic Higgs decays.

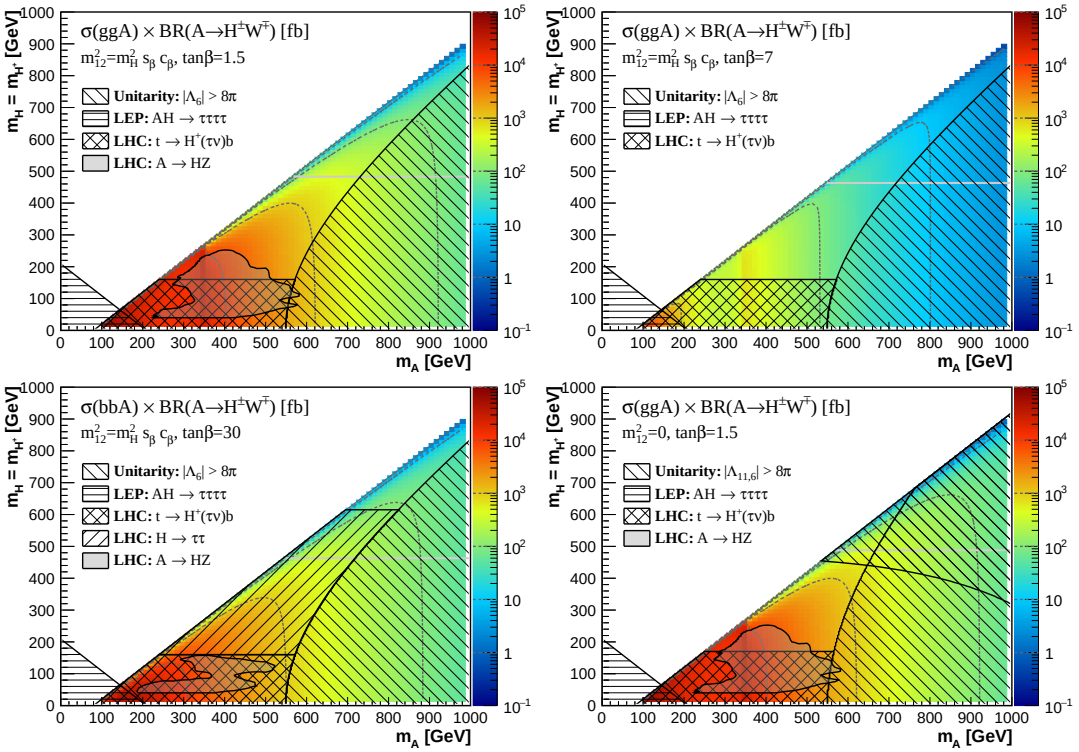

Figure 5. $\sigma \times$ BR for the exotic decay $A \to H^{\pm}W^{\mp}$ in BP IA: m_A vs $m_H = m_{H^{\pm}}$ plane, for Case 1 with $t_\beta = 1.5$ (upper left), 7 (upper right), 30 (lower left) and Case 2 with $t_\beta = 1.5$ (lower right). Contour lines of 10, 10^2, 10^3 and 10^4 fb are drawn as light grey dashed curves to guide the eye. Shaded and hatched regions are ruled out by theoretical and experimental constraints (see text for details). The solid horizontal grey line indicates the flavour constraint $m_{H^{\pm}} > 480$ GeV.

5.1 Exotic Decays in the Alignment Limit

5.1.1 BP IA: $m_A > m_H = m_{H^{\pm}}$

In this scenario, and for a sufficient mass splitting, there are two dominant exotic decay channels: $A \to H^{\pm}W^{\mp}$ and $A \to HZ$, for which we respectively show the $\sigma \times$ BR in Figures 5 and 6. In each case, we show four panels corresponding to the choices of m_{12}^2 and t_β described in Table 3. Note that for $t_\beta = 1.5, 7$ we consider the dominant ggA production, while for $t_\beta = 30$ the bbA production dominates and is considered instead. For each panel, contour lines of 10, 10^2, 10^3 and 10^4 fb are drawn as light grey dashed curves to guide the eye. Large cross sections $\sigma \times \text{BR} \gtrsim 1$ pb are possible for $t_\beta \sim 1$ and $t_\beta \gg 1$, respectively due to the enhanced top and bottom Yukawa coupling contribution, even for large CP-odd scalar masses $m_A \sim 500 - 600$ GeV. Shaded regions in Figures 5 and 6 are excluded by the CMS $A \to HZ$ search [22, 23], which already constrains a sizable portion

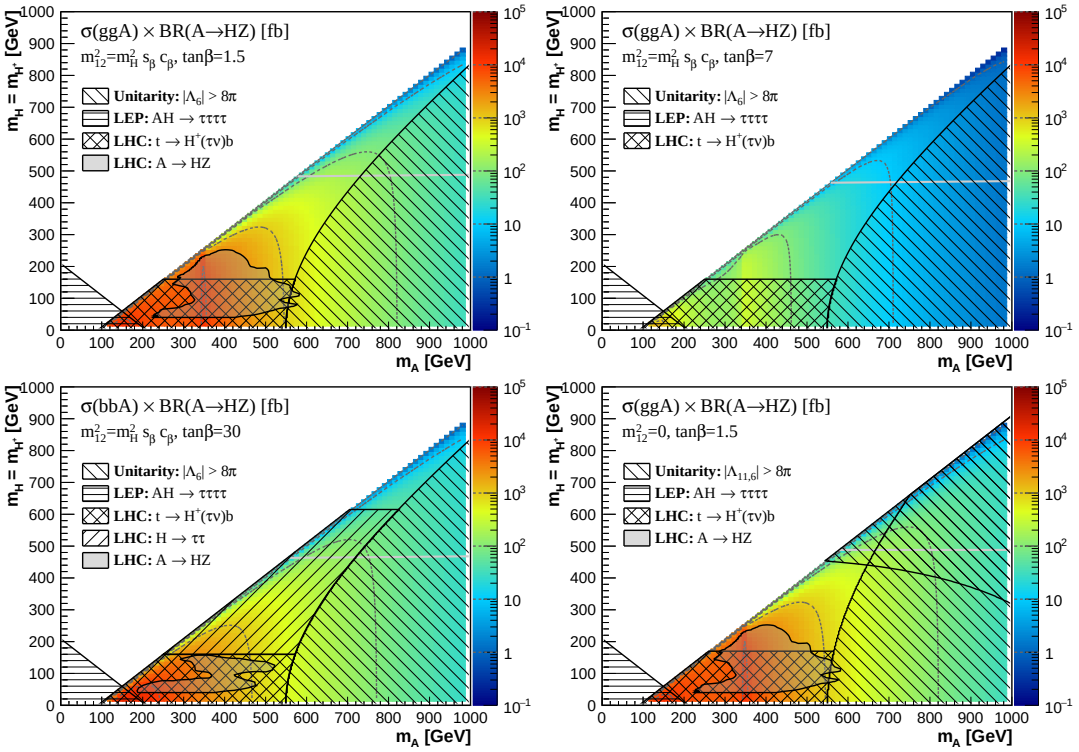

Figure 6. $\sigma \times \mathrm{BR}$ for the exotic decay $A \to HZ$ in BP IA: m_A vs $m_H = m_{H^\pm}$ plane (see caption of Figure 5 for further details). For $t_\beta = 1.5$, the contour line at $\sigma \times \mathrm{BR} = 10$ pb around $m_A = 350$ GeV is caused by the enhanced $gg \to A$ production cross section at the top threshold.

of parameter space and highlights the potential of such a search at LHC 13 TeV in the $bb\ell\ell$ and $\tau\tau\ell\ell$ final states, as a probe of both A and H.

Hatched regions show the parameter space excluded by other experimental searches, as well as unitarity constraints. The former exclusions are mainly due to $t \to H^+ b$ searches, which yield a limit $m_{H^\pm} > m_t$, as well as $H \to \tau\tau$ searches for large t_β, which rule out $m_H < 600$ GeV for $t_\beta = 30$. We also show the flavour bound $m_{H^\pm} > 480$ GeV as a horizontal grey line for indicative purposes.

Regarding unitarity, for Case 1 ($m_{12}^2 = m_H^2 s_\beta c_\beta$) with $m_A > m_H = m_{H^\pm}$ the eigenvalues of the scattering matrix are $|\Lambda_{i\neq 6}| = m_A^2 - m_H^2 \pm \mathcal{O}(m_h^2)$ and $|\Lambda_6| = 5(m_A^2 - m_H^2) + m_h^2$. The latter imposes the strongest constraint, which rules out regions with a very large mass splitting $m_A - m_H$ (as indicated by the hatched region in the lower-right corner of each panel in Figures 5 and 6). For Case 2 ($m_{12}^2 = 0$) with $m_A > m_H = m_{H^+}$, the strongest unitarity constraints come from $|\Lambda_6| = 5m_A^2 - 3m_H^2 \pm \mathcal{O}(m_h^2)$ and $|\Lambda_{11}| = \frac{1}{2}m_H^2(\frac{1}{t_\beta^2} + t_\beta^2) + \frac{1}{2}\sqrt{9m_H^4(\frac{1}{t_\beta^2} - t_\beta^2)^2 + 4m_A^4} \pm \mathcal{O}(m_h^2)$. In particular, $|\Lambda_{11}|$ rules out the large m_H region (upper hatched region in the lower right panel in Figures 5 and 6).

Taking into account both the theoretical and experimental constraints, relatively large regions of m_A vs. $m_H = m_{H^\pm}$ remain viable and having a sizable signal cross section for small to intermediate values of t_β for Case I. For $t_\beta \gg 1$, only the region $m_A \gtrsim$

$m_H = m_{H^\pm} > 600$ GeV still survives. For Case 2, given the unitary constraints ruling out large values of m_H and m_A, only the region 200 GeV $< m_A <$ 650 GeV and 175 GeV $< m_H = m_{H^\pm} <$ 450 GeV remains viable.

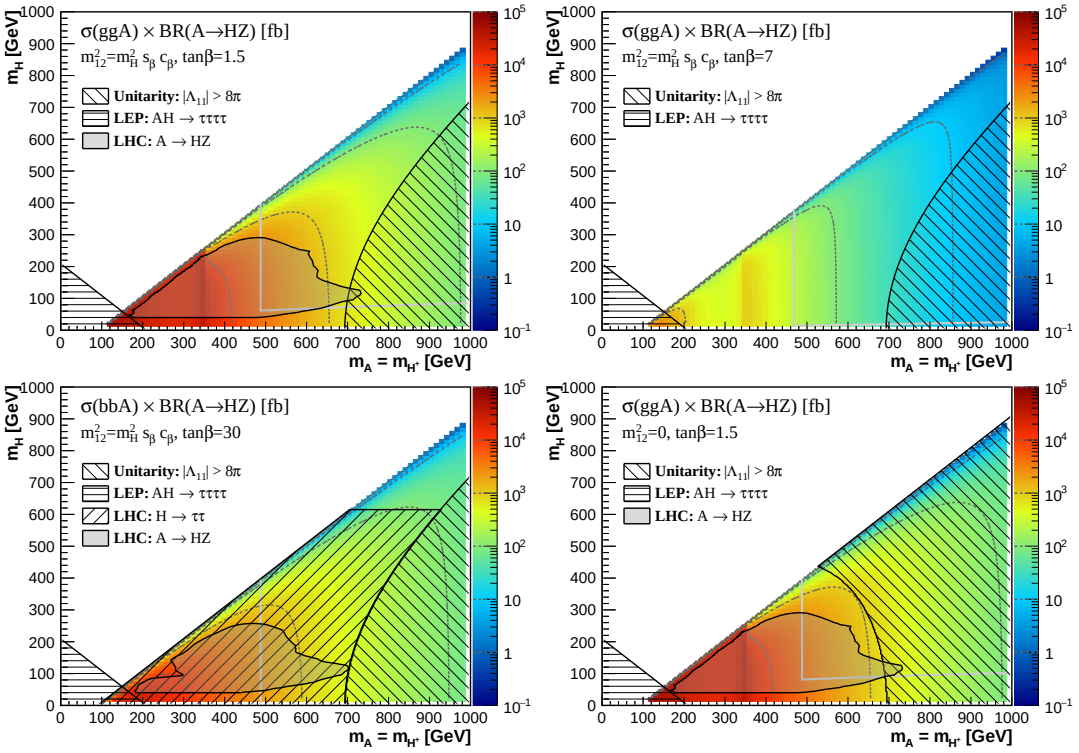

Figure 7. $\sigma \times$ BR for the exotic decay $A \to HZ$ in BP IIB: $m_A = m_{H^\pm}$ vs m_H plane (see caption of Figure 5 for further details). The solid horizontal and vertical light grey lines indicate the various flavour constraints.

5.1.2 BP IIB: $m_H < m_A = m_{H^\pm}$

For $m_H < m_A = m_{H^\pm}$, the dominant exotic decay channels are $A \to HZ$ and $H^\pm \to HW^\pm$. We show the $\sigma \times$ BR for $A \to HZ$ and $H^\pm \to HW^\pm$ respectively in Figures 7 and 8. The low $m_A + m_H$ region is ruled out by the LEP search $e^+e^- \to AH$ (recall the discussion in Section 3.5), while unitarity constraints bound large values for m_A, m_H: For Case I the strongest constraints arise from $|\Lambda_{2,4,5,6,11,12}| = 3(m_A^2 - m_H^2) \pm \mathcal{O}(m_h^2)$, which limit $m_A^2 - m_H^2$ for large m_H and/or m_A. For Case 2, large values of either m_A or m_H are excluded, since the strongest unitarity constraint comes from $|\Lambda_{11}| = \frac{1}{2}m_H^2(\frac{1}{t_\beta^2} + t_\beta^2) + \frac{1}{2}\sqrt{9m_H^4(\frac{1}{t_\beta^2} - t_\beta^2)^2 + 4(3m_A^2 - 2m_H^2)^2} \pm \mathcal{O}(m_h^2)$.

For Case 1 with $t_\beta = 1.5$ (upper left panel of Figure 7), signal cross sections for $A \to HZ$ in excess of 10 pb are viable given all the constraints, while we note that the LHC Run 1 CMS $A \to HZ$ search rules out a large portion of the parameter space with $m_H < 300$ GeV and $m_A < 650$ GeV. Intermediate values of t_β (exemplified by the $t_\beta = 7$

case shown in the upper right panel of Figure 7) only permit signal cross sections below 1 pb, due to the small gluon fusion production cross section (for $m_A > 600$ GeV the $\sigma\times$ BR values are in fact below 20 fb). For $t_\beta = 30$ (lower left panel of Figure 7), the current collider search of $H \to \tau\tau$ rules out $m_H < 600$ GeV, leaving only a small corner of parameter space allowed, with signal cross sections $\sigma\times$ BR $\lesssim 100$ fb. For Case 2, the lower right panel of Figure 7 shows that the CMS $A \to HZ$ search constrains most of the viable parameter space, which may in turn be probed completely by LHC 13.

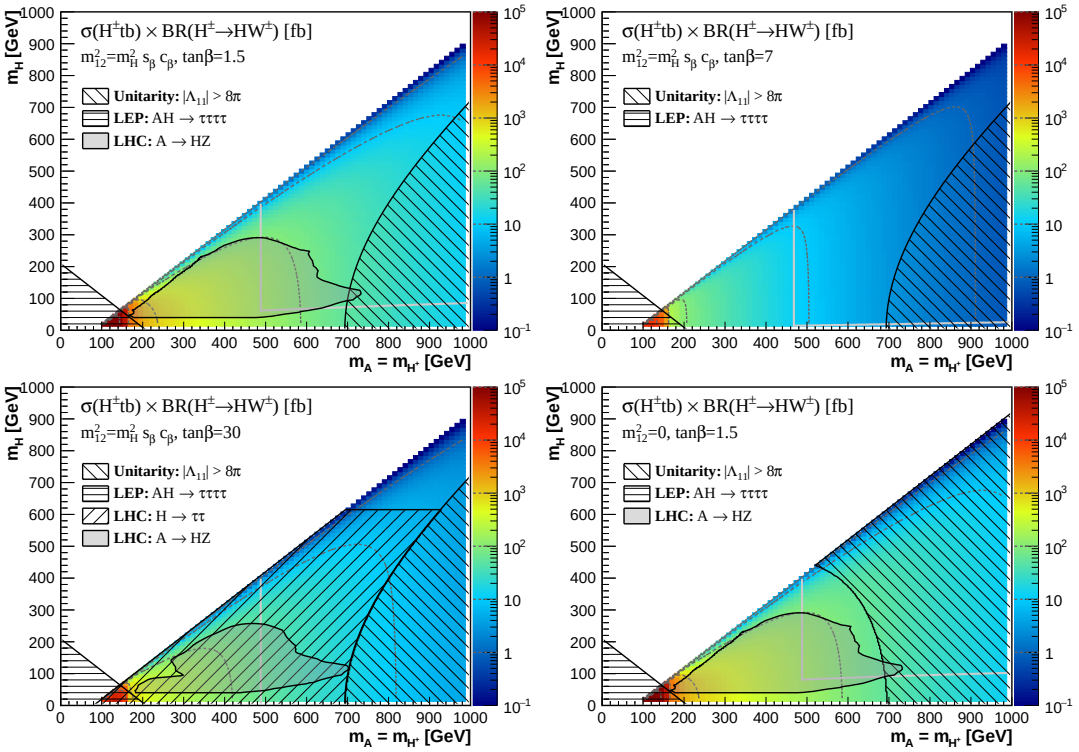

Figure 8. $\sigma \times$ BR for the exotic decay $H^\pm \to HW^\pm$ in BP IIB: $m_A = m_{H^\pm}$ vs. m_H plane (see caption of Figure 5 for further details). The solid horizontal and vertical light grey lines indicate the various flavour constraints.

While the generic features for $H^\pm \to HW^\pm$ are similar to those of $A \to HZ$, the signal cross sections are about two order of magnitude smaller, due to the suppressed production cross section of $pp \to H^\pm tb$. This, in addition to the complicated final state HW^+W^-bb which results, makes this channel challenging for LHC studies at 13 TeV.

5.1.3 BP IB: $m_A < m_{H^\pm} = m_H$

In this scenario, only Case 2 ($m_{12}^2 = 0$) is viable. The $\sigma\times$ BR for the three possible exotic decay channels $H \to AZ$, $H^\pm \to AW^\pm$ and $H \to AA$ is shown in Figure 9 for our benchmark $t_\beta = 1.5$. The $m_H > 460$ GeV region is excluded by unitarity, the strongest unitarity constraint coming from $|\Lambda_{11}| = \frac{1}{2}m_H^2(\frac{1}{t_\beta^2}+t_\beta^2)+\frac{1}{2}\sqrt{9m_H^4(\frac{1}{t_\beta^2}-t_\beta^2)^2+4m_A^4} \pm \mathcal{O}(m_h^2)$.

Below the unitarity limit on m_H, the ATLAS/CMS limits on $A \to \tau\tau$ at low t_β (ggA production) [46, 47] combined with the bounds from the CMS $H \to AZ$ search [22, 23] rule out $m_A > 40$ GeV down to $m_H \lesssim 350$ GeV. As can be seen from Figure 9, only a small region of parameter space survives the unitarity and LHC 8 TeV constraints. We also stress that in this case including the flavour constraint $m_{H^\pm} > 480$ GeV would rule out this benchmark scenario completely.

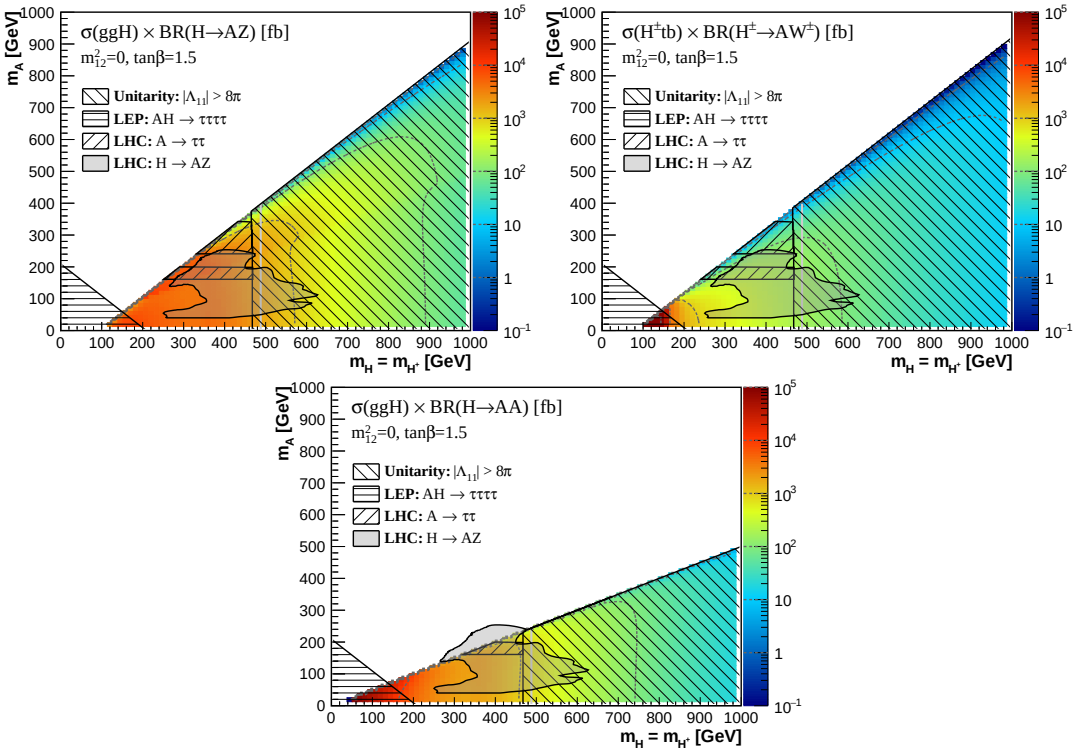

Figure 9. $\sigma \times$ BR for the exotic decays $H \to AZ$ (up left), $H^\pm \to AW^\pm$ (up right) and $H \to AA$ (down) in BP IB: $m_H = m_{H^\pm}$ vs. m_A plane, for Case 2 ($m^2_{12} = 0$) with $t_\beta = 1.5$. Contour lines of 10, 10^2 and 10^3 fb are drawn as light grey dashed curves to guide the eye. Shaded and hatched regions are ruled out by theoretical and experimental constraints (see text for details). The solid (vertical) light grey lines indicate the flavour constraint $m_{H^\pm} > 480$ GeV.

5.1.4 BP IIA: $m_H > m_A = m_{H^\pm}$

Four exotic Higgs decay channels, $H \to AZ$, $H \to H^\pm W^\mp$, $H \to AA$, and $H \to H^+H^-$ are possible for BP IIA (which we recall is only allowed for Case 2), shown respectively in the four panels of Figure 10. Comparing to BP IIB, the additional collider search limit $m_{H^\pm} > m_t$ applies, which overlaps with the 8 TeV LHC exclusion from $A \to \tau\tau$. This results in only a small stripe in parameter space, corresponding to 200 GeV $< m_A = m_{H^\pm} <$ 240 GeV and 300 GeV $< m_H <$ 450 GeV, being viable. Moreover, we note that the decays $H \to AA$ and $H \to H^+H^-$ are essentially not kinematically allowed in the viable region, as shown in the lower panels of Figure 10. This benchmark scenario should indeed be possible to probe completely at LHC 13 TeV.

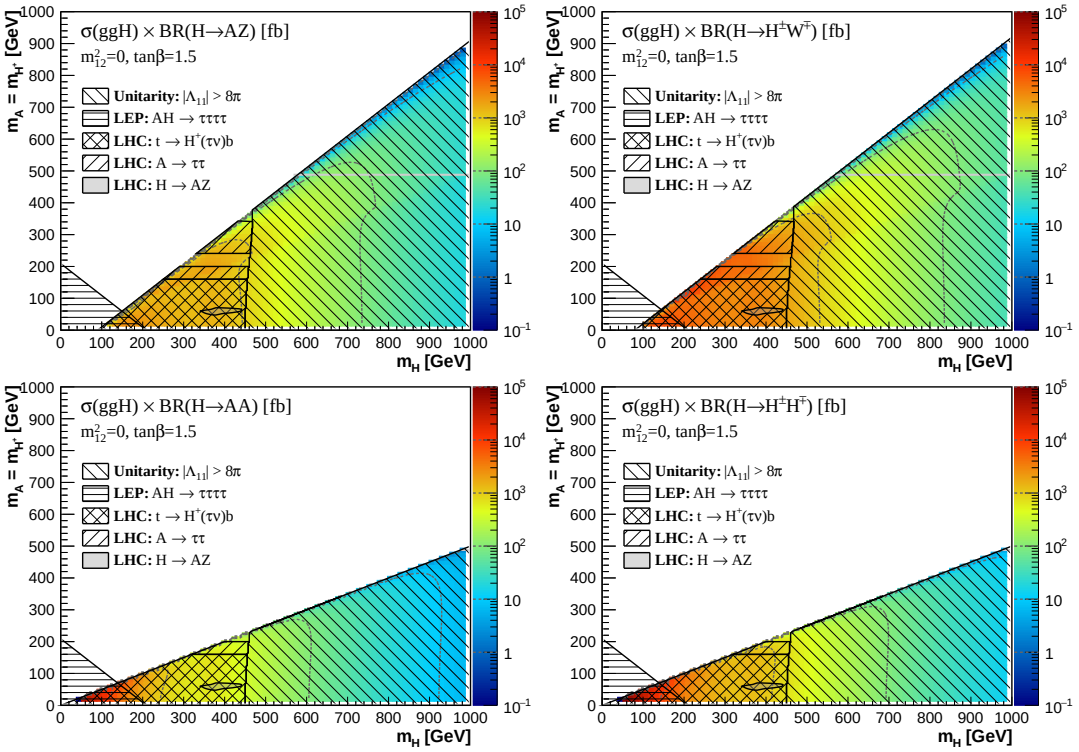

Figure 10. $\sigma \times$ BR for the exotic decays $H \to AZ$ (up left), $H^\pm \to H^\pm W^\mp$ (up right), $H \to AA$ (down left) and $H \to H^+H^-$ (down right) in BP IIA: m_H vs. $m_A = m_{H^\pm}$ plane (see caption of Figure 9 for further details).

5.2 Exotic Decays into h Away from Alignment

5.2.1 BP III: $m_A = m_H = m_{H^\pm}$ vs. $c_{\beta-\alpha}$

Exotic decays with the SM-like Higgs h in the final state are possible away from the alignment limit $c_{\beta-\alpha} = 0$, as the AhZ, $H^\pm hW^\mp$ and Hhh couplings are proportional to $c_{\beta-\alpha}$. In Figures 11, 12, and 13 we respectively show the $\sigma \times$BR for $A \to hZ$, $H^\pm \to hW^\pm$ and $H \to hh$, in each case for Case 1 with $t_\beta = 1.5$, 7, 30 and Case 2 with $t_\beta = 1.5$ in the ($c_{\beta-\alpha}$ vs $m_A = m_H = m_{H^\pm}$) plane.

For Case 1 with $t_\beta = 1.5$, only the region $|c_{\beta-\alpha}| \lesssim 0.2$ (close to the alignment limit) is viable as a result of Higgs signal strength measurements (mainly driven by the g_{hVV} couplings) considering all the theoretical and experimental constraints. The allowed range for $c_{\beta-\alpha}$ shrinks as the masses of the heavy 2HDM scalars grow due to stability constraints, being already restricted to $-0.02 < c_{\beta-\alpha} < 0.06$ for $m_A = m_H = m_{H^\pm} \simeq 500$ GeV. At the same time, LHC bounds on $H \to ZZ$ and $A \to \tau\tau$ rule out $m_A = m_H = m_{H^\pm} < 350$ GeV. For significantly higher values of t_β (as our $t_\beta = 7$, 30 scenarios) the stability constraints rule out almost completely the region $c_{\beta-\alpha} < 0$, while unitarity imposes a strong constraint on $c_{\beta-\alpha} > 0$ for high scalar masses $m_A = m_H = m_{H^\pm} > 600$ GeV. In addition, for $t_\beta = 7$ the vacuum stability constraint rules out the region $c_{\beta-\alpha} > 0.3$ while Higgs signal strengths rule out the region $0.05 < c_{\beta-\alpha} < 0.24$. For $t_\beta = 30$, Higgs signal strengths

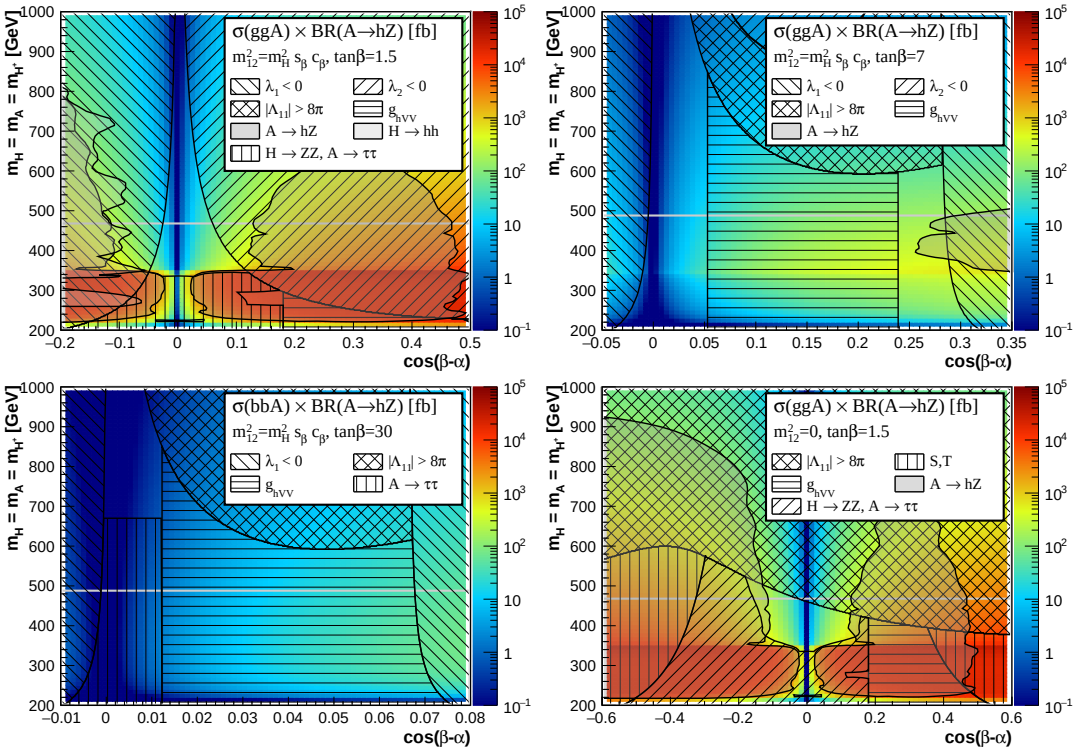

Figure 11. $\sigma \times \mathrm{BR}$ for $A \to hZ$ for the gluon fusion production in Case 1, $\tan\beta = 1.5$ (upper left), 7 (upper right), as well as Case 2, $\tan\beta = 1.5$ (lower right), and bbA associated production for Case 1, $\tan\beta = 30$ (lower left) in BPIII: $c_{\beta-\alpha}$ vs. $m_A = m_H = m_{H^\pm}$. Hatched regions are excluded by either theoretical or experimental constraints (as indicated in the legend), while shaded regions indicate the parameter space constrained by LHC searches for exotic (non-SM) Higgs decays: $A \to hZ$ and $H \to hh$. The solid horizontal light grey lines indicate the flavour constraint $m_{H^\pm} > 480$ GeV.

rule out $c_{\beta-\alpha} \gtrsim 0.01$, while $A \to \tau\tau$ searches restrict the allowed parameter space to $m_A = m_H = m_{H^\pm} > 650$ GeV, leaving only a very narrow stripe as viable parameter space. For Case 2 with $t_\beta = 1.5$, satisfying the constraints from $H \to ZZ$ and $A \to \tau\tau$ requires $m_A = m_H = m_{H^\pm} > 350$ GeV and $|c_{\beta-\alpha}| \lesssim 0.2$, while unitarity imposes an upper bound on the scalar masses in the range 450 GeV – 550 GeV depending on $c_{\beta-\alpha}$. As shown in Figure 11, the cross sections for $A \to hZ$ in the allowed region of parameter space could reach 1 pb or higher for $t_\beta = 1.5$ both in Case 1 and 2. For $t_\beta = 7$ (Case 1) the cross section for $A \to hZ$ is still sizable in the allowed region $0.24 < c_{\beta-\alpha} < 0.3$, reaching values ~ 100 fb. For $t_\beta = 30$ the signal cross section is however very small due to the suppressed branching ratio $\mathrm{BR}(A \to hZ)$ close to the alignment limit. The signal cross sections for $H^\pm \to hW^\pm$ shown in Figure 12 follow a trend similar to those for $A \to hZ$, but being typically a factor 10 – 100 smaller due to the suppressed production cross section for $H^\pm$ above m_t (see Appendix A.1). Finally for $H \to hh$ the signal cross sections, shown in Figure 13, are about factor of 10 smaller than those of $A \to hZ$, and

an additional suppression of the branching ratio BR($H \to hh$) occurs for certain values of $c_{\beta-\alpha}$ (e.g. $c_{\beta-\alpha} \sim 0.22$ for $t_\beta = 7$ and $c_{\beta-\alpha} \sim 0.052$ for $t_\beta = 30$, as seen from Figure 13).

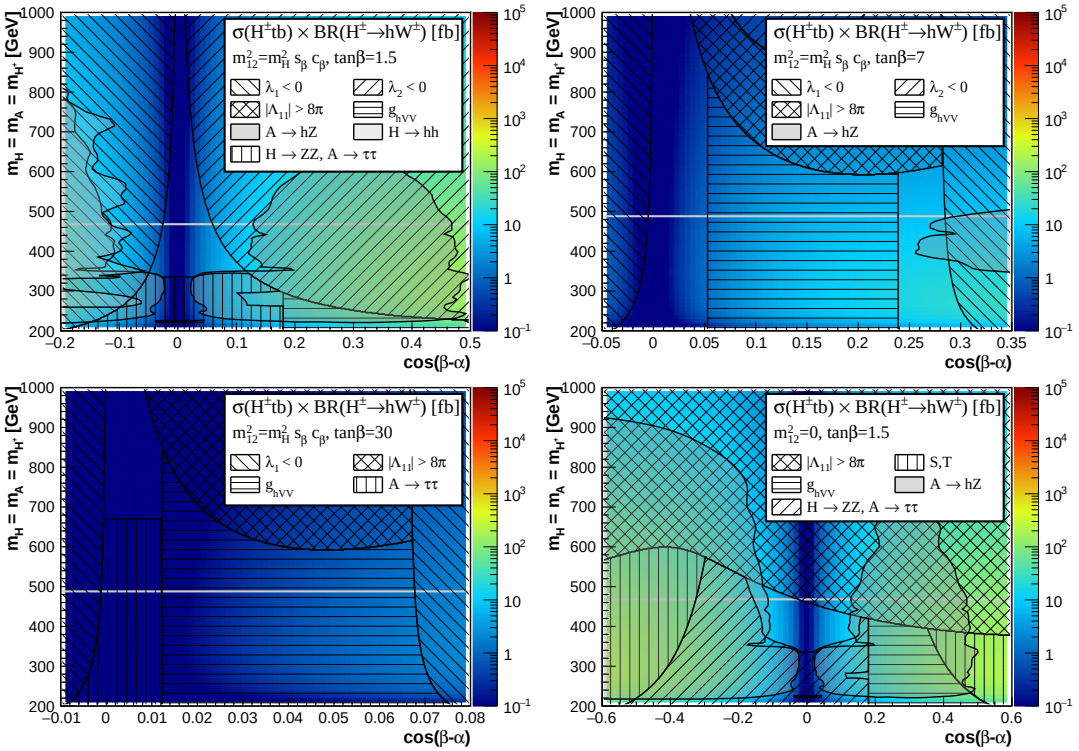

Figure 12. $\sigma \times$BR for $H^\pm \to hW^\pm$ in BPIII: $c_{\beta-\alpha}$ vs. $m_A = m_H = m_{H^\pm}$ (see caption of Figure 11 for further details).

6 Conclusions

In the 2HDM, other than decaying to pairs of SM quarks, leptons, and gauge bosons, the exotic decays of heavy Higgses into two lighter Higgses or one light Higgs and a SM gauge boson are likely to dominate once they are kinematically open. While the collider search bounds for heavy Higgses based on conventional search modes WW, ZZ, $\gamma\gamma$, bb and $\tau\tau$ for neutral Higgses, and $\tau\nu$ and cs modes for charged Higgses would be relaxed once those exotic modes are open, the exotic decay modes offer new discovery channels in large regions of the 2HDM parameter space.

Away from the 2HDM alignment limit, exotic decays into the SM-like 125 GeV Higgs boson h, namely $H \to hh$, $A \to hZ$ and $H^\pm \to hW^\pm$, are potentially important, and there is already an ongoing ATLAS and CMS search programme for $A \to hZ$ [51, 52] and $H \to hh$ [53–55]. In contrast, close to the alignment limit, as favoured by measurements of Higgs signal strengths, exotic decays among the new 2HDM scalars become particularly relevant. The experimental searches based on those channels, however, have just started with $H/A \to AZ/HZ$ [22, 23]. In this work, we carefully examine the exotic Higgs decay

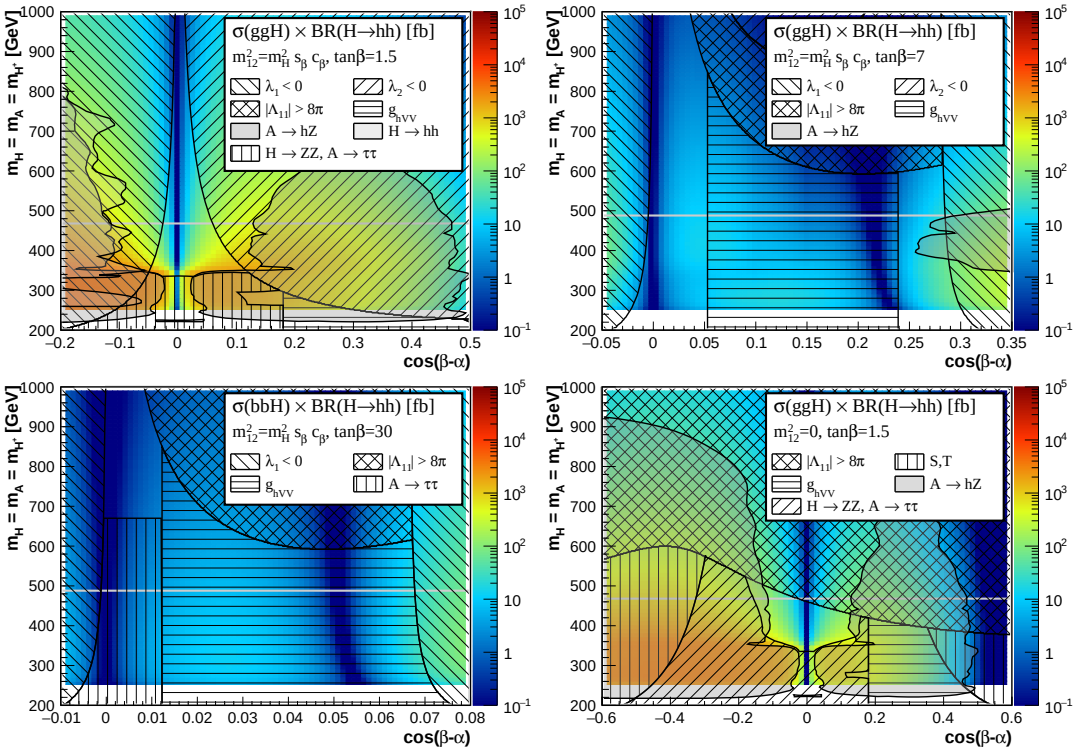

Figure 13. $\sigma \times$ BR for $H \to hh$ in BPIII: $c_{\beta-\alpha}$ vs. $m_A = m_H = m_{H^\pm}$ (see caption of Figure 11 for further details).

channels in the 2HDM, both in the presence of a hierarchy between Higgses and away from alignment when this hierarchy is not present. By taking into account the various theoretical and experimental constraints, we propose 2HDM benchmark plane scenarios for LHC searches at 13 TeV:

- BP IA: $m_A > m_H = m_{H^\pm}$, with $A \to HZ,\ H^\pm W^\mp$.
- BP IB: $m_A < m_H = m_{H^\pm}$, with $H \to AZ,\ AA$ and $H^\pm \to AW^\pm$.
- BP IIA: $m_H > m_A = m_{H^\pm}$, with $H \to AZ,\ H^\pm W^\mp,\ AA,\ H^+H^-$.
- BP IIB: $m_H < m_A = m_{H^\pm}$, with $A \to HZ$ and $H^\pm \to HW^\pm$.
- BP III: $m_A = m_H = m_{H^\pm}$ vs. $c_{\beta-\alpha}$, with $A \to hZ$, $H^\pm \to hW^\pm$, and $H \to hh$.

In each case, we analyze the allowed regions of parameter space and the LHC 13 TeV $\sigma \times$ BR for the relevant exotic Higgs decay modes in those regions.

To summarize, exotic Higgs decays provide new discovery avenues for heavy Higgses. In turn, the exploration of the proposed benchmarks via these decays could help to understand the structure of the electroweak symmetry breaking sector beyond the SM.

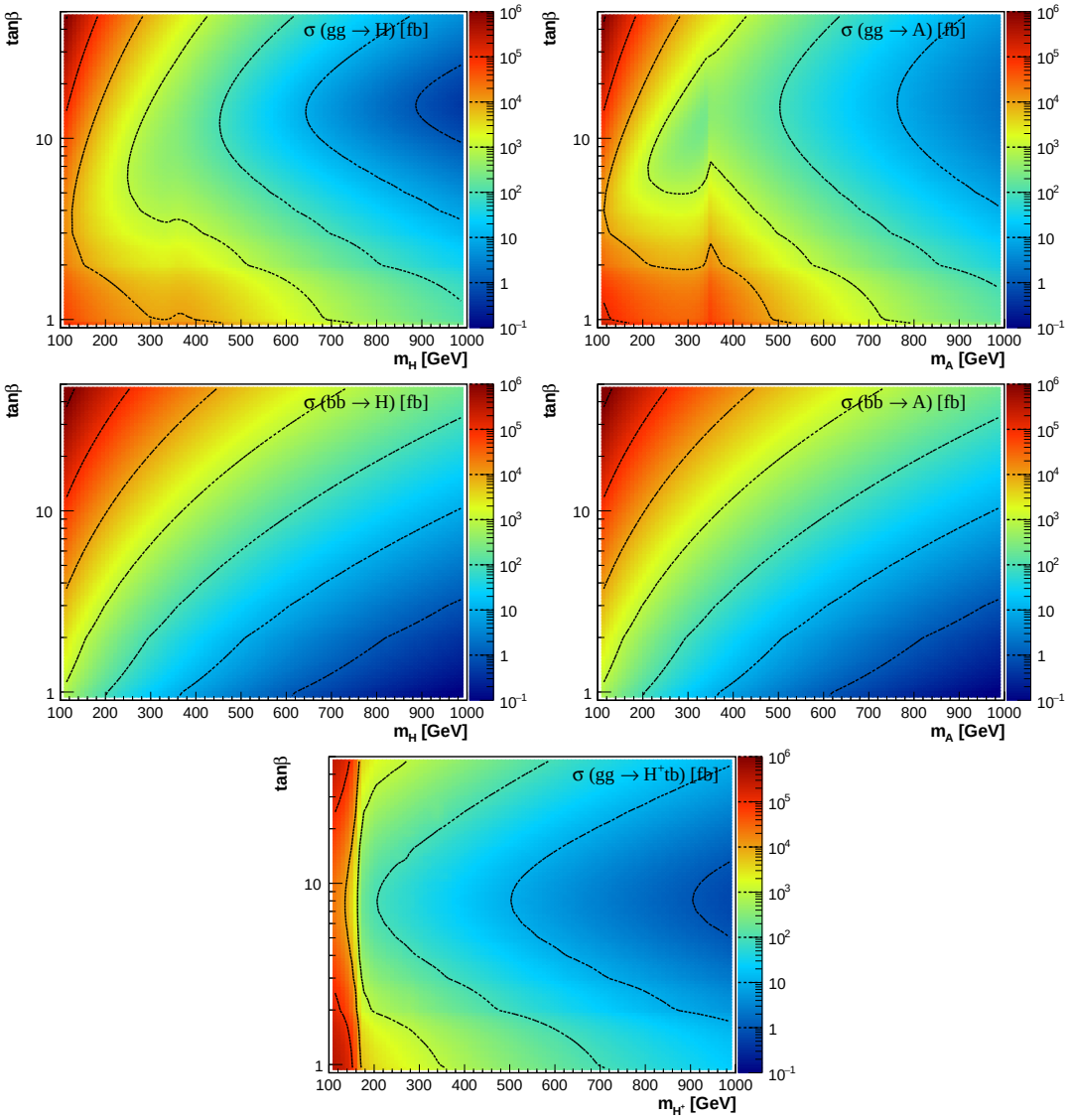

Figure 14. Production cross section for H, A and H^+ at LHC 13 TeV. The contour lines indicate the cross section of 1, 10, 10^2, 10^3, 10^4, 10^5 and 10^6 fb.

Acknowledgments

We would like to thank Baradhwaj Coleppa, Tao Han, Tao Liu, Ken Mimasu and Adarsh Pyarelal for helpful discussions. We also thank the Munich Institute for Astro- and Particle Physics (MIAPP) of the DFG cluster of excellence "Origin and Structure of the Universe" for support and hospitality during the initial stages of this work. The work of S.S. and F.K. was supported by US Department of Energy under Grant DE-FG02-04ER-41298. F.K. also acknowledges support from the Fermilab Graduate Student Research Program in Theoretical Physics operated by Fermi Research Alliance, LLC under Contract No. DE-

AC02-07CH11359 with the United States Department of Energy. J.M.N. is supported by the People Programme (Marie Curie Actions) of the European Union Seventh Framework Programme (FP7/2007-2013) under REA grant agreement PIEF-GA-2013-625809.

A Production Cross Sections and Branching Ratios of 2HDM Higgses

A.1 2HDM Production Cross Sections

In Figure 14, we show the gluon fusion production cross section for H (upper left panel) and A (upper right panel), bb-associated production cross section for H (middle left panel) and A (middle right panel), and $tbH^{\pm}$ production cross section (bottom) for the charged scalar (details are given in Section 4).

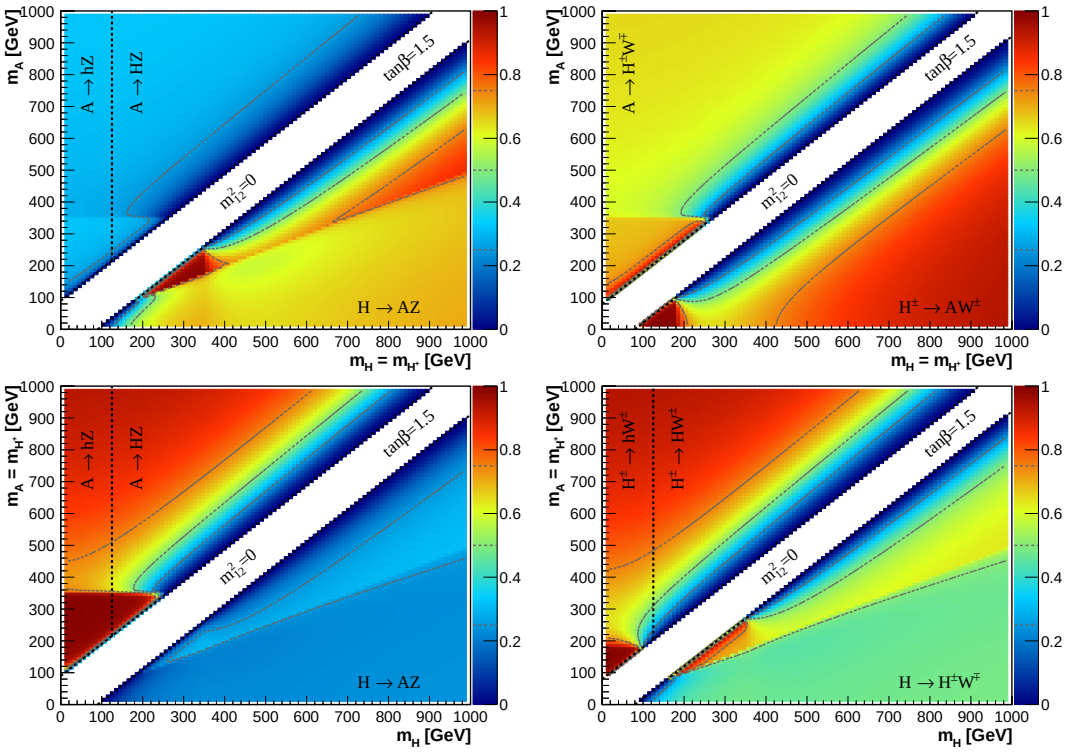

Figure 15. Left: Exotic decay BR $H/A \to AZ/H(h)Z$ for Plane I (top) and Plane II (bottom) for Case 2 ($m_{12}^2 = 0$) with $t_\beta = 1.5$. For $A \to H(h)Z$, we consider $A \to HZ$ for $m_H > m_h = 125$ GeV and $A \to hZ$ for $m_h < m_H = 125$ GeV (so that the BR into the non-SM like Higgs boson is shown in each case). Right: Exotic decay BR $A/H^{\pm} \to H^{\pm}W^{\mp}/AW^{\pm}$ for Plane I (top) and $H/H^{\pm} \to H^{\pm}W^{\mp}/HW^{\pm}$ for Plane II (bottom), for Case 2 ($m_{12}^2 = 0$) with $t_\beta = 1.5$.

A.2 2HDM Branching Ratios for Exotic Higgs Decays

For illustration, we show in Figure 15 the branching ratios of $H_a \to H_b V$ (with $H_{a,b} = H$, A, $H^{\pm}$ and $V = W^{\pm}$, Z) for Plane I (top) and Plane II (bottom) for Case 2 ($m_{12}^2 = 0$) with $t_\beta = 1.5$ (being the scenario allowed for the four benchmarks BP IA, BP IB, BP

IIA and BP IIB). The decay branching ratios for $H/A \to AZ/H(h)Z$ are shown on the left panels of Figure 15, while those for $A/H^\pm \to H^\pm W^\mp/AW^\pm$ (Plane I) and $H/H^\pm \to H^\pm W^\mp/HW^\pm$ (Plane II) are shown on the right panels.

References

[1] G. Aad *et al.* [ATLAS Collaboration], Eur. Phys. J. C **76** (2016) 1, 6 [arXiv:1507.04548 [hep-ex]].

[2] V. Khachatryan *et al.* [CMS Collaboration], Eur. Phys. J. C **75** (2015) 5, 212 [arXiv:1412.8662 [hep-ex]].

[3] A. Djouadi, Phys. Rept. **459** (2008) 1 [hep-ph/0503173].

[4] J. Mrazek, A. Pomarol, R. Rattazzi, M. Redi, J. Serra and A. Wulzer, Nucl. Phys. B **853** (2011) 1 [arXiv:1105.5403 [hep-ph]]; E. Bertuzzo, T. S. Ray, H. de Sandes and C. A. Savoy, JHEP **1305** (2013) 153 [arXiv:1206.2623 [hep-ph]].

[5] J. M. Cline, K. Kainulainen and A. P. Vischer, Phys. Rev. D **54** (1996) 2451 [hep-ph/9506284]; J. M. Cline and P. A. Lemieux, Phys. Rev. D **55** (1997) 3873 [hep-ph/9609240]; L. Fromme, S. J. Huber and M. Seniuch, JHEP **0611** (2006) 038 [hep-ph/0605242]; G. C. Dorsch, S. J. Huber and J. M. No, JHEP **1310** (2013) 029 [arXiv:1305.6610 [hep-ph]].

[6] A. Celis, V. Ilisie and A. Pich, JHEP **1307** (2013) 053 [arXiv:1302.4022 [hep-ph]].

[7] B. Grinstein and P. Uttayarat, JHEP **1306** (2013) 094 [JHEP **1309** (2013) 110] [arXiv:1304.0028 [hep-ph]].

[8] B. Coleppa, F. Kling and S. Su, JHEP **1401**, 161 (2014) [arXiv:1305.0002 [hep-ph]].

[9] C. Y. Chen, S. Dawson and M. Sher, Phys. Rev. D **88** (2013) 015018 [Phys. Rev. D **88** (2013) 039901] [arXiv:1305.1624 [hep-ph]].

[10] O. Eberhardt, U. Nierste and M. Wiebusch, JHEP **1307** (2013) 118 [arXiv:1305.1649 [hep-ph]].

[11] B. Dumont, J. F. Gunion, Y. Jiang and S. Kraml, Phys. Rev. D **90** (2014) 035021 [arXiv:1405.3584 [hep-ph]].

[12] J. Bernon, B. Dumont and S. Kraml, Phys. Rev. D **90** (2014) 071301 [arXiv:1409.1588 [hep-ph]].

[13] N. Craig, F. D'Eramo, P. Draper, S. Thomas and H. Zhang, JHEP **1506** (2015) 137 [arXiv:1504.04630 [hep-ph]].

[14] J. Bernon, J. F. Gunion, H. E. Haber, Y. Jiang and S. Kraml, Phys. Rev. D **92** (2015) 7, 075004 [arXiv:1507.00933 [hep-ph]].

[15] G. C. Dorsch, S. J. Huber, K. Mimasu and J. M. No, arXiv:1601.04545 [hep-ph].

[16] B. Coleppa, F. Kling and S. Su, arXiv:1308.6201 [hep-ph].

[17] B. Coleppa, F. Kling and S. Su, JHEP **1409**, 161 (2014) [arXiv:1404.1922 [hep-ph]].

[18] G. C. Dorsch, S. J. Huber, K. Mimasu and J. M. No, Phys. Rev. Lett. **113** (2014) 21, 211802 [arXiv:1405.5537 [hep-ph]].

[19] B. Coleppa, F. Kling and S. Su, JHEP **1412**, 148 (2014) [arXiv:1408.4119 [hep-ph]].

[20] T. Li and S. Su, JHEP **1511** (2015) 068 [arXiv:1504.04381 [hep-ph]].

[21] F. Kling, A. Pyarelal and S. Su, JHEP **1511**, 051 (2015) [arXiv:1504.06624 [hep-ph]].

[22] CMS Collaboration [CMS Collaboration], CMS-PAS-HIG-15-001.

[23] V. Khachatryan *et al.* [CMS Collaboration], arXiv:1603.02991 [hep-ex].

[24] J. F. Gunion, H. E. Haber, G. L. Kane and S. Dawson, Front. Phys. **80**, 1 (2000).

[25] J. Bernon, J. F. Gunion, H. E. Haber, Y. Jiang and S. Kraml, arXiv:1511.03682 [hep-ph].

[26] J. F. Gunion and H. E. Haber, Phys. Rev. D **67**, 075019 (2003) [hep-ph/0207010].

[27] G. Abbiendi *et al.* [ALEPH and DELPHI and L3 and OPAL and LEP Collaborations], Eur. Phys. J. C **73** (2013) 2463 [arXiv:1301.6065 [hep-ex]].

[28] J. Bernon, J. F. Gunion, Y. Jiang and S. Kraml, Phys. Rev. D **91** (2015) 7, 075019 [arXiv:1412.3385 [hep-ph]].

[29] S. L. Glashow and S. Weinberg, Phys. Rev. D **15**, 1958 (1977).

[30] G. C. Branco, P. M. Ferreira, L. Lavoura, M. N. Rebelo, M. Sher and J. P. Silva, Phys. Rept. **516**, 1 (2012) [arXiv:1106.0034 [hep-ph]].

[31] G. Aad *et al.* [ATLAS Collaboration], JHEP **1511** (2015) 206 [arXiv:1509.00672 [hep-ex]].

[32] P. M. Ferreira, J. F. Gunion, H. E. Haber and R. Santos, Phys. Rev. D **89**, no. 11, 115003 (2014) [arXiv:1403.4736 [hep-ph]].

[33] I. F. Ginzburg and I. P. Ivanov, Phys. Rev. D **72** (2005) 115010 [hep-ph/0508020].

[34] D. Eriksson, J. Rathsman and O. Stål, Comput. Phys. Commun. **181** (2010) 189 [arXiv:0902.0851 [hep-ph]].

[35] M. Baak *et al.* [Gfitter Group Collaboration], Eur. Phys. J. C **74** (2014) 3046 [arXiv:1407.3792 [hep-ph]].

[36] M. Gorbahn, J. M. No and V. Sanz, JHEP **1510** (2015) 036 [arXiv:1502.07352 [hep-ph]].

[37] Y. Amhis *et al.* [Heavy Flavor Averaging Group (HFAG) Collaboration], arXiv:1412.7515 [hep-ex].

[38] F. Mahmoudi, Comput. Phys. Commun. **180** (2009) 1579 [arXiv:0808.3144 [hep-ph]].

[39] F. Mahmoudi, Comput. Phys. Commun. **180** (2009) 1718.

[40] J. P. Lees *et al.* [BaBar Collaboration], Phys. Rev. Lett. **109** (2012) 101802 [arXiv:1205.5442 [hep-ex]].

[41] M. Huschle *et al.* [Belle Collaboration], Phys. Rev. D **92** (2015) no.7, 072014 [arXiv:1507.03233 [hep-ex]].

[42] A. Abdesselam *et al.* [Belle Collaboration], arXiv:1603.06711 [hep-ex].

[43] M. Misiak *et al.*, Phys. Rev. Lett. **114** (2015) 22, 221801 [arXiv:1503.01789 [hep-ph]].

[44] T. Han, T. Li, S. Su and L. T. Wang, JHEP **1311**, 053 (2013) [arXiv:1306.3229 [hep-ph]].

[45] S. Schael *et al.* [ALEPH and DELPHI and L3 and OPAL and LEP Working Group for Higgs Boson Searches Collaborations], Eur. Phys. J. C **47** (2006) 547 [hep-ex/0602042].

[46] G. Aad *et al.* [ATLAS Collaboration], JHEP **1411** (2014) 056 [arXiv:1409.6064 [hep-ex]].

[47] V. Khachatryan *et al.* [CMS Collaboration], JHEP **1410** (2014) 160 [arXiv:1408.3316 [hep-ex]].

[48] [ATLAS Collaboration], ATLAS-CONF-2013-013.

[49] G. Aad *et al.* [ATLAS Collaboration], Phys. Rev. D **92** (2015) 1, 012006 [arXiv:1412.2641 [hep-ex]].

[50] V. Khachatryan *et al.* [CMS Collaboration], JHEP **1510** (2015) 144 [arXiv:1504.00936 [hep-ex]].

[51] G. Aad *et al.* [ATLAS Collaboration], Phys. Lett. B **744** (2015) 163 [arXiv:1502.04478 [hep-ex]].

[52] V. Khachatryan *et al.* [CMS Collaboration], Phys. Lett. B **748** (2015) 221 [arXiv:1504.04710 [hep-ex]].

[53] G. Aad *et al.* [ATLAS Collaboration], Phys. Rev. Lett. **114** (2015) 8, 081802 [arXiv:1406.5053 [hep-ex]].

[54] CMS Collaboration [CMS Collaboration], CMS-PAS-HIG-13-032.

[55] V. Khachatryan *et al.* [CMS Collaboration], Phys. Lett. B **749** (2015) 560 [arXiv:1503.04114 [hep-ex]].

[56] G. Aad *et al.* [ATLAS Collaboration], JHEP **1503** (2015) 088 [arXiv:1412.6663 [hep-ex]].

[57] V. Khachatryan *et al.* [CMS Collaboration], JHEP **1511** (2015) 018 [arXiv:1508.07774 [hep-ex]].

[58] R. V. Harlander, S. Liebler and H. Mantler, Comput. Phys. Commun. **184** (2013) 1605 [arXiv:1212.3249 [hep-ph]].

[59] M. Flechl, R. Klees, M. Kramer, M. Spira and M. Ubiali, Phys. Rev. D **91**, no. 7, 075015 (2015) [arXiv:1409.5615 [hep-ph]]; S. Heinemeyer *et al.* [LHC Higgs Cross Section Working Group Collaboration], arXiv:1307.1347 [hep-ph]; S. Dittmaier, M. Kramer, M. Spira and M. Walser, Phys. Rev. D **83**, 055005 (2011) [arXiv:0906.2648 [hep-ph]]; E. L. Berger, T. Han, J. Jiang and T. Plehn, Phys. Rev. D **71**, 115012 (2005) [hep-ph/0312286].

[60] M. Czakon and A. Mitov, Comput. Phys. Commun. **185**, 2930 (2014) [arXiv:1112.5675 [hep-ph]].

[61] H. E. Haber and O. Stål, Eur. Phys. J. C **75** (2015) no.10, 491 [arXiv:1507.04281 [hep-ph]].

Appendix C

Exotic Decays of a Heavy Neutral Higgs through HZ/AZ Channel

The article *Exotic Decays of a Heavy Neutral Higgs through HZ/AZ Channel* has been submitted to arXiv and accepted for publication in the Journal of High Energy Physics [23].

Published for SISSA by Springer

Received: *April 28, 2014*
Revised: *August 12, 2014*
Accepted: *August 30, 2014*
Published: *September 26, 2014*

Exotic decays of a heavy neutral Higgs through HZ/AZ channel

Baradhwaj Coleppa, Felix Kling and Shufang Su

Department of Physics, University of Arizona,
1118 E. 4th st., P.O. Box 210081, Tucson, AZ 85721, U.S.A.

E-mail: baradhwa@email.arizona.edu, kling@email.arizona.edu, shufang@email.arizona.edu

Abstract: Models of electroweak symmetry breaking with extended Higgs sectors are theoretically well motivated. In this study, we focus on the Two Higgs Doublet Model with a low energy spectrum containing scalars H and a pseudoscalar A. We study the decays $A \to HZ$ or $H \to AZ$, which could reach sizable branching fractions in certain parameter regions. With detailed collider analysis, we obtain model independent exclusion bounds as well as discovery reach at the 14 TeV LHC for the process: $gg \to A/H \to HZ/AZ$, looking at final states $bb\ell\ell$, $\tau\tau\ell\ell$ and $ZZZ(4\ell + 2j)$ for $\ell = e, \mu$. We further interpret these bounds in the context of the Type II Two Higgs Doublet Model, considering three different classes of processes: $A \to h^0 Z$, $A \to H^0 Z$, and $H^0 \to AZ$, in which h^0 and H^0 are the light and heavy CP-even Higgses respectively. For 100 fb^{-1} integrated luminosity at the 14 TeV LHC, we find that for parent particle mass around 300–400 GeV, $A \to h^0 Z$ has the greatest reach when H^0 is interpreted as the 126 GeV Higgs: most regions in the $\tan\beta$ versus $\sin(\beta - \alpha)$ plane can be excluded and a significant fraction at small and large $\tan\beta$ can be covered by discovery. For 126 GeV h^0, only relatively small $\tan\beta \lesssim 10\,(5)$ can be reached by exclusion (discovery) while a wide range of $\sin(\beta - \alpha)$ is accessible. For $A \to H^0 Z$, the reach is typically restricted to $\sin(\beta - \alpha) \sim \pm 1$ with $\tan\beta \lesssim 10$ in $bb\ell\ell$ and $\tau\tau\ell\ell$ channels. The $ZZZ(4\ell 2j)$ channel, on the other hand, covers a wide range of $0.3 < |\sin(\beta - \alpha)| < 1$ for $\tan\beta \lesssim 4$. $H^0 \to AZ$ typically favors negative values of $\sin(\beta - \alpha)$, with exclusion/discovery reach possibly extending to all values of $\tan\beta$. A study of exotic decays of extra Higgses appearing in extensions of the Standard Model would extend the reach at the LHC and provides nice complementarity to conventional Higgs search channels.

Keywords: Higgs Physics, Beyond Standard Model

ArXiv ePrint: 1404.1922

doi:10.1007/JHEP09(2014)161

JHEP09(2014)161

Contents

1 Introduction

The greatest experimental triumph of the Large Hadron Collider (LHC) till date is the discovery of a scalar resonance at 126 GeV with properties consistent with that of the Standard Model (SM) Higgs [1–4]. The mass of this particle along with its spin [2, 4, 5] has now been established, and a complete characterization of all its possible decay modes is underway. At the same time, from the theoretical front, we have now known for a while that the SM, though in excellent agreement with experiments, has to be supplanted with other dynamics if it is to explain many puzzles facing particle physics today, viz., the hierarchy problem, neutrino masses, and the nature of dark matter, to name a few. Many beyond the SM scenarios are constructed to explain one or many of these puzzles, and are becoming more constrained by the Higgs observation at the LHC. This is particularly true for theories constructed with an extended Higgs sector. Well known examples are the Minimal Supersymmetric Standard Model (MSSM) [6–8], Next to Minimal Supersymmetric Standard Model (NMSSM) [9, 10] and Two Higgs Doublet Models (2HDM) [11–14]. In addition to the SM-like Higgs boson in these models, the low energy spectrum includes other CP-even Higgses, CP-odd Higgses, as well as charged ones.

Models with an extended Higgs sector hold a lot of phenomenological interest. The discovery of extra Higgses would be an unambiguous evidence for new physics beyond the SM. Other than the decay of these extra Higgses into the SM final states $\gamma\gamma$, ZZ, WW, bb and $\tau\tau$, which have been the focus of the current Higgs searches, the decay of heavy

JHEP09(2014)161

Higgses into light Higgses, or Higgs plus gauge boson final states could also be sizable. Such decays are particularly relevant as the 126 GeV resonance could show up as a decay of a heavier state, opening up the interesting possibility of using the SM-like Higgs to discover its heavier counterparts. It is thus timely to study these exotic Higgs decay channels and fully explore the experimental discovery potential for the enlarged Higgs sector.

In this paper, we focus on the decays $H \to AZ$ or $A \to HZ$, with H and A referring to generic CP-even and CP-odd Higgs, respectively.[1] We consider leptonic decays of the Z, with the A/H in the final states decaying to either a pair of fermions (bb or $\tau\tau$) or ZZ and explore the exclusion bounds as well as discovery reach at the LHC for various combinations of (m_A, m_H).

In the 2HDM or NMSSM, both decays $H_i \to A_j Z$ and $A_i \to H_j Z$ could appear with large branching fractions as shown in [15–18]. Ref. [19] also argued that $A \to h^0 Z$ could have a sizable branching fraction in the low $\tan\beta$ region of the MSSM with the light CP-even h^0 being SM-like. A brief Snowmass study of $A/H \to HZ/AZ$ with $bb\ell\ell$ final state can be found in ref. [20]. Another Snowmass study of heavy Higgses [21] explored sensitivities in the $H^0 \to ZZ \to 4\ell$ and $A \to Zh^0 \to bb\ell\ell$, $\tau\tau\ell\ell$ channels at the 14 TeV and 33 TeV LHC, focusing on the case with h^0 being the 126 GeV Higgs. In our study, we consider a variety of daughter Higgs masses in $bb\ell\ell$ and $\tau\tau\ell\ell$ channels, and analyze $A \to H^0 Z \to ZZZ$ in addition. We also interpret the search results in the context of the Type II 2HDM.

The paper is organized as follows. In section 2, we present a brief overview of models and parameter regions where the channels under consideration can be significant. In section 3, we summarize the current experimental search limits on heavy Higgses. In section 4.1, we present the details of the analysis of the HZ/AZ with the $bb\ell\ell$ final states. We also show model-independent results of 95% C.L. exclusion as well as 5σ discovery limits for $\sigma \times \mathrm{BR}(gg \to A/H \to HZ/AZ \to bb\ell\ell)$ at the 14 TeV LHC with 100, 300 and 1000 fb^{-1} integrated luminosity. In sections 4.2 and 4.3, we present the analysis for the $\tau\tau\ell\ell$ and ZZZ final states, respectively. In section 5, we study the implications of the collider search limits on the parameter regions of the Type II 2HDM. We conclude in section 6.

2 Scenarios with large $H \to AZ$ or $A \to HZ$

In the 2HDM, we introduce two SU(2) doublets Φ_i, $i = 1, 2$:

$$\Phi_i = \begin{pmatrix} \phi_i^+ \\ (v_i + \phi_i^0 + iG_i)/\sqrt{2} \end{pmatrix}, \tag{2.1}$$

where v_1 and v_2 are the vacuum expectation values of the neutral components which satisfy the relation: $\sqrt{v_1^2 + v_2^2} = 246$ GeV after electroweak symmetry breaking. Assuming a discrete $\mathcal{Z}_2$ symmetry imposed on the Lagrangian, we are left with six free parameters, which can be chosen as four Higgs masses (m_h, m_H, m_A, $m_{H^\pm}$), the mixing angle α between the two CP-even Higgses, and the ratio of the two vacuum expectation values,

[1] Note that we use h^0 and H^0 to refer to the lighter or the heavier CP-even Higgs for models with two CP-even Higgs bosons. When there is no need to specify, we use H to refer to the CP-even Higgses.

JHEP09(2014)161

$\tan\beta = v_2/v_1$. In the case in which a soft breaking of the $\mathcal{Z}_2$ symmetry is allowed, there is an additional parameter m_{12}^2.

The mass eigenstates contain a pair of CP-even Higgses: h^0, H^0, one CP-odd Higgs, A and a pair of charged Higgses $H^\pm$:[2]

$$\begin{pmatrix} H^0 \\ h^0 \end{pmatrix} = \begin{pmatrix} \cos\alpha & \sin\alpha \\ -\sin\alpha & \cos\alpha \end{pmatrix} \begin{pmatrix} \phi_1^0 \\ \phi_2^0 \end{pmatrix}, \qquad \begin{aligned} A &= -G_1 \sin\beta + G_2 \cos\beta \\ H^\pm &= -\phi_1^\pm \sin\beta + \phi_2^\pm \cos\beta \,. \end{aligned} \tag{2.2}$$

Two types of couplings that are of particular interest are ZAH^0/h^0 couplings and H^0/h^0VV couplings, with V being the SM gauge bosons $W^\pm$ and Z. Both are determined by the gauge coupling structure and the mixing angles. The couplings for ZAH^0 and ZAh^0 are [22]:

$$g_{ZAH^0} = -\frac{g\sin(\beta-\alpha)}{2\cos\theta_w}(p_{H^0} - p_A)_\mu \,, \qquad g_{ZAh^0} = \frac{g\cos(\beta-\alpha)}{2\cos\theta_w}(p_{h^0} - p_A)_\mu \,, \tag{2.3}$$

with g being the SU(2) coupling, θ_w being the Weinberg angle and p_μ being the incoming momentum of the corresponding particle.

The H^0VV and h^0VV couplings are:

$$g_{H^0VV} = \frac{m_V^2}{v}\cos(\beta-\alpha) \,, \qquad g_{h^0VV} = \frac{m_V^2}{v}\sin(\beta-\alpha) \,. \tag{2.4}$$

Note that A always couples to the non-SM-like Higgs more strongly. If we demand h^0 (H^0) to be SM-like, then $|\sin(\beta-\alpha)| \sim 1$ ($|\cos(\beta-\alpha)| \sim 1$) is preferred, and the ZAH^0 (ZAh^0) coupling is unsuppressed. Therefore, in the h^0-126 case, A is more likely to decay to H^0Z than h^0Z, unless the former decay is kinematically suppressed. $H^0 \to AZ$ could also be dominant once it is kinematically open. Particularly for a heavy H^0, as we will demonstrate later in section 5, $H^0 \to AZ$ can have a large branching fraction in the $\sin(\beta-\alpha) = \pm 1$ regions. On the contrary, for H^0 being SM-like with $|\cos(\beta-\alpha)| \sim 1$, $A \to h^0Z$ dominates over H^0Z channel. For very light m_A, $h^0 \to AZ$ could also open. The detectability of this channel, however, is challenging given the soft or collinear final decay products from a light A. Therefore, for our discussion below, we will focus on the cases $A \to h^0Z$, H^0Z and $H^0 \to AZ$ only.

In the generic 2HDM, there are no mass relations between the pseudoscalar and the scalar states. Thus, the decays $A \to h^0Z$, H^0Z and $H^0 \to AZ$ can happen in different regions of parameter spaces. It was shown in ref. [23] that in the Type II 2HDM with $\mathcal{Z}_2$ symmetry, imposing all experimental and theoretical constraints still leaves sizable regions in the parameter space. In those parameter spaces, such exotic decays can have unsuppressed decay branching fractions. It was also pointed out in ref. [11] that in the Type I 2HDM, for $\cos^2(\alpha-\beta) > 1/2$, the decay $h^0 \to AZ$ will actually dominate the WW decay for a light A. Results obtained in this study can also be applied to the CP-violating 2HDM in which $H_i \to H_jZ$ could be sizable with $H_{i,j}$ being mixtures of CP-even and CP-odd states. Appropriate rescaling of the production cross sections and decay branching fractions is needed to recast the results.

[2]For more details about the model, see ref. [11].

JHEP09(2014)161

The Higgs sector in the MSSM is more restricted, given that the quartic Higgs couplings are fixed by the gauge couplings and the tree-level Higgs mass matrix only depends on m_A and $\tan\beta$. In the usual decoupling region with large m_A, the light CP-even Higgs h^0 is SM-like while the other Higgses are almost degenerate: $m_{H^0} \sim m_A \sim m_{H^\pm}$. Thus, $A \to ZH^0$ or $H^0 \to ZA$ is not allowed kinematically. $A \to Zh^0$ is typically suppressed by the small coupling: $\cos(\beta-\alpha) \sim 0$, and is only relevant for small $\tan\beta$. In the NMSSM, the Higgs sector of MSSM is enlarged to include an additional singlet. It was shown in ref. [17] that there are regions of parameter space where the decay $A_i \to H_j Z$ can be significant.

3 Current experimental limits

Searches for the non-SM like Higgses, mainly in the bb, $\mu\mu$, $\tau\tau$ or WW/ZZ channels have been performed both by ATLAS and CMS. No evidence for a neutral non-SM like Higgs was found.

Searches for the neutral Higgs bosons Φ of the MSSM in the process $pp \to \Phi \to \mu^+\mu^-/\tau^+\tau^-$ have been performed by the ATLAS [24], and in the $\tau^+\tau^-$channel at CMS [25]. Limits in the $\mu\mu$ channel are much weaker given the extremely small branching fraction in the MSSM. The production mechanisms considered were both gluon fusion and bb associated production, and the exclusion results were reported for the MSSM m_h^{max} scenario. The ATLAS study was performed at $\sqrt{s} = 7\,\text{TeV}$ with 4.7–4.8 fb^{-1} integrated luminosity looking at three different possible $\tau\tau$ final states, $\tau_e\tau_\mu$, $\tau_{\text{lep}}\tau_{\text{had}}$, and $\tau_{\text{had}}\tau_{\text{had}}$. The ATLAS search rules out a fairly sizable portion of the MSSM parameter space, extending from about $\tan\beta$ of 10 for $m_A \sim 130\,\text{GeV}$, to $\tan\beta \approx 60$ for $m_A = 500\,\text{GeV}$. The corresponding exclusion in $\sigma_\Phi \times \text{BR}(\Phi \to \tau\tau)$ extends from roughly 40 pb to 0.3 pb in that mass range. The CMS study was performed with 19.7 fb^{-1} integrated luminosity at 8 TeV and 4.9 fb^{-1} at 7 TeV in the $\tau_e\tau_\mu$, $\tau_\mu\tau_\mu$, $\tau_{\text{lep}}\tau_{\text{had}}$, and $\tau_{\text{had}}\tau_{\text{had}}$ final states. The search excludes roughly between $\tan\beta$ of 4 for $m_A = 140\,\text{GeV}$ and $\tan\beta \approx 60$ for $m_A = 1000\,\text{GeV}$. The corresponding exclusion in $\sigma_\Phi \times \text{BR}(\Phi \to \tau\tau)$ extends from roughly 2 pb to 13 fb in that mass range.

In figure 1, we recast the current 95% C.L. limit of $pp \to \Phi \to \tau^+\tau^-$ in the $(m_A, \tan\beta)$ parameter space of the Type II 2HDM [25] (left panel) and the projected 5σ reach at the 14 TeV LHC with 30 fb^{-1} luminosity [26] (right panel). In both plots, the solid black curves correspond to the limits in the MSSM, when $m_A \approx m_{H^0}$ with both A and H^0 contributing to the signal. The solid red curves correspond to the limits in the type II 2HDM, when only contribution from A is included and H^0 is decoupled. The reach is considerably weaker: the current exclusion is about $\tan\beta \sim 12$ at $m_A = 160\,\text{GeV}$, and $\tan\beta \sim 46$ for $m_A = 600\,\text{GeV}$. At the 14 TeV LHC with 30 fb^{-1} luminosity, the 5σ reach extends beyond the current exclusion for large m_A. Dashed lines indicate the reduced reach in the $\tau\tau$ channel once $A \to h^0 Z$ mode opens, for a benchmark point of $\sin(\beta-\alpha) = 0$, $m_{h^0} = 50\,\text{GeV}$ and $m_{H^0} = 126\,\text{GeV}$.

Searches with bb final states have also been performed for the MSSM Higgs in the associated production $pp \to b\Phi + X$. The CMS search, done with 2.7–4.8 fb^{-1} of data at

JHEP09(2014)161

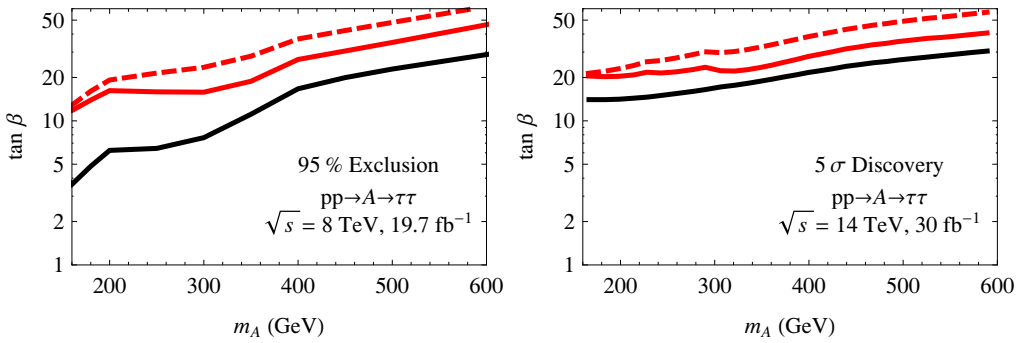

Figure 1. The reach of $pp \to A \to \tau\tau$ in $m_A - \tan\beta$ parameter space of the Type II 2HDM. Left panel shows the current 95% C.L. exclusion limits from CMS [25] with 19.7 fb^{-1} data collected at the $\sqrt{s} = 8$ TeV LHC. Right panel shows the projected 5σ discovery reach at the 14 TeV LHC with 30 fb^{-1} luminosity [26]. In both plots, the solid black curves correspond to the limits in the MSSM, when $m_A \approx m_{H^0}$ with both A and H^0 contributing to the signal. The solid red curves correspond to the limits in the type II 2HDM, when only contribution from A is included and H^0 is decoupled. Also shown in the red dashed curves are the reduced $\tau\tau$ channel limits when $A \to h^0 Z$ is open with the parameter choice of $\sin(\beta - \alpha) = 0$, $m_{h^0} = 50$ GeV and $m_{H^0} = 126$ GeV.

$\sqrt{s} = 7$ TeV excludes $\tan\beta$ values between 18 and 42 in the mass range 90 GeV $< m_A <$ 350 GeV [27].

The ATLAS collaboration has also looked for the heavier CP-even Higgs in the Type I and Type II 2HDM, assuming the lighter CP-even Higgs is the discovered 126 GeV boson [28]. The study was performed with 13 fb^{-1} integrated luminosity at 8 TeV and considered both gluon fusion and vector boson fusion production. Searches in the process $H^0 \to WW \to e\mu\nu_e\nu_\mu$ exclude a significant region of the $m_{H^0} - \cos\alpha$ parameter space in the mass range 135 GeV $< m_{H^0} <$ 200 GeV for the Type II 2HDM. The excluded region shrinks for higher $\tan\beta$ due to the reduced branching ratio to WW. This would serve as a useful constraint if we were to look at decays of the relatively light H^0 to light A's. In this paper, we consider values of m_H outside this mass range so this constraint does not apply.

The CMS collaboration has also searched for the heavier CP-even Higgs H^0 and a heavy CP-odd Higgs A in 2HDM via the processes $gg \to A \to h^0 Z$ and $gg \to H^0 \to h^0 h^0$, assuming the lighter Higgs h^0 is the discovered 126 GeV boson [29]. The study was performed with 19.5 fb^{-1} integrated luminosity at 8 TeV. Various possible decays of the SM-Higgs were taken into account. Assuming SM branching ratios for h^0, this study gives an upper bound on $\sigma \times \mathrm{BR}(A \to h^0 Z)$ of roughly 1.5 pb for m_A between 260 and 360 GeV and $\sigma \times \mathrm{BR}(H^0 \to h^0 h^0)$ between 8 pb and 6 pb for masses m_{H^0} between 260 GeV and 360 GeV. The corresponding excluded parameter space for the Type II 2HDM in the $\tan\beta - \cos(\beta - \alpha)$ plane was also analyzed. In the analysis presented in this paper, we do not necessarily require that the daughter Higgs in $A \to HZ$ to be the SM-like Higgs or have SM-like branching ratios. Furthermore we also analyze the process $H \to AZ$ for light A and its implication in the Type II 2HDM.

JHEP09(2014)161

4 Collider analysis

In this section, we will present model *independent* limits on the $\sigma \times \mathrm{BR}$ for both 95% C.L. exclusion and 5σ discovery for $A/H \to HZ/AZ$ in the various final states of $bb\ell\ell$, $\tau\tau\ell\ell$ and $ZZZ(4\ell 2j)$. In this study we focus on the leptonic decay of the Z, which allows precise mass reconstruction and suppresses the background sufficiently. Other decay modes of the Z, for example $Z \to \tau\tau$, might be useful in studying this channel as well. In the discussion of the analyses and results below, we use the decay $A \to HZ$ for $m_A > m_H + m_Z$ as an illustration. Since we do not make use of angular correlations, the bounds obtained for $A \to HZ$ apply to $H \to AZ$ as well with the values of m_A and m_H switched.

4.1 $A/H \to HZ/AZ \to bb\ell\ell$

We start our analysis by looking at the channel $A/H \to HZ/AZ \to bb\ell\ell$ for $\ell = e, \mu$, focusing only on the gluon fusion production channels. We use H to refer to either the light or the heavy CP-even Higgs. Since the only allowed couplings are of the type $H-A-Z$, if the parent particle is a scalar H, the daughter particle is necessarily a pseudoscalar A and vice versa.

The dominant SM backgrounds for $bb\ell\ell$ final states are $Z/\gamma^* bb$ with leptonic Z/γ^* decay, $t\bar{t}$ with leptonically decaying top quarks, $ZZ \to bb\ell\ell$, and $H_{\mathrm{SM}}Z$ [30–33]. We have ignored the subdominant backgrounds from WZ, WW, $H_{\mathrm{SM}} \to ZZ$, Wbb, Multijet QCD Background, Zjj, $Z\ell\ell$ as well as tWb. These backgrounds either have small production cross sections, or can be sufficiently suppressed by the cuts imposed. We have included $H_{\mathrm{SM}}Z$ here even if the cross section is very small because it has the same final state as the process under consideration, especially for the $A \to H_{\mathrm{SM}}Z$ case. The total cross sections for these backgrounds can be found in table 1.

We use Madgraph 5/MadEvent v1.5.11 [34] to generate our signal and background events. These events are passed to Pythia v2.1.21 [35] to simulate initial and final state radiation, showering and hadronization. The events are further passed through Delphes 3.09 [36] with the Snowmass combined LHC detector card [37] to simulate detector effects.

For the signal process, we generated event samples at the 14 TeV LHC for $gg \to A \to HZ$ with the daughter particle mass fixed at 50, 126, and 200 GeV while varying the parent particle mass in the range of 150–600 GeV. We applied the following cuts to identify the signal from the backgrounds:[3]

1. *Two isolated leptons, two tagged b's.*

$$n_\ell = 2\,,\ n_b = 2\,,\ \text{with } |\eta_{\ell,b}| < 2.5\,,\ p_{T,\ell} > 10\,\mathrm{GeV},\ p_{T,b} > 15\,\mathrm{GeV}. \tag{4.1}$$

   For jet reconstruction, the anti-k_T jet algorithm with $R = 0.5$ is used.

2. *Lepton trigger [38, 39].*

$$p_{T,\ell_1} > 30\,\mathrm{GeV} \text{ or } p_{T,\ell_1} > 20\,\mathrm{GeV},\ p_{T,\ell_2} > 10\,\mathrm{GeV}. \tag{4.2}$$

[3] Requiring the missing transverse energy to be small would potentially greatly reduce the $t\bar{t}$ background. However, including pile-up effects introduces $\not{E}_T$ in the signal events, which renders the cut inefficient. We thank Meenakshi Narain and John Stupak for pointing this out to us.

JHEP09(2014)161

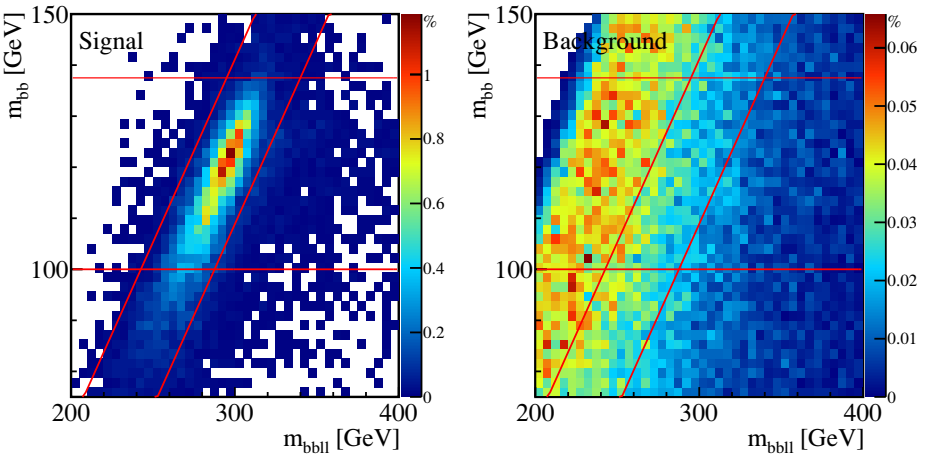

Figure 2. Normalized distribution (in percent as given by the color code along the y-axis) of m_{bb} versus $m_{bb\ell\ell}$ for the signal (left panel), and the backgrounds ($Z/\gamma^* bb + ZZ + H_{\rm SM} + t\bar{t}$) (right panel) for $m_A = 300\,\text{GeV}$ and $m_H = 126\,\text{GeV}$. Two horizontal lines indicate the m_{bb} range and two slanted lines indicate the $m_{bb\ell\ell}$ range, as given in eq. (4.4).

3. *Dilepton mass* $m_{\ell\ell}$. We require the dilepton mass to be in the Z-mass window:

$$80\,\text{GeV} < m_{\ell\ell} < 100\,\text{GeV}. \tag{4.3}$$

4. m_{bb} *versus* $m_{bb\ell\ell}$. We require the dijet mass m_{bb} to be close to the daughter-Higgs mass m_H and the mass $m_{bb\ell\ell}$ to be close to the parent-Higgs mass m_A. These two invariant masses are correlated, i.e., if we underestimate m_{bb} we also underestimate $m_{bb\ell\ell}$. To take this into account we apply a two-dimensional cut:

$$\begin{aligned} (0.95-w_{bb})\times m_H < m_{bb} < (0.95+w_{bb})\times m_H \text{ with } w_{bb} = 0.15\,, \\ \frac{m_Z+m_H}{m_A}\times(m_{bb\ell\ell}-m_A-w_{bb\ell\ell}) < m_{bb}-m_H < \frac{m_Z+m_H}{m_A}\times(m_{bb\ell\ell}-m_A+w_{bb\ell\ell})\,, \end{aligned} \tag{4.4}$$

where $w_{bb}\times m_H$ is the width of the dijet mass window. Note that the slightly shifted reconstructed Higgs mass m_{bb} ($0.95\,m_H$ instead of m_H) is due to the reconstruction of the b-jet with a small size of $R = 0.5$. The second condition describes two lines going through the points $(m_A \pm w_{bb\ell\ell}, m_H)$ with slope $(m_Z + m_H)/m_A$. We choose a width for the $m_{bb\ell\ell}$ peak of $w_{bb\ell\ell} = \text{Max}(\Gamma_{H_{\rm SM}}|_{m_A}, 0.075 m_A)$ where $\Gamma_{H_{\rm SM}}|_{m_A}$ is the width of a SM Higgs with mass m_A [40]. This accounts for both small Higgs masses for which the width of the peak is caused by detector effects and large Higgs masses for which the physical width dominates.

The effectiveness of this cut is shown in figure 2 for $m_A = 300\,\text{GeV}$ and $m_H = 126\,\text{GeV}$, with two horizontal lines indicating the m_{bb} range and two slanted lines indicating the $m_{bb\ell\ell}$ range as given in eq. (4.4). Left and right panels show the normalized distributions for the signal and the backgrounds, respectively. The color coding is such that points in dark red are most likely, with the probability falling as

JHEP09(2014)161

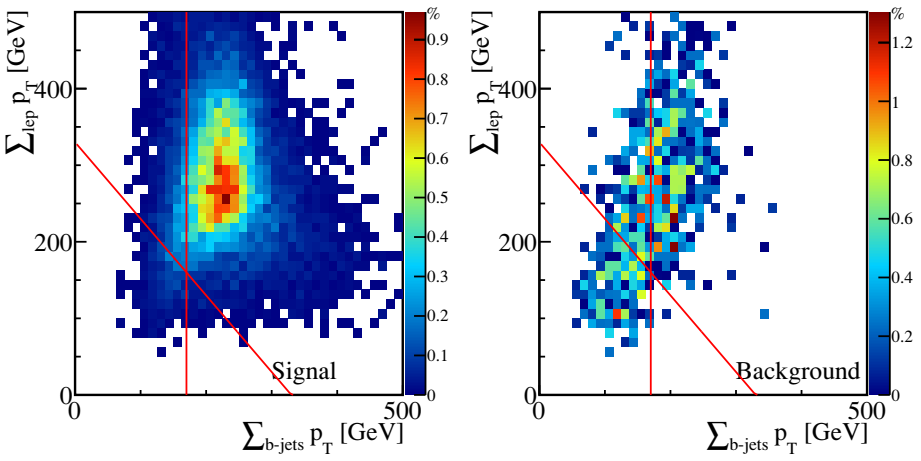

Figure 3. Normalized transverse momentum distribution $\sum_\ell p_T$ versus $\sum_{b\,\text{jets}} p_T$ for the signal (left panel) and the backgrounds (right panel) for $m_A = 500\,\text{GeV}$ and $m_H = 126\,\text{GeV}$. Two red lines indicate the conditions used in the cuts as given in eq. (4.5).

we reach dark blue as indicated on the right color panel in each plot. The numbers in this panel represent the percentage of the number of events that survive in each bin for the corresponding color. The signal region in each plot is the region bounded by the two pairs of slanting and horizontal lines. As expected, we see that most of the signal events fall within this strip, while the backgrounds mostly lie outside it.

5. *Transverse momentum.* We require the sum of the transverse momenta of the bottom jets and the sum of the transverse momenta of the bottom jets and leptons to satisfy:

$$\begin{aligned} \sum_{b\,\text{jets}} p_T &> 0.6 \times \frac{m_A^2 + m_H^2 - m_Z^2}{2m_A}\,, \\ \sum_{\ell,\, b\,\text{jets}} p_T &> 0.66 \times m_A\,. \end{aligned} \tag{4.5}$$

The cuts given in eq. (4.5) follow from simple relativistic kinematics applied to the process as applicable to the entire momenta, i.e., $\sum_{b\,\text{jets}} p_{b_i} = \frac{m_A^2+m_H^2-m_Z^2}{2m_A}$ assuming that the parent Higgs A is at rest. We have chosen to specialize this formula to the transverse part alone, including an optimization factor of 0.6. In figure 3, we show how this p_T cut helps in extracting the signal over the backgrounds for the case where the parent mass is 500 GeV and the daughter mass is 126 GeV. The regions of the plot to the left of the two lines are excluded. It can be seen that while the signal is largely intact, a good portion of the backgrounds gets cut out.

In table 1, we show the signal and background cross sections with cuts for signal benchmark point of $m_A = 300\,\text{GeV}$ and $m_H = 126\,\text{GeV}$ at the 14 TeV LHC. We have chosen a nominal value for $\sigma \times \text{BR}(gg \to A/H \to HZ/AZ \to bb\ell\ell)$ of 100 fb to illustrate the cut efficiencies for the signal process. In the last column, $S/\sqrt{B}$ is shown for an integrated

JHEP09(2014)161

Cut	Signal [fb]	$bb\ell\ell$ [fb]	$H_{\rm SM}Z$ [fb]	$t\bar{t}$ [fb]	S/B	$S/\sqrt{B}$
$\sigma_{\rm total}$		2.21×10^6	883	9.20×10^5	–	–
Leptonic decay	100	2.21×10^6	59.4	2.15×10^4	–	–
Two leptons, two b's [eq. (4.1)]	6.35	343	3.44	1409	0.0036	2.63
Lepton trigger [eq. (4.2)]	6.35	336	3.44	1394	0.0037	2.65
$m_{\ell\ell}$ [eq. (4.3)]	5.76	285	3.13	189	0.012	4.59
m_{bb} vs $m_{bb\ell\ell}$ [eq. (4.4)]	3.03	11.5	0.401	11.5	0.14	11.5
$\sum p_{T,b}$, $\sum(p_{T,b}+p_{T,\ell})$ [eq. (4.5)]	2.81	8.11	0.361	8.38	0.17	12.0

Table 1. Signal and background cross sections with cuts for the signal benchmark point $m_A = 300\,\text{GeV}$ and $m_H = 126\,\text{GeV}$ at the 14 TeV LHC. We have chosen a nominal value for $\sigma\times\text{BR}(gg\to A\to HZ\to bb\ell\ell)$ of 100 fb to illustrate the cut efficiencies for the signal process. In the last column, $S/\sqrt{B}$ is shown for an integrated luminosity of $\mathcal{L} = 300\,\text{fb}^{-1}$.

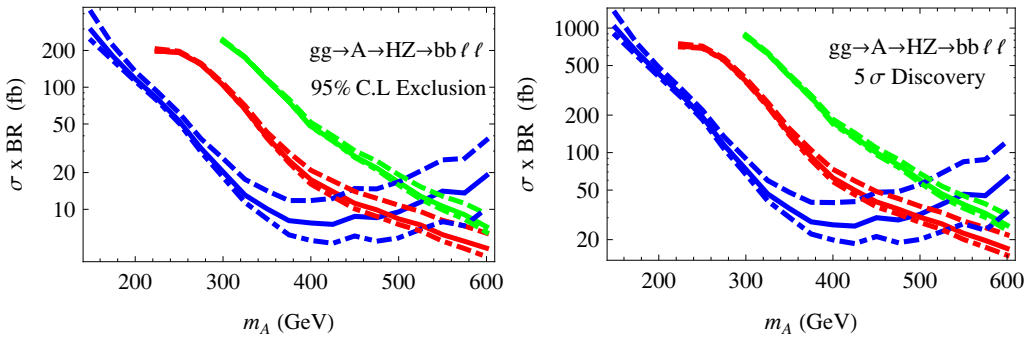

Figure 4. The 95% C.L. exclusion (left) and 5σ discovery (right) limits for $\sigma\times\text{BR}(gg\to A\to HZ\to bb\ell\ell)$ for $m_H = 50\,\text{GeV}$ (blue), 126 GeV (red), and 200 GeV (green) at the 14 TeV LHC. The dashed, solid and dot-dashed lines correspond to an integrated luminosity of 100, 300 and $1000\,\text{fb}^{-1}$, respectively. Here, we have assumed a 10% systematic error on the backgrounds. These results are equally applicable to the $H\to AZ$ process for the same parent and daughter Higgs masses.

luminosity of $\mathcal{L} = 300\,\text{fb}^{-1}$. Note that for both the signal and the backgrounds, the biggest reduction of the cross sections arises upon demanding exactly two isolated leptons and b jets. In fact, the signal cross section drops from 100 fb to 6.35 fb at this stage. The two b tag efficiencies bring down the cross section by $0.7^2\approx 50\%$. Other contributing factors are leptons and b jets that are either soft or in the forward direction, or non-isolated leptons and b jets. We also remark that the $m_{\ell\ell}$ cut does not have a significant effect on either the signal or the $bb\ell\ell$ and $H_{\rm SM}Z$ backgrounds since these are dominated by the leptons coming from Z, but does have a pronounced effect on the $t\bar{t}$ background. The second to last row clearly demonstrates the efficacy of the two dimensional cut in the $m_{bb}-m_{bb\ell\ell}$ plane.

In figure 4, we display the results at the 14 TeV LHC for 95% C.L. exclusion (left panel) and 5σ discovery (right panel) limits for $\sigma\times\text{BR}(gg\to A\to HZ\to bb\ell\ell)$, which applies for $H\to AZ$ as well with m_A and m_H switched. The blue, red, and green curves correspond to the daughter particle being 50 GeV, 126 GeV, and 200 GeV, respectively. The masses of the daughter particle are chosen such that they represent cases with a light Higgs, a SM-like Higgs, as well as a heavy Higgs that can decay to WW/ZZ. For each mass,

JHEP09(2014)161

we have displayed the results for three luminosities: $100\,\text{fb}^{-1}$ (dashed), $300\,\text{fb}^{-1}$ (solid), and $1000\,\text{fb}^{-1}$ (dot-dashed), with 10% systematic error included [41]. Better sensitivity is achieved for larger m_A since the mass cuts on m_{bb} and $m_{bb\ell\ell}$ have a more pronounced effect on SM backgrounds for larger masses. The limit, however, gets worse for the $m_H = 50\,\text{GeV}$ case when $m_A \gtrsim 400\,\text{GeV}$ (blue curves). This is due to the decrease of the signal cut efficiency for a highly boosted daughter particle with two collimated b jets. For the interesting case where the daughter particle is 126 GeV, it is seen that the discovery limits for a $300\,\text{fb}^{-1}$ collider fall from about 0.7 pb for m_A of 225 GeV, to less than 20 fb for a 600 GeV parent particle. These numbers do not change appreciably between the three chosen luminosity values, except for the case of $m_H = 50\,\text{GeV}$ and $m_A \gtrsim 400\,\text{GeV}$. This is because we have chosen a uniform 10% systematic error on the backgrounds, which dominates the statistical errors for most of the parameter region. For a given parent particle mass m_A, limits are better for smaller $m_H = 50\,\text{GeV}$. This is because the m_{bb} distribution for the dominating Zbb and tt backgrounds peaks around higher masses $m_{bb} \approx$ 70–200 GeV and therefore the background rejection efficiency for $m_{bb} \approx 50\,\text{GeV}$ is high. For $m_H = 126$ and 200 GeV the background rejection efficiencies are comparable but for $m_H = 200\,\text{GeV}$ the signal cut efficiency is worse and hence the exclusion limits are the highest for $m_H = 200\,\text{GeV}$.

We reiterate here these exclusion and discovery limits are completely model independent. Whether or not discovery/exclusion is actually feasible in this channel should be answered within the context of a particular model, in which the theoretically predicted cross sections and branching fractions can be compared with the exclusion or discovery limits. We will do this in section 5 using Type II 2HDM as a specific example.

4.2 $A/H \to HZ/AZ \to \tau\tau\ell\ell$

We now turn to the process $gg \to A/H \to HZ/AZ \to \tau\tau\ell\ell$. Since we want to reconstruct the final state particles unambiguously, we will employ τ tags and thus will only consider fully hadronic τ decays. While the signal is typically suppressed compared to the $bb\ell\ell$ case due to the smaller $H \to \tau\tau$ branching fraction, the SM backgrounds [32, 33] are much smaller due to the absence of b jets in the final states. The dominant background is ZZ. We have also included $H_{\text{SM}}Z$ background even though it is negligible for most cases.

Here, we list the cuts employed:

1. *Two isolated leptons and two tagged τ's.*

$$n_\ell = 2\,,\ n_\tau = 2\,,\ \text{with } |\eta_{\ell,\tau}| < 2.5\,,\ p_{T,\ell} > 10\,\text{GeV},\ p_{T,\tau} > 20\,\text{GeV}. \tag{4.6}$$

   We do not impose jet veto.

2. *Lepton trigger.*

$$p_{T,\ell_1} > 30\,\text{GeV or } p_{T,\ell_1} > 20\,\text{GeV},\ p_{T,\ell_2} > 10\,\text{GeV}. \tag{4.7}$$

3. *Dilepton mass $m_{\ell\ell}$.*

$$80\,\text{GeV} < m_{\ell\ell} < 100\,\text{GeV}. \tag{4.8}$$

JHEP09(2014)161

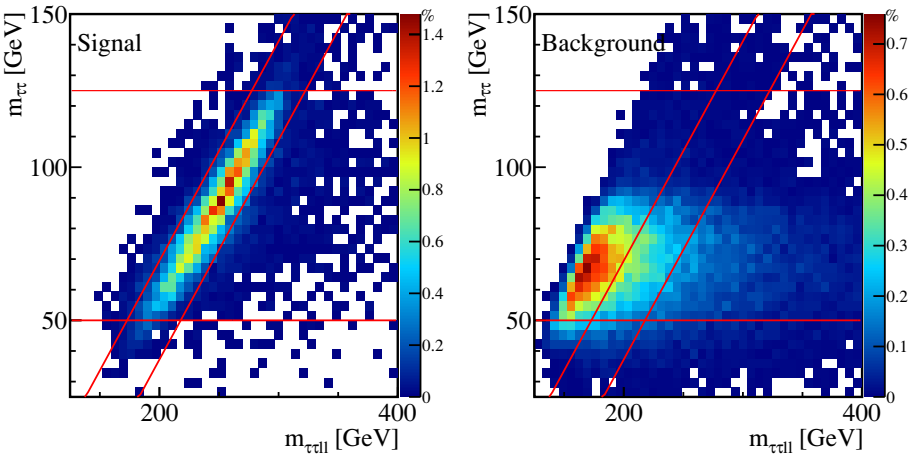

Figure 5. Normalized distribution of $m_{\tau\tau}$ versus $m_{\tau\tau\ell\ell}$ for the signal (left panel), the backgrounds (right panel) for $m_A = 300\,\text{GeV}$ and $m_H = 126\,\text{GeV}$. Two horizontal lines indicate the $m_{\tau\tau}$ range and two slanted lines indicate the $m_{\tau\tau\ell\ell}$ range, as given in eq. (4.9).

4. *$m_{\tau\tau}$ versus $m_{\tau\tau\ell\ell}$.* The expected Higgs mass is shifted more towards smaller values compared to the bb case. This is because of the hadronic decay of τ with missing energy carried away by neutrinos. Our 2-D cuts are modified as follows:

$$\begin{aligned} (0.7-w_{\tau\tau})\times m_H < m_{\tau\tau} < (0.7+w_{\tau\tau})\times m_H \text{ with } w_{\tau\tau} = 0.3\,; \\ \frac{m_Z+m_H}{m_A}\times(m_{\tau\tau\ell\ell}-m_A-w_{\tau\tau\ell\ell}) < m_{\tau\tau}-m_H < \frac{m_Z+m_H}{m_A}\times(m_{\tau\tau\ell\ell}-m_A+w_{\tau\tau\ell\ell})\,, \end{aligned} \tag{4.9}$$

with $w_{\tau\tau\ell\ell} = \text{Max}(\Gamma_{H_{\text{SM}}}|_{m_A}, 0.075 m_A)$. We show the normalized 2-D distribution as well as cuts imposed as indicated by red lines in figure 5 for the signal (left panel) and the backgrounds (right panel). The cut filters out most of the backgrounds while retaining the signal, yielding a good $S/\sqrt{B}$ value.

5. *Transverse momentum.*

$$\begin{aligned} \sum_{\tau} p_T &> 0.4 \times \frac{m_A^2 + m_H^2 - m_Z^2}{2m_A}\,, \\ \sum_{\ell,\tau} p_T &> 0.66 \times m_A\,. \end{aligned} \tag{4.10}$$

The looser cut on $\sum_\tau p_T$ compared to the $bb\ell\ell$ case is again due to the extra missing E_T in the τ decay.

In table 2, we present the cross sections after the individual cut is imposed sequentially. We take a nominal signal cross section of 10 fb to illustrate the efficiency of the chosen cuts. Again, the 2-D $m_{\tau\tau} - m_{\tau\tau\ell\ell}$ cut improves the $S/\sqrt{B}$ value significantly.

In figure 6, we show the 95% C.L. exclusion and 5σ discovery reach in $\sigma \times \text{BR}(gg \to A \to HZ \to \tau\tau\ell\ell)$ for the 14 TeV LHC. The general feature of these plots follows that of

JHEP09(2014)161

Cut	Signal [fb]	$\tau\tau\ell\ell$ [fb]	$H_{\rm SM}Z$ [fb]	S/B	$S/\sqrt{B}$
$\sigma_{\rm total}$		218	883	–	–
leptonic decay	10	218	3.02	–	–
Two leptons, two τ's [eq. (4.6)]	0.43	1.622	0.1136	0.2684	5.921
Lepton trigger [eq. (4.7)]	0.43	1.572	0.1134	0.2768	6.011
$m_{\ell\ell}$ [eq. (4.8)]	0.39	1.312	0.1031	0.301	5.869
$m_{\tau\tau}$ vs $m_{\tau\tau\ell\ell}$ [eq. (4.9)]	0.29	0.3029	0.023	0.9643	9.192
$\sum p_{T,\tau}$, $\sum(p_{T,\tau}+p_{T,\ell})$ [eq. (4.10)]	0.18	0.064	0.013	2.872	12.68

Table 2. Signal and background cross sections with cuts for signal benchmark point of $m_A = 300\,\text{GeV}$ and $m_H = 126\,\text{GeV}$ at the 14 TeV LHC. We have chosen a nominal value for $\sigma \times \text{BR}(gg \to A \to HZ \to \tau\tau\ell\ell)$ of 10 fb to illustrate the cut efficiencies for the signal process. In the last column, $S/\sqrt{B}$ is shown for an integrated luminosity of $\mathcal{L} = 300\,\text{fb}^{-1}$.

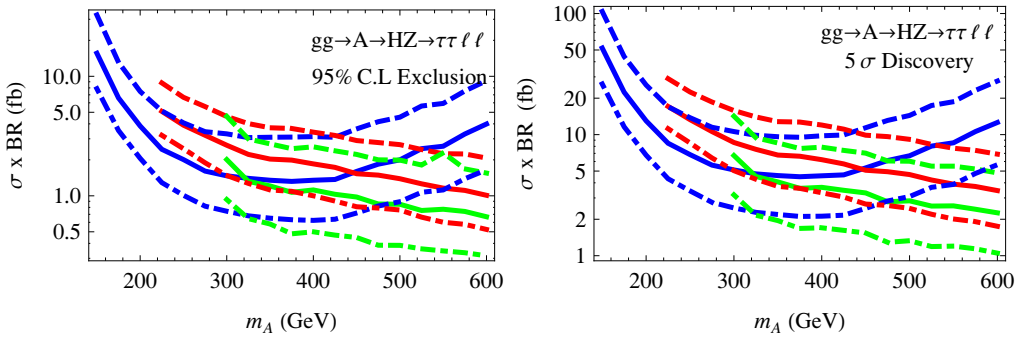

Figure 6. The 95% C.L. exclusion (left) and 5σ discovery (right) limits for $\sigma \times \text{BR}(gg \to A \to HZ \to \tau\tau\ell\ell)$ for $m_H = 50\,\text{GeV}$ (blue), 126 GeV (red), and 200 GeV (green) at the 14 TeV LHC. The dashed, solid and dot-dashed lines correspond to an integrated luminosity of 100, 300 and $1000\,\text{fb}^{-1}$, respectively. A 10% systematic error on the backgrounds is assumed as well.

figure 4, particularly with highly boosted daughter particles making τ identification more challenging, as shown by the blue curves for 50 GeV daughter particle mass, which exhibit worse limits for $m_A > 400\,\text{GeV}$. The exclusion limits are lowest for small $m_H = 50\,\text{GeV}$ and also for high $m_H = 200\,\text{GeV}$ since the dominating ZZ background peaks at $m_{\tau\tau} \approx 90\,\text{GeV}$ and therefore our $m_{\tau\tau}$ mass cut leads to a high background rejection for lower or higher m_H. Since the statistical error dominates the 10% systematic error, the $\sigma \times \text{BR}$ limits scale roughly with $1/\sqrt{L}$, as indicated by the dashed, solid and dot-dashed lines for different luminosities.

Compared to the $bb\ell\ell$ case, the $\sigma \times \text{BR}$ reach in $\tau\tau\ell\ell$ case is better due to significantly lower SM backgrounds. For the 126 GeV daughter particle case with $300\,\text{fb}^{-1}$, the 5σ discovery reach varies from about 20 fb for parent mass of 225 GeV to about 3 fb for 600 GeV. Thus, given the typical ratio of $\text{Br}(H/A \to bb) : \text{Br}(H/A \to \tau\tau) \sim 3m_b^2/m_\tau^2$, the reach in $\tau\tau\ell\ell$ can be comparable or even better than $bb\ell\ell$ channel, in particular, for smaller parent Higgs masses.

JHEP09(2014)161

4.3 $A \to HZ \to ZZZ \to 4\ell + 2j$

We now consider the case where the daughter particle decays to a pair of Z bosons, which only applies to $A \to HZ \to ZZZ$. This process involves a trade-off between having a clean final state with suppressed backgrounds and suppressed signal cross section for detection. We find that the best final states combination that yields signal cross sections that are not too suppressed in realistic models with controllable backgrounds is the $4\ell + 2j$ final state: $A \to HZ \to ZZZ \to 4\ell + 2j$. The SM backgrounds for this process come from the single, double and triple vector boson processes including additional jets as well as $t\bar{t}$ background [37, 42, 43].

Note that the Z's from the H decay could be either on-shell or off-shell depending on m_H. We will display our results for two cases: one where one of the final state Z's is necessarily off-shell, and another where both are on-shell. We will find that the latter case leads to much better discovery prospects.

We applied the following set of cuts:

- *Four isolated leptons, two jets.*

$$n_\ell = 4\,,\ n_j \geq 2\,,\ \text{with } |\eta_\ell| < 2.5\,,\ p_{T,\ell} > 10\,\text{GeV},\ |\eta_j| < 5\,,\ p_{T,j} > 20\,\text{GeV}. \tag{4.11}$$

  For jet reconstruction, we use the anti-k_T jet algorithm with $R = 0.5$. We also require the leptons to satisfy the lepton trigger as in eq. (4.2).

- *Three Z-candidates.* We reconstruct the hadronically decaying Z using the 2 hardest jets. To reconstruct the leptonically decaying Z's:

  - $4e$ *or* 4μ. If we have $4e$ or 4μ, we first find the combination of electrons or muons with opposite charge that is closest to the Z-mass. The other 2 electrons or muons are combined to find the last Z.
  - $2e2\mu$. Here, we combine the same flavored leptons in a straightforward manner.

- *Z masses.* We require the hardonically decaying Z_1, the well reconstructed leptonically decaying Z_2 and the final reconstructed leptonically decaying Z_3 to be in the following windows:

$$\begin{aligned} 60\,\text{GeV} < m_{Z_1} < 115\,\text{GeV}. \\ 80\,\text{GeV} < m_{Z_2} < 100\,\text{GeV}. \\ m_{\text{min}} < m_{Z_3} < 115\,\text{GeV}. \end{aligned} \tag{4.12}$$

  Here, we assume Z_1 to be on-shell. However, we allow for the possibility that Z_3 could be far off-shell. The m_{min} employed here mimics the LHC search strategy for the SM Higgs, and its value depends on the Higgs mass and can be found in table 2 of ref. [44].

- *m_H and m_A.* The Z produced in the A decay typically has a higher p_T than the Z's produced in H decay. Therefore we assume that the lower p_T Z's are coming from the H. For the reconstructed H with mass m_{ZZ} and A with mass m_{ZZZ} we require:

$$0.9\,m_H < m_{ZZ} < 1.1\,m_H \tag{4.13}$$

$$0.875\,m_A < m_{ZZZ} < 1.125\,m_A\,. \tag{4.14}$$

JHEP09(2014)161

Cut	$m_H = 126\,\text{GeV}$	$m_H = 200\,\text{GeV}$	BG [fb]	S/B	$S/\sqrt{B}$
Leptonic decay	1.0	10			–
Four leptons, two jets [eq. (4.11)]	0.14	2.78	2.592	1.07	29.9
Z-mass [eq. (4.12)]	0.027	1.03	0.6027	1.71	23.1
m_{ZZ} [eq. (4.13)]	0.012	0.73	0.2118	3.49	27.9
m_{ZZZ} [eq. (4.14)]	0.0094	0.54	0.0905	5.98	31.2

Table 3. Signal and background cross sections with cuts for signal benchmark point of $m_A = 400\,\text{GeV}$ and $m_H = 126$ or $200\,\text{GeV}$ at the 14 TeV LHC. We have chosen a nominal value for $\sigma \times \text{BR}(gg \to A \to HZ \to ZZZ \to 4\ell + 2j)$ of 1.0 fb (for 126 GeV m_H) and 10 fb (for 200 GeV m_H) to illustrate the cut efficiencies for the signal process. The total background cross section after cuts is shown by imposing the cuts for the $m_H = 200\,\text{GeV}$ case. S/B and $S/\sqrt{B}$ are given for the $m_H = 200\,\text{GeV}$ benchmark point. In the last column, $S/\sqrt{B}$ is shown for an integrated luminosity of $\mathcal{L} = 300\,\text{fb}^{-1}$.

In table 3, we show the cross sections after cuts for two signal benchmark points $m_H = 126\,\text{GeV}$ and 200 GeV with m_A fixed at 400 GeV, as well as for the SM backgrounds. For $m_H = 126\,\text{GeV}$, we choose a signal cross section of 1 fb.[4] For $m_H = 200\,\text{GeV}$, we use a cross section of 10 fb assuming $\text{BR}(H \to ZZ)$ is 25% for $m_H = 200\,\text{GeV}$. For the $m_H = 126\,\text{GeV}$ case, due to the off-shell Z decay, the cut efficiencies for identifying four leptons and two jets, as well as reconstructed m_{ZZ} cuts are fairly low. Coupled with the small branching fraction of $H \to ZZ^*$, the number of surviving events is about 1 for $100\,\text{fb}^{-1}$ after all cuts are imposed. However, this channel becomes quite promising for heavier daughter masses when all Z's in the final state are on-shell, as shown for the benchmark point of $m_H = 200\,\text{GeV}$.

We note that the nominal value for the cross section that is used in table 3 can, in typical BSM scenarios, be enhanced at small $\tan\beta$, due to the top loop contributions to the gluon fusion production, as well as the suppression of the $H \to bb$ branching fraction.

Figure 7 shows the 95% C.L. exclusion and 5σ discovery at the 14 TeV LHC for different integrated luminosities: $\mathcal{L} = 100\,\text{fb}^{-1}$, $300\,\text{fb}^{-1}$, and $1000\,\text{fb}^{-1}$. Even for $\mathcal{L} = 300\,\text{fb}^{-1}$, the discovery limits vary only between about 3 fb and 1.5 fb with 200 GeV m_H for m_A between 300 GeV and 600 GeV. Thus, the only challenge in this channel is to have high enough signal cross sections, as the SM backgrounds prove to be less of a threat compared to the $bb\ell\ell$ final state.

5 Implications for the Type II 2HDM

The decays $A/H \to HZ/AZ$ appear in many models that have an extension of the SM Higgs sector. In this section, we illustrate the implications of the exclusion or discovery limits of $bb\ell\ell$, $\tau\tau\ell\ell$ and $ZZZ(4\ell 2j)$ searches on these models using Type II 2HDM as an explicit example.

[4] Particularly, the number is arrived at by taking gluon fusion cross section of 9 pb for a 400 GeV CP-odd Higgs, and assuming $\text{BR}(A \to HZ) = 50\%$ and $\text{Br}(H \to ZZ^*) = 2.64\%$ for a 126 GeV Higgs.

JHEP09(2014)161

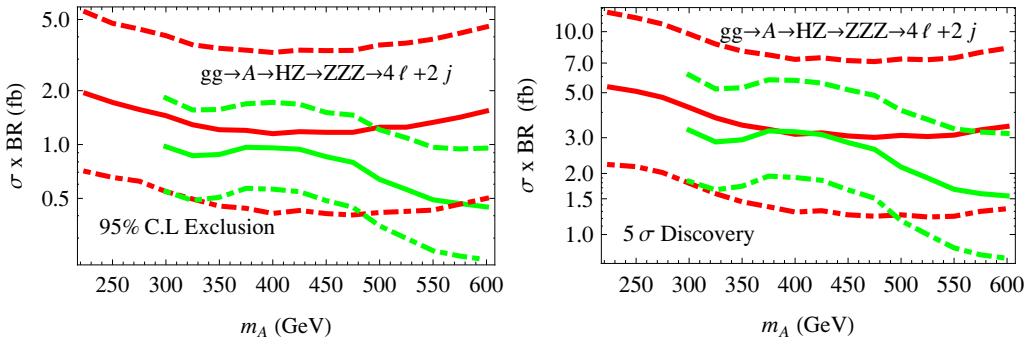

Figure 7. The 95% C.L. discovery and 5σ exclusion limits at the 14 TeV LHC in the channel $gg \to A \to HZ \to ZZZ \to 4\ell + 2j$ for $m_H = 126\,\text{GeV}$ (red) and $m_H = 200\,\text{GeV}$ (green). The dashed, solid and dot-dashed lines correspond to an integrated luminosity of 100, 300 and $1000\,\text{fb}^{-1}$, respectively. A 10% systematic error on the backgrounds is assumed as well.

$\xi^{VV}_{h^0}$	$\sin(\beta-\alpha)$	$\xi^{VV}_{H^0}$	$\cos(\beta-\alpha)$	ξ^{VV}_{A}	0
$\xi^{u}_{h^0}$	$\cos\alpha/\sin\beta$	$\xi^{u}_{H^0}$	$\sin\alpha/\sin\beta$	ξ^{u}_{A}	$\cot\beta$
$\xi^{d,l}_{h^0}$	$-\sin\alpha/\cos\beta$	$\xi^{d,l}_{H^0}$	$\cos\alpha/\cos\beta$	$\xi^{d,l}_{A}$	$\tan\beta$

Table 4. The multiplicative factors ξ by which the couplings of the CP-even Higgses and the CP-odd Higgs to the gauge bosons and fermions scale with respect to the SM value. The superscripts u, d, l and VV refer to the up-type quarks, down-type quarks, leptons, and WW/ZZ respectively.

In the Type II 2HDM, one Higgs doublet Φ_1 provides masses for the down-type quarks and charged leptons, while the other Higgs doublet Φ_2 provides masses for the up-type quarks. The couplings of the CP-even Higgses h^0, H^0 and the CP-odd Higgs A to the SM gauge bosons and fermions are scaled by a factor ξ relative to the SM value, which are presented in table 4.

The implication of the current Higgs search results on the Type II 2HDM has been studied in the literature [15, 16, 18, 23, 45–48]. In particular, a detailed analysis of the surviving regions of the Type II 2HDM was performed in [23], considering various theoretical constraints and including the latest experimental results from both the ATLAS and the CMS. Either the light or the heavy CP-even Higgs can be interpreted as the observed 126 GeV SM-like Higgs, with very different preferred parameter regions. In the h^0-126 case, we are restricted to narrow regions with $\sin(\beta-\alpha) \sim \pm\,1$ with $\tan\beta$ up to 4 or an extended region in $0.55 < \sin(\beta-\alpha) < 0.9$ with $1.5 < \tan\beta < 4$. The masses m_{H^0}, $m_{H^\pm}$, and m_A are, however, relatively unconstrained. In the H^0-126 case, we are restricted to a narrow region of $\sin(\beta-\alpha) \sim 0$ with $\tan\beta$ up to about 8, or an extended region of $\sin(\beta-\alpha)$ between -0.8 to -0.05, with $\tan\beta$ extending to 30 or higher. m_A and $m_{H^\pm}$ are nearly degenerate due to $\Delta\rho$ constraints. Imposing the flavor constraints in addition further narrows down the preferred parameter space.

Given the different parameter dependence of the gluon fusion cross section for A and H^0, the branching fractions of h^0, H^0 and A, as well as the coupling difference between

JHEP09(2014)161

$\{m_A, m_{H^0}, m_{h^0}\}$ GeV	$A \to h^0 Z$	$A \to H^0 Z$	$H^0 \to AZ$	Favored region
BP1: $\{400, 126, 50\}$	✓	✓	✗	$\sin(\beta-\alpha) \approx 0$
BP2: $\{400, 200, 126\}$	✓	✓	✗	$\sin(\beta-\alpha) \approx \pm 1$
BP3: $\{300, 400, 126\}$	✓	✗	Marginal	$\sin(\beta-\alpha) \approx \pm 1$
BP4: $\{50, 400, 126\}$	✗	✗	✓	$\sin(\beta-\alpha) \approx \pm 1$
BP5: $\{200, 400, 126\}$	✗	✗	✓	$\sin(\beta-\alpha) \approx \pm 1$

Table 5. Benchmark points shown for illustrating the discovery and exclusion limits in the processes considered in the context of the Type II 2HDM. The checkmarks indicate kinematically allowed channels. Also shown are the typical favored region of $\sin(\beta-\alpha)$ for each case (see ref. [23]).

h^0AZ and H^0AZ, we can identify three different classes of processes: $gg \to A \to h^0Z$, $gg \to A \to H^0Z$, and $gg \to H^0 \to AZ$ when interpreting the exclusion and discovery limits from the previous sections. We do not consider the decay of $h^0 \to AZ$ since this channel is experimentally challenging given that both h^0 and A are relatively light.

In table 5, we list the benchmark points that we use for the interpretation of the exclusion and discovery bounds in the Type II 2HDM. BP1 is the only H^0-126 case while BP2–BP5 are for the h^0-126 case. Both BP1 with $(m_A, m_{H^0}, m_{h^0}) = (400, 126, 50)$ GeV and BP2 with $(m_A, m_{H^0}, m_{h^0}) = (400, 200, 126)$ GeV are designed for both $gg \to A \to H^0Z$ and $gg \to A \to h^0Z$ as both modes are kinematically open. BP2 with $m_{H^0} = 200$ GeV, in particular, allow us to study the implication of $ZZZ(4\ell 2j)$ search through $gg \to A \to H^0Z$. BP3 with $(m_A, m_{H^0}, m_{h^0}) = (300, 400, 126)$ GeV is designed for $A \to h^0Z$ with the H^0 decoupled. We also choose m_A to be below the $t\bar{t}$ threshold. BP4 with $(m_A, m_{H^0}, m_{h^0}) = (50, 400, 126)$ GeV and BP5 with $(m_A, m_{H^0}, m_{h^0}) = (200, 400, 126)$ GeV are designed for the study of $gg \to H^0 \to AZ$. Also shown in table 5 are the preferred regions in $\sin(\beta-\alpha)$ once all the theoretical and experimental constraints are imposed, following ref. [23].

Note that in our study, we have decoupled the charged Higgs so that it does not appear in the decay products of A or H. For a light charged Higgs that is accessible in the decays of $A/H \to H^\pm W^\mp, H^+H^-$, decay branching fractions of $A/H \to HZ/AZ$ will decrease correspondingly, which reduces the reach of this channel. However, the new decay channels involving the charged Higgs might provide new discovery modes for A or H, which have been explored elsewhere [49–53]. In particular, for $A/H \to H^\pm W^\mp, H^+H^-$ with $H^\pm \to \tau^\pm\nu$, the spin correlation in the τ decay can be used to identify the signal from the SM backgrounds. The sensitivity of this channel involving $H^\pm$ in the intermediate to large $\tan\beta$ region provides a nice complementarity to the $A/H \to HZ/AZ$ channels [49].

To be more general, in the discussion below when we interpret the search results of $bb\ell\ell$, $\tau\tau\ell\ell$ and $ZZZ(4\ell 2j)$ channels in the model parameter space, we do not restrict ourselves to the narrow preferred parameter regions for h^0-126 or H^0-126 case as shown in ref. [23]. In particular, we consider the broad range of $-1 \leq \sin(\beta-\alpha) \leq +1$ and $1 \leq \tan\beta \leq 50$. This is because the allowed regions would change if a soft $\mathcal{Z}_2$ symmetry breaking is incorporated which ref. [23] did not deal with. Furthermore, the Higgs sector of 2HDM and the subsequent symmetry breaking structure is rather general and the results

JHEP09(2014)161

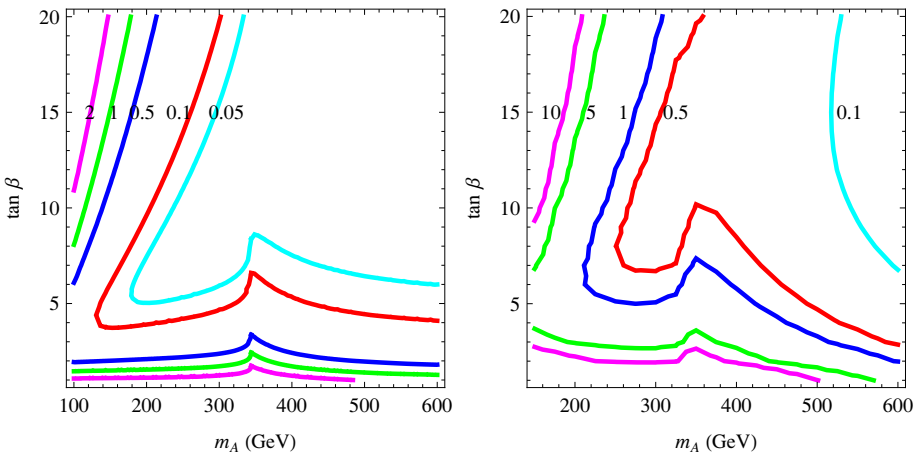

Figure 8. Contours of $\sigma(gg \to A)$ normalized to the SM value in the $m_A - \tan\beta$ plane (left panel) and $\sigma(gg \to A)$ at the 14 TeV LHC in unit of pb (right panel).

presented in this section can be interpreted in the context of any such model if the Higgs couplings to the fermions follow a similar pattern. We do, however, point out the interplay between the exotic Higgs decay channels and the SM-like Higgs search results at the end of each discussion.

5.1 $gg \to A \to h^0 Z$

We compute the production cross section for the CP-odd Higgs A by a simple rescaling of the SM Higgs cross section as follows:

$$\sigma(gg \to A) = \sigma_{\rm SM} \times \frac{|\cot\beta\, F^A_{1/2}(\tau_t) + \tan\beta\, F^A_{1/2}(\tau_b)|^2}{|F^h_{1/2}(\tau_t) + F^h_{1/2}(\tau_b)|^2}\,, \tag{5.1}$$

where $\tau_f = 4m_f^2/m_A^2$ and the scalar and pseudoscalar loop factors $F^h_{1/2}$ and $F^A_{1/2}$ are given by [22]:

$$F^A_{1/2} = -2\tau f(\tau)\,, \qquad F^h_{1/2} = -2\tau\big[1 + (1-\tau)f(\tau)\big]\,, \tag{5.2}$$

and

$$f(\tau) = \begin{cases} \big[\sin^{-1}(1/\sqrt{\tau})\big]^2 & \tau \geq 1\,, \\ -\frac{1}{4}\big[\ln(\eta_+/\eta_-) - i\pi\big]^2 & \tau < 1\,, \end{cases} \tag{5.3}$$

with $\eta_\pm \equiv 1 \pm \sqrt{1-\tau}$. We have ignored the contribution from other Higgses in the loop, which is typically small. The left panel of figure 8 shows the contour plot of the $\sigma(gg \to A)$ normalized to that of the SM Higgs with the same mass. The $\tan\beta$ dependence is due to the Att and Abb couplings, while the mass dependence comes from the different dependence of $F_{1/2}(\tau_f)$ on τ_f for pseudoscalar compared to a scalar. Enhancements over the SM value is possible for large $\tan\beta$ at small m_A due to the bottom loop, or small $\tan\beta$ for all values of m_A due to the top loop. The bump in the plot for m_A around 350 GeV corresponds to top threshold effects. Note that for A, the production cross section only depends on

JHEP09(2014)161

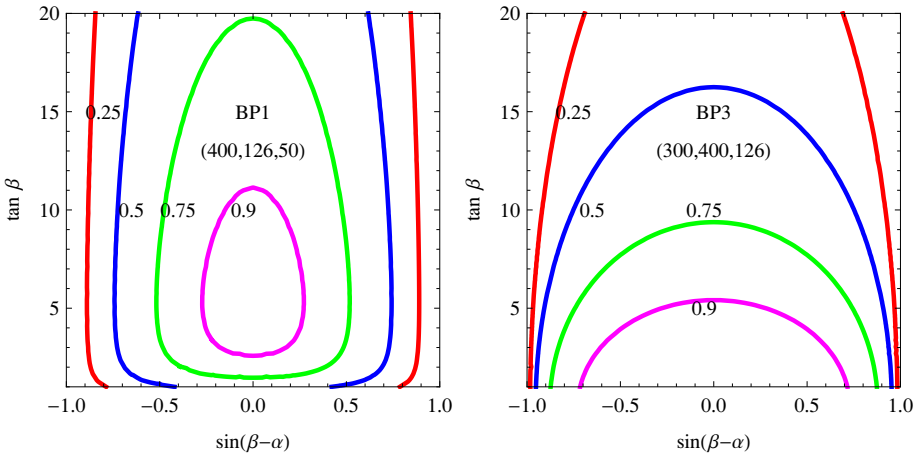

Figure 9. Contour plot of BR($A \to h^0 Z$) for BP1 (left panel), and BP3 (right panel). Also marked in each plot is the corresponding values of (m_A, m_{H^0}, m_{h^0}) for each benchmark point.

$\tan\beta$ and is independent of α. Also shown in the right panel of figure 8 are contours of $\sigma(gg \to A)$ in the $m_A - \tan\beta$ plane for the 14 TeV LHC, with the cross sections for the SM Higgs production obtained from refs. [40, 54]. Significant cross sections of 10 pb or more are possible for large m_A up to 500 GeV for small $\tan\beta$. Cross sections of similar magnitude are also possible at large $\tan\beta$ due to the bottom loop enhancement effects, albeit only for relatively small m_A.

In figure 9, we show contour plots of BR($A \to h^0 Z$) for BP1 (left panel) and BP3 (right panel). BR($A \to h^0 Z$) always maximizes at $\sin(\beta-\alpha) = 0$, and decreases for larger $|\sin(\beta-\alpha)|$, since $g_{ZAh^0} \sim \cos(\beta-\alpha)$. For BP1 with $(m_A, m_{H^0}, m_{h^0}) = (400, 126, 50)$ GeV, both $A \to h^0 Z$ and $A \to H^0 Z$ open, with the coupling of the latter process proportional to $\sin(\beta-\alpha)$. Therefore, BR($A \to h^0 Z$) decreases more rapidly when $|\sin(\beta-\alpha)|$ gets bigger. BR($A \to h^0 Z$) decreases at large $\tan\beta$ as $A \to bb$ becomes more and more important. For $m_A > 2m_t$, $A \to tt$ becomes competitive at low $\tan\beta$, which correspondingly reduces BR($A \to h^0 Z$) further in that region. For BP2 with $(m_A, m_{H^0}, m_{h^0}) = (400, 200, 126)$ GeV, the behavior of BR($A \to h^0 Z$) is very similar to that of BP1.

For BP3 with $(m_A, m_{H^0}, m_{h^0}) = (300, 400, 126)$ GeV, only $A \to h^0 Z$ opens with no competitive process from $A \to H^0 Z$ and $A \to tt$. Therefore, comparing to BP1, BR($A \to h^0 Z$) decreases much slower as $\sin(\beta-\alpha)$ approaches ± 1. BR($A \to h^0 Z$) is also maximized at smaller $\tan\beta$ due to both the absence of $A \to tt$ and the suppression of $A \to bb$.

To compare with the exclusion and discovery limits in the $bb\ell\ell$, $\tau\tau\ell\ell$ channels, it is also important to know the branching fractions of $h^0 \to bb, \tau\tau$, which depend mostly on m_{h^0}. For BP1 with $m_{h^0} = 50$ GeV, we used BR($h^0 \to bb$) = 82% and BR($h^0 \to \tau\tau$) = 8%. For the other benchmark points with h^0 being the SM-like 126 GeV Higgs, the branching fraction is obtained by rescaling the SM value of the BR with relevant coupling coefficients as given in table 4. We show a contour plot of BR($h^0 \to bb$) in figure 10 for h^0 being the 126 GeV Higgs. While $h^0 \to bb$ reaches 80% and saturates in most of the parameter space,

JHEP09(2014)161

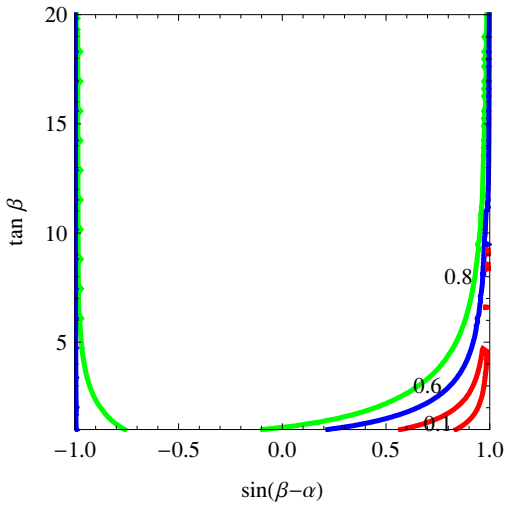

Figure 10. Branching ratio of $h^0 \to bb$ for h^0 being the 126 GeV Higgs.

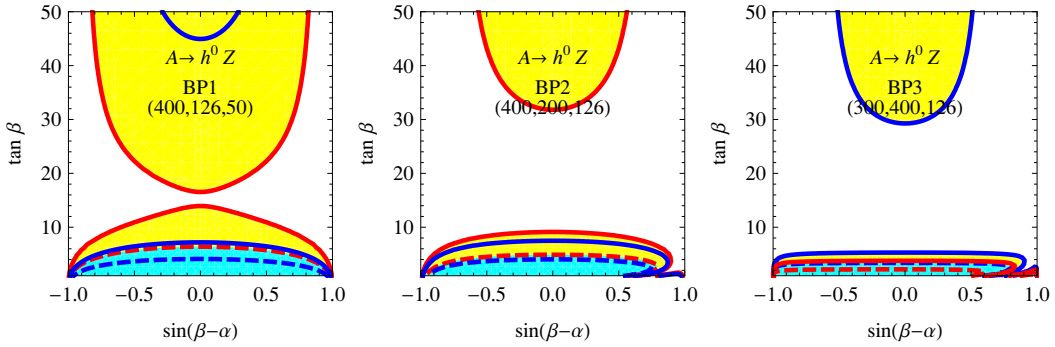

Figure 11. The 95% exclusion (yellow regions encoded by the solid lines) and 5σ discovery (cyan regions enclosed by the dashed lines) for $gg \to A \to h^0 Z$ in the $\tan\beta$ versus $\sin(\beta-\alpha)$ plane, corresponding to an integrated luminosity of 100 fb^{-1} at the 14 TeV LHC for BP1 (left panel), BP2 (middle panel) and BP3 (right panel). The red curves correspond to the $bb\ell\ell$ final state while the blue curves are the results for $\tau\tau\ell\ell$. Also marked in each plot is the corresponding values of (m_A, m_{H^0}, m_{h^0}) for each benchmark point.

there is a wedge shaped region around $0.5 < \sin(\beta-\alpha) < 1$ at small $\tan\beta$ in which $h^0 \to bb$ could be suppressed.

In figure 11, we show the LHC 100 fb^{-1} discovery/exclusion reach for $gg \to A \to h^0 Z$ in the $bb\ell\ell$ (red curves) and $\tau\tau\ell\ell$ (blue curves) channels for BP1 (left panel), BP2 (middle panel) and BP3 (right panel). 95% Exclusion regions are shown as yellow regions enclosed by the solid lines while the 5σ discovery regions are the cyan regions enclosed by the dashed lines. Each plot also indicates the corresponding values of (m_A, m_{H^0}, m_{h^0}) for each specific benchmark point. For all the plots, the discovery region for either case is restricted to $\tan\beta \leq 5$ where the gluon-fusion cross section is enhanced from the top-loop contribution. For BP1 with $m_A = 400$ GeV and a small mass of $m_{h^0} = 50$ GeV,

JHEP09(2014)161

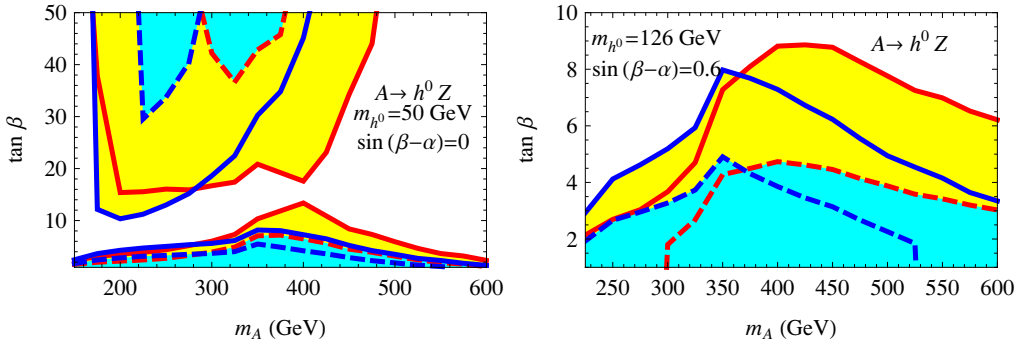

Figure 12. The 95% exclusion (yellow regions enclosed by the solid curves) and 5σ discovery (cyan regions enclosed by dashed curves) in the $m_A - \tan\beta$ plane for $gg \to A \to h^0 Z$ with $m_{h^0} = 50\,\text{GeV}$, $\sin(\beta-\alpha) = 0$, $m_{H^0} = 126\,\text{GeV}$ (left panel) and $m_{h^0} = 126\,\text{GeV}$, $\sin(\beta-\alpha) = 0.6$, $m_{H^0} = 1\,\text{TeV}$ (right panel), corresponding to an integrated luminosity of $100\,\text{fb}^{-1}$ at the 14 TeV LHC. In either plot, the red and blue curves refer to the limits of $bb\ell\ell$ and $\tau\tau\ell\ell$ channels respectively.

the experimental reach on $\sigma \times \text{BR}$ is the best. Discovery is possible for all values of $-1 < \sin(\beta-\alpha) < 1$ for $\tan\beta$ up to 5, while the exclusion region covers $\tan\beta \lesssim 14$ or large $\tan\beta \gtrsim 16$ with $-0.8 < \sin(\beta-\alpha) < 0.8$. Exclusion or discovery regions with $\tau\tau\ell\ell$ channel, shown in regions enclosed by the blue curves, are smaller compared to the regions in the $bb\ell\ell$ channel.

For BP2 with $m_A = 400\,\text{GeV}$ and $m_{h^0} = 126\,\text{GeV}$, regions of $\tan\beta < 10$ or $\tan\beta > 32$ will be excluded if no signal is detected, and regions of $\tan\beta < 4$ can be discovered if there are positive signals. For BP3 with $m_A = 300\,\text{GeV}$ and $m_{h^0} = 126\,\text{GeV}$, the exclusion and discovery regions shrink further at small $\tan\beta$. The wedge-shaped region toward $\sin(\beta-\alpha) = 1$ corresponds to the wedge region in figure 10. Our results agree with that of ref. [21] for $A \to h^0 Z$ with h^0 being the SM-like Higgs.

We note the interesting feature that the $bb\ell\ell$ limits are better than the $\tau\tau\ell\ell$ ones for BP1 and BP2, while the behavior flipped for BP3. This is because $\tau\tau\ell\ell$ typically has better reach than $bb\ell\ell$ process at small m_A, while $bb\ell\ell$ does better at large m_A, when the $\text{BR}(h^0 \to bb)/\text{BR}(h^0 \to \tau\tau) \sim 3m_b^2/m_\tau^2$ is taken into account.

Given the smallness of the branching fraction of $h^0 \to ZZ$ for the m_{h^0} values chosen, the ZZZ channel will not be useful in probing the parameter space with $gg \to A \to h^0 Z$. We also note that for the H^0-126 case (BP1) with the favored region to interpret H^0 as the SM-like Higgs being around $\sin(\beta-\alpha) \sim 0$, $gg \to A \to h^0 Z$ will be extremely useful in probing this region. For the h^0-126 case (BP2 and BP3), the favored region to interpret h^0 as the SM-like Higgs is around $\sin(\beta-\alpha) = \pm 1$. Even though the $A \to h^0 Z$ branching ratio is typically suppressed when $\sin(\beta-\alpha)$ approaches ± 1, we could still have reach in $\sin(\beta-\alpha)$ extending fairly close to ± 1.

In the left panel of figure 12, we show the reach in $\tan\beta$ versus m_A plane for $m_{h^0} = 50\,\text{GeV}$ and $\sin(\beta-\alpha) = 0$, with 95% C.L. exclusion (yellow regions enclosed by the solid curves) and 5σ discovery (cyan regions enclosed by dashed curves) given for $bb\ell\ell$ channel (red lines) and $\tau\tau\ell\ell$ channel (blue lines). While $\tau\tau\ell\ell$ is more sensitive at low m_A, $bb\ell\ell$

JHEP09(2014)161

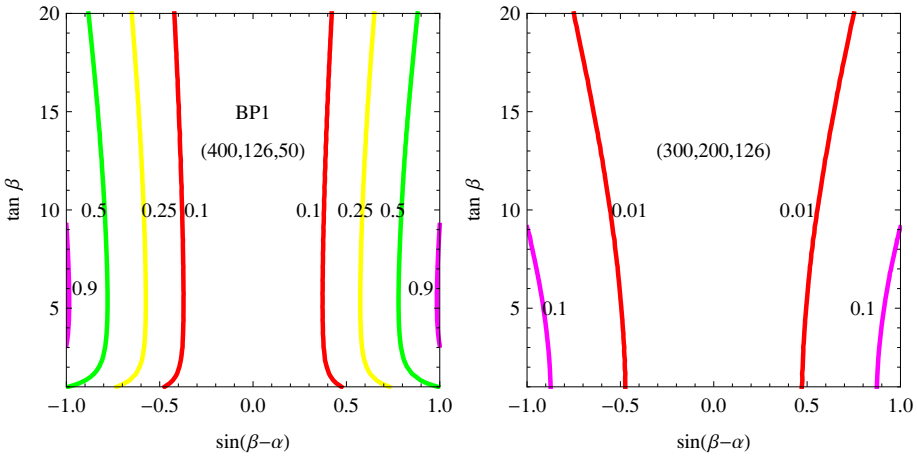

Figure 13. Contour plot of BR($A \to H^0 Z$) for BP1 (left panel) and a comparison point of $(m_A, m_{H^0}, m_{h^0}) = (300, 200, 126)$ GeV (right panel).

extends the reach at large m_A. In general, small $\tan\beta$ (lower region) or large $\tan\beta$ (top region) are within reach due to the enhancement of the top and bottom Yukawa couplings in those regions. For small $\tan\beta \sim 1$, almost all values of m_A up to 600 GeV can be covered, with regions of m_A shrink for increasing $\tan\beta$. At large $\tan\beta \gtrsim 10$, small m_A can not be approached due to the weakening of the experimental limit, while large m_A can not be approached due to the decreasing of the signal cross sections.

In the right panel of figure 12, we show the reach in $m_A - \tan\beta$ plane for $m_{h^0} = 126$ GeV and $\sin(\beta - \alpha) = 0.6$. Note that we have chose a value for $\sin(\beta - \alpha)$ that is consistent with the current Higgs search results [23] of a 126 GeV h^0 while still allowing a sizable branching fraction for $A \to h^0 Z$. We have decoupled the heavy CP-even Higgs H^0 so that $A \to H^0 Z$ does not occur. Given the reduced branching fraction for $A \to h^0 Z$, as well as the worse exclusion/discovery limits, the exclusion and discovery regions are smaller, compared to the left panel with $m_{h^0} = 50$ GeV, $\sin(\beta - \alpha) = 0$. In particular, only regions with $\tan\beta \lesssim 8$ or a small region in $\tan\beta \gtrsim 50$ around $m_A \sim 450$ GeV are viable.

5.2 $gg \to A \to H^0 Z$

$A \to H^0 Z$ opens once it is kinematically accessible. Since $m_{h^0} < m_{H^0}$, $A \to h^0 Z$ is always accessible and more favorable in phase space. Whether $A \to H^0 Z$ dominates or not depends largely on $\sin(\beta - \alpha)$, which controls the coupling of ZAH^0 as well as ZAh^0. Figure 13 shows the contours of BR($A \to H^0 Z$) in the parameter space of $\tan\beta$ versus $\sin(\beta - \alpha)$, for BP1 in the left panel. Contrary to the $A \to h^0 Z$ case as shown in figure 9, the branching ratios become larger for larger $|\sin(\beta - \alpha)|$, which is maximized at $\sin(\beta - \alpha) = \pm 1$, consistent with eq. (2.3). While the branching fractions are largely independent of $\tan\beta$, for small $\tan\beta \lesssim 2$, BR($A \to H^0 Z$) decreases due to the competition from $A \to tt$. The behavior of BR($A \to H^0 Z$) in BP2 with $(m_A, m_{H^0}, m_{h^0}) = (400, 200, 126)$ GeV is very similar to that of BP1 with $(m_A, m_{H^0}, m_{h^0}) = (400, 126, 50)$ GeV. The branching fraction is slightly smaller compared to that of BP1 due to the relatively larger phase space suppression of

JHEP09(2014)161

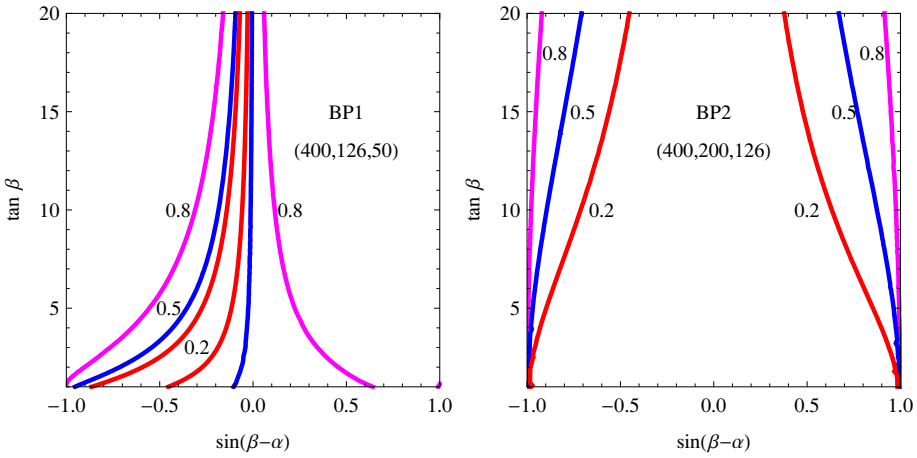

Figure 14. Contour plots of BR($H^0 \to bb$) for BP1 (left panel) and BP2 (right panel).

$A \to H^0 Z$. As a comparison of the phase space effects, we show BR($A \to H^0 Z$) for $(m_A, m_{H^0}, m_{h^0}) = (300, 200, 126)\,\text{GeV}$ in the right panel. The branching fraction is less than 10% over almost the entire parameter space. It is also evident that unlike BP1 and BP2, there is no suppression of the branching fractions at small $\tan\beta$ due to the absence of the tt decay mode.

In figure 14, we show contours of the branching ratio $H^0 \to bb$ for BP1 (left panel) and BP2 (right panel) in $\tan\beta$ versus $\sin(\beta-\alpha)$ plane. For BP1 with $m_{H^0} = 126\,\text{GeV}$, $H^0 \to bb$ is more than 80% for $\sin(\beta-\alpha) > 0.1$ or $\sin(\beta-\alpha) < -0.2$ for large $\tan\beta$. The branching fraction decreases for smaller $\tan\beta$ due to the reduction of the bottom Yukawa coupling. The further reduction of the branching fraction in negative $\sin(\beta-\alpha)$ is due to the scaling of $H^0 bb$ coupling as $\cos\alpha/\cos\beta$. For BP2 with $m_H = 200\,\text{GeV}$, $H^0 \to VV$ is kinematically accessible, which reduces $H^0 \to bb$ further for small $\sin(\beta-\alpha)$. Note that for all the benchmark points chosen, $m_{H^0} < 2\,m_t$, and hence there is no suppression of the bb mode for small $\tan\beta$ when the tt mode would potentially dominate.

Figure 15 shows the exclusion reach (yellow regions enclosed by the solid lines) and discovery (cyan region enclosed by the dashed lines) of $A \to H^0 Z$ for both the $bb\ell\ell$ (red) and $\tau\tau\ell\ell$ (blue) channels. Regions around $\sin(\beta-\alpha) \sim \pm 1$ are reachable while regions around $\sin(\beta-\alpha) \sim 0$ are inaccessible due to the suppression of $A \to H^0 Z$. For BP1, $\tan\beta \lesssim 10$ can be excluded while $\tan\beta \lesssim 5$ is discoverable for $\sin(\beta-\alpha) = \pm 1$. The bottom loop effect kicks in at $\tan\beta \gtrsim 32$, excluding slices of parameter space around $\sin(\beta-\alpha) = \pm 1$. For $\tan\beta \sim 3$, $-1 \lesssim \sin(\beta-\alpha) \lesssim -0.5$ can be excluded, while for $\sin(\beta-\alpha) > 0$, the exclusion reach extends to $\sin(\beta-\alpha) \gtrsim 0.2$ for small $\tan\beta$. There is also a small additional bump around $\sin(\beta-\alpha) = -0.6$, mainly due to the increasing of BR($H^0 \to bb$), as shown in the left panel of figure 14. The reach is greatly reduced for BP2 due to the suppression of $H^0 \to bb$, except for $\sin(\beta-\alpha) \sim \pm 1$. Only thin slices of parameter region near $\sin(\beta-\alpha) \sim \pm 1$ can be covered, which extends to $\tan\beta \lesssim 8$ for the exclusion, and $\tan\beta \lesssim 4.5$ for discovery.

JHEP09(2014)161

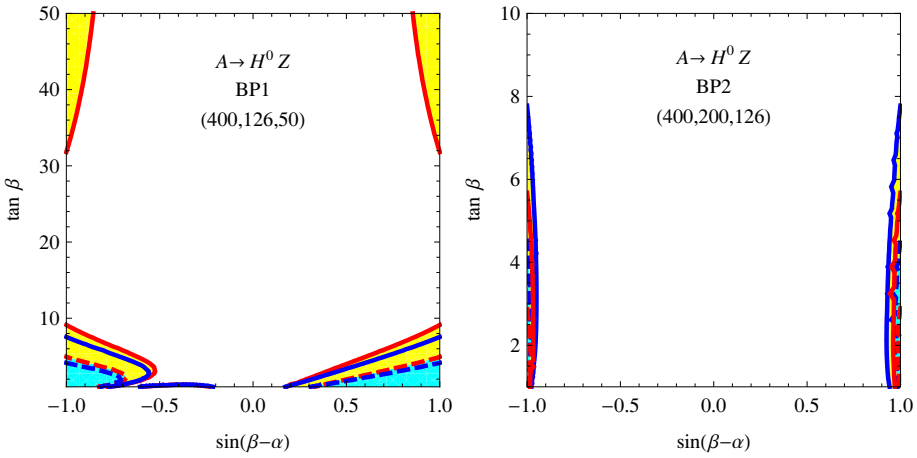

Figure 15. The exclusion and discovery region for $gg \to A \to H^0 Z$ in the $bb\ell\ell$ and $\tau\tau\ell\ell$ channels in the $\tan\beta$ versus $\sin(\beta-\alpha)$ plane, corresponding to an integrated luminosity of $100\,\text{fb}^{-1}$ for BP1 (left panel) and BP2 (right panel). Color coding is the same as in figure 11.

Note that for BP1 with $(m_A, m_{H^0}, m_{h^0}) = (400, 126, 50)$, both $A \to h^0 Z$ and $A \to H^0 Z$ open. The former is more sensitive to the $\sin(\beta-\alpha) \sim 0$ region, as shown in the left panel of figure 11, while the latter is more sensitive to $\sin(\beta-\alpha) \sim \pm 1$, as shown in the left panel of figure 15. Searches in these two channels are complementary to each other. When combined, they could cover the entire region of $\sin(\beta-\alpha)$, in particular, for $\tan\beta \lesssim 10$. Note that when combined with the current experimental search results for the 126 GeV Higgs being the H^0, the region with $\sin(\beta-\alpha) \sim 0$ is favored, with a thin slice of extended region at negative $-0.8 < \sin(\beta-\alpha) < -0.05$ as well [23].

Similar complementarity between $A \to h^0 Z$ and $A \to H^0 Z$ can be found for BP2 with $(m_A, m_{H^0}, m_{h^0}) = (400, 200, 126)\,\text{GeV}$, for the entire region of $\sin(\beta-\alpha)$. Interpreting h^0 being the 126 GeV observed Higgs boson, furthermore, favors $\sin(\beta-\alpha) \sim \pm 1$ or a thin slice of extended region at $0.55 \lesssim \sin(\beta-\alpha) \lesssim 0.9$ [23].

In the left panel of figure 16, we present the exclusion and discovery reach in the $\tan\beta$ versus m_A plane for $A \to H^0 Z$ with $m_{H^0} = 126\,\text{GeV}$, $m_{h^0} = 50\,\text{GeV}$ and $\sin(\beta-\alpha) = -0.8$. We have chosen the value of $\sin(\beta-\alpha)$ such that the branching faction of $A \to H^0 Z$ is sizable while still consistent with the experimental Higgs search results [23] with a 126 GeV H^0. We see that $\tan\beta$ up to about 6.5 can be reached for exclusion, and $\tan\beta$ up to about 3.5 can be reached for discovery.

In the right panel of figure 16, we present the exclusion and discovery reach in the $\tan\beta$ versus m_A plane for $m_H = 200\,\text{GeV}$, $m_{h^0} = 126\,\text{GeV}$ and $\sin(\beta-\alpha) = 1$. For $350\,\text{GeV} \lesssim m_A \lesssim 600\,\text{GeV}$, $\tan\beta$ up to about 6 can be excluded, and up to about 3 can be discovered in the $bb\ell\ell$ channel. $\tau\tau\ell\ell$ channel does better in the low m_A region.

For BP2 with $m_A = 400\,\text{GeV}$, $m_{H^0} = 200\,\text{GeV}$, we can also study the parameter reach of $A \to H^0 Z$ with $H^0 \to ZZ$. In figure 17, we show $\text{BR}(H^0 \to ZZ)$ in the left panel, which reaches a maximum of 25% for $|\sin(\beta-\alpha)| \lesssim 0.2$. It gets larger for small $\tan\beta$ when $H^0 \to bb$ is further suppressed. In the right panel of figure 17, we show the discovery and

JHEP09(2014)161

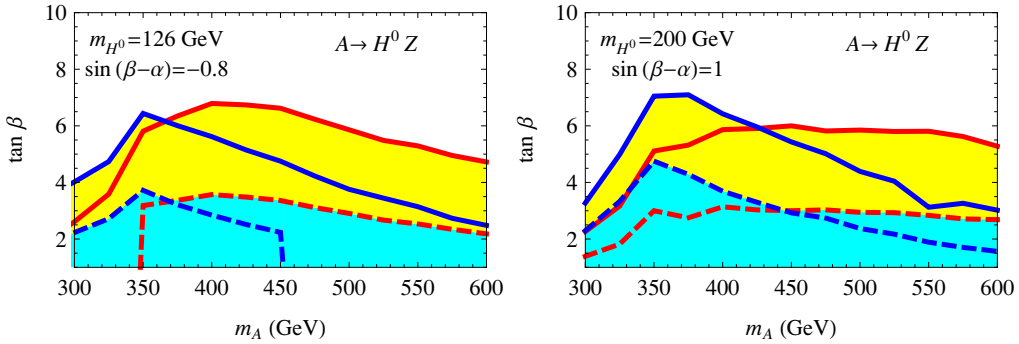

Figure 16. The discovery and exclusion regions in the $m_A - \tan\beta$ plane for $gg \to A \to H^0 Z$ in $bb\ell\ell$ and $\tau\tau\ell\ell$ final states with $m_{H^0} = 126\,\text{GeV}$, $m_{h^0} = 50\,\text{GeV}$, $\sin(\beta-\alpha) = -0.8$ (left panel) and $m_{H^0} = 200\,\text{GeV}$, $m_{h^0} = 126\,\text{GeV}$, $\sin(\beta-\alpha) = 1$ (right panel), corresponding to an integrated luminosity of $100\,\text{fb}^{-1}$ at the 14 TeV LHC. Color coding is the same as in figure 12.

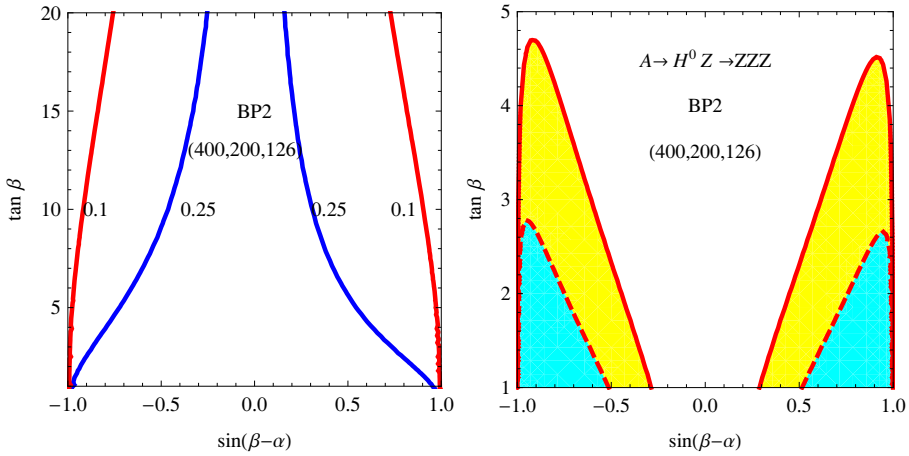

Figure 17. Left: contour plots of $\text{BR}(H^0 \to ZZ)$ for BP2. Right: the exclusion (yellow regions enclosed by the solid lines) and the discovery (cyan regions enclosed by the dashed lines) in the $\sin(\beta-\alpha) - \tan\beta$ plane for $gg \to A \to H^0 Z \to ZZZ$, corresponding to an integrated luminosity of $100\,\text{fb}^{-1}$ at the 14 TeV LHC for the $4\ell + 2j$ final state.

exclusion contours in the $\tan\beta$ versus $\sin(\beta-\alpha)$ plane for $100\,\text{fb}^{-1}$ luminosity at the LHC. While $H^0 \to ZZ$ maximizes at $\sin(\beta-\alpha) \sim 0$, $A \to H^0 Z$ is minimized in this region. As a result, regions of $0.3 \lesssim |\sin(\beta-\alpha)| \lesssim 1$ with $\tan\beta$ up to 4.7 can be excluded while the discovery regions are $0.5 \lesssim |\sin(\beta-\alpha)| \lesssim 1$ with $\tan\beta \lesssim 2.8$. Note also that this channel is complementary to $A \to H^0 Z \to bb/\tau\tau\ell\ell$ as shown in figure 15, which is sensitive to $\sin(\beta-\alpha) \sim \pm 1$ region.

In figure 18, we present the exclusion and discovery in $\tan\beta$ versus m_A plane for $gg \to A \to H^0 Z \to ZZZ(4\ell 2j)$ with $m_H = 200\,\text{GeV}$, $\sin(\beta-\alpha) = 0.9$. We have chosen the value of $\sin(\beta-\alpha)$ such that the branching fractions of both $A \to H^0 Z$ and $H^0 \to ZZ$ is sizable while still consistent with the experimental Higgs search results [23] with a 126 GeV h^0. We see that the whole region of $300\,\text{GeV} < m_A < 600\,\text{GeV}$ can be covered at small

JHEP09(2014)161

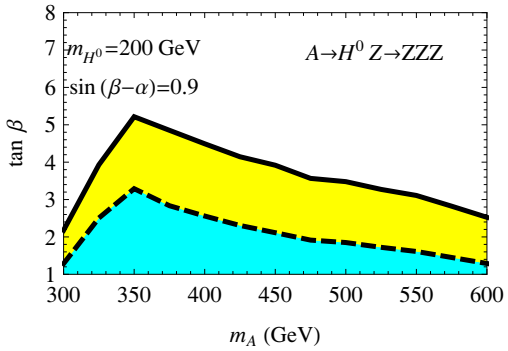

Figure 18. The exclusion (yellow region enclosed by the solid lines) and the discovery (cyan region enclosed by the dashed lines) in the $m_A - \tan\beta$ plane with $m_{H^0} = 200\,\text{GeV}$, $m_{h^0} = 126\,\text{GeV}$, and $\sin(\beta-\alpha) = 0.9$, corresponding to an integrated luminosity of $100\,\text{fb}^{-1}$ at the 14 TeV LHC for the $4\ell + 2j$ final state.

$\tan\beta$, with the maximum reach in $\tan\beta$ obtained for $m_A \sim 350\,\text{GeV}$: $\tan\beta \lesssim 3$ for discovery and $\tan\beta \lesssim 5$ for exclusion.

5.3 $gg \to H^0 \to AZ$

For this process, we restrict to the $m_{h^0} = 126\,\text{GeV}$ case with a heavier H^0. We use BP4 with $(m_A, m_{H^0}, m_{h^0}) = (50, 400, 126)\,\text{GeV}$ and BP5 with $(m_A, m_{H^0}, m_{h^0}) = (200, 400, 126)\,\text{GeV}$ as an illustration. The gluon fusion production cross section for H^0 can be rescaled from the SM cross section:

$$\sigma(gg \to H^0) = \sigma_{\text{SM}} \times \frac{\left|\left(\frac{\sin\alpha}{\sin\beta}\right) F^h_{1/2}(\tau_t) + \left(\frac{\cos\alpha}{\cos\beta}\right) F^h_{1/2}(\tau_b)\right|^2}{|F^h_{1/2}(\tau_t) + F^h_{1/2}(\tau_b)|^2}\,, \tag{5.4}$$

where the loop factors F's are defined in eq. (5.2). We note that in contrast to the production of A in eq. (5.1), the production of H^0 involves both α and β. In the left panel of figure 19, we show contours of the production cross section of H^0 normalized to the SM value in the $\sin(\beta-\alpha) - \tan\beta$ plane for $m_{H^0} = 400\,\text{GeV}$. We see that for positive $\sin(\beta-\alpha)$, the cross section is always relatively more suppressed than that for negative $\sin(\beta-\alpha)$, introduced by the interference between the top and bottom loops in eq. (5.4). For $\sin(\beta-\alpha) = \pm 1$, which is preferred by the interpretation of h^0 being the SM-like Higgs, the cross section receives the strongest suppression: only 10% of the corresponding SM value. In the right panel of figure 19, we show contours of the production cross section at 14 TeV LHC in the $m_{H^0} - \tan\beta$ plane. We see that cross sections of 10 pb or more is possible for m_{H^0} up to 425 GeV for small $\tan\beta$ — slightly lower than the corresponding numbers for $\sigma(gg \to A)$ as shown in figure 8. However, the bottom loop enhancement plays a slightly more significant role in this case at large $\tan\beta$, compared to the A case.

Figure 20 shows the $\text{BR}(H^0 \to AZ)$ for BP4 (left panel) and BP5 (right panel). Since $g_{ZAH^0} \propto \sin(\beta-\alpha)$, the branching fraction gets bigger for larger $|\sin(\beta-\alpha)|$, and is maximized at $\sin(\beta-\alpha) = \pm 1$. Branching fractions in BP4 is larger than that of BP5 due

JHEP09(2014)161

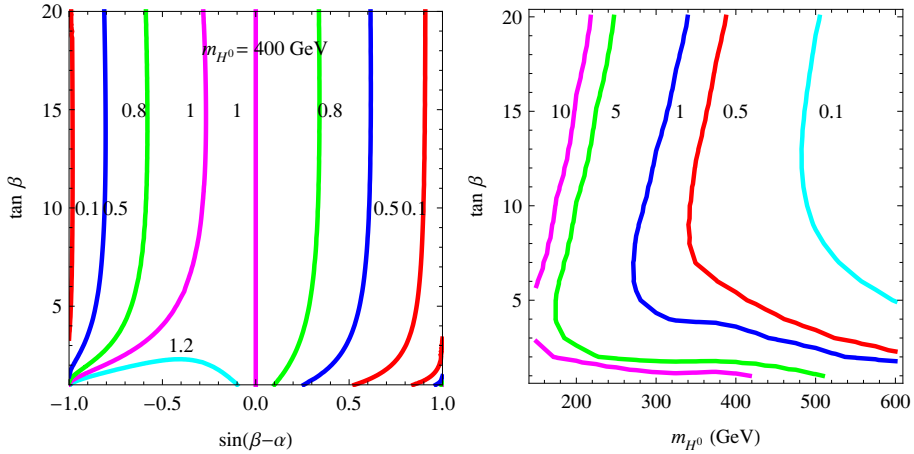

Figure 19. Contours of the cross section normalized to the SM value in the $\sin(\beta-\alpha)-\tan\beta$ plane (left panel) for $m_{H^0}=400\,\text{GeV}$ and $gg\to H^0$ cross section at the 14 TeV LHC in unit of pb in the $m_{H^0}-\tan\beta$ plane (right panel) with $\sin(\beta-\alpha)=-1$.

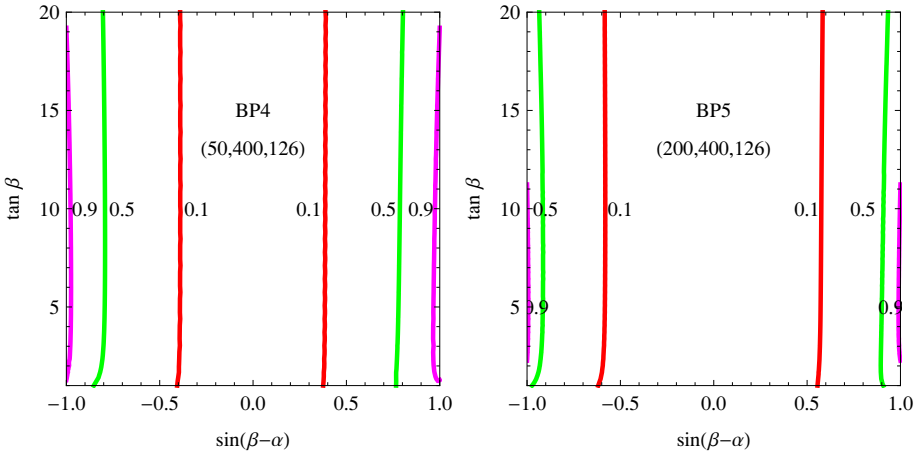

Figure 20. Contour plot of $\text{BR}(H^0\to AZ)$ (left panel) for BP4 (left panel) and BP5 (right panel).

to the bigger phase space for $H^0\to AZ$. For $A\to bb$ and $\tau\tau$, the branching fraction is about 94% and 6% respectively, which does not vary much for BP4 with $m_A=50\,\text{GeV}$ and BP5 with $m_A=200\,\text{GeV}$.

In figure 21, we display the discovery/exclusion reach in $gg\to H^0\to AZ$ for the $bb\ell\ell$ (red) and $\tau\tau\ell\ell$ (blue) final states for BP4 (left panel) and BP5 (right panel). For BP4, large regions of parameter spaces in $\tan\beta$ versus $\sin(\beta-\alpha)$ can be excluded, except for $-0.15<\sin(\beta-\alpha)<0.2$ when $H^0\to AZ$ is highly suppressed. The discovery region shrinks to $-1\lesssim\sin(\beta-\alpha)\lesssim-0.3$ and $0.35\lesssim\sin(\beta-\alpha)\lesssim0.9$ for all values of $\tan\beta$. For BP5, regions of $-1\lesssim\sin(\beta-\alpha)\lesssim-0.5$ for all $\tan\beta$ and $0.6\lesssim\sin(\beta-\alpha)\lesssim0.8$ with $6\lesssim\tan\beta\lesssim26$ can be excluded and a smaller region in $-1\lesssim\sin(\beta-\alpha)\lesssim-0.6$ with

JHEP09(2014)161

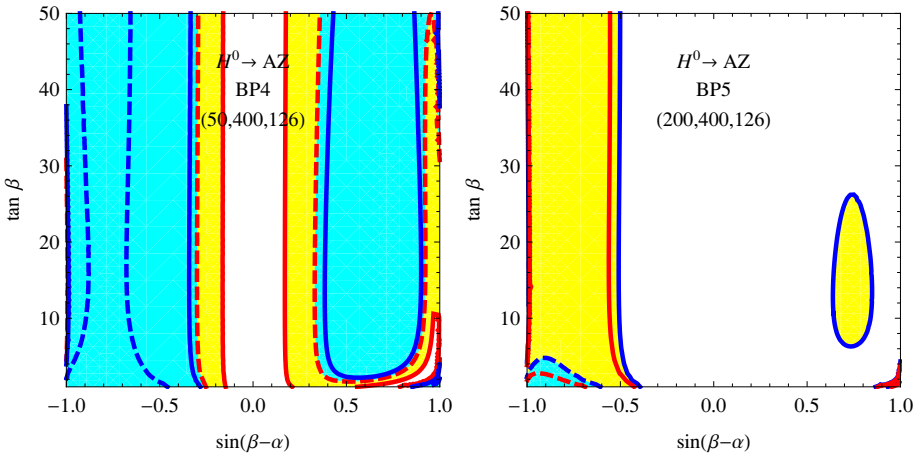

Figure 21. The exclusion and discovery regions in the $\tan\beta$ versus $\sin(\beta-\alpha)$ plane for $gg \to H^0 \to AZ$ with $bb\ell\ell$ (red) and $\tau\tau\ell\ell$ (blue) final states for BP4 (left panel) and BP5 (right panel), corresponding to $100\,\text{fb}^{-1}$ integrated luminosity at the 14 TeV LHC. Color coding is the same as in figure 11.

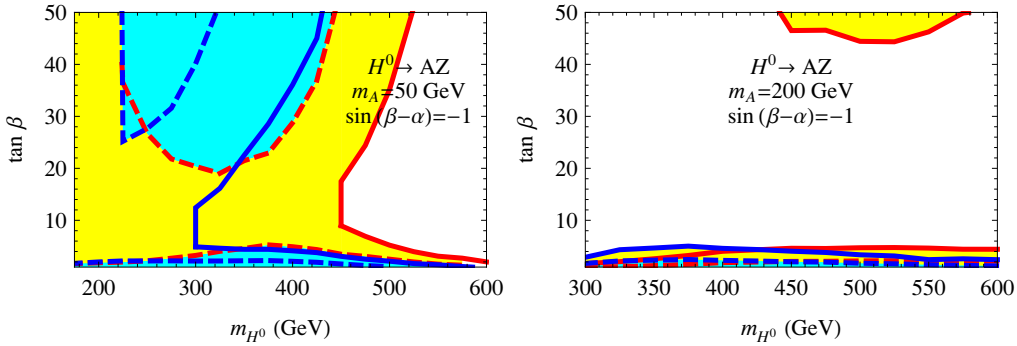

Figure 22. The discovery and exclusion region in the $m_{H^0} - \tan\beta$ plane for $gg \to H^0 \to AZ$ with $bb\ell\ell$ (red) and $\tau\tau\ell\ell$ (blue) final states, corresponding to $100\,\text{fb}^{-1}$ integrated luminosity at the 14 TeV LHC. The left panel is for $m_A = 50\,\text{GeV}$ with $\sin(\beta-\alpha) = -1$ and the right panel is for $m_A = 200\,\text{GeV}$ with $\sin(\beta-\alpha) = -1$. Color coding is the same as in figure 12.

$\tan\beta \lesssim 5$ can be discovered. While $bb\ell\ell$ channel has better reach for BP4, $\tau\tau\ell\ell$ channel has a slightly better sensitivity for BP5. The reach is also much better for negative $\sin(\beta-\alpha)$ because of the less suppressed cross sections of $gg \to H^0$.

In the left panel of figure 22, we show the exclusion and discovery each with $100\,\text{fb}^{-1}$ luminosity at 14 TeV LHC in $\tan\beta$ versus m_H plane, for $gg \to H^0 \to AZ$ with $bb\ell\ell$ (red) and $\tau\tau\ell\ell$ (blue) final states. We have chosen $m_A = 50\,\text{GeV}$ and $\sin(\beta-\alpha) = -1$. Discovery is possible for small values of $\tan\beta \lesssim 5$ or larger values of $\tan\beta \gtrsim 20$. The exclusion reach, however, is much more extended. All values of $\tan\beta$ can be covered for m_{H^0} up to 450 GeV, with reach extended further at larger and smaller values of $\tan\beta$. The reach with daughter particle mass $m_A = 200\,\text{GeV}$ is shown in the right panel of figure 22. Both the exclusion

JHEP09(2014)161

and discovery regions shrink greatly. Only very small $\tan\beta \lesssim 4$ or very large $\tan\beta \gtrsim 44$ can be excluded. Note that while $\sin(\beta-\alpha) = \pm 1$ is preferred by the interpretation of the h^0 being the SM-like Higgs, the suppression of $gg \to H^0$ in that region results in a reduced exclusion/discovery reach. Even a small deviation of $\sin(\beta-\alpha)$ away from ± 1 would introduce a much larger reach in $gg \to H^0 \to AZ$.

6 Conclusion

Given the discovery of a 126 GeV SM-like Higgs boson at the LHC, it is now time to use the experimental data to constrain new physics models while also exploring the detectability of extra Higgs bosons in the extensions of the SM. In this spirit, we explored the production and decay of heavy scalar and pseudoscalar states via the processes $gg \to H^0 \to AZ$ and $gg \to A \to h^0 Z/H^0 Z$ with both fermionic (bb, $\tau\tau$) and possible bosonic (ZZ) decays of the daughter Higgs. This channel provides nice complementarity to the conventional search channel $pp \to A/H \to \tau\tau$, which is mostly sensitive to the large $\tan\beta$ region. We presented model independent limits on the 95% C.L. exclusion and 5σ discovery in those channels at the 14 TeV LHC. The possibilities include the interesting case of having the 126 GeV SM-like Higgs as a decay product of a heavy pseudoscalar.

For the 14 TeV LHC with 300 fb^{-1} integrated luminosity, the 95% C.L. limits on $\sigma \times \mathrm{BR}$ for the $bb\ell\ell$ final state (where the b's come from the Higgs in the final state) for a 126 GeV daughter Higgs particle vary between 200 fb to a few fb for the parent heavy Higgs mass in the range of 200 GeV to 600 GeV, while the limit for 5σ discovery is about 3–5 times larger. For the $\tau\tau\ell\ell$ channel with the same range of A mass, the exclusion bounds are around 5–1 fb and the discovery reach is about 20 fb–3 fb. While the $\sigma \times \mathrm{BR}$ reach in the $\tau\tau\ell\ell$ channel is in general much better than the $bb\ell\ell$ channel, owing mostly to more suppressed backgrounds, it is comparable to $bb\ell\ell$ mode once the branching fraction difference between bb and $\tau\tau$ modes are taken into account in a given model. $gg \to A \to H^0 Z \to ZZZ \to 4\ell 2j$ is useful for heavy Higgses with $m_{H^0} > 2m_Z$. For $m_{H^0} = 200$ GeV and $m_A = 400$ GeV, exclusion in this channel with 300 fb^{-1} integrated luminosity requires as little as 1 fb in $\sigma \times \mathrm{BR}$ while 5σ discovery needs about 3 fb.

We then discussed the implication of the exclusion and discovery bounds of $bb\ell\ell$, $\tau\tau\ell\ell$ and ZZZ channels in the Type II 2HDM, studying three classes of processes: $gg \to A \to h^0 Z$, $gg \to A \to H^0 Z$, and $gg \to H^0 \to AZ$. We find, in general, that there is a significant portion of the $\tan\beta$ versus $\sin(\beta-\alpha)$ plane that allows discovery/exclusion possibilities in the $bb\ell\ell$ and $\tau\tau\ell\ell$ final states. $bb\ell\ell$ and $\tau\tau\ell\ell$ have comparable reach, with $\tau\tau\ell\ell$ being slightly better for low parent Higgs masses and $bb\ell\ell$ being better for higher parent Higgs masses.

Specifically, in the channel $gg \to A \to h^0 Z$ when H^0 is identified as the SM-like Higgs, 95% exclusion covers most of the $\tan\beta$ versus $\sin(\beta-\alpha)$ plane for m_A around 400 GeV. $\tan\beta < 5$ can also be covered by 5σ discovery. On the other hand, the exclusion/discovery range is more restricted when h^0 is identified as the SM Higgs. Typically, we find that for $m_A = 400$ GeV, discovery region lies between $-1 < \sin(\beta-\alpha) \lesssim 0.8$ and $\tan\beta \leq 5$, while the exclusion region extends to $\tan\beta \lesssim 10$ or $\gtrsim 30$. Note also that even though the reach

JHEP09(2014)161

is always maximized at $\sin(\beta-\alpha)\sim 0$, it extends to larger values of $|\sin(\beta-\alpha)|$ close to ± 1 as well. A wide range of m_A can be covered at low $\tan\beta \lesssim 10$, while high $\tan\beta$ can only be approached for $m_A \lesssim 500\,\text{GeV}$.

The case where A decays to $H^0 Z$ is complementary to $A \to h^0 Z$ in that the discovery and exclusion regions split into two distinct regions around $\sin(\beta-\alpha)\sim \pm 1$. We find that in both the $bb\ell\ell$ and $\tau\tau\ell\ell$ channels, the discovery reach covers $\tan\beta$ up to about 4, while the exclusion region extends to about 7 for m_A up to about 600 GeV. Moreover, for $m_{H^0} \geq 200\,\text{GeV}$, this channel also allows for an exclusion reach with ZZZ final states with $0.3 < |\sin(\beta-\alpha)| < 1$, and $\tan\beta$ up to 4.5 for m_A around 400 GeV. For small values of $\tan\beta$, a wide range of m_A can be covered either by exclusion or discovery.

In the last class $gg \to H^0 \to AZ$, we find that discovery/exclusion regions favor the negative $\sin(\beta-\alpha)$ regions, largely due to the parameter dependence of gluon fusion production $\sigma(gg\to H^0)$. For $m_{H^0} = 400\,\text{GeV}$ and $m_A = 50\,\text{GeV}$, a wide range of $\tan\beta$ versus $\sin(\beta-\alpha)$ space can be covered, except for a small stripe around $-0.15 < \sin(\beta-\alpha) < 0.2$. For $m_A = 200\,\text{GeV}$, the regions $-1 \lesssim \sin(\beta-\alpha) \lesssim -0.5$ can be excluded for all values of $\tan\beta$, while only a smaller region at low $\tan\beta$ can be discovered. For $m_A = 50\,\text{GeV}$ and $\sin(\beta-\alpha) = -1$, the exclusion reach in m_H can be as large as 450 GeV for $\tan\beta$ around 10, which extends even further for smaller and larger $\tan\beta$.

While extra Higgs bosons other than the observed 126 GeV SM-like Higgs exist in many extension of the SM, the searches for those Higgses in unconventional decay channels have just started. Compared to conventional search channels of bb, $\tau\tau$, WW, ZZ and $\gamma\gamma$, these exotic decay modes of heavier Higgses decaying into two light Higgses or one Higgs with one gauge boson can be dominant in certain regions of parameter space. In this paper, we explored $A/H \to HZ/AZ$ in $bb\ell\ell$, $\tau\tau\ell\ell$ and ZZZ modes. Other channels, in particular, those involving charged Higgses can be very promising as well [49–53].

Acknowledgments

We thank Nathaniel Craig, Tao Han, Meenakshi Narain, Peter Loch, and John Stupak for helpful discussions. This work was supported by the Department of Energy under Grant DE-FG02-13ER41976.

References

[1] ATLAS collaboration, *Observation of a new particle in the search for the standard model Higgs boson with the ATLAS detector at the LHC*, *Phys. Lett.* **B 716** (2012) 1 [arXiv:1207.7214] [INSPIRE].

[2] ATLAS collaboration, *Combined coupling measurements of the Higgs-like boson with the ATLAS detector using up to 25 fb^{-1} of proton-proton collision data*, ATLAS-CONF-2013-034 (2013).

JHEP09(2014)161

[3] CMS collaboration, *Observation of a new boson at a mass of 125 GeV with the CMS experiment at the LHC*, *Phys. Lett.* **B 716** (2012) 30 [arXiv:1207.7235] [INSPIRE].

[4] CMS collaboration, *Combination of standard model Higgs boson searches and measurements of the properties of the new boson with a mass near 125 GeV*, CMS-PAS-HIG-13-005 (2013).

[5] ATLAS collaboration, *Evidence for the spin-0 nature of the Higgs boson using ATLAS data*, *Phys. Lett.* **B 726** (2013) 120 [arXiv:1307.1432] [INSPIRE].

[6] H.P. Nilles, *Supersymmetry, supergravity and particle physics*, *Phys. Rept.* **110** (1984) 1 [INSPIRE].

[7] H.E. Haber and G.L. Kane, *The search for supersymmetry: probing physics beyond the standard model*, *Phys. Rept.* **117** (1985) 75 [INSPIRE].

[8] R. Barbieri, *Looking beyond the standard model: the supersymmetric option*, *Riv. Nuovo Cim.* **11N4** (1988) 1 [INSPIRE].

[9] J.R. Ellis, J.F. Gunion, H.E. Haber, L. Roszkowski and F. Zwirner, *Higgs bosons in a nonminimal supersymmetric model*, *Phys. Rev.* **D 39** (1989) 844 [INSPIRE].

[10] M. Drees, *Supersymmetric models with extended Higgs sector*, *Int. J. Mod. Phys.* **A 4** (1989) 3635 [INSPIRE].

[11] G.C. Branco et al., *Theory and phenomenology of two-Higgs-doublet models*, *Phys. Rept.* **516** (2012) 1 [arXiv:1106.0034] [INSPIRE].

[12] H.E. Haber, G.L. Kane and T. Sterling, *The fermion mass scale and possible effects of Higgs bosons on experimental observables*, *Nucl. Phys.* **B 161** (1979) 493 [INSPIRE].

[13] L.J. Hall and M.B. Wise, *Flavor changing Higgs-boson couplings*, *Nucl. Phys.* **B 187** (1981) 397 [INSPIRE].

[14] J.F. Donoghue and L.F. Li, *Properties of charged Higgs bosons*, *Phys. Rev.* **D 19** (1979) 945 [INSPIRE].

[15] N. Craig and S. Thomas, *Exclusive signals of an extended Higgs sector*, *JHEP* **11** (2012) 083 [arXiv:1207.4835] [INSPIRE].

[16] C.-W. Chiang and K. Yagyu, *Implications of Higgs boson search data on the two-Higgs doublet models with a softly broken Z_2 symmetry*, *JHEP* **07** (2013) 160 [arXiv:1303.0168] [INSPIRE].

[17] N.D. Christensen, T. Han, Z. Liu and S. Su, *Low-mass Higgs bosons in the NMSSM and their LHC implications*, *JHEP* **08** (2013) 019 [arXiv:1303.2113] [INSPIRE].

[18] B. Grinstein and P. Uttayarat, *Carving out parameter space in type-II two Higgs doublets model*, *JHEP* **06** (2013) 094 [*Erratum ibid.* **09** (2013) 110] [arXiv:1304.0028] [INSPIRE].

[19] I.M. Lewis, *Closing the wedge with 300 fb^{-1} and 3000 fb^{-1} at the LHC: a Snowmass white paper*, arXiv:1308.1742 [INSPIRE].

[20] B. Coleppa, F. Kling and S. Su, *Exotic Higgs decay via AZ/HZ channel: a Snowmass whitepaper*, arXiv:1308.6201 [INSPIRE].

[21] E. Brownson et al., *Heavy Higgs scalars at future hadron colliders (a Snowmass whitepaper)*, arXiv:1308.6334 [INSPIRE].

[22] J.F. Gunion, H.E. Haber, G.L. Kane and S. Dawson, *The Higgs hunter's guide*, *Front. Phys.* **80** (2000) 1 [INSPIRE].

JHEP09(2014)161

[23] B. Coleppa, F. Kling and S. Su, *Constraining type II 2HDM in light of LHC Higgs searches*, *JHEP* **01** (2014) 161 [arXiv:1305.0002] [INSPIRE].

[24] ATLAS collaboration, *Search for the neutral Higgs bosons of the minimal supersymmetric standard model in pp collisions at $\sqrt{s} = 7$ TeV with the ATLAS detector*, *JHEP* **02** (2013) 095 [arXiv:1211.6956] [INSPIRE].

[25] CMS collaboration, *Search for MSSM neutral Higgs bosons decaying to tau pairs in pp collisions*, CMS-PAS-HIG-13-021 (2013).

[26] ATLAS collaboration, *Discovery potential of $A/H \to \tau\tau \to \ell h$ in ATLAS*, ATL-PHYS-PUB-2010-011 (2010).

[27] CMS collaboration, *Search for a Higgs boson decaying into a b-quark pair and produced in association with b quarks in proton-proton collisions at 7 TeV*, *Phys. Lett.* **B 722** (2013) 207 [arXiv:1302.2892] [INSPIRE].

[28] ATLAS collaboration, *Search for Higgs bosons in two-Higgs-doublet models in the $H \to WW \to e\nu\mu\nu$ channel with the ATLAS detector*, ATLAS-CONF-2013-027 (2013).

[29] CMS collaboration, *Search for extended Higgs sectors in the $H \to hh$ and $A \to Zh$ channels in $\sqrt{s} = 8$ TeV pp collisions with multileptons and photons final states*, CMS-PAS-HIG-13-025 (2013).

[30] F. Febres Cordero, L. Reina and D. Wackeroth, *W- and Z-boson production with a massive bottom-quark pair at the Large Hadron Collider*, *Phys. Rev.* **D 80** (2009) 034015 [arXiv:0906.1923] [INSPIRE].

[31] N. Kidonakis, *Differential and total cross sections for top pair and single top production*, arXiv:1205.3453 [INSPIRE].

[32] J.M. Campbell, R.K. Ellis and C. Williams, *Vector boson pair production at the LHC*, *JHEP* **07** (2011) 018 [arXiv:1105.0020] [INSPIRE].

[33] LHC Higgs Cross Section Working Group collaboration, S. Dittmaier et al., *Handbook of LHC Higgs cross sections: 1. Inclusive observables*, arXiv:1101.0593 [INSPIRE].

[34] J. Alwall, M. Herquet, F. Maltoni, O. Mattelaer and T. Stelzer, *MadGraph 5: going beyond*, *JHEP* **06** (2011) 128 [arXiv:1106.0522] [INSPIRE].

[35] T. Sjöstrand, S. Mrenna and P.Z. Skands, *PYTHIA 6.4 physics and manual*, *JHEP* **05** (2006) 026 [hep-ph/0603175] [INSPIRE].

[36] DELPHES 3 collaboration, J. de Favereau et al., *DELPHES 3, a modular framework for fast simulation of a generic collider experiment*, *JHEP* **02** (2014) 057 [arXiv:1307.6346] [INSPIRE].

[37] J. Anderson et al., *Snowmass energy frontier simulations*, arXiv:1309.1057 [INSPIRE].

[38] ATLAS collaboration, *Performance of the ATLAS muon trigger in 2011*, ATLAS-CONF-2012-099 (2012).

[39] ATLAS collaboration, *Performance of the ATLAS electron and photon trigger in p-p collisions at $\sqrt{s} = 7$ TeV in 2011*, ATLAS-CONF-2012-048 (2012).

[40] LHC Higgs Cross Section Working Group collaboration, S. Heinemeyer et al., *Handbook of LHC Higgs cross sections: 3. Higgs properties*, arXiv:1307.1347 [INSPIRE].

[41] http://www-ekp.physik.uni-karlsruhe.de/~ott/theta/theta-auto/.

JHEP09(2014)161

[42] A. Avetisyan et al., *Methods and results for standard model event generation at $\sqrt{s} = 14$ TeV, 33 TeV and 100 TeV proton colliders (a Snowmass whitepaper)*, arXiv:1308.1636 [INSPIRE].

[43] A. Avetisyan et al., *Snowmass energy frontier simulations using the open science grid (a Snowmass 2013 whitepaper)*, arXiv:1308.0843 [INSPIRE].

[44] ATLAS collaboration, *Search for the standard model Higgs boson in the decay channel $H \to ZZ^{(*)} \to 4\ell$ with 4.8 fb^{-1} of pp collision data at $\sqrt{s} = 7$ TeV with ATLAS*, *Phys. Lett.* **B 710** (2012) 383 [arXiv:1202.1415] [INSPIRE].

[45] H.S. Cheon and S.K. Kang, *Constraining parameter space in type-II two-Higgs doublet model in light of a 126 GeV Higgs boson*, *JHEP* **09** (2013) 085 [arXiv:1207.1083] [INSPIRE].

[46] A. Drozd, B. Grzadkowski, J.F. Gunion and Y. Jiang, *Two-Higgs-doublet models and enhanced rates for a 125 GeV Higgs*, *JHEP* **05** (2013) 072 [arXiv:1211.3580] [INSPIRE].

[47] S. Chang et al., *Comprehensive study of two Higgs doublet model in light of the new boson with mass around 125 GeV*, *JHEP* **05** (2013) 075 [arXiv:1210.3439] [INSPIRE].

[48] C.-Y. Chen and S. Dawson, *Exploring two Higgs doublet models through Higgs production*, *Phys. Rev.* **D 87** (2013) 055016 [arXiv:1301.0309] [INSPIRE].

[49] T. Li and S. Su, *Exotic Higgs decay via charged Higgs*, in preparation.

[50] L. Basso et al., *Probing the charged Higgs boson at the LHC in the CP-violating type-II 2HDM*, *JHEP* **11** (2012) 011 [arXiv:1205.6569] [INSPIRE].

[51] R. Dermisek, J.P. Hall, E. Lunghi and S. Shin, *A new avenue to charged Higgs discovery in multi-Higgs models*, *JHEP* **04** (2014) 140 [arXiv:1311.7208] [INSPIRE].

[52] U. Maitra, B. Mukhopadhyaya, S. Nandi, S.K. Rai and A. Shivaji, *Searching for an elusive charged Higgs at the Large Hadron Collider*, *Phys. Rev.* **D 89** (2014) 055024 [arXiv:1401.1775] [INSPIRE].

[53] B. Coleppa, F. Kling and S. Su, *Charged Higgs search in $H^\pm \to AW^\pm/HW^\pm$*, in preparation.

[54] T. Hahn, S. Heinemeyer, W. Hollik, H. Rzehak and G. Weiglein, *FeynHiggs 2.7*, *Nucl. Phys. Proc. Suppl.* **205-206** (2010) 152 [arXiv:1007.0956] [INSPIRE].

JHEP09(2014)161

Appendix D

Charged Higgs Search via $AW^{\pm}/HW^{\pm}$ Channel

The article *Charged Higgs Search via* $AW^{\pm}/HW^{\pm}$ *Channel* has been submitted to arXiv and accepted for publication in the Journal of High Energy Physics [24].

Published for SISSA by Springer

Received: *August 30, 2014*
Revised: *November 14, 2014*
Accepted: *December 8, 2014*
Published: *December 22, 2014*

Charged Higgs search via $AW^{\pm}/HW^{\pm}$ channel

Baradhwaj Coleppa, Felix Kling and Shufang Su

Department of Physics, University of Arizona,
1118 E. Fourth Street, Tucson, AZ 85721, U.S.A.

E-mail: baradhwa@email.arizona.edu, kling@email.arizona.edu, shufang@email.arizona.edu

Abstract: Models of electroweak symmetry breaking with extended Higgs sectors are theoretically well motivated. In this study, we focus on models with a low energy spectrum containing a pair of charged scalars $H^{\pm}$, as well as a light scalar H and/or a pseudoscalar A. We study the $H^{\pm}tb$ associated production with $H^{\pm} \to AW^{\pm}/HW^{\pm}$, which could reach sizable branching fractions in certain parameter regions. With detailed collider analysis, we obtain the exclusion bounds as well as discovery reach at the 14 TeV LHC for the process $pp \to H^{\pm}tb \to AW^{\pm}tb/HW^{\pm}tb \to \tau\tau bbWW, bbbbWW$. We find that for a daughter particle mass of 70 GeV, the 95% C.L. exclusion reach in $\sigma \times$ BR varies from about 60 fb to 25 fb, for $m_{H^{\pm}}$ ranging from 150 GeV to 500 GeV with 300 fb^{-1} integrated luminosity in the $\tau\tau$ mode. We further interpret these bounds in the context of Type II Two Higgs Doublet Model. The exclusion region in the $m_{H^{\pm}} - \tan\beta$ plane can be extended to $m_{H^{\pm}} = 600$ GeV, while discovery is possible for $m_{H^{\pm}} \lesssim 400$ GeV with 300 fb^{-1} integrated luminosity. The exotic decay mode $H^{\pm} \to AW^{\pm}/HW^{\pm}$ offers a complementary channel to the conventional mode $H^{\pm} \to \tau\nu$ for charged Higgs searches.

Keywords: Higgs Physics, Beyond Standard Model

ArXiv ePrint: 1408.4119

doi:10.1007/JHEP12(2014)148

JHEP12(2014)148

Contents

JHEP12(2014)148

1 Introduction

The discovery of the Standard Model (SM)-like Higgs at the LHC [1–4] marks the final and one of the most important discoveries within the SM of particle physics as regards its particle content. The ATLAS and CMS experiments have reported precise measurements of the mass of this particle, as well as the determination of its spin [2, 4, 5]. The present scenario raises interesting questions about the origin of Electroweak Symmetry Breaking (EWSB). It is conceivable that the scalar sector of the SM does indeed engineer all of EWSB, but at the same time we have compelling evidence from theoretical and experimental fronts that the SM needs to be supplanted with other dynamics for it to consistently explain issues like the naturalness problem, neutrino masses and the dark matter in the universe. Thus it is entirely possible that the scalar sector of the SM responsible for EWSB itself has a richer structure. Early attempts toward enlarging the scalar sector resulted in the Two Higgs Doublet Models (2HDM) [6–9]. Other examples also involving an enlarged scalar sector include the Minimal Supersymmetric Standard Model (MSSM) [10–12] and the Next to Minimal Supersymmetric Standard Model (NMSSM) [13, 14].

Models with extended Higgs sectors hold a lot of phenomenological interest. The discovery of extra Higgs bosons would serve as unambiguous evidence for new physics beyond the SM. A clear indication for a non-minimal Higgs sector as a source of EWSB would be the observation of charged Higgs bosons $H^\pm$ which are absent in the SM. The discovery of the charged Higgs, however, is quite challenging at colliders. If the mass of the charged Higgs $m_{H^\pm}$ is smaller than the top mass m_t, the dominant production mechanism

of the charged Higgs is via top decay: $t \to bH^+$. Most studies performed at LEP, Tevatron and LHC focus on such light charged Higgs bosons which are assumed to either decay leptonically ($H^\pm \to \tau\nu$), or into jets ($H^\pm \to cs$). In the case of a heavy charged Higgs with $m_{H^\pm} > m_t$, the main production mode is the top quark associated production $H^\pm tb$. For the dominant decay $H^\pm \to tb$, it is difficult to identify the $ttbb$ signal given the huge irreducible SM backgrounds. The current heavy charged Higgs searches thus mostly focus on the subdominant decays $H^\pm \to \tau\nu$ or cs in order to take advantage of the cleaner signal and suppressed backgrounds.

Other possible decay channels like $H^\pm \to AW^\pm, HW^\pm$ open up once they are kinematically accessible, where H and A refer to the generic CP-even and CP-odd Higgs, respectively.[1] In the 2HDM, the couplings $H^\pm AW^\mp / H^\pm HW^\mp$ are controlled by the electroweak gauge coupling g. While the coupling to A is independent of the mixing angles, the coupling to H is maximized for non-SM-like CP-even Higgses. These exotic decays quickly dominate over $\tau\nu, cs$ once they are open, and could be even larger than the tb mode for a large range of $\tan\beta$. It was shown that in the 2HDM or NMSSM, both decays $H^\pm \to A_i W^\pm, H_i W^\pm$ could appear with large branching fractions[2] [15–18]. It is thus timely to study such charged Higgs decay channels and fully explore the experimental discovery potential for an enlarged Higgs sector.

In this paper, we focus on $H^\pm tb$ associated production of the charged Higgs with the subsequent exotic decay of $H^\pm \to AW^\pm / HW^\pm$. We consider leptonic decay of one of the $W^\pm$ either coming from $H^\pm$ or top decay, with the A/H in the final state decaying into a pair of fermions (bb or $\tau\tau$) and explore the exclusion bounds as well as the discovery reach at the LHC for various combinations of $(m_{H^\pm}, m_{H/A})$. ATLAS investigated this decay mode in an early study [19–21] focusing on the $A/H \to bb$ mode only. So far no analysis has been done for the more promising $A/H \to \tau\tau$ mode.

A light charged Higgs could have a large impact on precision and flavor observables [22]. For example, in the 2HDM, the bounds on $b \to s\gamma$ restrict the charged Higgs to be heavier than 300 GeV. A detailed analysis of precision and flavor bounds in the 2HDM can be found in refs. [23, 24]. Flavor constraints on the Higgs sector are, however, typically model-dependent, and could be alleviated when there are contributions from other new particles in the model. Our focus in this work is on collider searches for the charged Higgs and its implications for the Type II 2HDM. Therefore, we consider a wide range of charged Higgs mass.

The paper is organized as follows. In section 2, we present a brief overview of models and parameter regions where $H^\pm \to AW^\pm / HW^\pm$ can be significant. In section 3, we summarize the current experimental search limits on charged Higgses. Section 4 describes the collider analysis in detail. After describing the signal process and event generation in section 4.1, we present the details of the analysis for the $A/H \to \tau\tau$ channel in section 4.2. We show the model independent results of 95% C.L. exclusion as well as 5σ discovery limits for $\sigma(pp \to H^\pm tb \to A/HW^\pm tb \to \tau\tau bbWW)$ at the 14 TeV LHC with 100, 300 and

[1] Note that we use h^0 and H^0 to refer to the lighter or the heavier CP-even Higgs for models with two CP-even Higgs bosons. When there is no need to specify, we use H to refer to the CP-even Higgses.

[2] $H^\pm \to AW^\pm, HW^\pm$ is less likely to open in the MSSM due to kinematical constraints that force $m_{H^\pm} \sim m_A \sim m_H$ for the non SM-like Higgses.

JHEP12(2014)148

1000 fb^{-1} integrated luminosity. In section 4.3 we present the analysis for the $H/A \to bb$ final state and derive the corresponding cross section limits. In section 5, we study the implications of the collider search limits on the Type II 2HDM. We conclude in section 6.

2 Scenarios with large $H^\pm \to AW^\pm/HW^\pm$

In the 2HDM, we introduce two SU(2)$_L$ doublets Φ_i, $i = 1, 2$:

$$\Phi_i = \begin{pmatrix} \phi_i^+ \\ (v_i + \phi_i^0 + iG_i)/\sqrt{2} \end{pmatrix}, \tag{2.1}$$

where v_1 and v_2 are the vacuum expectation values (vev) of the neutral components which satisfy the relation $\sqrt{v_1^2 + v_2^2} = 246\,\text{GeV}$ after EWSB. Assuming an additional discrete $\mathcal{Z}_2$ symmetry imposed on the Lagrangian, we are left with six free parameters, which can be chosen as the four Higgs masses (m_{h^0}, m_{H^0}, m_A, $m_{H^\pm}$), a mixing angle α between the two CP-even Higgses, and the ratio of the two vacuum expectation values, $\tan\beta = v_2/v_1$. In the case where a soft breaking of the $\mathcal{Z}_2$ symmetry is allowed, there is an additional parameter m_{12}^2.

The Higgs mass eigenstates containing a pair of CP-even Higgses (h^0, H^0), one CP-odd Higgs A and a pair of charged Higgses $H^\pm$ can be written as:[3]

$$\begin{pmatrix} H^0 \\ h^0 \end{pmatrix} = \begin{pmatrix} \cos\alpha & \sin\alpha \\ -\sin\alpha & \cos\alpha \end{pmatrix} \begin{pmatrix} \phi_1^0 \\ \phi_2^0 \end{pmatrix}, \quad \begin{aligned} A &= -G_1 \sin\beta + G_2 \cos\beta \\ H^\pm &= -\phi_1^\pm \sin\beta + \phi_2^\pm \cos\beta \end{aligned}. \tag{2.2}$$

The couplings that are of particular interest are of the type $H^\pm AW^\mp$ and $H^\pm HW^\mp$. They are determined by the gauge coupling structure, as well as the mixing angles [25]:

$$g_{H^\pm h^0 W^\mp} = \frac{g\cos(\beta-\alpha)}{2}(p_{h^0} - p_{H^\pm})^\mu, \tag{2.3}$$

$$g_{H^\pm H^0 W^\mp} = \frac{g\sin(\beta-\alpha)}{2}(p_{H^0} - p_{H^\pm})^\mu, \tag{2.4}$$

$$g_{H^\pm A W^\mp} = \frac{g}{2}(p_A - p_{H^\pm})^\mu, \tag{2.5}$$

with g being the SU(2)$_L$ coupling, and p_μ being the incoming momentum for the corresponding particle.

An interesting feature here is that $H^\pm$ always couples to the non-SM-like CP-even Higgs more strongly. If we demand h^0 (H^0) to be SM-like, then $|\sin(\beta-\alpha)| \sim 1$ ($|\cos(\beta-\alpha)| \sim 1$), and the $H^\pm H^0 W^\mp$ ($H^\pm h^0 W^\mp$) coupling is unsuppressed. Therefore, in the h^0-126 case, $H^\pm$ is more likely to decay to $H^0 W^\pm$ than $h^0 W^\pm$ unless the former decay is kinematically suppressed. In the H^0-126 case, $H^\pm$ is more likely to decay to $h^0 W^\pm$ than $H^0 W^\pm$. The $H^\pm AW^\mp$ coupling, on the other hand, does not depend on any mixing angle and therefore this decay is not suppressed once it is kinematically allowed.

In the generic 2HDM, there are no mass relations between the charged scalar, the scalar and pseudoscalar states. Thus, the decays $H^\pm \to h^0 W^\pm$, $H^0 W^\pm$ and $H^\pm \to AW^\pm$ can all

[3] For more details about the 2HDM model, see ref. [6].

JHEP12(2014)148

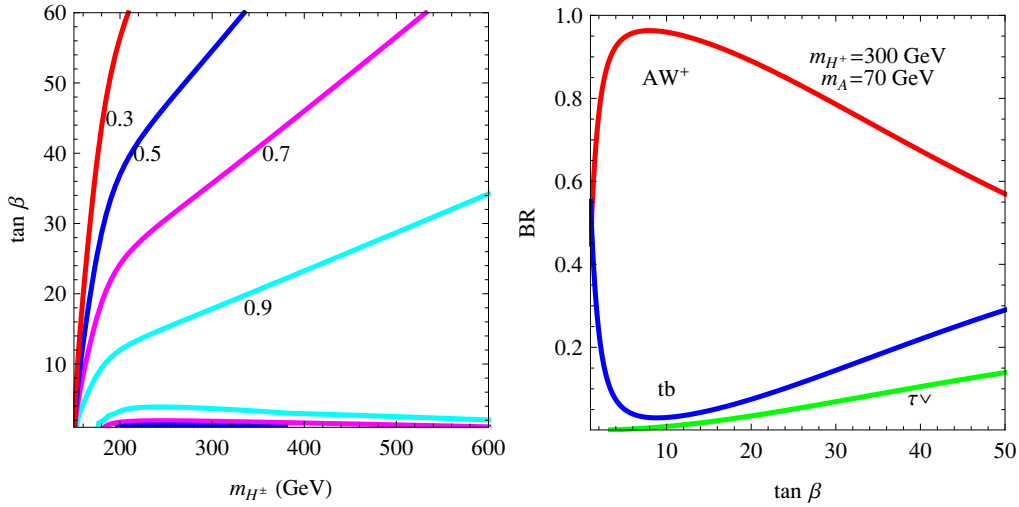

Figure 1. Left panel: branching fraction BR($H^\pm \to AW^\pm$) in the $m_{H^\pm} - \tan\beta$ plane, for $m_A = 70\,\text{GeV}$ and $\sin(\beta-\alpha)$ =1. Right panel: the branching fractions of $H^\pm$ as a function of $\tan\beta$ for various decay modes: $H^\pm \to AW^\pm$ (red), tb (blue), $\tau\nu$ (green) for $m_{H^\pm} = 300\,\text{GeV}$, $m_A = 70\,\text{GeV}$ and $\sin(\beta-\alpha) = 1$.

be kinematically accessible and dominate in different regions of parameter spaces. It was shown in ref. [23] that in the Type II 2HDM with $\mathcal{Z}_2$ symmetry, imposing all experimental and theoretical constraints still left sizable regions in the parameter space that permit such exotic decays with unsuppressed decay branching fractions.

The dominant competing mode is $H^\pm \to tb$, which is controlled by the $H^\pm tb$ coupling

$$g_{H^\pm tb} = \frac{g}{2\sqrt{2}m_W}\left[(m_b \tan\beta + m_t \cot\beta) \pm (m_b \tan\beta - m_t \cot\beta)\gamma_5\right] \tag{2.6}$$

in the Type II 2HDM. At both small and large $\tan\beta$, $\Gamma(H^\pm \to tb)$ is increased given the enhanced top and bottom Yukawa coupling, respectively. The subdominant channel $H^\pm \to \tau\nu$ has similar enhancement at large $\tan\beta$ as well.

In the left panel of figure 1, we present contours of the branching fraction BR($H^\pm \to AW^\pm$) in the $m_{H^\pm} - \tan\beta$ plane fixing $\sin(\beta-\alpha) = 1$, $m_A = 70\,\text{GeV}$ and decoupling H^0. It is seen that there is a "kink" at the tb threshold which brings down the steeply increasing values of BR($H^\pm \to AW^\pm$). Even so, the $AW^\pm$ mode can be 90% or higher in the band $1.5 \lesssim \tan\beta \lesssim 30$ for $m_{H^\pm}$ between 175 and 600 GeV. For large or small values of $\tan\beta$, BR($H^\pm \to AW^\pm$) is reduced due to competition from $H^\pm \to tb, \tau\nu$ modes. The $H^\pm \to H^0 W^\pm$ mode, when kinematically accessible, would show similar features with additional phase space suppression. $H^\pm \to h^0 W^\pm$ mode is maximized at $\sin(\beta-\alpha) = 0$, which could be a potentially useful search channel for $H^\pm$ in the H^0-126 case. The current searches for the charged Higgs focus on the $H^\pm \to \tau\nu$ channel, which is sensitive to the large $\tan\beta$ region. We expect the $H^\pm \to AW^\pm/HW^\pm$ channel to be complementary for small or intermediate $\tan\beta$.

JHEP12(2014)148

In the right panel of figure 1, we show the branching fractions of $H^\pm$ as a function of $\tan\beta$ for various decay modes of $H^\pm \to AW^\pm$, $tb, \tau\nu$ for $m_{H^\pm} = 300\,\text{GeV}$, $m_A = 70\,\text{GeV}$ and $\sin(\beta-\alpha) = 1$. For almost all values of $\tan\beta$, the decay to the $AW^\pm$ mode exceeds that of tb.

The Higgs sector in the MSSM is more restricted, given that the quartic Higgs couplings are fixed by the gauge couplings and the tree-level Higgs mass matrix only depends on m_A and $\tan\beta$. The decay $H^\pm \to h^0 W^\pm$ is typically suppressed by the small coupling $\cos(\beta-\alpha) \sim 0$, and is only relevant for small $\tan\beta$. The branching fraction is typically about 10% or less [26]. In the usual decoupling region with large m_A, the light CP-even Higgs h^0 is SM-like while the other Higgses are almost degenerate: $m_{H^0} \sim m_A \sim m_{H^\pm}$. Thus, $H^\pm \to H^0 W^\pm$ or $H^\pm \to AW^\pm$ is not kinematically allowed. However, it has been shown that there are scenarios with large μ in which next-to-leading order (NLO) corrections can increase the mass difference between the charged and neutral Higgses [27], which could make this channel kinematically accessible. In the NMSSM, the Higgs sector of MSSM is enlarged to include an additional singlet. It was shown in refs. [15, 16] that in this model, there are regions of parameter space where the decay $H^\pm \to H_i W^\pm / A_i W^\pm$ can be significant.

3 Current limits

Searches for a light charged Higgs boson with mass $m_{H^\pm} < m_t$ have been performed both by ATLAS and CMS [28, 29] with 19.7 fb^{-1} integrated luminosity at 8 TeV and 4.6 fb^{-1} integrated luminosity at 7 TeV. The production mechanism considered is top pair production in which one top quark decays into a charged Higgs $t \to bH^\pm$ while the other top decays into bW. Assuming a branching fraction $\text{BR}(H^\pm \to \tau\nu) = 100\%$, the null search results from CMS [29] imply an upper bound for the top quark branching fraction $\text{BR}(t \to bH^\pm) = 1.2\%$ to 0.16% for charged Higgs masses between 80 GeV and 160 GeV. This result can be translated into bounds on the MSSM parameter space. In the m_h^{max} scenario of the MSSM, this excludes $m_{H^\pm} < 155\,\text{GeV}$ for all values of $\tan\beta$. Only the small region $155\,\text{GeV} < m_{H^\pm} < 160\,\text{GeV}$ around $\tan\beta = 8$ is still allowed. The ATLAS results [28] are similar.

A search with the $H^\pm \to cs$ final state has been performed by ATLAS [30] using $4.7\,\text{fb}^{-1}$ integrated luminosity at 7 TeV. Assuming $\text{BR}(H^\pm \to cs) = 100\%$, this implies an upper bound for the top quark branching fraction $\text{BR}(t \to bH^\pm) = 5\%$ to 1% for charged Higgs masses between 90 GeV and 150 GeV.

Both ATLAS and CMS have also searched for a heavy charged Higgs boson with mass $m_{H^\pm} > m_t$ produced in association with a top quark [28, 29]. With 19.5 fb^{-1} integrated luminosity at 8 TeV and assuming a branching fraction $\text{BR}(H^\pm \to \tau\nu) = 100\%$, the null search results at ATLAS imply an upper bound on the production cross section $\sigma(pp \to H^\pm tb)$ between 0.9 pb and 0.017 pb [28] for charged Higgs masses between 180 GeV and 600 GeV. When interpreting in the m_h^{max} scenario of the MSSM, $\tan\beta$ above 47 to 65 is excluded for $m_{H^\pm}$ between 230 GeV and 310 GeV. The CMS results [29] are very similar, which are slightly better for low $m_{H^\pm}$ and slightly worse for large $m_{H^\pm}$.

As demonstrated in figure 1, the conventional decay modes $\tau\nu$ and cs would be highly suppressed in regions of parameter space where the exotic decay modes $H^\pm \to AW^\pm / HW^\pm$

JHEP12(2014)148

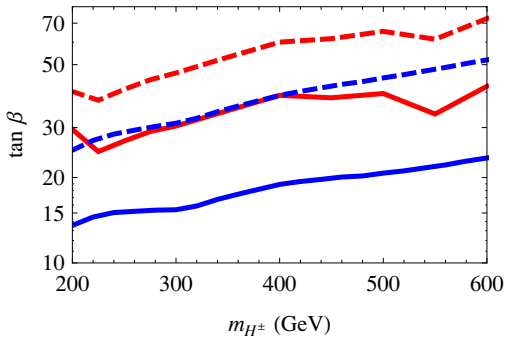

Figure 2. The recast of the current ATLAS 95% CL exclusion limits (solid red curves) [28] with 19.5 fb^{-1} integrated luminosity and the projected 5σ reach (solid blue curves) [31] with 100 fb^{-1} integrated luminosity at the 14 TeV LHC for the process $pp \to H^\pm tb \to (\tau\nu)(bbjj)$ in the context of the Type II 2HDM. Also shown in dashed curves are the reduced limits with the opening of $H^\pm \to AW^\pm$, with $m_A = 70$ GeV, $\sin(\beta - \alpha) = 1$ and H^0 decoupled.

open. In figure 2, we recast the current 95% C.L. exclusion limits (solid red curve) [29] and future projection of 5σ discovery (solid blue curve) [31] with 100 fb^{-1} integrated luminosity at the 14 TeV LHC for the process $pp \to H^\pm tb \to (\tau\nu)(bbjj)$ in the context of the Type II 2HDM. The dashed curves show the reduced reach when $H^\pm \to AW^\pm$ opens up, shown here for the parameter choice $m_A = 70$ GeV, $\sin(\beta - \alpha) = 1$, and with the H^0 decoupled. The inclusion of the exotic decay modes thus substantially weakens the current and future limits.

There have been other theoretical studies on the charged Higgs detectability at the LHC. The authors of [32, 33] analyzed the possibility of observing light charged Higgs decay $H^\pm \to \tau\nu$ via the single top production mode. The possibility of the $H^\pm \to \mu\nu$ decay with a light charged Higgs produced via top decay in top pair production has been investigated in [34]. Furthermore the decay of a heavy charged Higgs into tb has been studied, considering charged Higgs production via $qq' \to H^\pm$ [35], $H^\pm tb$ associate production [36–39] and $W^\mp H^\pm$ associate production [40].

Furthermore, the authors of [41] studied electroweak charged Higgs boson pair production with the charged Higgses decaying into a W boson and a very light $[m_\phi = \mathcal{O}(eV)]$ neutral scalar which decays invisibly. A search strategy for $H^\pm \to h^0 W^\pm$ for a SM-like h^0 using the $H^\pm W^\mp$ production mode has been suggested by the authors of [42] and analysed in the context of CP-violating Type-II 2HDM. This study considers both electroweak production and the production via the decay of heavy scalars, if it is kinematically allowed. Charged Higgs production via the decay of a heavy scalar $pp \to H \to WH^\pm$ with $H^\pm \to AW^\pm$ was investigated in [43].

The $H^\pm tb$ associated production with $H^\pm \to HW^\pm \to bbW^\pm$ has been analyzed in early studies [19–21]. While refs. [19, 20] concluded that the $H^\pm \to h^0 W^\pm / H^0 W^\pm$ is not promising in MSSM searches, the authors of [21] found that this channel is indeed promising in NMSSM. However, neither paper considers the possibility of analyzing this channel with the $\tau\tau$ mode. In particular, the $\tau\tau$ mode allows two same sign lepton signature with the accompanying leptonic decay of W [44], which leads to a better reach than the existing

JHEP12(2014)148

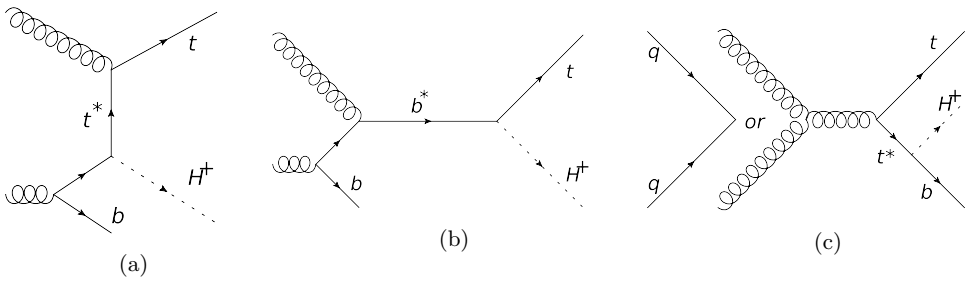

Figure 3. Dominant t-channel (a), s-channel (b) and $t\bar{t}$-like (c) diagrams contributing to heavy quark associated charged Higgs production [48].

studies of the $H/A \to bb$ channel. Therefore, in our study, we analyze the discovery and exclusion prospects in both $H^\pm \to AW^\pm/HW^\pm \to bbW^\pm$ and $H^\pm \to AW^\pm/HW^\pm \to \tau\tau W^\pm$ channels.

Our study also assumes the existence of a light neutral Higgs A/H, which has been constrained by the $A/H \to \tau\tau$ searches at the LHC [45, 46], in particular, for $m_{A/H} > 90\,\text{GeV}$ and relatively large $\tan\beta$. No limit, however, exists for $m_{A/H} < 90\,\text{GeV}$ due to the difficulties in the identification of the relatively low p_T taus and the overwhelming SM backgrounds for low p_T leptons and τ-jets. Furthermore, LEP limits [47] based on VH associated production do not apply for the CP-odd A or the non-SM like CP-even Higgs. LEP limits based on AH pair production also do not apply as long as $m_A + m_H > 208\,\text{GeV}$. Therefore, in our analyses below, we choose the daughter neutral Higgs mass to be 70,[4] 126, and 200 GeV to represent the cases with a light, SM-like, and a heavy neutral Higgs respectively.

4 Collider analysis

4.1 Signal process

In our analysis we study the associated production $pp \to H^\pm tb$ in which the charged Higgs boson decays into a neutral Higgs (A or H) and a W. The dominant leading order Feynman diagrams contributing to this production are shown in figure 3 [48]. For large charged Higgs masses, diagrams (a) and (b) dominate while for smaller charged Higgs masses, top pair production in panel (c) with the decay of one (possibly offshell) top into a charged Higgs dominates.[5] The exclusion and discovery reach in $\sigma \times \text{BR}$ obtained in this section will cover the entire kinematically possible mass range. When interpreting the results in the Type II 2HDM in section 5, we focus on the high mass region: $m_{H^\pm} > m_t$. For the low mass range where the $t\bar{t}$ production dominates, the bounds are usually translated into limits on the branching fraction $\text{BR}(t \to H^\pm b)$ [49].

In principle the neutral Higgs boson can either be CP-even (denoted by H) or CP-odd (denoted by A). In the analysis that follows, we use the decay $H^\pm \to AW^\pm$ as an

[4]The mass of 70 GeV was choose to be above the $h_{\text{SM}} \to AA$ threshold to avoid significant deviations of the 126 GeV SM-like Higgs branching fractions from current measurements.

[5]All possible production diagrams are taken into account for event generation.

JHEP12(2014)148

illustration. Since we do not make use of angular correlations, the bounds obtained for $H^\pm \to AW^\pm$ apply to $H^\pm \to HW^\pm$ as well.

The neutral Higgs boson itself will further decay. We only look at the fermionic decays $A \to bb, \tau\tau$. While the bb case has the advantage of a large branching fraction BR($A \to bb$), the $\tau\tau$ case has less SM backgrounds and therefore leads to a cleaner signal. We study both leptonic and hadronic τ decays and consider the three cases: $\tau_{had}\tau_{had}$, $\tau_{lep}\tau_{had}$ and $\tau_{lep}\tau_{lep}$. The $\tau_{lep}\tau_{had}$ case is particularly promising since we can utilize the same sign dilepton signal with the leptons from W decay and from τ decay. Exotic decays of A/H into pairs of vector bosons or other Higgs bosons will most likely be suppressed or have a very complex final state. Since the top quark decays to bW, the final state contains two W bosons. To reduce the backgrounds, in our analysis we assume one of these two W bosons decays leptonically, with the other W decaying hadronically.

We use Madgraph 5/MadEvent v1.5.11 [50, 51] to generate our signal and background events. These events are passed to Pythia v2.1.21 [52] to simulate initial and final state radiation, showering and hadronization. The events are further passed through Delphes 3.07 [53] with the Snowmass combined LHC detector card [54] to simulate detector effects. The discovery reach and exclusion bounds have been determined using the program RooStats [55, 56] and theta-auto [57].

In this section, we will present model *independent* limits on the $\sigma \times$ BR for both 95% C.L. exclusion and 5σ discovery for both possible final states $\tau\tau bbWW$ and $bbbbWW$. For the signal process, we generated event samples at 14 TeV LHC for $pp \to H^\pm tb \to AW^\pm tb$ with the daughter particle mass fixed at $m_A = 70, 126, 200$ GeV to represent the cases with a light, SM-like, and a heavy Higgs respectively. For each case, we vary the parent particle mass $m_{H^\pm}$ in the range $150 - 600$ GeV.

4.2 $A \to \tau\tau$ mode

We start our analysis by looking at the channel $pp \to H^\pm tb \to AW^\pm tb \to \tau\tau bbWW$. We only require to identify one b jet from top decay. We do not require to find the b jet produced in association with the charged Higgs since it is likely to be soft. As mentioned above, we will distinguish three cases depending on how the taus decay:

- **Case A:** both taus decay hadronically.
- **Case B:** one tau decays hadronically, and the other tau decays leptonically.
- **Case C:** both taus decay leptonically.

For the two W bosons, we require one decay leptonically and the other decay hadronically. The dominant SM background for this final state is semi- and fully leptonic (where leptonic includes decaying into τ) $t\bar{t}$ pair production, which we generate with up to one additional jet. We also take into account $tt\tau\tau$ production, where the taus come from the decay of a boson $Z/H/\gamma^*$. Furthermore we include $W\tau\tau$ production with up to two additional jets (including b jets) and $WW\tau\tau$ production with up to one additional jet (including b jet), where the taus are produced in the decay of a boson $Z/H/\gamma^*$. We ignored the subdominant

JHEP12(2014)148

backgrounds from single vector boson production, WW, ZZ, single top production, as well as multijet QCD Background. Those backgrounds are either small or can be sufficiently suppressed by the cuts imposed.

We apply the following cuts to extract the signal from the backgrounds:

1. **Identification cuts:**
   Case A: one lepton $\ell = e$ or μ , one or two b jets, two τ tagged jets and at least two untagged jets:
   $$n_\ell = 1,\ n_b = 1, 2,\ n_\tau = 2,\ n_j \geq 2. \tag{4.1}$$
   We require that the τ tagged jets have opposite charge.
   Case B: two leptons, one or two b jets, one τ tagged jet and at least two untagged jets:
   $$n_\ell = 2,\ n_b = 1, 2,\ n_\tau = 1,\ n_j \geq 2. \tag{4.2}$$
   We require that both leptons have the same sign, which is opposite to the sign of the τ tagged jet.
   Case C: three leptons, one or two b jets, no τ tagged jet and at least two untagged jets:
   $$n_\ell = 3,\ n_b = 1, 2,\ n_\tau = 0,\ n_j \geq 2. \tag{4.3}$$
   We adopt the following selection cuts for the identification of leptons, b jets and jets.
   $$|\eta_{\ell,b,\tau}| < 2.5,\ |\eta_j| < 5,\ p_{T;\ell_1,j,b} > 20 \text{ GeV and } p_{T;\ell_2} > 10 \text{ GeV}, \tag{4.4}$$
   where $\ell_{1,2}$ refer to the hardest and the sub-leading lepton. For jet reconstruction, the anti-k_T jet algorithm with $R = 0.5$ is used.

2. **Two W candidates:** our analysis assumes that one W decays leptonically and the other decays hadronically. We look for the combination of two untagged jets that gives an invariant mass closest to the W mass and reconstruct the jets to form the hadronic W_{had}. The momentum of the neutrino coming from the leptonic W decay is determined using the missing transverse momentum and imposing the mass conditions [58]. Using the momenta of the reconstructed neutrino and the lepton, the momentum of the leptonic W_{lep} can be deduced. In cases B and C which contain more than one lepton, the hardest lepton is used for W reconstruction. In these cases the neutrino reconstruction will be relatively poor since there is additional missing energy from the τ decay.

3. **Top candidate:** we look for the combination of the b tagged jet and a reconstructed (either leptonic or hadronic) W that gives an invariant mass closest to the top mass and combine them to form the top candidate t.

4. **Neutral Higgs candidate (H):** the τ jets (case A), the τ jet and the softer lepton (case B) or the two softer leptons (case C) are combined to form the neutral Higgs candidate. In cases B and C the Higgs reconstruction will be relatively poor for

JHEP12(2014)148

reasons mentioned above which in turn forces us to employ more relaxed mass cuts (see below).

5. **Charged Higgs candidate ($H^\pm$):** the Higgs candidate and the W candidate not used for the top reconstruction are combined to form the charged Higgs candidate $H^\pm$.

6. **$m_{\tau\tau}$ versus $m_{\tau\tau W}$:** we require the ditau mass $m_{\tau\tau}$ to be close to the daughter Higgs mass m_A and the mass of the two taus and the W ($m_{\tau\tau W}$) to be close to the parent Higgs mass $m_{H^\pm}$. The two masses are correlated, i.e., if we underestimate $m_{\tau\tau}$ we also underestimate $m_{\tau\tau W}$. To take this into account we apply a two-dimensional cut:

$$\begin{aligned} (1-\Delta-w_{\tau\tau})\cdot m_A < m_{\tau\tau} < (1-\Delta+w_{\tau\tau})\cdot m_A, \\ \frac{m_A}{E_A}(m_{\tau\tau W}-m_{H^\pm}-w_{\tau\tau W}) < m_{\tau\tau}-m_A < \frac{m_A}{E_A}(m_{\tau\tau W}-m_{H^\pm}+w_{\tau\tau W}). \end{aligned} \tag{4.5}$$

   Here $w_{\tau\tau} = 0.225$ (case A) or 0.25 (cases B and C) is the width of the ditau mass window. Note that the slightly shifted reconstructed Higgs mass $m_{\tau\tau}$ around $(1-\Delta)m_A$ instead of m_A is due to the reconstruction of the τ using a jet with a small size of $R = 0.5$ or a lepton. We use $\Delta = 0.3$ (case A), 0.4 (case B) and 0.66 (case C). The second condition describes two lines going through the points $(m_{H^\pm} \pm w_{\tau\tau W}, m_A)$ with slope $\frac{m_A}{E_A}$ where E_A is the energy of the neutral Higgs in the rest frame of the charged Higgs.[6] We choose a width for the $m_{\tau\tau W}$ peak of $w_{\tau\tau W} = 0.2 m_{H^\pm}$, based on the theoretical decay width estimation of $w_{H^\pm} \sim 0.1 m_{H^\pm}$ as well as detector resolutions. The effectiveness of this cut is shown in figure 4 for $m_{H^\pm} = 240\,\text{GeV}$ and $m_A = 70\,\text{GeV}$ in case A, with two horizontal lines indicating the $m_{\tau\tau}$ range and two slanted lines indicating the $m_{\tau\tau W}$ range as given in eq. (4.5).

No mass cuts are applied for the reconstructed W and t candidates since both signal and the dominant backgrounds contain a top quark and an additional W boson. In table 1, we show the signal and background cross sections with cuts for a signal benchmark point of $M_{H^\pm} = 240\,\text{GeV}$ and $m_A = 70\,\text{GeV}$ at the 14 TeV LHC. The first row shows the total cross section before cuts calculated using MadGraph. The following rows show the cross sections after applying the identification cuts and mass cuts for all three cases as discussed above. We have chosen a nominal value for $\sigma \times BR(pp \to H^\pm tb \to \tau\tau bbWW)$ of 100 fb[7] to illustrate the cut efficiencies for the signal process. The last column shows the $S/\sqrt{B}$ value for an integrated luminosity of 300 fb^{-1}.

We can see that the dominant background contributions are $t\bar{t}$ (case A) and $t\bar{t}\tau\tau$ (cases B and C) while the vector boson backgrounds do not contribute much. It turns out that

[6] We choose $E_A = \frac{m_{H^\pm}^2 + m_A^2 - m_W^2}{2m_A}$, which is the energy of A in the rest frame of the charged Higgs. The slope in eq. (4.5) can be motivated by relativistic kinematics and works well even when the charged Higgs is not produced at rest.

[7] For the Type II 2HDM the cross section for $m_{H^\pm} = 240\,\text{GeV}$ is typically in the range of $\sigma(pp \to H^\pm tb) = 0.1-1.5$ pb (see figure 7.). Assuming a branching fraction $\text{BR}(H^\pm \to AW^\pm) = 100\%$ and $\text{BR}(A \to \tau\tau) = 10\%$ leads to the stated $\sigma\times$ BR of around 100 fb.

JHEP12(2014)148

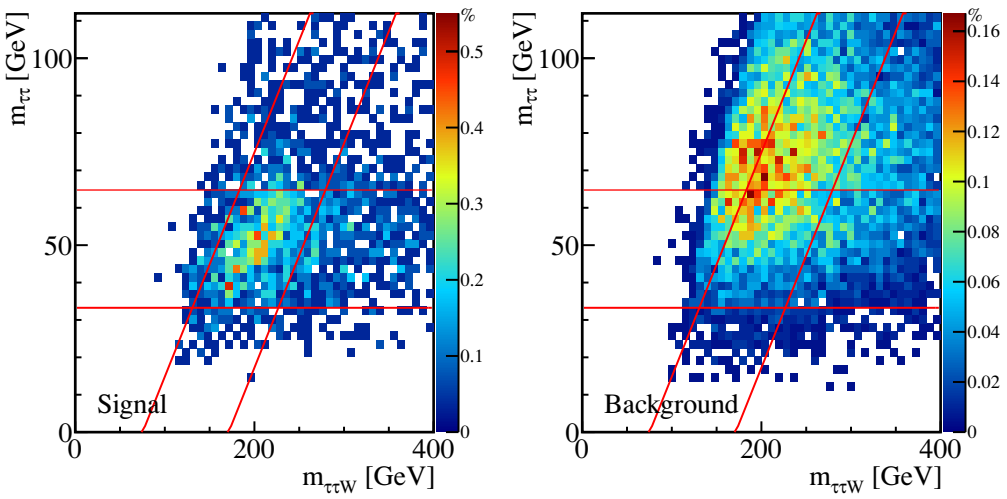

Figure 4. Normalized distribution (in percent as given by the color code in the panel along the y-axis) of $m_{\tau\tau}$ versus $m_{\tau\tau W}$ for the signal (left) and the backgrounds (right) assuming $m_{H^\pm} = 240\,\text{GeV}$ and $m_A = 70\,\text{GeV}$ for case A. Two horizontal lines indicate the $m_{\tau\tau}$ range and two slanted lines indicate the $m_{\tau\tau W}$ range, as given in eq. (4.5).

Cut	Signal [fb]	$t\bar{t}$ [fb]	$t\bar{t}\tau\tau$ [fb]	$W(W)\tau\tau$ [fb]	S/B	$S/\sqrt{B}$
σ	100	$6.3 \cdot 10^5$	247	2000	-	-
A: identification [eq. (4.1)]	0.57	22.9	0.58	0.078	0.02	2.04
$m_{\tau\tau}$ vs $m_{\tau\tau W}$ [eq. (4.5)]	0.16	1.67	0.054	0.010	0.10	2.20
B: identification [eq. (4.2)]	0.47	0.35	0.697	0.073	0.42	7.81
$m_{\tau\tau}$ vs $m_{\tau\tau W}$ [eq. (4.5)]	0.15	0.043	0.104	0.018	0.94	6.67
C: identification [eq. (4.3)]	0.48	2.35	5.11	0.059	0.06	3.05
$m_{\tau\tau}$ vs $m_{\tau\tau W}$ [eq. (4.5)]	0.15	0.56	0.56	0.010	0.13	2.54

Table 1. Signal and background cross sections with cuts for the signal benchmark point $m_{H^\pm} = 240\,\text{GeV}$ and $m_A = 70\,\text{GeV}$ at the 14 TeV LHC. We have chosen a nominal value for $\sigma \times \text{BR}(pp \to H^\pm tb \to \tau\tau bbWW)$ of 100 fb to illustrate the cut efficiencies for the signal process. The last column of $S/\sqrt{B}$ is shown for an integrated luminosity of $\mathcal{L} = 300\ \text{fb}^{-1}$.

case B, in which one τ decays leptonically and the other τ decays hadronically, gives the best reach. This is because the same sign lepton signature can reduce the $t\bar{t}$ background sufficiently. This analysis is sensitive to the tagging and misidentification rate of the τ tagger. Most of the top pair background, especially in case A, includes mistagged τ jets. We assume a tagging rate of $\epsilon_{tag} = 60\%$ and a mistagging rate of $\epsilon_{miss} = 0.4\%$ as suggested in [54]. A better rejection of non-τ initiated jets would increase the significance of this channel.

In figure 5, we display the results at the 14 TeV LHC for 95% C.L. exclusion (left panel) and 5σ discovery (right panel) limits for $\sigma \times \text{BR}(pp \to H^\pm tb \to \tau\tau bbWW)$, which applies for $H^\pm \to HW^\pm$ as well with m_A replaced by m_H. We have combined all three cases of tau decays. The blue, red, and green curves correspond to the daughter particle being 70 GeV,

JHEP12(2014)148

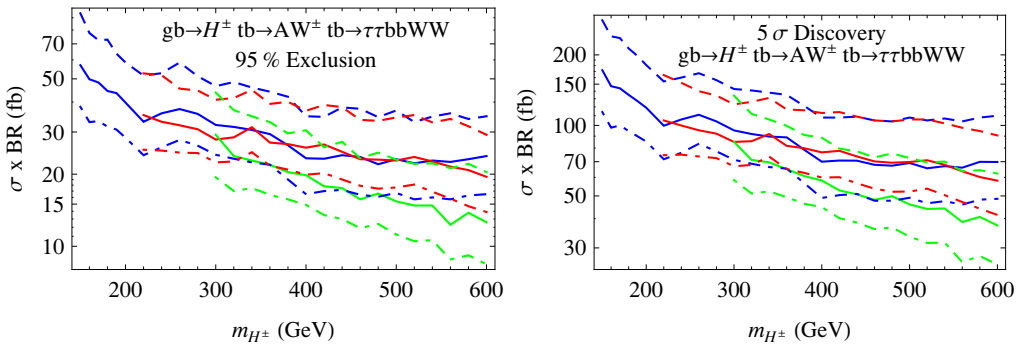

Figure 5. The 95% C.L. exclusion (left) and 5σ discovery (right) limits for $\sigma \times \mathrm{BR}(pp \to H^\pm tb \to \tau\tau bbWW)$ for $m_A = 70\,\mathrm{GeV}$ (blue), 126 GeV (red), and 200 GeV (green) at the 14 TeV LHC. We have combined all three cases of tau decays. The dashed, solid and dot-dashed lines correspond to an integrated luminosity of 100, 300 and $1000\,\mathrm{fb}^{-1}$, respectively. Here, we have assumed a 10% systematic error on the backgrounds. These results are equally applicable to the $H^\pm \to HW^\pm$ process for the same parent and daughter Higgs masses.

126 GeV, and 200 GeV, respectively. For each mass, we have displayed the results for three luminosities: $100\,\mathrm{fb}^{-1}$ (dashed), $300\,\mathrm{fb}^{-1}$ (solid), and $1000\,\mathrm{fb}^{-1}$ (dot-dashed), with 10% systematic error included [57]. Due to the small number of events, the statistical error dominates in this channel and therefore higher luminosities lead to a better reach. Better sensitivity is achieved for larger $m_{H^\pm}$ since the mass cuts on $m_{\tau\tau}$ and $m_{\tau\tau W}$ have a more pronounced effect on the SM backgrounds for larger masses.

The $m_{\tau\tau}$ distribution for the dominating tt backgrounds peaks around higher masses $m_{\tau\tau} \approx 70$ - 200 GeV and therefore the background rejection efficiency for $m_{\tau\tau} \approx 70\,\mathrm{GeV}$ is high compared to the cases with larger daughter particle masses. On the other hand a small daughter Higgs mass causes the taus to be either soft (low $m_{H^\pm}$) or collimated (high $m_{H^\pm}$) and decreases the identification efficiency compared to higher daughter particles masses. Taking into account these two effects, the limits do not change significantly for m_A being 70 GeV or 125 GeV. The limit for $m_A = 200\,\mathrm{GeV}$ is better by about a factor of 1.5.

The limit, however, gets slightly worse for the $m_A = 70\,\mathrm{GeV}$ case when $m_{H^\pm} \gtrsim 500\,\mathrm{GeV}$ (blue curves). This is due to the decrease of the signal cut efficiency for a highly boosted daughter particle with two collimated τ jets. For the interesting case where the daughter particle is 70 GeV, it is seen that the exclusion limits for a $300\,\mathrm{fb}^{-1}$ collider fall from about 60 fb for $m_{H^\pm}$ of 150 GeV, to less than 25 fb for a 500 GeV charged Higgs. The 5σ discovery limits are about a factor of 3−4 higher.

We reiterate here that these exclusion and discovery limits are completely model independent. Whether or not discovery/exclusion is actually feasible in this channel should be answered within the context of a particular model, in which the theoretically predicted cross sections and branching fractions can be compared with the exclusion or discovery limits. We will do this in section 5 using the Type II 2HDM as a specific example.

JHEP12(2014)148

4.3 $A \to bb$ mode

We now turn to the channel $pp \to H^{\pm}tb \to bbbbWW$, with one W decaying leptonically and the other decaying hadronically. The dominant SM backgrounds for this final state are semi- and fully leptonic top pair production, which we generate with up to one additional jet. We also take into account $ttbb$ production where the two bottom jets either come from the decay of a boson $Z/H/\gamma^*$ or are produced through gluon splitting. We have ignored the subdominant backgrounds including V+jets, VV+jets or VVV+jets, single top production, as well as multijet QCD Background. These backgrounds either have small production cross sections, or can be sufficiently suppressed by the cuts imposed.

Much of the analysis for this case is similar to the $\tau\tau$ case described above. We apply the following cuts to identify the signal from the backgrounds:

1. **One lepton, three or 4 b jets, at least two untagged jets:**

$$\begin{gathered} n_\ell = 1,\ n_b = 3, 4,\ n_j \geq 2 \text{ with} \\ |\eta_{\ell,b}| < 2.5,\ |\eta_j| < 5,\ p_{T,\ell,j,b} > 20 \text{ GeV}. \end{gathered} \tag{4.6}$$

2. **Two W candidates and one top candidate:** similar to that in section 4.2. For top reconstruction, we look for the combination of a b tagged jet and a reconstructed W that gives an invariant mass closest to the top mass.

3. **Neutral Higgs candidate (A):** the remaining b jets are combined to form the Higgs candidate A with mass m_{bb}.

4. **Charged Higgs candidate ($H^{\pm}$):** the Higgs candidate and the W candidate not used for the top reconstruction are combined to form the charged Higgs candidate $H^{\pm}$ with mass m_{bbW}.

5. **m_{bb} versus m_{bbW}:** there is no Higgs mass shift Δ as in the $\tau\tau$ case since there is no missing energy carried away by neutrinos from tau decay anymore. Our 2-D cuts are thus modified as follows:

$$\begin{gathered} (1 - w_{bb}) \cdot m_A < m_{bb} < (1 + w_{bb}) \cdot m_A, \\ \frac{m_A}{E_A}(m_{bbW} - m_{H^\pm} - w_{bbW}) < m_{bb} - m_A < \frac{m_A}{E_A}(m_{bbW} - m_{H^\pm} + w_{bbW}). \end{gathered} \tag{4.7}$$

   The mass window chosen is slightly tighter due to a better mass reconstruction in the bb case: $w_{bb} = 0.2$ and $w_{bbW} = 0.175 m_{H^\pm}$.

In table 2, we present the cross sections after the individual cuts are imposed sequentially. We take a nominal signal cross section of 1000 fb to illustrate the efficiency of the chosen cuts. Since the expected number of events is large, the systematic uncertainty will dominate and a large ratio S/B is desired. Although $S/\sqrt{B}$ does not improve using the mass cut, S/B improves and therefore the systematic uncertainty, which dominates the overall uncertainty, decreases. The dominant background comes from top pair production.

In figure 6, we show the 95% C.L. exclusion and 5σ discovery reach in $\sigma \times \text{BR}(pp \to H^{\pm}tb \to bbbbWW)$ for the 14 TeV LHC. The general feature of these plots follows that of

JHEP12(2014)148

Cut	Signal [fb]	$t\bar{t}$ [fb]	$t\bar{t}bb$ [fb]	S/B	$S/\sqrt{B}$
σ	1000	$6.5 \cdot 10^5$	11310	-	-
Identification [eq. (4.6)]	13.3	903	143	0.012	7.1
m_{bb} vs m_{bbW} [eq. (4.7)]	0.83	28	3.8	0.026	2.5

Table 2. Signal and background cross sections with cuts for the signal benchmark point $m_{H^\pm} = 240\,\text{GeV}$ and $m_A = 70\,\text{GeV}$ at the 14 TeV LHC. We have chosen a nominal value for $\sigma \times BR(pp \to H^\pm tb \to bbbWW)$ of 1000 fb to illustrate the cut efficiencies for the signal process. The last column of $S/\sqrt{B}$ is shown for an integrated luminosity of $\mathcal{L} = 300\ \text{fb}^{-1}$.

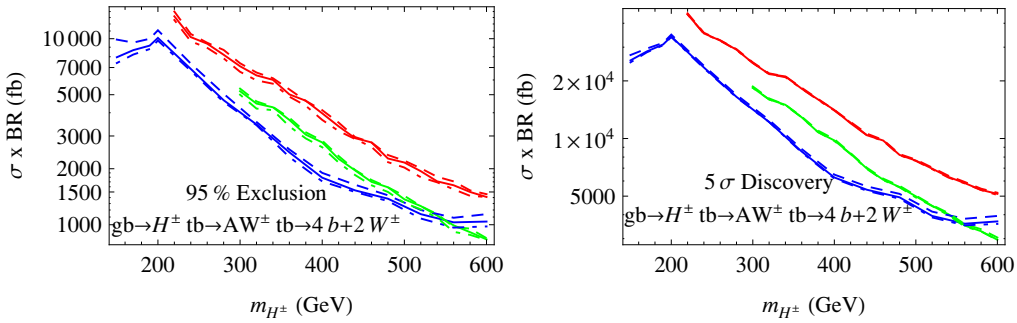

Figure 6. The 95% C.L. exclusion (left) and 5σ discovery (right) limits for $\sigma \times \text{BR}(pp \to H^\pm tb \to bbbWW)$ for $m_A = 70\,\text{GeV}$ (blue), 126 GeV (red), and 200 GeV (green) at the 14 TeV LHC. The dashed, solid and dot-dashed lines correspond to an integrated luminosity of 100, 300 and 1000 fb^{-1} respectively. Here, we have assumed a 10% systematic error on the backgrounds.

figure 5, particularly with highly boosted daughter particles making b identification more challenging, as shown by the flattening of the blue curves for 70 GeV daughter particle mass when $m_{H^\pm} \gtrsim 550\,\text{GeV}$. Unlike the $\tau\tau$ case, different luminosities do not change the limits significantly as the errors on the backgrounds are dominated by systematic uncertainties. Thus, in our analysis, we have chosen a uniform 10% systematic error on the backgrounds. With the possible reduction of systematic errors in the future, the cross section limits can be improved. For example, a 5% systematic error would lead to the cross section limits improved by about a factor of 2. The exclusion limits are lowest for small $m_A = 70\,\text{GeV}$ since the dominating $t\bar{t}$ background peaks around $m_{bb} \approx 70{-}200\,\text{GeV}$ and therefore the background rejection efficiency for $m_{bb} \approx 70\,\text{GeV}$ is high. The improvement of the sensitivity for the $m_A = 70\,\text{GeV}$ case when $m_{H^\pm} < 200\,\text{GeV}$ is due to the suppression of the $t\bar{t}$ background with the m_{bbW} cut.

Compared to the $\tau\tau$ case, the $\sigma \times \text{BR}$ reach in the bb case is worse due to significantly higher SM backgrounds. For the 70 GeV daughter particle case with 300 fb^{-1}, the exclusion limit varies from about 10 pb for a parent mass of 200 GeV to about 1.5 pb for 500 GeV. Thus, given the typical ratio of BR $(A/H \to bb) : \text{Br}(A/H \to \tau\tau) \sim 3m_b^2/m_\tau^2$, we conclude that the reach in the bb case is much worse than that in the $\tau\tau$ case for all masses.

JHEP12(2014)148

5 Implication for the type II 2HDM

The discussion thus far has been completely model independent, and the discovery and exclusion limits displayed in figures 5 and 6 apply to any model in which $H^\pm \to AW^\pm/HW^\pm$ occurs. In this section, we will analyze the feasibility of this channel at the 14 TeV LHC in the context of the Type II 2HDM.

5.1 Cross section and branching fractions

In the Type II 2HDM, one Higgs doublet Φ_1 provides masses for the down-type quarks and charged leptons, while the other Higgs doublet Φ_2 provides masses for the up-type quarks. The couplings of the CP-even Higgses h^0, H^0 and the CP-odd Higgs A to the SM particles can be found in ref. [6].

The discovery of the 126 GeV SM-like Higgs imposes restrictions on the couplings and masses of the various Higgses in the 2HDM, and several studies in the literature mapped out the available parameter space after all the theoretical and experimental constraints are imposed [17, 18, 23, 59–63]. Note that the 2HDM offers two possibilities: either the h^0 or the H^0 could be interpreted as the observed 126 GeV resonance, and accordingly, the available parameter spaces differ. In the h^0-126 case with $m_{12}^2 = 0$, we are restricted to narrow regions with $\sin(\beta-\alpha) \sim \pm 1$ with $\tan\beta$ up to 4 or an extended region in $0.55 < \sin(\beta-\alpha) < 0.9$ with $1.5 < \tan\beta < 4$. The masses $m_{H^0}, m_{H^\pm}$, and m_A are, however, relatively unconstrained. In the H^0-126 case with $m_{12}^2 = 0$, we are restricted to a narrow region of $\sin(\beta-\alpha) \sim 0$ with $\tan\beta$ up to about 8, or an extended region of $\sin(\beta-\alpha)$ between -0.8 to -0.05, with $\tan\beta$ extending to 30 or higher [23]. m_A and $m_{H^\pm}$ are nearly degenerate due to $\Delta\rho$ constraints. Imposing the flavor constraints further narrows down the preferred parameter space. In what follows, we will specify the Higgs masses for each benchmark point considered, but will display our results for all values of $\sin(\beta-\alpha)$ and $\tan\beta$.

Figure 7 shows contours of NLO $\sigma(gg \to H^\pm tb)$ in the $m_{H^\pm} - \tan\beta$ plane at the 14 TeV LHC, with values taken from the LHC Higgs Working Group [64].[8] The production is controlled by the $H^\pm tb$ vertex, which is given in eq. (2.6). This coupling is enhanced for both small and large $\tan\beta$, due to the enhancement of the top and bottom Yukawa coupling, respectively. Correspondingly, the cross section can reach up to 1.5 pb for $m_{H^\pm} \leq 300$ GeV for either $\tan\beta > 40$, or $\tan\beta < 2$. However, we note that the cross section decreases rapidly with increasing mass, falling below 50 fb in most regions of $m_{H^\pm} > 400$ GeV. This makes the charged Higgs search challenging in the high mass regions unless we get a particularly clean signal with minimal backgrounds.

The results of section 4, in principle, could be interpreted within the context of three processes: $H^\pm \to AW^\pm$, $H^\pm \to h^0W^\pm$, and $H^\pm \to H^0W^\pm$. The decay width of the first of these is independent of $\sin(\beta-\alpha)$, while decay to $h^0W^\pm$ or $H^0W^\pm$ is proportional to $\cos(\beta-\alpha)$ or $\sin(\beta-\alpha)$. Therefore, the decay to non-SM-like Higgs is preferable. In this section, we will consider two cases for illustration: i) $H^\pm \to AW^\pm$ for the h^0-126 case with H^0 decoupled and ii) $H^\pm \to h^0W^\pm$ for the h^0-126 and H^0-126 cases with A decoupled.

[8] The NLO cross sections are available only for $m_{H^\pm} \geq 200$ GeV. Thus, for $m_{H^\pm}$ less than this value, we simply using the leading order numbers calculated using FeynHiggs [65–69].

JHEP12(2014)148

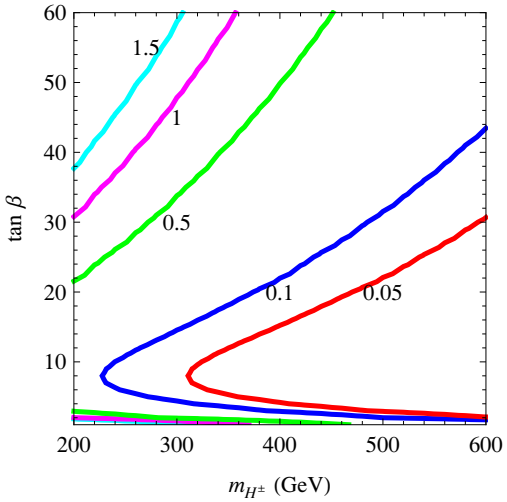

Figure 7. Contours of NLO $\sigma(pp \to H^\pm tb)$ (in pb) in the $m_{H^\pm} - \tan\beta$ plane at the 14 TeV LHC for the Type II 2HDM.

$\{m_{H^\pm}, m_A, m_{h^0}, m_{H^0}\}$ GeV	$H^\pm \to AW^\pm$	$H^\pm \to h^0 W^\pm$	Favored Region
BP1: $\{200, 70, 126, 700\}$	✓	✗	$\sin(\beta-\alpha) \approx \pm 1$
BP2: $\{300, 126, 126, 700\}$	✓	✓	$\sin(\beta-\alpha) \approx \pm 1$
BP3: $\{300, 700, 70, 126\}$	✗	✓	$\sin(\beta-\alpha) \approx 0$
BP4: $\{300, 700, 126, 700\}$	✗	✓	$\sin(\beta-\alpha) \approx \pm 1$

Table 3. Benchmark points shown for illustrating the discovery and exclusion limits for the processes $pp \to H^\pm tb \to AW^\pm/HW^\pm tb \to \tau\tau bbWW$ in the context of Type II 2HDM. The checkmarks indicate kinematically allowed channels. Also shown are the typical favored region of $\sin(\beta-\alpha)$ for each case (see ref. [23]).

We do not consider the decay $H^\pm \to H^0 W^\pm$ as its reach is similar to the $H^\pm \to AW^\pm$ channel in the h^0-126 case while being suppressed in the H^0-126 case. We do not consider the decay $H^\pm \to AW^\pm$ in the H^0-126 case since the reach is always worse that that in the h^0-126 case due to competition from the $H^\pm \to h^0 W^\pm$ mode.

We list the specific benchmark points considered in table 3. BP1 and BP2 are chosen to illustrate the reach for the $H^\pm \to AW^\pm$ decay. A smaller $m_{H^\pm}$ is chosen for BP1 to illustrate the effect of a larger production cross section. BP3 and BP4 are chosen to illustrate the reach for the $H^\pm \to h^0 W^\pm$ decay, with unsuppressed decay in BP3 (H^0-126 case) and suppressed decay in BP4 (h^0-126 case) when preferred value of $\sin(\beta-\alpha)$ is considered. Note that BP1 and BP4 admit only one exotic decay ($AW^\pm$ for the former and $h^0 W^\pm$ for the latter), thus representing the simplest scenario where the reach is maximized in these two modes for the chosen $m_{H^\pm}$ value.

In figure 8, we display the branching fraction of the $H^\pm \to AW^\pm$ and $h^0 W^\pm$ for the various benchmark points listed in table 3 in the $\sin(\beta-\alpha) - \tan\beta$ plane. For BP1

JHEP12(2014)148

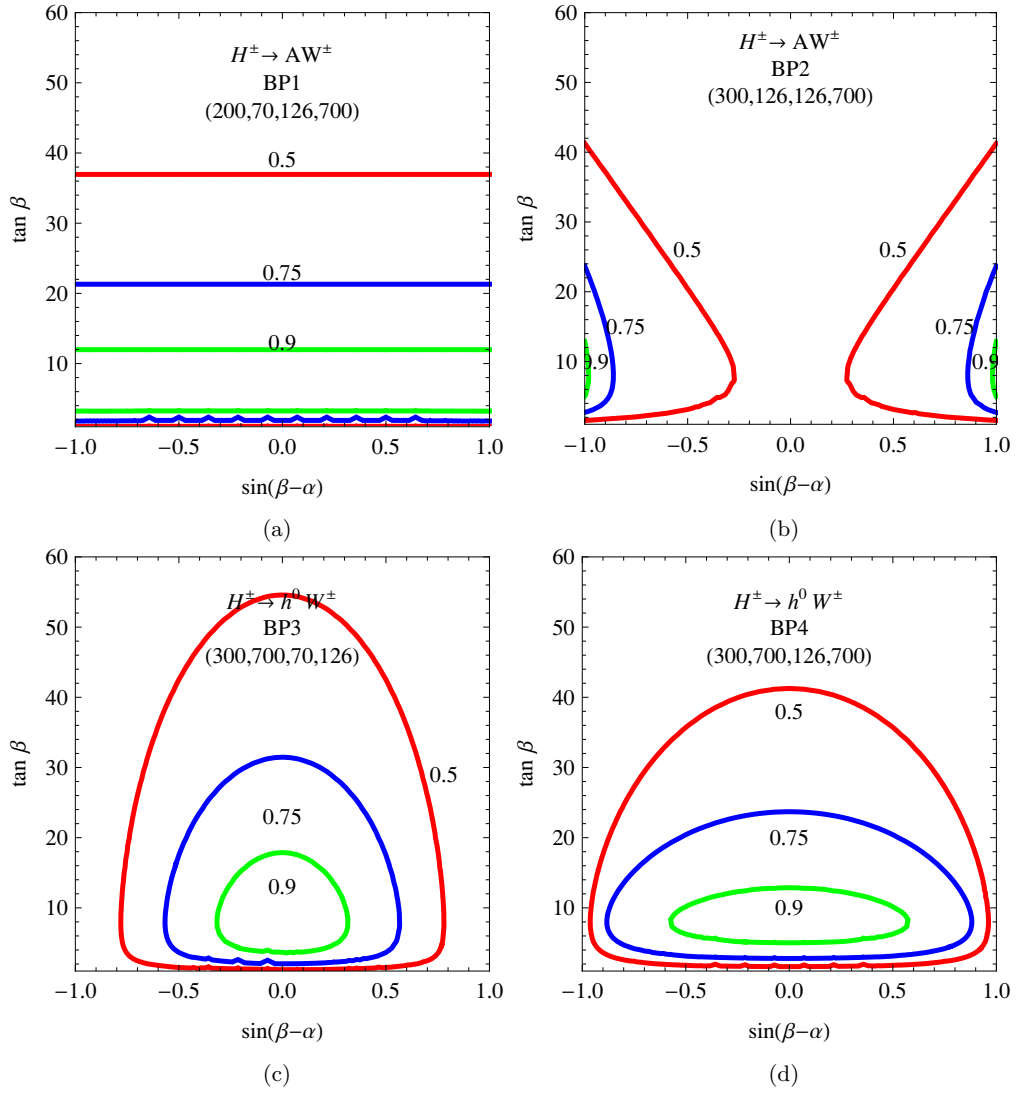

Figure 8. Contours of branching fractions of $H^\pm \to AW^\pm$ [(a) and (b)] and $H^\pm \to h^0 W^\pm$ [(c) and (d)] for each benchmark point.

with $(m_{H^\pm}, m_A, m_{h^0}, m_{H^0})$=(200, 70, 126, 700) GeV in panel (a), BR($H^\pm \to AW^\pm$) is independent of $\sin(\beta-\alpha)$, while decreasing at both large and very small $\tan\beta$, due to the competition of $H^\pm \to tb$ mode. BR($H^\pm \to AW^\pm$) can reach 90% or larger in the range $3 \lesssim \tan\beta \lesssim 12$. Even for $\tan\beta = 37$, BR($H^\pm \to AW^\pm$) can be around 50%.

For BP2 with $(m_{H^\pm}, m_A, m_{h^0}, m_{H^0})$=(300, 126, 126, 700) GeV in panel (b), BR($H^\pm \to AW^\pm$) decreases at small $|\sin(\beta-\alpha)|$ due to the opening of the $H^\pm \to h^0 W^\pm$ channel. BR($H^\pm \to AW^\pm$) is maximized for $\sin(\beta-\alpha) = \pm 1$ and intermediate $\tan\beta$, which is also the preferred region in the h^0-126 case.

For BP3 with $(m_{H^\pm}, m_A, m_{h^0}, m_{H^0})$=(300, 700, 70, 126) GeV in panel (c), maximal branching fraction for $H^\pm \to h^0 W^\pm$ is obtained around $\sin(\beta-\alpha) = 0$ where the cou-

JHEP12(2014)148

pling is maximal. The decreasing of the branching fraction at large and small $\tan\beta$ is caused by the enhanced tb and $\tau\nu$ modes, while the decreasing of the branching fraction at $\sin(\beta-\alpha)\sim\pm1$ is caused by the suppressed $H^\pm\to h^0W^\pm$ decay width as well as the enhanced $H^\pm\to H^0W$ mode.

For BP4 with $(m_{H^\pm}, m_A, m_{h^0}, m_{H^0})$=(300, 700, 126, 700) GeV in panel (d), BR($H^\pm\to h^0W^\pm$) is suppressed at large $\tan\beta$ compared to BP3, since $H^\pm\to h^0W^\pm$ has more phase space suppression. The reduction of BR($H^\pm\to h^0W^\pm$) at larger $|\sin(\beta-\alpha)|$, however, is milder since $H^\pm\to H^0W^\pm$ is kinematically forbidden. In the preferred regions $\sin(\beta-\alpha)\sim\pm1$ and $0.55<\sin(\beta-\alpha)<0.9$ (for $1.5<\tan\beta<4$) in the h^0-126 case, BR($H^\pm\to h^0W^\pm$) is still large enough to allow sensitivity in this channel.

5.2 Reach in parameter spaces

To translate the discovery and exclusion limits on $\sigma\times$BR in the $\tan\beta$ versus $\sin(\beta-\alpha)$ plane, we focus on the model implication for the $\tau\tau$ channel only since the limits for the bb channel are too weak to be realized within the Type II 2HDM.

In figure 9, we display the 95% exclusion (yellow regions enclosed by the solid lines) and 5σ discovery limits (cyan regions enclosed by the dashed lines) for the various benchmark points at the 14 TeV LHC with 300 fb^{-1} integrated luminosity. For BP1 with $H^\pm\to AW^\pm$ [panel (a)] , discovery is possible for small $\tan\beta\lesssim1.5$ independent of $\sin(\beta-\alpha)$, and for large $\tan\beta\geq34$. The exclusion regions are much larger: $\tan\beta\lesssim4$ and $\tan\beta\gtrsim15$. Note that while the branching fraction is relatively suppressed at small and large $\tan\beta$, as shown in figure 8, the $H^\pm$ production cross section is enhanced in those regions, which is more than sufficient to offset the slightly reduced branching fractions. Therefore, we typically find exclusion and discovery regions appear in both the small and large $\tan\beta$ regions, so long as $\sigma\times$ BR values are large enough for exclusion/discovery.

The reach for BP2 [panel (b)] is smaller compared to BP1 because of smaller cross sections associated with a 300 GeV $H^\pm$. The model could still be excluded in quite a large range: $\tan\beta\lesssim3$, and $\tan\beta\gtrsim22$. These values, however, are dependent on $\sin(\beta-\alpha)$. The maximum reach is achieved around $\sin(\beta-\alpha)=\pm1$ where BR($H^\pm\to AW^\pm$) is maximized. 5σ discovery, however, is not possible for this benchmark point except for very high $\tan\beta\geq55$, and $\sin(\beta-\alpha)\approx\pm1$.

For BP3 in panel (c), the reach is best for $\sin(\beta-\alpha)=0$: $\tan\beta\gtrsim20$ or $\lesssim3$ for 95% C.L. exclusion and $\tan\beta\gtrsim46$ or $\lesssim1$ for 5σ discovery. The reach gets significantly weaker when $\sin(\beta-\alpha)$ approaches ±1 with the regions $|\sin(\beta-\alpha)|>0.9$ providing no reach. Note that for BP3 with $m_{H^0}=126$ GeV, $\sin(\beta-\alpha)\approx0$ is also the favored region given the SM-like Higgs consideration.

BP4 is an interesting case as this corresponds to the charged Higgs decaying to a SM-like Higgs h^0. The exclusion reach is almost the same as in BP3, while the discovery reach is relatively weaker due to the suppression of the branching fractions at large or small $\tan\beta$, as shown in figure 8 (d). There are small regions of parameter space around $\sin(\beta-\alpha)=0$ and $\tan\beta\gtrsim55$ or $\tan\beta\leq1$ that permit discovery. These exclusion or discovery regions do not lie in the preferred region $\sin(\beta-\alpha)\approx\pm1$ for the h^0-126 case. Note, however

JHEP12(2014)148

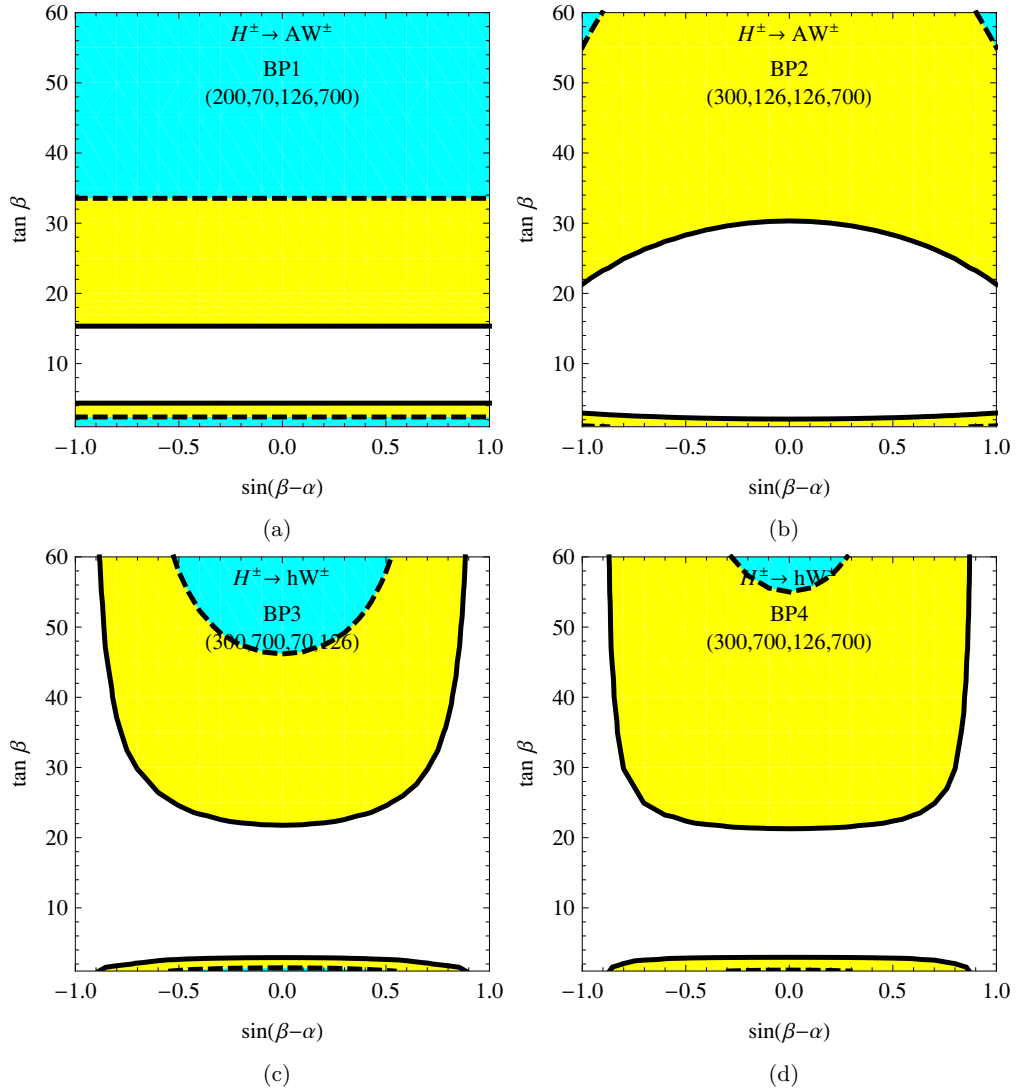

Figure 9. The 95% exclusion (yellow regions enclosed by the solid lines) and the 5σ discovery reach (cyan regions enclosed by the dashed lines) for $pp \to H^\pm tb \to AW^\pm tb/HW^\pm tb \to \tau\tau bbWW$ in the $\tan\beta$ versus $\sin(\beta-\alpha)$ plane for each benchmark point, with an integrated luminosity of $300\,\text{fb}^{-1}$ at the 14 TeV LHC.

that the exclusion region for $H^\pm \to h^0 W^\pm$ is indeed sensitive to part of the region that is consistent with the observed Higgs signal: $0.55 < \sin(\beta-\alpha) < 0.9$ with small $\tan\beta$ [23].

Figure 10 shows the reach in the $m_{H^\pm} - \tan\beta$ for $H^\pm \to AW^\pm$, with $m_A = 70\,\text{GeV}$ (left panel) and 126 GeV (right panel). We have fixed $\sin(\beta-\alpha) = 1$ and decoupled H^0 such that both $H^\pm \to h^0 W^\pm, H^0 W^\pm$ are absent. Superimposed on the plot in black dashed line is the projected ATLAS $H^\pm \to \tau\nu$ discovery reach with $100\,\text{fb}^{-1}$ luminosity [31] for comparison. The $m_A = 70\,\text{GeV}$ represents the best case scenario for discovery/exclusion. While the reach in the exotic channel $H^\pm \to AW^\pm$ is smaller compared to the standard

JHEP12(2014)148

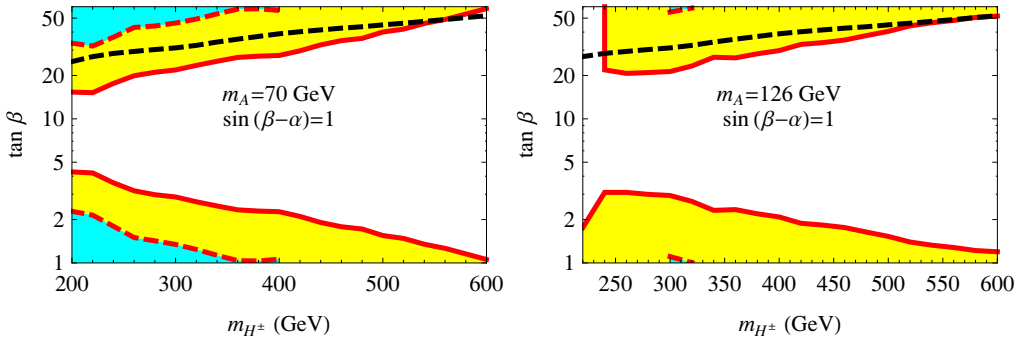

Figure 10. 95% exclusion (yellow regions bounded by solid red lines) and the 5σ discovery (cyan regions bounded by the dashed red lines) in the $m_{H^\pm} - \tan\beta$ parameter space for 300 fb^{-1} luminosity in the $pp \to H^\pm tb \to AW^\pm tb \to \tau\tau bbWW$ channel, with $m_A = 70$ GeV (left panel) and 126 GeV (right panel). Superimposed in black dashed line is the projected ATLAS $H^\pm \to \tau\nu$ 5σ discovery contours with 100 fb^{-1} luminosity. $\sin(\beta - \alpha)$ is chosen to be 1 and H^0 is decoupled.

$H^\pm \to \tau\nu$ searches in the high $\tan\beta$ region, $AW^\pm$ channel provides a reach in the small $\tan\beta$ regions which is absent in the $\tau\nu$ mode. Additionally, the model can be excluded at the 95% C.L. for masses extending all the way to 600 GeV for both small and large $\tan\beta$ in this channel. The $m_A = 126$ case has limited sensitivity for discovery (constrained to only small regions 300 GeV $< m_{H^\pm} <$ 320 GeV), but does provide an exclusion range that is comparable to the $m_A = 70$ GeV case.

We conclude this section with the following observations:

- The best case scenario are the decays $H^\pm \to AW^\pm$ for the $h^0{-}126$ case and $H^\pm \to h^0W^\pm$ in the $H^0{-}126$ case for small daughter Higgs masses.
- The potentially interesting scenario $H^\pm \to h^0W^\pm$ with h^0 being SM-like has sensitivity for 95% C.L. exclusion at small and large $\tan\beta$ for $\sin(\beta - \alpha)$ different from ± 1. The sensitivity for discovery, however, is constrained mostly to high $\tan\beta$ regions.
- There is sizeable reach in both small and large $\tan\beta$ for exclusion for $m_A = 70$ GeV and $\sin(\beta - \alpha) = 1$, while discovery is also possible for small $\tan\beta$ as seen in figure 10. Specifically, discovery of the charged Higgs is possible for $m_{H^\pm}$ up to 400 GeV in both the small and large $\tan\beta$ regions.
- The reach in this exotic channel $H^\pm \to AW^\pm/HW^\pm$ is complementary to the conventional search channel $H^\pm \to \tau\nu$, in particular, for small $\tan\beta$.

6 Conclusion

The discovery of the Higgs at 126 GeV has not only confirmed the predictions of the SM, but has also ushered in a new era of discovery of beyond the SM physics. Many such scenarios incorporate an extended Higgs sector, which predict the existence of extra Higgs bosons other than the SM-like one. Most of the current searches for those extra Higgs

JHEP12(2014)148

bosons focus on the conventional channels of bb, $\tau\tau$, $\gamma\gamma$, WW and ZZ for the neutral ones, and $\tau\nu$, cs for the charged ones. However, there have been efforts recently to study the exotic decay of these Higgs bosons to enhance their collider reaches [41–43, 70–75].

Charged Higgses, compared to their neutral counterparts, are harder to discover. This is mostly due to the relatively small associated production cross section of $H^\pm tb$ (compared to the gluon fusion process for the neutral ones), as well as the large SM backgrounds for the dominant decay mode $H^\pm \to tb$. The conventional search channel $H^\pm \to \tau\nu$ suffers from relatively small decay branching fraction and thus, it behooves us to consider other possible decays of the $H^\pm$ to enhance its reach at colliders. In this paper, we analyzed the feasibility of discovering a charged Higgs boson in the process $H^\pm \to AW^\pm/HW^\pm$, with the daughter Higgs decaying to either $\tau\tau$ or bb.

We obtained model independent limits on $\sigma \times \mathrm{BR}(pp \to H^\pm tb \to AW^\pm tb/HW^\pm tb \to \tau\tau bbWW, bbbbWW)$ at the 14 TeV LHC. For the $\tau\tau$ channel, we considered all three cases: $\tau_{had}\tau_{had}$, $\tau_{lep}\tau_{had}$, and $\tau_{lep}\tau_{lep}$. It turns out that $\tau_{lep}\tau_{had}$ affords the best possible reach as we can take advantage of the same sign dilepton signal. Combining all three channels, we find for a daughter particle mass of 70 GeV, that the 95% C.L. exclusion reach ranges from about 60 fb to 25 fb, when $m_{H^\pm}$ is varied in the range 150 GeV−500 GeV with 300 fb^{-1} integrated luminosity at the 14 TeV LHC. The 5σ reach is about a factor of 3−4 higher. This channel is statistically limited and the reach enhances with increased luminosity. The reach in the bb channel is significantly worse.

We studied the implication of the $\sigma \times$ BR reach in the Type II 2HDM, focusing on $H^\pm \to AW^\pm$ and $H^\pm \to h^0 W^\pm$ decays. We find that in this model, the $pp \to H^\pm tb \to bbbbWW$ cross section is too low for $H^\pm$ to be either discovered or excluded. However, for the $\tau\tau$ mode, large regions of parameter space in $\tan\beta$ versus $\sin(\beta-\alpha)$ can be covered when the daughter Higgs mass is relatively light, in particular, for small and large $\tan\beta$. The exclusion region in the $m_{H^\pm} - \tan\beta$ plane can be extended to $m_{H^\pm} = 600$ GeV, while discovery is possible for $m_{H^\pm} \lesssim 400$ GeV. While the model can be excluded for a wide range of $\tan\beta$ values, discovery regions are mostly restricted to either small ($\lesssim 2$) or large ($\gtrsim 34$) values. Since the conventional search channel $H^\pm \to \tau\nu$ is only sensitive to the large $\tan\beta$ region, the exotic decay mode $H^\pm \to AW^\pm/HW^\pm$ offers a complementary channel for charged Higgs searches.

Given the difficulties of the charged Higgs detection at hadron colliders, other search channels, for example, $qq' \to H^\pm$, electroweak pair production of H^+H^-, H^+W^-, as well as charged Higgs produced in the decay of a heavy Higgs [35, 40–43, 75, 76] should be studied to fully explore the discovery potential of the charged Higgses at the LHC. A future lepton machine with high center of mass energy would certainly be useful for charged Higgs discovery.

Acknowledgments

We thank Peter Loch, John Paul Chou, John Stupak and Martin Flechl for helpful discussions. We also wishes to acknowledge the hospitality of the Aspen Center for Physics

JHEP12(2014)148

where part of the work was finished. This work was supported by the Department of Energy under Grant DE-FG02-13ER41976.

References

[1] ATLAS collaboration, *Observation of a new particle in the search for the standard model Higgs boson with the ATLAS detector at the LHC*, *Phys. Lett.* **B 716** (2012) 1 [arXiv:1207.7214] [INSPIRE].

[2] ATLAS collaboration, *Combined coupling measurements of the Higgs-like boson with the ATLAS detector using up to* $25\,\text{fb}^{-1}$ *of proton-proton collision data*, ATLAS-CONF-2013-034, CERN, Geneva Switzerland (2013).

[3] CMS collaboration, *Observation of a new boson at a mass of* 125 *GeV with the CMS experiment at the LHC*, *Phys. Lett.* **B 716** (2012) 30 [arXiv:1207.7235] [INSPIRE].

[4] CMS collaboration, *Combination of standard model Higgs boson searches and measurements of the properties of the new boson with a mass near* 125 *GeV*, CMS-PAS-HIG-13-005, CERN, Geneva Switzerland (2013).

[5] ATLAS collaboration, *Evidence for the spin-*0 *nature of the Higgs boson using ATLAS data*, *Phys. Lett.* **B 726** (2013) 120 [arXiv:1307.1432] [INSPIRE].

[6] G.C. Branco et al., *Theory and phenomenology of two-Higgs-doublet models*, *Phys. Rept.* **516** (2012) 1 [arXiv:1106.0034] [INSPIRE].

[7] H.E. Haber, G.L. Kane and T. Sterling, *The fermion mass scale and possible effects of Higgs bosons on experimental observables*, *Nucl. Phys.* **B 161** (1979) 493 [INSPIRE].

[8] L.J. Hall and M.B. Wise, *Flavor changing Higgs-boson couplings*, *Nucl. Phys.* **B 187** (1981) 397 [INSPIRE].

[9] J.F. Donoghue and L.F. Li, *Properties of charged Higgs bosons*, *Phys. Rev.* **D 19** (1979) 945 [INSPIRE].

[10] H.P. Nilles, *Supersymmetry, supergravity and particle physics*, *Phys. Rept.* **110** (1984) 1 [INSPIRE].

[11] H.E. Haber and G.L. Kane, *The search for supersymmetry: probing physics beyond the standard model*, *Phys. Rept.* **117** (1985) 75 [INSPIRE].

[12] R. Barbieri, *Looking beyond the standard model: the supersymmetric option*, *Riv. Nuovo Cim.* **11N4** (1988) 1 [INSPIRE].

[13] J.R. Ellis, J.F. Gunion, H.E. Haber, L. Roszkowski and F. Zwirner, *Higgs bosons in a nonminimal supersymmetric model*, *Phys. Rev.* **D 39** (1989) 844 [INSPIRE].

[14] M. Drees, *Supersymmetric models with extended Higgs sector*, *Int. J. Mod. Phys.* **A 4** (1989) 3635 [INSPIRE].

[15] N.D. Christensen, T. Han, Z. Liu and S. Su, *Low-mass Higgs bosons in the NMSSM and their LHC implications*, *JHEP* **08** (2013) 019 [arXiv:1303.2113] [INSPIRE].

JHEP12(2014)148

[16] M. Drees, M. Guchait and D.P. Roy, *Signature of charged to neutral Higgs boson decay at the LHC in SUSY models*, *Phys. Lett.* **B 471** (1999) 39 [hep-ph/9909266] [INSPIRE].

[17] B. Grinstein and P. Uttayarat, *Carving out parameter space in type-II two Higgs doublets model*, *JHEP* **06** (2013) 094 [*Erratum ibid.* **09** (2013) 110] [arXiv:1304.0028] [INSPIRE].

[18] C.-W. Chiang and K. Yagyu, *Implications of Higgs boson search data on the two-Higgs doublet models with a softly broken Z_2 symmetry*, *JHEP* **07** (2013) 160 [arXiv:1303.0168] [INSPIRE].

[19] B. Mohn, N. Gollub and K.A. Assamagan, *The ATLAS discovery potential for a heavy charged Higgs boson in a large mass splitting MSSM scenario*, ATL-PHYS-PUB-2005-017, CERN, Geneva Switzerland (2005).

[20] K.A. Assamagan, *Signature of the charged Higgs decay $H^{\pm} \to W h_0$ with the ATLAS detector*, *Acta Phys. Polon.* **B 31** (2000) 881 [INSPIRE].

[21] K.A. Assamagan, Y. Coadou and A. Deandrea, *ATLAS discovery potential for a heavy charged Higgs boson*, *Eur. Phys. J. direct* **C 4** (2002) 9 [hep-ph/0203121] [INSPIRE].

[22] Particle Data Group collaboration, J. Beringer et al., *Review of particle physics (RPP)*, *Phys. Rev.* **D 86** (2012) 010001 [INSPIRE] and 2013 partial update for the 2014 edition.

[23] B. Coleppa, F. Kling and S. Su, *Constraining type II 2HDM in light of LHC Higgs searches*, *JHEP* **01** (2014) 161 [arXiv:1305.0002] [INSPIRE].

[24] F. Mahmoudi and O. Stal, *Flavor constraints on the two-Higgs-doublet model with general Yukawa couplings*, *Phys. Rev.* **D 81** (2010) 035016 [arXiv:0907.1791] [INSPIRE].

[25] J.F. Gunion, H.E. Haber, G.L. Kane and S. Dawson, *The Higgs hunter's guide*, *Front. Phys.* **80** (2000) 1 [INSPIRE].

[26] LHC Higgs Cross section Working Group collaboration, S. Heinemeyer et al., *Handbook of LHC Higgs cross sections: 3. Higgs properties*, arXiv:1307.1347 [INSPIRE].

[27] A.G. Akeroyd and S. Baek, *Large mass splittings between charged and neutral Higgs bosons in the MSSM*, *Phys. Lett.* **B 525** (2002) 315 [hep-ph/0105228] [INSPIRE].

[28] ATLAS collaboration, *Search for charged Higgs bosons in the τ+jets final state with pp collision data recorded at $\sqrt{s} = 8$ TeV with the ATLAS experiment*, ATLAS-CONF-2013-090, CERN, Geneva Switzerland (2013).

[29] CMS collaboration, *Search for charged Higgs bosons with the $H^+ \to \tau\nu$ decay channel in the fully hadronic final state at $\sqrt{s} = 8$ TeV*, CMS-PAS-HIG-14-020, CERN, Geneva Switzerland (2014).

[30] ATLAS collaboration, *Search for a light charged Higgs boson in the decay channel $H^+ \to c\bar{s}$ in $t\bar{t}$ events using pp collisions at $\sqrt{s} = 7$ TeV with the ATLAS detector*, *Eur. Phys. J.* **C 73** (2013) 2465 [arXiv:1302.3694] [INSPIRE].

[31] B. Mohn, M. Flechl and J. Alwall, *ATLAS discovery potential for the charged Higgs boson in $H^+ \to \tau\nu$ decays*, ATL-PHYS-PUB-2007-006, CERN, Geneva Switzerland (2007).

[32] R. Guedes, S. Moretti and R. Santos, *Charged Higgs bosons in single top production at the LHC*, *JHEP* **10** (2012) 119 [arXiv:1207.4071] [INSPIRE].

[33] M. Hashemi, *Single top events as a source of light charged Higgs in the fully hadronic final state at LHC*, *JHEP* **05** (2013) 112 [arXiv:1305.2096] [INSPIRE].

JHEP12(2014)148

[34] M. Hashemi, *Observability of light charged Higgs decay to muon in top quark pair events at LHC*, *Eur. Phys. J.* **C 72** (2012) 1994 [arXiv:1109.5356] [INSPIRE].

[35] M. Hashemi, *Observability of heavy charged Higgs through s-channel single top events at LHC*, *JHEP* **11** (2013) 005 [arXiv:1310.5209] [INSPIRE].

[36] Q.-H. Cao, X. Wan, X.-P. Wang and S.-H. Zhu, *Searching for charged Higgs boson in polarized top quark*, *Phys. Rev.* **D 87** (2013) 055022 [arXiv:1301.6608] [INSPIRE].

[37] S. Yang and Q.-S. Yan, *Searching for heavy charged Higgs boson with jet substructure at the LHC*, *JHEP* **02** (2012) 074 [arXiv:1111.4530] [INSPIRE].

[38] K.A. Assamagan and N. Gollub, *The ATLAS discovery potential for a heavy charged Higgs boson in $gg \to tbH^{\pm}$ with $H^{\pm} \to tb$*, *Eur. Phys. J.* **C 39S2** (2005) 25 [hep-ph/0406013] [INSPIRE].

[39] P.S.B. Dev and A. Pilaftsis, *Maximally symmetric two Higgs doublet model with natural standard model alignment*, *JHEP* **12** (2014) 024 [arXiv:1408.3405] [INSPIRE].

[40] S.-S. Bao, X. Gong, H.-L. Li, S.-Y. Li and Z.-G. Si, *Identify charged Higgs boson in $W^{\pm}H^{\mp}$ associated production at LHC*, *Phys. Rev.* **D 85** (2012) 075005 [arXiv:1112.0086] [INSPIRE].

[41] U. Maitra, B. Mukhopadhyaya, S. Nandi, S.K. Rai and A. Shivaji, *Searching for an elusive charged Higgs at the Large Hadron Collider*, *Phys. Rev.* **D 89** (2014) 055024 [arXiv:1401.1775] [INSPIRE].

[42] L. Basso et al., *Probing the charged Higgs boson at the LHC in the CP-violating type-II 2HDM*, *JHEP* **11** (2012) 011 [arXiv:1205.6569] [INSPIRE].

[43] R. Dermisek, J.P. Hall, E. Lunghi and S. Shin, *A new avenue to charged Higgs discovery in multi-Higgs models*, *JHEP* **04** (2014) 140 [arXiv:1311.7208] [INSPIRE].

[44] CMS collaboration, *Searches for electroweak production of charginos, neutralinos and sleptons decaying to leptons and W, Z and Higgs bosons in pp collisions at 8 TeV*, *Eur. Phys. J.* **C 74** (2014) 3036 [arXiv:1405.7570] [INSPIRE].

[45] CMS collaboration, *Search for neutral MSSM Higgs bosons decaying to a pair of τ leptons in pp collisions*, *JHEP* **10** (2014) 160 [arXiv:1408.3316] [INSPIRE].

[46] ATLAS collaboration, *Search for neutral Higgs bosons of the minimal supersymmetric standard model in pp collisions at $\sqrt{s} = 8$ TeV with the ATLAS detector*, *JHEP* **11** (2014) 056 [arXiv:1409.6064] [INSPIRE].

[47] *LEP Higgs Working Group webpage*, http://lephiggs.web.cern.ch/LEPHIGGS/www/Welcome.html.

[48] S. Dittmaier, M. Krämer, M. Spira and M. Walser, *Charged-Higgs-boson production at the LHC: NLO supersymmetric QCD corrections*, *Phys. Rev.* **D 83** (2011) 055005 [arXiv:0906.2648] [INSPIRE].

[49] B. Coleppa, F. Kling, A. Pyarelal and S. Su, *LHC reach for a light charged Higgs*, to appear.

[50] J. Alwall, M. Herquet, F. Maltoni, O. Mattelaer and T. Stelzer, *MadGraph 5: going beyond*, *JHEP* **06** (2011) 128 [arXiv:1106.0522] [INSPIRE].

[51] J. Alwall et al., *The automated computation of tree-level and next-to-leading order differential cross sections and their matching to parton shower simulations*, *JHEP* **07** (2014) 079 [arXiv:1405.0301] [INSPIRE].

JHEP12(2014)148

[52] T. Sjöstrand, S. Mrenna and P.Z. Skands, *PYTHIA* 6.4 *physics and manual*, *JHEP* **05** (2006) 026 [hep-ph/0603175] [INSPIRE].

[53] S. Ovyn, X. Rouby and V. Lemaitre, *DELPHES, a framework for fast simulation of a generic collider experiment*, arXiv:0903.2225 [INSPIRE].

[54] J. Anderson et al., *Snowmass energy frontier simulations*, arXiv:1309.1057 [INSPIRE].

[55] L. Moneta et al., *The RooStats project*, PoS(ACAT2010)057 [arXiv:1009.1003] [INSPIRE].

[56] RooStats Team collaboration, G. Schott, *RooStats for searches*, arXiv:1203.1547 [INSPIRE].

[57] *Theta-auto testing documentation webpage*, http://www-ekp.physik.uni-karlsruhe.de/~ott/theta/theta-auto/.

[58] ATLAS collaboration, *Measurement of the t-channel single top-quark production cross section in pp collisions at* $\sqrt{s} = 7$ *TeV with the ATLAS detector*, *Phys. Lett.* **B 717** (2012) 330 [arXiv:1205.3130] [INSPIRE].

[59] N. Craig and S. Thomas, *Exclusive signals of an extended Higgs sector*, *JHEP* **11** (2012) 083 [arXiv:1207.4835] [INSPIRE].

[60] H.S. Cheon and S.K. Kang, *Constraining parameter space in type-II two-Higgs doublet model in light of a* 126 *GeV Higgs boson*, *JHEP* **09** (2013) 085 [arXiv:1207.1083] [INSPIRE].

[61] A. Drozd, B. Grzadkowski, J.F. Gunion and Y. Jiang, *Two-Higgs-doublet models and enhanced rates for a* 125 *GeV Higgs*, *JHEP* **05** (2013) 072 [arXiv:1211.3580] [INSPIRE].

[62] S. Chang et al., *Comprehensive study of two Higgs doublet model in light of the new boson with mass around* 125 *GeV*, *JHEP* **05** (2013) 075 [arXiv:1210.3439] [INSPIRE].

[63] C.-Y. Chen and S. Dawson, *Exploring two Higgs doublet models through Higgs production*, *Phys. Rev.* **D 87** (2013) 055016 [arXiv:1301.0309] [INSPIRE].

[64] M. Flechl, M. Kramer, S. Lehti and S. Heinemeyer, *MSSM Charged Higgs webpage*, https://twiki.cern.ch/twiki/bin/view/LHCPhysics/LHCHXSWGMSSMCharged.

[65] T. Hahn, S. Heinemeyer, W. Hollik, H. Rzehak and G. Weiglein, *High-precision predictions for the light CP-even Higgs boson mass of the minimal supersymmetric standard model*, *Phys. Rev. Lett.* **112** (2014) 141801 [arXiv:1312.4937] [INSPIRE].

[66] M. Frank et al., *The Higgs boson masses and mixings of the complex MSSM in the Feynman-diagrammatic approach*, *JHEP* **02** (2007) 047 [hep-ph/0611326] [INSPIRE].

[67] G. Degrassi, S. Heinemeyer, W. Hollik, P. Slavich and G. Weiglein, *Towards high precision predictions for the MSSM Higgs sector*, *Eur. Phys. J.* **C 28** (2003) 133 [hep-ph/0212020] [INSPIRE].

[68] S. Heinemeyer, W. Hollik and G. Weiglein, *The masses of the neutral CP-even Higgs bosons in the MSSM: accurate analysis at the two loop level*, *Eur. Phys. J.* **C 9** (1999) 343 [hep-ph/9812472] [INSPIRE].

[69] S. Heinemeyer, W. Hollik and G. Weiglein, *FeynHiggs: a program for the calculation of the masses of the neutral CP-even Higgs bosons in the MSSM*, *Comput. Phys. Commun.* **124** (2000) 76 [hep-ph/9812320] [INSPIRE].

[70] B. Coleppa, F. Kling and S. Su, *Exotic decays of a heavy neutral Higgs through* HZ/AZ *channel*, *JHEP* **09** (2014) 161 [arXiv:1404.1922] [INSPIRE].

JHEP12(2014)148

[71] Heavy Flavor Averaging Group collaboration, Y. Amhis et al., *Averages of b-hadron, c-hadron and τ-lepton properties as of early* 2012, arXiv:1207.1158 [INSPIRE].

[72] *Heavy Flavor Averaging Group (HFAG) online updates webpage*, http://www.slac.stanford.edu/xorg/hfag.

[73] E. Brownson et al., *Heavy Higgs scalars at future hadron colliders (a Snowmass whitepaper)*, arXiv:1308.6334 [INSPIRE].

[74] D. Curtin et al., *Exotic decays of the* 125 *GeV Higgs boson*, *Phys. Rev.* **D 90** (2014) 075004 [arXiv:1312.4992] [INSPIRE].

[75] L. Tong and S. Su, *Exotic Higgs decay via charged Higgs*, in preparation.

[76] N.D. Christensen, T. Han and T. Li, *Pair production of MSSM Higgs bosons in the non-decoupling region at the LHC*, *Phys. Rev.* **D 86** (2012) 074003 [arXiv:1206.5816] [INSPIRE].

JHEP12(2014)148

Appendix E

Light Charged Higgs Bosons to AW/HW via Top Decay

The article *Light Charged Higgs Bosons to AW/HW via Top Decay* has been submitted to arXiv and accepted for publication in the Journal of High Energy Physics [25].

Published for SISSA by Springer

Received: *May 13, 2015*
Revised: *September 1, 2015*
Accepted: *September 30, 2015*
Published: *November 9, 2015*

Light charged Higgs bosons to AW/HW via top decay

Felix Kling, Adarsh Pyarelal and Shufang Su

Department of Physics, University of Arizona, Tucson, AZ 85721, U.S.A.

E-mail: kling@email.arizona.edu, adarsh@email.arizona.edu, shufang@email.arizona.edu

Abstract: While current ATLAS and CMS measurements exclude a light charged Higgs ($m_{H^\pm} < 160\,\text{GeV}$) for most of the parameter region in the context of the MSSM scenarios, these bounds are significantly weakened in the Type II 2HDM once the exotic decay channel into a lighter neutral Higgs, $H^\pm \to AW/HW$, is open. In this study, we examine the possibility of a light charged Higgs produced in top decay via single top or top pair production, which is the most prominent production channel for a light charged Higgs at the LHC. We consider the subsequent decay $H^\pm \to AW/HW$, which can reach a sizable branching fraction at low $\tan\beta$ once it is kinematically permitted. With a detailed collider analysis, we obtain exclusion and discovery bounds for the 14 TeV LHC assuming the existence of a 70 GeV neutral scalar. Assuming $\text{BR}(H^\pm \to AW/HW) = 100\%$ and $\text{BR}(A/H \to \tau\tau) = 8.6\%$, the 95% exclusion limits on $\text{BR}(t \to H^+ b)$ are about 0.2% and 0.03% for single top and top pair production respectively, with an integrated luminosity of 300 fb^{-1}. The discovery reaches are about 3 times higher. In the context of the Type II 2HDM, discovery is possible at both large $\tan\beta > 17$ for $155\,\text{GeV} < m_{H^\pm} < 165\,\text{GeV}$, and small $\tan\beta < 6$ over the entire mass range. Exclusion is possible in the entire $\tan\beta$ versus $m_{H^\pm}$ plane except for charged Higgs masses close to the top threshold. The exotic decay channel $H^\pm \to AW/HW$ is therefore complementary to the conventional $H^\pm \to \tau\nu$ channel.

Keywords: Supersymmetry Phenomenology, Hadronic Colliders

ArXiv ePrint: 1504.06624

doi:10.1007/JHEP11(2015)051

JHEP11(2015)051

Contents

JHEP11(2015)051

1 Introduction

In July 2012, both the ATLAS and the CMS collaborations announced the discovery of a new resonance with a mass of 126 GeV, which is consistent with the predictions of the Standard Model (SM) Higgs boson [1, 2]. The data obtained in the following years allowed measurements of its mass and couplings and a determination of its CP properties and spin [3–5]. Nevertheless, there are many reasons, both from theoretical considerations and experimental observations, to expect physics beyond the SM, such as the hierarchy problem, neutrino masses and dark matter. There have been numerous attempts to build new physics models which can explain these puzzles. Some well known examples are the Minimal Supersymmetric Standard Model (MSSM) [6–8], the Next to Minimal Supersymmetric Standard Model (NMSSM) [9, 10] and the Two Higgs Doublet Models (2HDM) [11–14].

Many of these new physics models involve an extended Higgs sector with an interesting phenomenology that might be testable at the LHC. In addition to the SM-like Higgs boson in these models, the low energy spectrum includes other CP-even Higgses[1] H, CP-odd Higgses A, and a pair of charged Higgses $H^{\pm}$. The discovery of one or more of these new particles would be a clear indication of an extended Higgs sector as the source of electroweak symmetry breaking (EWSB). A number of searches have been performed at the LEP, Tevatron and the LHC, mainly focusing on decays of Higgses into SM particles [15–22]. However, exotic decay channels, in which a heavy Higgs decays into either two lighter Higgses, or a Higgs plus an SM gauge boson, open up and can even dominate if kinematically allowed, reducing the reach of the conventional search channels. Some of these channels have already been studied both in a theoretical [23–31] and experimental [32–34]

[1]Note that we use h^0 and H^0 to refer to the lighter or the heavier CP-even Higgs for models with two CP-even Higgs bosons. When there is no need to specify, we use H to refer to the CP-even Higgses.

setting. Soon, more of those exotic Higgs decay channels will be accessible at the LHC. It is therefore timely to study the LHC reach of those channels more carefully.

In the current study we examine the detectability of a light charged Higgs boson, with $m_{H^\pm} < m_t$. The dominant production mode for such a light charged Higgs at the LHC is via top decay, given the large top production rate at the LHC. BR($t \to H^\pm b$) can be enhanced at both large and small $\tan\beta$, due to the enhanced top and bottom Yukawa couplings. Current search strategies assume that the charged Higgs decays either leptonically ($H^\pm \to \tau\nu$) or hadronically ($H^\pm \to cs$). The null search results at both the ATLAS and CMS exclude a light charged Higgs below a mass of about 160 GeV for most of the parameter space [16, 17]. However, if there exists a neutral Higgs (A/H) light enough such that the $H^\pm \to AW^\pm/HW^\pm$ channel is kinematically open, the branching fractions into the conventional final states $\tau\nu$ and cs are suppressed and the exclusion bounds can be significantly weakened. Due to experimental challenges at low energies, such a light neutral Higgs has not been fully excluded yet. A relatively large region of $m_{H^\pm} > 150\,\text{GeV}$ and $\tan\beta \lesssim 20$ is still allowed, while no limits exist for $m_{H^\pm} > 160\,\text{GeV}$.

The exotic decay channel of $H^\pm \to AW/HW$, on the other hand, offers an additional opportunity for the detection of a light charged Higgs, closing the loophole of the current light charged Higgs searches. While there are strong constraints on the mass of the light charged Higgs from flavor [35–37] and precision [38–42] observables, those limits are typically model dependent and could be relaxed when there are contributions from the other sectors of the model [43]. A direct search for a light charged Higgs, on the other hand, provides a model-independent and complementary reach. It is thus timely and worthwhile to fully explore the discovery or exclusion potential of the light charged Higgs at the LHC.

In this paper we study the exotic decay of a charged Higgs $H^\pm \to AW/HW$ with A/H decaying into $\tau\tau$. We focus on the light charged Higgs produced via top decay, considering both the single top and top pair production channels. The exclusion bounds and discovery reach will be explored and interpreted in the context of the Type II 2HDM. A collider analysis considering the same decay channel of a heavy charged Higgs produced in $H^\pm tb$ associate production has been performed in [26].

We will proceed as follows. In section 2, we briefly introduce the Type II 2HDM and present scenarios that permit a large branching fraction for the process $H^\pm \to AW/HW$. In section 3, we summarize the current experimental constraints on a light charged Higgs. In section 4, we present the details of our collider analysis. We investigate the single top and top pair production channels in section 4.1 and 4.2, respectively, and present the model independent 95% C.L. exclusion and 5σ discovery limits for both processes at the 14 TeV LHC with various luminosities in section 4.3. In section 5, we discuss the implications of our analysis for the Type II 2HDM and translate our results into reaches in parameter space. We conclude in section 6.

2 Theoretical motivation

In the 2HDM, we introduce two $\text{SU}(2)_L$ doublets Φ_i, $i = 1, 2$:

$$\Phi_i = \begin{pmatrix} \phi_i^+ \\ (v_i + \phi_i^0 + iG_i)/\sqrt{2} \end{pmatrix}, \tag{2.1}$$

where v_1 and v_2 are the vacuum expectation values of the neutral components which satisfy the relation $\sqrt{v_1^2 + v_2^2} = 246\,\text{GeV}$ after EWSB. Assuming an additional discrete $\mathcal{Z}_2$ symmetry imposed on the Lagrangian, we are left with six free parameters, which can be chosen as four Higgs masses (m_{h^0}, m_{H^0}, m_A, $m_{H^\pm}$), a mixing angle α between the two CP-even Higgses, and the ratio of the two vacuum expectation values ($\tan\beta = v_2/v_1$). In the case where a soft breaking of the $\mathcal{Z}_2$ symmetry is allowed, there is an additional parameter, m_{12}^2. In the Type II 2HDM, Φ_1 couples to the leptons and down type quarks, while Φ_2 couples to the up type quarks. Details of the Type II 2HDM can be found in the review paper [11].

The Higgs mass eigenstates contain a pair of CP-even Higgses (h^0, H^0), one CP-odd Higgs A and a pair of charged Higgses $H^\pm$, which can be written as:

$$\begin{pmatrix} H^0 \\ h^0 \end{pmatrix} = \begin{pmatrix} \cos\alpha & \sin\alpha \\ -\sin\alpha & \cos\alpha \end{pmatrix} \begin{pmatrix} \phi_1^0 \\ \phi_2^0 \end{pmatrix}, \quad \begin{aligned} A &= -G_1 \sin\beta + G_2 \cos\beta \\ H^\pm &= -\phi_1^\pm \sin\beta + \phi_2^\pm \cos\beta \end{aligned}. \tag{2.2}$$

If the charged Higgs is light, the top quark can either decay into Wb or into $H^\pm b$. The first decay is controlled by the SM gauge coupling

$$g_{W^\pm tb} = \frac{g}{\sqrt{2}} \gamma^\mu \frac{1-\gamma_5}{2}, \tag{2.3}$$

with g being the SM $\text{SU}(2)_L$ coupling, while the second decay depends on $\tan\beta$ in the Type II 2HDM or MSSM:

$$g_{H^\pm tb} = \frac{g}{2\sqrt{2} m_W} \left[(m_b \tan\beta + m_t \cot\beta) \pm (m_b \tan\beta - m_t \cot\beta)\gamma_5 \right]. \tag{2.4}$$

This coupling is enhanced for both small and large $\tan\beta$. In figure 1, we present contours of the branching fraction $\text{BR}(t \to H^\pm b)$ in the $m_{H^\pm} - \tan\beta$ plane, calculated using the 2HDMC [44]. We can see that the decay branching fraction $\text{BR}(t \to H^\pm b)$ can reach values of 5% and above for both large and small $\tan\beta$, but reaches a minimum at $\tan\beta = \sqrt{m_t/m_b} \sim 8$. The branching fraction decreases rapidly when the charged Higgs mass becomes close to the top mass.

Conventionally, a light charged Higgs is assumed to either decay into $\tau\nu$ or cs, with the corresponding couplings being

$$g_{H^\pm \tau\nu} = \frac{g}{2\sqrt{2} m_W} m_\tau \tan\beta (1 \pm \gamma_5), \tag{2.5}$$

$$g_{H^\pm cs} = \frac{g}{2\sqrt{2} m_W} \left[(m_s \tan\beta + m_c \cot\beta) \pm (m_s \tan\beta - m_c \cot\beta)\gamma_5 \right]. \tag{2.6}$$

If there is an additional light neutral Higgs boson h^0 or A, additional decay channels into $h^0 W/AW$ open up. The couplings are determined by the gauge coupling structure, as well as the mixing angles [45]:

$$g_{H^\pm h^0 W^\mp} = \frac{g \cos(\beta - \alpha)}{2} (p_{h^0} - p_{H^\pm})^\mu, \tag{2.7}$$

$$g_{H^\pm A W^\mp} = \frac{g}{2} (p_A - p_{H^\pm})^\mu, \tag{2.8}$$

with p_μ being the incoming momentum for the corresponding particle.

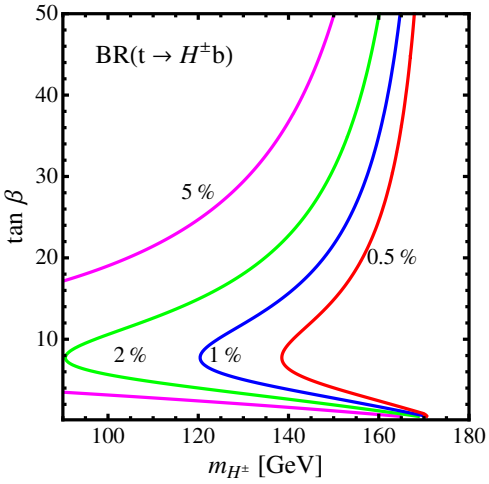

Figure 1. Branching fractions of BR($t \to H^{\pm} b$) in the $m_{H^{\pm}} - \tan\beta$ plane.

The $H^{\pm} \to h^0 W$ channel for a light charged Higgs is open only if we demand the heavy CP-even neutral Higgs H^0 to be the observed 126 GeV SM-like Higgs. In this case $|\cos(\beta - \alpha)| \sim 1$ is preferred by experiments and the $H^{\pm} h^0 W^{\pm}$ coupling is unsuppressed. The $H^{\pm} A W^{\pm}$ coupling is independent of $\sin(\beta - \alpha)$ and always unsuppressed. There is no $H^{\pm} \to H^0 W$ channel since it is kinematically forbidden given $m_{H^{\pm}} < m_t$ and $m_{H^0} \geq 126\,\text{GeV}$.

In the generic 2HDM, there are no mass relations between the charged scalars, the scalar and pseudoscalar states. Therefore both the decays $H^{\pm} \to h^0 W$ and $H^{\pm} \to A W$ can be accessible or even dominant in certain regions of the parameter space. It was shown in ref. [37] that in the Type II 2HDM with $\mathcal{Z}_2$ symmetry, imposing all experimental and theoretical constraints still leaves large regions in the parameter space that permit such exotic decays with unsuppressed decay branching fractions.

In the left panel of figure 2, we show the contours of the branching fraction BR($H^{\pm} \to AW$) in the $m_{H^{\pm}} - \tan\beta$ plane assuming $m_A = 70\,\text{GeV}$, h^0 being the SM-like Higgs and m_{H^0} decoupled. This branching fraction dominates for values of $\tan\beta$ less than 10 to 30 for charged Higgs masses in the range between 155 GeV and 170 GeV. For large values of $\tan\beta$, the $\tau\nu$ channel dominates, as shown in the right panel of figure 2 for $m_{H^{\pm}} = 160\,\text{GeV}$. For small charged Higgs masses close to the $m_A + m_W$ threshold, the decay is kinematically suppressed. Similar results can be obtained for $H^{\pm} \to h^0 W$ with $m_{h^0} = 70\,\text{GeV}$, $\sin(\beta - \alpha) \sim 0$ and decoupled m_A.

The MSSM Higgs mass spectrum is more restricted. At tree level, the mass matrix depends on m_A and $\tan\beta$ only, and the charged Higgs mass is related to m_A by $m^2_{H^{\pm}} = m^2_A + m^2_W$. Large loop corrections are needed to increase the mass splitting to permit the decay of $H^{\pm} \to AW$. In the non-decoupling region of MSSM with H^0 being the SM-like Higgs, the light CP-even Higgs h^0 can be light: $m_{h^0} < m_{H^{\pm}} - m_W$. The branching fractions can reach values up to 10% [46] in some regions of parameter space. In the NMSSM the Higgs sector is enlarged by an additional singlet. The authors of [47, 48] have shown that decays of $H^{\pm} \to A_i W / H_i W$ can be significant in certain regions of parameter space.

JHEP11(2015)051

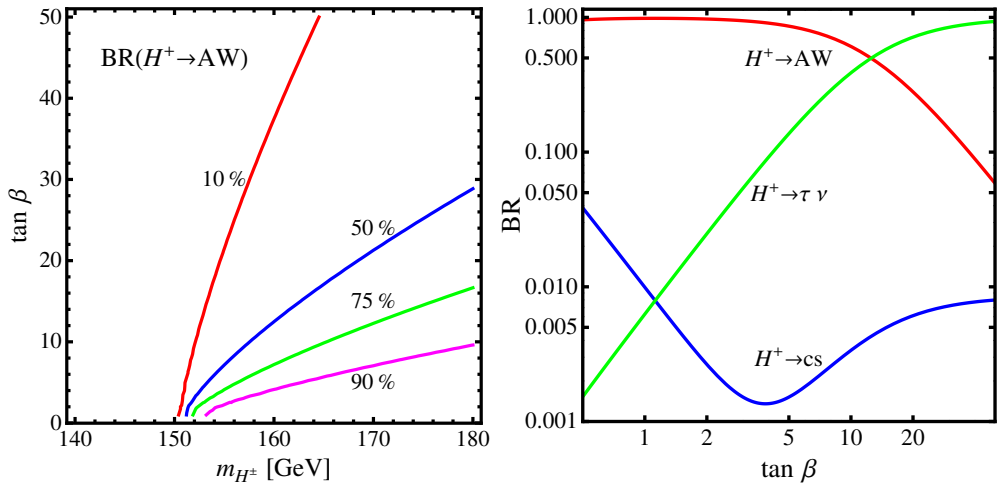

Figure 2. The left panel shows the branching fraction BR($H^\pm \to AW$) in the Type II 2HDM in $m_{H^\pm} - \tan\beta$ plane. The right panel shows the branching fractions of $H^\pm \to AW$ (red), $\tau\nu$ (green) and cs (blue) as a function of $\tan\beta$ for a 160 GeV $H^\pm$. Both plots assume the existence of a 70 GeV CP-odd scalar A, h^0 being the SM-like Higgs and H^0 decoupled.

3 Current limits

Searches for a light charged Higgs boson with mass $m_{H^\pm} < m_t$ have been performed by both ATLAS and CMS [16, 17] with 19.7 fb^{-1} integrated luminosity at 8 TeV and 4.6 fb^{-1} integrated luminosity at 7 TeV. The production mechanism considered is top pair production in which one top quark decays into $bH^\pm$ while the other decays into bW. These studies focus on the $H^\pm \to \tau\nu$ decay channel, which is dominant in most parts of the parameter space in the absence of decays into lighter Higgses. Assuming a branching fraction BR($H^\pm \to \tau\nu$) = 100%, the null search results from CMS [17] imply upper bounds for the top quark branching fraction BR($t \to H^\pm b$) varying between 1.2% to 0.16% for charged Higgs masses between 80 GeV and 160 GeV. This result can be translated into bounds on the MSSM parameter space. The obtained exclusion limits for the MSSM $m_h^{\max}$ scenario can be seen in the right panel of figure 3 (the region to the left of the red line). Only charged Higgs masses in the small region 155 GeV $< m_{H^\pm} <$ 160 GeV around $\tan\beta = 8$ are still allowed. The ATLAS results [16] are similar.

A search with the $H^\pm \to cs$ final states has been performed by ATLAS [18] using 4.7 fb^{-1} integrated luminosity at 7 TeV and by CMS [19] using 19.7 fb^{-1} integrated luminosity at 8 TeV. Assuming BR($H^\pm \to cs$) = 100%, the ATLAS results imply an upper bound for BR($t \to bH^\pm$) around 5% to 1% for charged Higgs masses between 90 GeV and 150 GeV while the CMS searches impose an upper bound of BR($t \to bH^\pm$) around 2% to 7% for a charged Higgs mass between 90 and 160 GeV.

These limits get weaker once we assume realistic branching fractions smaller than 100%. The left panel of figure 3 shows how the CMS limits on the branching fraction BR($t \to H^\pm b$) can change significantly in the presence of an additional light neutral Higgs.

JHEP11(2015)051

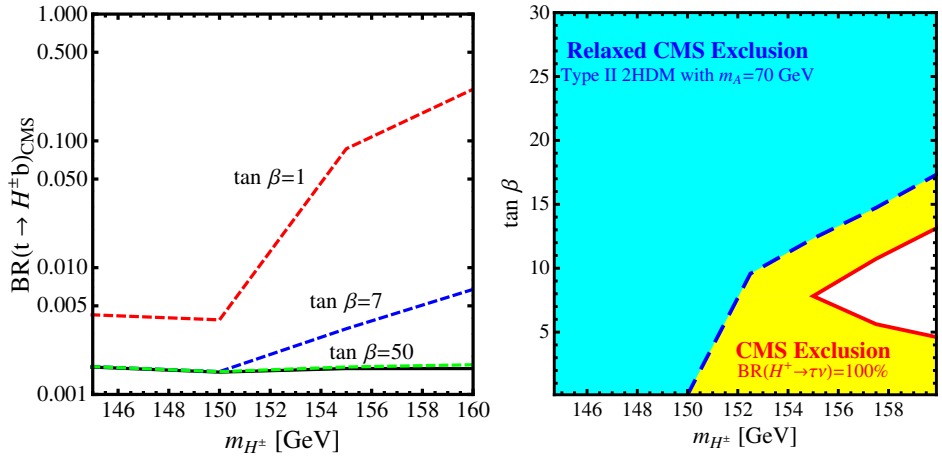

Figure 3. Left panel: CMS limits on the branching fraction BR($t \to H^{\pm} b$) assuming a 100% BR($H^{\pm} \to \tau\nu$) (black line) [17], as well as the weakened limits in the Type II 2HDM in the presence of a light neutral Higgs for $\tan\beta = 1$ (red), $\tan\beta = 7$ (blue) and $\tan\beta = 50$ (green). Right panel: the excluded region in $m_{H^{\pm}} - \tan\beta$ plane assuming a 100% BR($H^{\pm} \to \tau\nu$) (yellow and cyan regions) and the weakened limits with a light neutral Higgs (cyan region). Here we have assumed the light neutral Higgs to be a 70 GeV CP-odd scalar A.

The black curve shows the CMS limits presented in [17] assuming a 100% BR($H^{\pm} \to \tau\nu$). The modified limits assuming the presence of a 70 GeV CP-odd neutral Higgs are shown for $\tan\beta = 1$ (red), $\tan\beta = 7$ (blue) and $\tan\beta = 50$ (green). We can see that for large $\tan\beta$, the limits stay almost unchanged since $H^{\pm} \to \tau\nu$ is the dominating decay channel, but for smaller values of $\tan\beta$ these limits are weakened significantly.

The right panel of figure 3 shows how the CMS limits in the $m_{H^{\pm}} - \tan\beta$ plane weaken in the presence of an additional light Higgs. The yellow shaded region (plus the cyan region) assumes a 100% BR($H^{\pm} \to \tau\nu$) while the cyan region assumes the Type II 2HDM branching fractions in the presence of a 70 GeV CP-odd neutral Higgs. For $\tan\beta < 15$, the surviving region in $m_{H^{\pm}}$ is much more relaxed, extending down to about 150 GeV. Therefore, the presence of exotic decay modes substantially weakens the current and future limits based on searches for the conventional $H^{\pm} \to \tau\nu, cs$ decay modes.

A light charged Higgs could have a large impact on precision and flavor observables [49]. For example, in the 2HDM, the bounds on $b \to s\gamma$ restrict the charged Higgs to be heavier than 300 GeV. A detailed analysis of precision and flavor bounds in the 2HDM can be found in refs. [35–37]. Flavor constraints on the Higgs sector are, however, typically model-dependent, and could be alleviated when there are contributions from other new particles in the model [43]. Since our focus in this work is on collider searches for a light charged Higgs and their implications for the Type II 2HDM, we consider the scenario of a light charged Higgs: $m_{H^{\pm}} < m_t$, as long as it satisfies the direct collider Higgs search bounds.

Our study also assumes the existence of a light neutral Higgs A/H, which has been constrained by the $A/H \to \tau\tau$ searches at the LHC [20, 21], in particular, for $m_{A/H} > 90$ GeV and relatively large $\tan\beta$. No limit, however, exists for $m_{A/H} < 90$ GeV due

JHEP11(2015)051

to the difficulties in the identification of the relatively soft taus and the overwhelming SM backgrounds for soft leptons and τ-jets. Furthermore, LEP limits [22] based on VH associated production do not apply for the CP-odd A or the non-SM like CP-even Higgs. LEP limits based on AH pair production can also be avoided as long as $m_A + m_H > 208\,\text{GeV}$. Therefore, in our analyses below, we choose the daughter (neutral) Higgs mass to be 70 GeV.[2]

There have been theoretical studies on other light charged Higgs production and decay channels. The authors of [50, 51] analyzed the possibility of using the single top production mode to observe a light charged Higgs boson decaying into a $\tau\nu$ final state. The detectability of a charged Higgs decay into a $\mu\nu$ final state or a $\gamma\gamma W$ final state via AW with a light charged Higgs produced via top decay in top pair production has been investigated in [52] and [53].

The $H^\pm tb$ associated production with $H^\pm \to AW/HW^\pm$ has been analyzed in detail in ref. [26], which focuses on heavy charged Higgs bosons ($m_{H^\pm} > m_t$). Given the same final state of $bbWWA/H$, the same search strategy can be used to analyze light charged Higgs coming from top decay with top pair production. Furthermore, we analyze single top production with $pp \to tj$ and $t \to H^\pm b \to A/HWb$. This channel permits a cleaner signal due to its unique kinematic features.

4 Collider analysis

In our analysis we study the exotic decay $H^\pm \to AW/HW$ of light charged Higgs bosons ($m_{H^\pm} < m_t$) produced via top decay. We consider two production mechanisms: t-channel single top production[3] (tj) and top pair production ($t\bar{t}$) [54].

The light neutral Higgs boson can either be the CP-even H or the CP-odd A. In the analysis that follows, we use the decay $H^\pm \to AW^\pm$ as an illustration. Since we do not use angular correlations of the charged Higgs decay, the bounds obtained for $H^\pm \to AW^\pm$ apply to $H^\pm \to HW^\pm$ as well.

The neutral Higgs boson (A) itself will decay further. In this analysis we look at the fermionic decay $A \to \tau\tau$ for single top production and both the $\tau\tau$ and the hadronic bb modes for top pair production. While the bb mode would have the advantage of a large branching fraction $\text{BR}(A \to bb)$, the $\tau\tau$ case has smaller SM backgrounds and therefore leads to a cleaner signal. We study both leptonic and hadronic τ decays and consider three cases: $\tau_{had}\tau_{had}$, $\tau_{lep}\tau_{had}$ and $\tau_{lep}\tau_{lep}$. The $\tau_{lep}\tau_{had}$ case is particularly promising since we can utilize the same sign dilepton signal with the leptons from the decays of the W and the τ.

We use Madgraph 5/MadEvent v1.5.11 [55, 56] to generate our signal and background events. These events are passed to Pythia v2.1.21 [57] to simulate initial and final state radiation, showering and hadronization. The events are further passed through Delphes

[2] The mass of 70 GeV is also chosen to be above the $h_{\text{SM}} \to AA$ threshold to avoid significant deviations of the 126 GeV SM-like Higgs branching fractions from current measurements.

[3] We only consider the dominant t-channel single top mode since the s-channel mode suffers from a very small production rate and the tW mode has a final state similar to that of the top pair production case.

JHEP11(2015)051

3.07 [58] with the Snowmass combined LHC detector card [59] to simulate detector effects. The discovery reach and exclusion bounds have been determined using the program RooStats [60, 61] and theta-auto [62].

In this section, we will present model *independent* limits on the $\sigma \times \mathrm{BR}$ for both 95% C.L. exclusion and 5σ discovery for both single top and top pair production with possible final states $\tau\tau bWj$ and $\tau\tau bbWW/bbbbWW$. We consider the parent particle mass $m_{H^\pm}$ in the range $150 - 170\,\mathrm{GeV}$ and the daughter particle mass, $m_A = 70\,\mathrm{GeV}$.

4.1 Single top production

For single top production, we consider the channel

$$pp \to tj \to H^\pm bj \to AW^\pm bj \to \tau\tau Wbj. \tag{4.1}$$

The dominant SM backgrounds are $W\tau\tau$ production, which we generate with up to two additional jets (including b jets); and top pair production with both fully and semi-leptonic decay chains, which we generate with up to one additional jet. We also take into account the SM backgrounds $tj\tau\tau$ and $ttll$ with $l = (e, \mu, \tau)$.

The cuts that we have imposed are:

1. **Identification cuts.**

   Case A ($\tau_{had}\tau_{had}$). One lepton $\ell = e$ or μ, two τ tagged jets, zero or one b tagged jet and at least one untagged jet:

   $$n_\ell = 1,\ n_\tau = 2,\ n_b = 0, 1,\ n_j \geq 1. \tag{4.2}$$

   We require the τ-tagged jets to have charges of opposite signs.

   Case B ($\tau_{lep}\tau_{had}$). Two leptons, one τ tagged jet, zero or one b tagged jet and at least one untagged jet:

   $$n_\ell = 2,\ n_\tau = 1,\ n_b = 0, 1,\ n_j \geq 1. \tag{4.3}$$

   We require that both leptons have the same sign, which is opposite to the sign of the τ tagged jet.

   Case C ($\tau_{lep}\tau_{lep}$). Three leptons, no τ tagged jet, zero or one b tagged jet and at least one untagged jet:

   $$n_\ell = 3,\ n_\tau = 0,\ n_b = 0, 1,\ n_j \geq 1. \tag{4.4}$$

   The following selection cuts for the identification of leptons, b jets and jets are used:

   $$|\eta_{\ell,b,\tau}| < 2.5,\ |\eta_j| < 5,\ p_{T,\ell_1,j,b} > 20\ \mathrm{GeV} \text{ and } p_{T,\ell_2} > 10\ \mathrm{GeV}. \tag{4.5}$$

2. **Neutrino reconstruction.** We reconstruct the momentum of the neutrino using the missing transverse momentum and the momentum of the hardest lepton as described in [63], assuming that the missing energy is solely from $W \to \ell\nu$. In case B and C, the neutrino reconstruction is relatively poor since there is additional missing energy from the leptonic τ decay.

JHEP11(2015)051

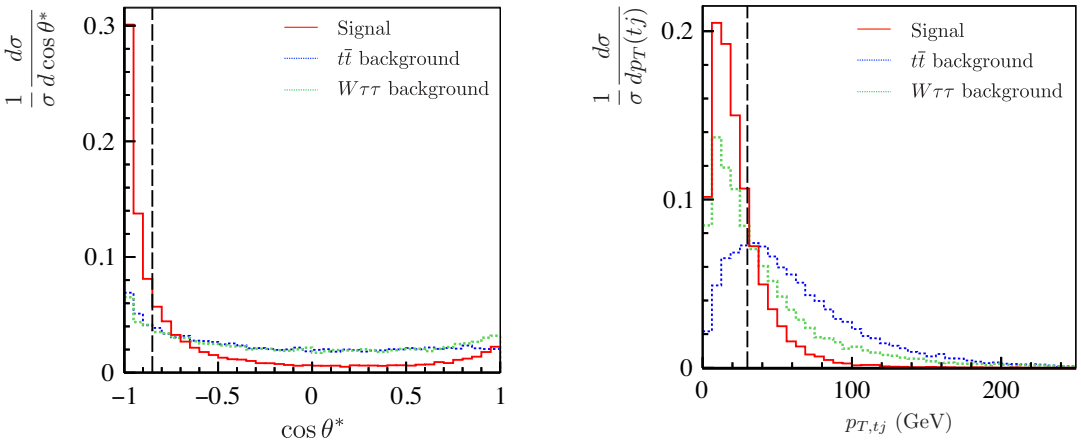

Figure 4. Normalized distribution of $\cos\theta^*$ (left panel) and the transverse momentum of the tj system $p_{T,tj}$ (right panel) for the signal (red, solid) and the dominant SM backgrounds: $t\bar{t}$ (blue, dotted) and $W\tau\tau$ (green, dotted). The imposed cuts are indicated by the vertical dashed lines. The histograms shown are for case A with $m_{H^\pm} = 160$ GeV and $m_A = 70\,\text{GeV}$.

3. **Neutral Higgs candidate A.** The τ jets (case A), the τ jet and the softer lepton (case B) or the two softer leptons (case C) are combined to form the neutral Higgs candidate. In cases B and C the mass reconstruction is relatively poor due to missing energy from the neutrino associated with the leptonic τ decay.

4. **Charged Higgs candidate $H^\pm$.** The neutral Higgs candidate, the reconstructed neutrino and the hardest lepton are combined to form the charged Higgs candidate.

5. **Mass cuts.** We place upper limits on the masses of the charged and neutral Higgs candidates, optimized for each mass combination. For $m_{H^\pm} = 160\,\text{GeV}$ and $m_A = 70\,\text{GeV}$, we impose

$$m_{\tau\tau} < 48 \text{ GeV and } m_{\tau\tau W} < 148 \text{ GeV}. \tag{4.6}$$

6. **Angular correlation.** A unique kinematical signature of single top production is the distribution of the angle θ^*, which is the angle between the top momentum in the tj system's rest frame and the tj system's momentum in the lab frame, as suggested in [64]. The differential distribution for $\cos\theta^*$ is shown in the left panel of figure 4 for signal (red, solid), $t\bar{t}$ (blue, dotted) and $W\tau\tau$ (green, dotted). The signal tends to peak around $\cos\theta^* \approx -1$ while the background is flat for $W\tau\tau$ and $t\bar{t}$.[4] In our analysis we require

$$\cos\theta^* < -0.8. \tag{4.7}$$

[4]As shown in [64], the $\cos\theta^*$ distribution for $t\bar{t}$ background would peak around $\cos\theta^* = 1$ if the top quark could be reliably identified. However, in this paper we approximate the top quark momentum by the momentum of the charged Higgs candidate, which results in a flat distribution of $\cos\theta^*$ for the $t\bar{t}$ system.

JHEP11(2015)051

Cut	Signal [fb]	$W(W)\tau\tau$ [fb]	$t\bar{t}$ [fb]	$tj\tau\tau/ttll$ [fb]	S/B	$S/\sqrt{B}$ ($300\,\text{fb}^{-1}$)
σ	100	2000	$6.3 \cdot 10^5$	257	–	–
A: Identification [eq. (4.2)]	0.29	5.36	130	1.39	0.002	0.43
Mass cuts [eq. (4.6)]	0.16	0.34	2.62	0.04	0.05	1.55
$\cos\theta^*$ and $p_{T,tj}$ [eq. (4.7), (4.8)]	0.07	0.03	0.07	0.001	0.67	3.72
B: Identification [eq. (4.3)]	0.25	4.45	2.46	1.33	0.03	1.51
Mass cuts [eq. (4.6)]	0.11	0.31	0.20	0.05	0.19	2.48
$\cos\theta^*$ and $p_{T,tj}$ [eq. (4.7), (4.8)]	0.06	0.04	0.02	0.002	0.91	3.99
C: Identification [eq. (4.4)]	0.18	3.07	6.77	6.74	0.01	0.78
Mass cuts [eq. (4.6)]	0.12	0.55	0.94	0.28	0.07	1.63
$\cos\theta^*$ and $p_{T,tj}$ [eq. (4.7), (4.8)]	0.07	0.08	0.10	0.01	0.38	2.84

Table 1. Signal and dominant background cross sections with cuts for the signal benchmark point $m_{H^\pm} = 160\,\text{GeV}$ and $m_A = 70\,\text{GeV}$ at the 14 TeV LHC. We have chosen a nominal value for $\sigma \times \text{BR}(pp \to tj \to H^\pm jb \to \tau\tau Wbj)$ of 100 fb to illustrate the cut efficiencies for the signal process. The last column of $S/\sqrt{B}$ is shown for an integrated luminosity of $\mathcal{L} = 300\ \text{fb}^{-1}$.

7. **Top and recoil jet system momentum.** In single top production, we expect that the transverse momentum of the top quark and recoil jet should balance each other, as shown in the right plot of figure 4 by the red solid curve. We impose the cut for the transverse momentum of the tj system:

$$p_{T,tj} < 30\ \text{GeV}. \tag{4.8}$$

This further suppresses the top pair background in the presence of additional jets coming from the second top.

In Table 1, we show the signal and major background cross sections with cuts for a signal benchmark point of $m_{H^\pm} = 160\,\text{GeV}$ and $m_A = 70\,\text{GeV}$ at the 14 TeV LHC. The first row shows the total cross section before cuts, calculated using MadGraph. The following rows show the cross sections after applying the identification cuts, mass cuts and the additional cuts on $\cos\theta^*$ and $p_{T,tj}$ for all three cases as discussed above. We have chosen a nominal value for $\sigma \times \text{BR}(pp \to H^\pm bj \to \tau\tau Wbj)$ of 100 fb.[5]

We can see that the dominant background contributions after particle identification are $t\bar{t}$ for cases A and C, and $W\tau\tau$ for case B. The reach is slightly better in case B in which the same sign dilepton signature can reduce the $t\bar{t}$ background sufficiently. Nevertheless, soft leptons from underlying events or b-decay can mimic the same sign dilepton signal. The obtained results are sensitive to the τ tagging efficiency as well as the misidentification rate. In our analyses, we have used a τ tagging efficiency of $\epsilon_{tag} = 60\%$ and a mistagging rate of $\epsilon_{miss} = 0.4\%$, as suggested in [59]. A better rejection of non-τ initiated jets would increase the significance of this channel.

[5]For the Type II 2HDM the top branching fraction into a charged Higgs for $m_{H^\pm} = 160\,\text{GeV}$ is typically between 0.1% and 1% (see figure 1). Using the single top production cross section, $\sigma_{tj} = 248$ pb [54] and assuming the branching fractions $\text{BR}(H^\pm \to AW^\pm) = 100\%$ and $\text{BR}(A \to \tau\tau) = 8.6\%$ leads to the stated $\sigma\times$ BR of around $21 - 210\,\text{fb}$.

JHEP11(2015)051

Cut	Signal [fb]	$t\bar{t}$ [fb]	$t\bar{t}ll$ [fb]	$W(W)\tau\tau$ [fb]	S/B	$S/\sqrt{B}$
σ	1000	$6.3 \cdot 10^5$	247	2000		
$\tau_{had}\tau_{had}$: Identification	4.1	23.3	0.58	0.078	0.17	14.9
$m_{\tau\tau}$ vs $m_{\tau\tau W}$	0.6	0.31	0.021	0.003	1.9	18.8
$\tau_{lep}\tau_{had}$: Identification	3.3	0.35	0.697	0.072	3.0	55.3
$m_{\tau\tau}$ vs $m_{\tau\tau W}$	0.69	0.035	0.042	0.007	8.1	41.1
$\tau_{lep}\tau_{lep}$: Identification	3.1	2.35	5.11	0.058	0.41	19.9
$m_{\tau\tau}$ vs $m_{\tau\tau W}$	0.62	0.25	0.16	0.006	1.4	16.5

Table 2. Signal and background cross sections with cuts for the signal benchmark point $m_{H^\pm} = 160\,\text{GeV}$ and $m_A = 70\,\text{GeV}$ at the 14 TeV LHC. We have chosen a nominal value for $\sigma \times \text{BR}(pp \to tt \to H^\pm tb \to \tau\tau bbWW)$ of 1000 fb to illustrate the cut efficiencies for the signal process. The last column of $S/\sqrt{B}$ is shown for an integrated luminosity of $\mathcal{L} = 300\ \text{fb}^{-1}$. See details in ref. [26] for the identification cuts and $m_{\tau\tau}$ vs $m_{\tau\tau W}$ cuts.

4.2 Top pair production

We now turn to the top pair production channel

$$pp \to tt \to H^\pm tb \to AbbWW \to \tau\tau bbWW/bbbbWW. \tag{4.9}$$

A detailed collider study with the same final states has been performed in [26] with a focus on high charged Higgs masses. The same strategy has been adopted for the light charged Higgs case and we refer to ref. [26] for details of the analysis.

To analyze this channel, we consider decay modes of the neutral Higgs into $\tau_{had}\tau_{had}$, $\tau_{had}\tau_{lep}$, $\tau_{lep}\tau_{lep}$ and bb. For the two W bosons, we require one to decay leptonically and the other to decay hadronically to reduce backgrounds.

The dominant SM background for the $\tau\tau$ channel is semi- and fully leptonic $t\bar{t}$ pair production. We also take into account $ttll$ production with $l = (e, \mu, \tau)$, as well as $W\tau\tau$ and $WW\tau\tau$. We ignored the subdominant backgrounds from single vector boson production, WW, ZZ, single top production, as well as multijet QCD background. Those backgrounds are either small or can be sufficiently suppressed by the cuts imposed. Similar backgrounds are considered for the bb process.

In Table 2, we show the signal and major background cross sections of the $\tau\tau$ channel with cuts for a signal benchmark point of $m_{H^\pm} = 160\,\text{GeV}$ and $m_A = 70\,\text{GeV}$ at the 14 TeV LHC, similar to Table 1. We have chosen a nominal value for $\sigma \times \text{BR}(pp \to tt \to H^\pm tb \to \tau\tau bbWW)$ of 1000 fb to illustrate the cut efficiencies for the signal process.

After the cuts, the dominant background contributions are $t\bar{t}$ ($\tau_{had}\tau_{had}$, $\tau_{lep}\tau_{lep}$) as well as $t\bar{t}ll$ ($\tau_{had}\tau_{lep}$) while the backgrounds including vector bosons do not contribute much. We find that the case in which one τ decays leptonically and the other τ decays hadronically gives the best reach. This is because the same sign dilepton signature can reduce the $t\bar{t}$ background sufficiently.

JHEP11(2015)051

4.3 Limits

Figure 5 displays the 95% C.L. exclusion (green curve) and 5σ discovery (red curve) limits at the 14 TeV LHC for both the single top (left) and top pair (right) channel . The dot-dashed, solid and dashed line show the results for three luminosities: $100\,\text{fb}^{-1}$, $300\,\text{fb}^{-1}$ and $1000\,\text{fb}^{-1}$, respectively. In these plots we have combined all three cases of τ decays. While in the single top channel, all three cases contribute roughly the same to the overall significance, the highest sensitivity in the top pair production channel comes from the $\tau_{lep}\tau_{had}$ case. Due to the small number of events in both channels, the statistical error dominates over the assumed 10% systematic error in the background cross sections. Therefore, higher luminosities lead to better reaches. Assuming 300 fb^{-1} integrated luminosity, the 95% C.L. limits on $\sigma \times \text{BR}$ are about 35 and 55 fb for the single top and top pair production processes respectively. The discovery reaches are about 3 times higher.

Assuming a 100% branching fraction $\text{BR}(H^\pm \to AW)$ and $\text{BR}(A \to \tau\tau) = 8.6\%$,[6] we can reinterpret $\sigma \times \text{BR}$ limits as limits on the branching fraction $\text{BR}(t \to H^\pm b)$ as indicated by the vertical axis on the right. While the cross section limits are better in the single top channel, the corresponding limits on the branching fraction $\text{BR}(t \to H^\pm b)$ are weaker due to the smaller single top production cross section. The 95% C.L. exclusion limit on $\text{BR}(t \to H^\pm b)$ is about 0.2% for the single top process and 0.03% for the top pair production process, respectively.

A study of the $A \to bb$ decay using the top pair production channel leads to worse results due to the significantly higher SM backgrounds. For the 14 TeV LHC with $300\,\text{fb}^{-1}$, the exclusion limit on $\sigma \times \text{BR}$ is about 7 pb for a charged Higgs with mass $m_{H^\pm} = 160\,\text{GeV}$, assuming the existence of a light neutral Higgs with mass $m_A = 70\,\text{GeV}$. Thus, given the typical ratio of $\text{BR}(A/H \to bb) : \text{Br}(A/H \to \tau\tau) \sim 3m_b^2/m_\tau^2$, we conclude that the reach in the bb case is much worse than that in the $\tau\tau$ case.

We reiterate here that the exclusion and discovery limits on $\sigma \times \text{BR}$ are completely model independent. Whether or not discovery/exclusion is actually feasible in this channel should be answered within the context of a particular model, in which the theoretically predicted cross sections and branching fractions can be compared with the exclusion or discovery limits. We will do this in section 5 using the Type II 2HDM as a specific example.

5 Implication for the type II 2HDM

The results in the previous section on $\text{BR}(t \to bH^\pm)$ can be applied to any beyond the SM scenarios containing a light charged Higgs boson with the $H^\pm \to AW/HW$ channel being kinematically accessible. To give a specific example of the implication of this channel, we will now apply the exclusion and discovery limits in the context of the Type II 2HDM.

The 2HDM allows us to interpret the observed Higgs signal either as the lighter CP-even Higgs (h^0-126) or the heavier CP-even Higgs (H^0-126). The authors of ref. [37] have identified the Type II 2HDM parameter space in both cases, assuming $m_{12}^2 = 0$ and including all the experimental and theoretical constraints. In the h^0-126 case, we are restricted to either a SM-like region at $\sin(\beta - \alpha) = \pm 1$ with $\tan\beta < 4$ or an extended

[6] Assuming bb and $\tau\tau$ are the dominant decay modes of a light A, $\text{BR}(A \to \tau\tau) = 8.6\%$ in the Type II 2HDM or MSSM for medium to large $\tan\beta$. This branching fraction decreases for small $\tan\beta$ when the cs-channel is enhanced.

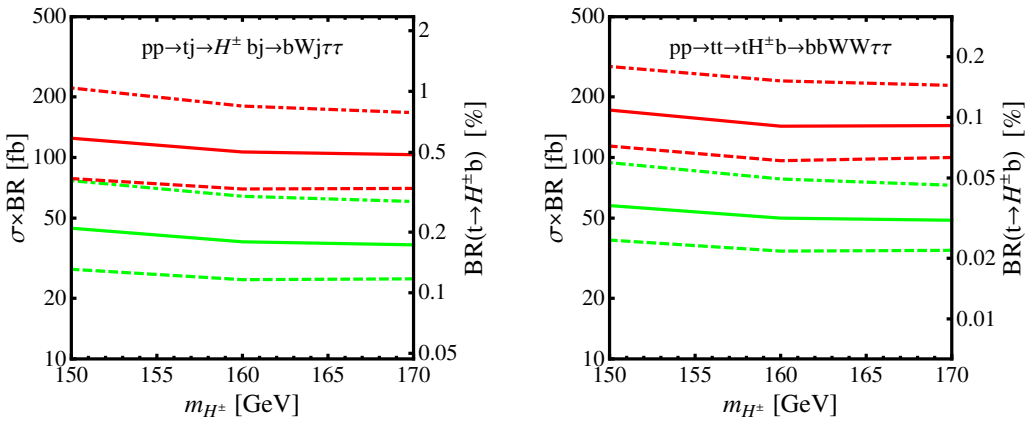

Figure 5. The 95% C.L. exclusion (green) and 5σ discovery (red) limits for $\sigma\times$BR and BR($t \to H^\pm b$) (right vertical axis) assuming BR($H^\pm \to AW$) = 100% and BR($A \to \tau\tau$) = 8.6% for $m_A = 70\,\text{GeV}$ at the 14 TeV LHC using the single top (left panel) and top pair (right panel) production channels. The dot-dashed, solid and dashed lines correspond to an integrated luminosity of 100, 300 and $1000\,\text{fb}^{-1}$ respectively. Here, we have assumed a 10% systematic error on the backgrounds.

$\{m_{H^\pm}, m_A, m_{h^0}, m_{H^0}\}$ GeV	$H^\pm \to AW$	$H^\pm \to h^0 W$	Favored Region
BP1: $\{160, 70, 126, 700\}$	✓	✗	$\sin(\beta-\alpha) \approx \pm 1$
BP2: $\{160, 700, 70, 126\}$	✗	✓	$\sin(\beta-\alpha) \approx 0$

Table 3. Benchmark points used for illustrating the discovery and exclusion limits in the context of the Type II 2HDM. The checkmarks indicate kinematically allowed channels. Also shown are the typical favored region of $\sin(\beta-\alpha)$ for each case (see ref. [37]).

region with $0.6 < \sin(\beta-\alpha) < 0.9$ and $1.5 < \tan\beta < 4$ with relatively unconstrained masses. In the H^0-126 case, an SM-like region, around $\sin(\beta-\alpha) = 0$ and $\tan\beta < 8$, and an extended region with $-0.8 < \sin(\beta-\alpha) < 0.05$ and $\tan\beta$ up to 30 or higher, survive all constraints.

We can interpret the results of the previous section in two ways: the light neutral Higgs in the charged Higgs decay could either be the light CP-even Higgs h^0 or the CP-odd Higgs A. The decay mode $H^\pm \to H^0 W$ is not possible given that $m_{H^0} \geq 126\,\text{GeV}$. The decay $H^\pm \to AW$ is possible in both the h^0-126 and H^0-126 case and the partial decay width is independent of $\sin(\beta-\alpha)$. The decay branching fraction, however, depends on whether $H^\pm \to h^0 W$ is open or not. For simplicity, we choose a benchmark point BP1, with $\{m_{H^\pm}, m_A, m_{h^0}, m_{H^0}\} = \{160, 70, 126, 700\}$ such that only $H^\pm \to AW$ is kinematically accessible. The decay width $H^\pm \to h^0 W$ depends on $\sin(\beta-\alpha)$ and is only sizable in the H^0-126 case. We illustrate this case with a second benchmark point BP2: $\{m_{H^\pm}, m_A, m_{h^0}, m_{H^0}\} = \{160, 700, 70, 126\}$, assuming that the CP-odd Higgs A decouples. We list the benchmark points in Table 3.

In the left panel of figure 6, we show the branching faction BR($H^\pm \to AW$) for BP1, which is independent of $\sin(\beta-\alpha)$ and decreases with increasing $\tan\beta$ due to the

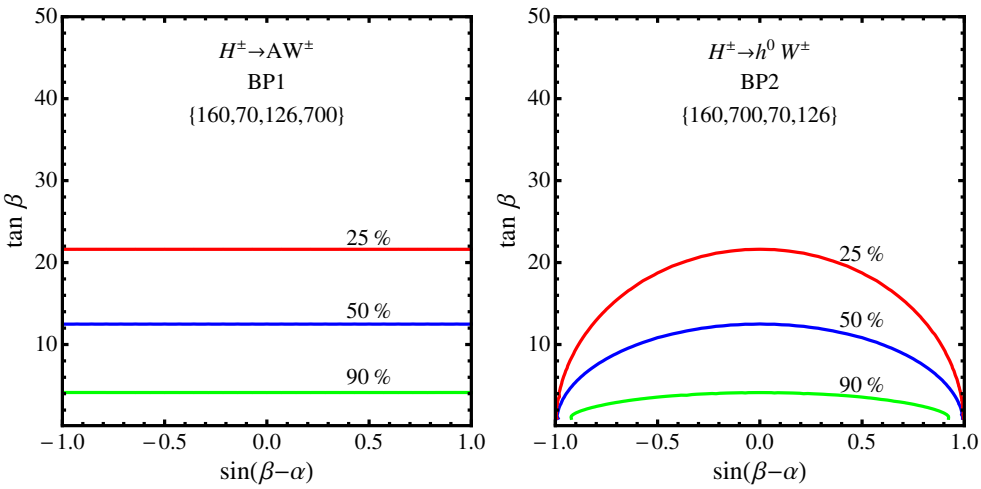

Figure 6. Contours of branching fractions of $H^\pm \to AW$ (left panel) and $H^\pm \to h^0 W$ (right panel) for BP1 and BP2, respectively.

enhancement of the $\tau\nu$ mode. The branching fraction can reach values of 90% or larger for small $\tan\beta < 4$ and stays the dominating channel until $\tan\beta = 12$.

The right panel of figure 6 shows the branching fraction, $\mathrm{BR}(H^\pm \to h^0 W)$, for BP2. It reaches maximal values around $\sin(\beta-\alpha) = 0$ and decreases for larger $|\sin(\beta-\alpha)|$ compared to BP1 due to the suppressed $H^\pm h^0 W$ coupling.

In figure 7, we display the 95% exclusion (yellow regions enclosed by the solid lines as well as the cyan regions) and 5σ discovery reach (cyan regions enclosed by the dashed lines) for BP1 (left panel) and BP2 (right panel) at the 14 TeV LHC with 300 fb^{-1} integrated luminosity. The red lines refer to the limits based on top pair production, and the blue lines refer to the limits based on single top production.

For the benchmark point BP1 with $H^\pm \to AW^\pm$, the exclusion reach based on top pair production covers the entire parameter space, while discovery is possible for small $\tan\beta < 6$ and large $\tan\beta > 18$, independent of $\sin(\beta-\alpha)$. Intermediate values of $\tan\beta$ have a reduced branching fraction $\mathrm{BR}(t \to H^\pm b)$ (see figure 1) and therefore the total $\sigma\times\mathrm{BR}$ is suppressed. At high $\tan\beta$, $\mathrm{BR}(t \to H^\pm b)$ is enhanced sufficiently to overcome the reduced branching fraction $\mathrm{BR}(H^\pm \to AW)$. The search based on single top production is only effective in the small $\tan\beta$ region, with an exclusion reach of $\tan\beta < 4$ and a discovery reach of $\tan\beta < 2$.

The right panel of figure 7 shows the reach for BP2. The exclusion region for top pair production covers the entire parameter space except for $|\sin(\beta-\alpha)| > 0.85$ and $\tan\beta > 4$. Discovery is possible for large $\tan\beta > 18$ with $|\sin(\beta-\alpha)| < 0.5$ and for small $\tan\beta < 6$. The reach for single top production is limited to the small $\tan\beta$ region.

In figure 8, we show the reach in the $m_{H^\pm} - \tan\beta$ plane for $H^\pm \to AW$ with $m_A = 70\,\mathrm{GeV}$ with both h^0 and H^0 outside the kinematic reach. These limits also apply for $H^\pm \to h^0 W$ with $m_{h^0} = 70\,\mathrm{GeV}$ and $\sin(\beta-\alpha) = 0$ with a decoupled A. We display the 95% exclusion (yellow regions enclosed by the solid lines as well as the cyan regions) and 5σ discovery limits (cyan regions enclosed by the dashed lines) for an integrated luminosity

JHEP11(2015)051

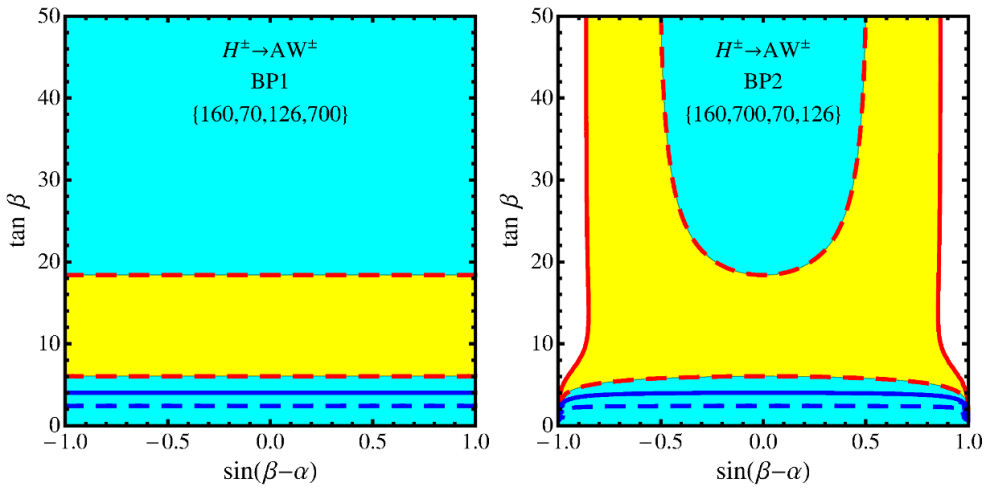

Figure 7. The 95% exclusion (yellow regions enclosed by the solid lines as well as the cyan regions) and the 5σ discovery reach (cyan regions enclosed by the dashed lines) obtained by the tj-channel (blue) and tt-channel (red) in the $\tan\beta$ versus $\sin(\beta-\alpha)$ plane for BP1 (left panel) and BP2 (right panel), with an integrated luminosity of 300 fb^{-1} at the 14 TeV LHC.

of 300 fb^{-1} at the 14 TeV LHC. Superimposed are the current CMS limits (black hatched region) [17] which exclude the large $\tan\beta$ region at $m_{H^\pm} < 160$ GeV.

The best reach is obtained by the top pair channel, as indicated by regions enclosed by the red lines. The model can be excluded up to 167 GeV for all $\tan\beta$ and up to 170 GeV for $\tan\beta < 4$ or $\tan\beta > 29$. Discovery is possible for both low $\tan\beta$ <6 in the entire region of 150 GeV $< m_{H^\pm} <$ 170 GeV and high $\tan\beta > 17$ with 155 GeV $< m_{H^\pm} <$ 165 GeV. The reach is weakened for intermediate $\tan\beta$ due to the reduced branching fraction $t \to H^\pm b$. The single top channel (blue lines) only provides sensitivity in the low $\tan\beta$ region and permits exclusion (discovery) for $\tan\beta \lesssim 4$ (3).

We conclude this section with the following observations:

- Once the AW/h^0W channels are kinematically accessible, they dominate for small and intermediate values of $\tan\beta$. The reach in the $H^\pm \to \tau\nu$ mode is significantly weakened in the presence of the $H^\pm \to AW/h^0W$ modes, in particular for small to intermediate $\tan\beta$, leaving the possibility of a light charged Higgs that has escaped detection so far.

- Both the $H^\pm \to AW$ channel for the h^0-126 case and the $H^\pm \to h^0W$ channel in the H^0-126 case permit exclusion and discovery in large regions of the parameter space.

- The reach in the exotic channels $H^\pm \to AW/h^0W$ is complementary to the reach in the conventional search channel $H^\pm \to \tau\nu$, especially for small to intermediate values of $\tan\beta$.

- While the top pair production channel covers a large region of parameter space, the single top channel permits discovery/exclusion in the low $\tan\beta$ region.

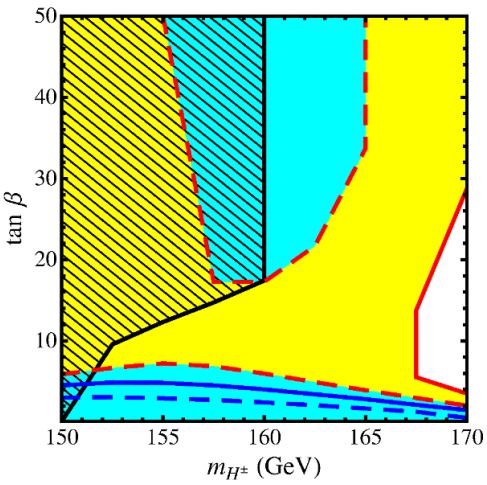

Figure 8. 95% exclusion (yellow regions bounded by solid lines as well as the cyan regions) and the 5σ discovery (cyan regions bounded by the dashed lines) imposed by the tj-channel (blue) and tt-channel (red) in the $m_{H^\pm} - \tan\beta$ parameter space for $300\,\text{fb}^{-1}$ luminosity with $m_A = 70\,\text{GeV}$. The same limits apply for $m_{h^0} = 70\,\text{GeV}$ and $\sin(\beta - \alpha) = 0$ if A is decoupled. The black hatched region indicates the region excluded by the CMS search based on $H^\pm \to \tau\nu$ [17].

6 Conclusion

After the discovery of the first fundamental scalar by both the ATLAS and CMS collaboration, it is now time to carefully measure its properties to determine the nature of this particle. Current measurements still permit the possibility that the discovered signal is not the SM Higgs particle, but just one scalar particle contained in a larger Higgs sector, as predicted by many extensions of the SM. While most of the current searches for the non-SM Higgs bosons focus on conventional search channels, increasing attention is being paid to exotic Higgs decay channels [23–34] into a pair of lighter Higgses or a Higgs plus vector boson final states that can become dominant once kinematically allowed.

In this paper we consider the possibility of a light charged Higgs $m_{H^\pm} < m_t$ produced via top decay $t \to H^\pm b$. Due to the large single top and top pair production cross section at the LHC, the charged Higgs can be produced copiously. Assuming that a light charged Higgs predominantly decays into $\tau\nu$, both ATLAS and CMS exclude a light charged Higgs for most regions of the MSSM and the Type II 2HDM parameter spaces. The branching fraction $\text{BR}(H^\pm \to \tau\nu)$ can be significantly reduced once the exotic decay channel into a light Higgs, $H^\pm \to AW/HW$, is open. In this case, the exclusion bounds from the $\tau\nu$ search get weakened, in particular for small and intermediate $\tan\beta$, leaving the possibility of a light charged Higgs open. This loophole, however, can be closed when we consider the alternative charged Higgs decay channel: $H^\pm \to AW/HW$.

In this paper we analyze the possibility of discovering a light charged Higgs via the $H^\pm \to AW/HW$ decay mode assuming that the light Higgs A/H decays into either $\tau\tau$ or bb. While the top pair channel benefits from a large production cross section, the single top channel permits a cleaner signal due to its unique kinematic features. Assuming

JHEP11(2015)051

the existence of a light neutral Higgs of mass 70 GeV, the model independent 95% C.L. exclusion limits on $\sigma \times \mathrm{BR}$ based on $\tau\tau$ channel are about 35 fb for the single top channel and 55 fb for the top pair channel. The discovery reaches are about three times higher. Assuming $\mathrm{BR}(H^\pm \to AW/HW) = 100\%$ and $\mathrm{BR}(A/H \to \tau\tau) = 8.6\%$, the exclusion limits on $\mathrm{BR}(t \to H^+ b)$ are about 0.2% and 0.03% for single top and top pair production, respectively. A significantly worse reach is obtained in the bb channel.

We discuss the implications of the obtained exclusion and discovery bounds in the context of the Type II 2HDM, focusing on two scenarios: the decay $H^\pm \to AW$ with a light A in the h^0-126 case and the decay $H^\pm \to h^0 W$ in the H^0-126 case. The top pair channel provides the best reach and permits discovery for both large $\tan\beta > 17$ around $m_{H^\pm} = 160$ GeV and small $\tan\beta < 6$ over the entire mass range, while exclusion is possible in the entire $\tan\beta$ versus $m_{H^\pm}$ plane except for charged Higgs masses close to the top threshold. The single top channel is sensitive in the low $\tan\beta$ region and permits discovery for $\tan\beta < 3$. In particular, the low $\tan\beta$ region is not constrained by searches in $\tau\nu$ channel, making the $H^\pm \to AW/h^0 W$ a complementary channel for charged Higgs searches.

While most of the recent searches for additional Higgs bosons have focused on conventional decay channels, searches using exotic decay channels have just started [23–34]. Studying all of the possibilities for the non-SM Higgs decays will allow us to explore the full potential of the LHC and future colliders in understanding the nature of electroweak symmetry breaking.

Acknowledgments

We thank B. Coleppa for his participation at the beginning of this project. We would also like to thank Peter Loch and Matt Leone for helpful discussions. This work was supported by the Department of Energy under Grant DE-FG02-13ER41976.

References

[1] ATLAS collaboration, *Observation of a new particle in the search for the Standard Model Higgs boson with the ATLAS detector at the LHC*, *Phys. Lett.* **B 716** (2013) 1 [arXiv:1207.7214] [INSPIRE].

[2] CMS collaboration, *Observation of a new boson at a mass of 125 GeV with the CMS experiment at the LHC*, *Phys. Lett.* **B 716** (2012) 30 [arXiv:1207.7235] [INSPIRE].

[3] ATLAS collaboration, *Combined coupling measurements of the Higgs-like boson with the ATLAS detector using up to 25 fb^{-1} of proton-proton collision data*, ATLAS-CONF-2013-034 (2013).

[4] CMS collaboration, *Combination of standard model Higgs boson searches and measurements of the properties of the new boson with a mass near 125 GeV*, CMS-PAS-HIG-13-005 (2013).

JHEP11(2015)051

[5] ATLAS collaboration, *Evidence for the spin-0 nature of the Higgs boson using ATLAS data*, *Phys. Lett.* **B 726** (2013) 120 [arXiv:1307.1432] [INSPIRE].

[6] H.P. Nilles, *Supersymmetry, Supergravity and Particle Physics*, *Phys. Rept.* **110** (1984) 1 [INSPIRE].

[7] H.E. Haber and G.L. Kane, *The Search for Supersymmetry: Probing Physics Beyond the Standard Model*, *Phys. Rept.* **117** (1985) 75 [INSPIRE].

[8] R. Barbieri, *Looking Beyond the Standard Model: The Supersymmetric Option*, *Riv. Nuovo Cim.* **11N4** (1988) 1 [INSPIRE].

[9] J.R. Ellis, J.F. Gunion, H.E. Haber, L. Roszkowski and F. Zwirner, *Higgs Bosons in a Nonminimal Supersymmetric Model*, *Phys. Rev.* **D 39** (1989) 844 [INSPIRE].

[10] M. Drees, *Supersymmetric Models with Extended Higgs Sector*, *Int. J. Mod. Phys.* **A 4** (1989) 3635 [INSPIRE].

[11] G.C. Branco, P.M. Ferreira, L. Lavoura, M.N. Rebelo, M. Sher and J.P. Silva, *Theory and phenomenology of two-Higgs-doublet models*, *Phys. Rept.* **516** (2012) 1 [arXiv:1106.0034] [INSPIRE].

[12] H.E. Haber, G.L. Kane and T. Sterling, *The Fermion Mass Scale and Possible Effects of Higgs Bosons on Experimental Observables*, *Nucl. Phys.* **B 161** (1979) 493 [INSPIRE].

[13] L.J. Hall and M.B. Wise, *Flavor Changing Higgs – Boson Couplings*, *Nucl. Phys.* **B 187** (1981) 397 [INSPIRE].

[14] J.F. Donoghue and L.F. Li, *Properties of Charged Higgs Bosons*, *Phys. Rev.* **D 19** (1979) 945 [INSPIRE].

[15] CMS collaboration, *Search for a Higgs Boson in the Mass Range from 145 to 1000 GeV Decaying to a Pair of W or Z Bosons*, arXiv:1504.00936 [INSPIRE].

[16] ATLAS collaboration, *Search for charged Higgs bosons in the τ+jets final state with pp collision data recorded at $\sqrt{s} = 8$ TeV with the ATLAS experiment*, ATLAS-CONF-2013-090 (2013).

[17] CMS collaboration, *Search for charged Higgs bosons with the H+ to tau nu decay channel in the fully hadronic final state at $\sqrt{s} = 8$ TeV*, CMS-PAS-HIG-14-020 (2014).

[18] ATLAS collaboration, *Search for a light charged Higgs boson in the decay channel $H^+ \to c\bar{s}$ in $t\bar{t}$ events using pp collisions at $\sqrt{s} = 7$ TeV with the ATLAS detector*, *Eur. Phys. J.* **C 73** (2013) 2465 [arXiv:1302.3694] [INSPIRE].

[19] CMS collaboration, *Search for H+ to cs-bar decay*, CMS-PAS-HIG-13-035 (2014).

[20] CMS collaboration, *Search for neutral MSSM Higgs bosons decaying to a pair of tau leptons in pp collisions*, *JHEP* **10** (2014) 160 [arXiv:1408.3316] [INSPIRE].

[21] ATLAS collaboration, *Search for neutral Higgs bosons of the minimal supersymmetric standard model in pp collisions at $\sqrt{s} = 8$ TeV with the ATLAS detector*, *JHEP* **11** (2014) 056 [arXiv:1409.6064] [INSPIRE].

[22] http://lephiggs.web.cern.ch/LEPHIGGS/www/Welcome.html.

[23] D. Curtin et al., *Exotic decays of the 125 GeV Higgs boson*, *Phys. Rev.* **D 90** (2014) 075004 [arXiv:1312.4992] [INSPIRE].

[24] E. Brownson et al., *Heavy Higgs Scalars at Future Hadron Colliders (A Snowmass Whitepaper)*, arXiv:1308.6334 [INSPIRE].

JHEP11(2015)051

[25] B. Coleppa, F. Kling and S. Su, *Exotic Decays Of A Heavy Neutral Higgs Through HZ/AZ Channel*, *JHEP* **09** (2014) 161 [arXiv:1404.1922] [INSPIRE].

[26] B. Coleppa, F. Kling and S. Su, *Charged Higgs search via $AW^{\pm}/HW^{\pm}$ channel*, *JHEP* **12** (2014) 148 [arXiv:1408.4119] [INSPIRE].

[27] T. Li and S. Su, *Exotic Higgs Decay via Charged Higgs*, arXiv:1504.04381 [INSPIRE].

[28] G.C. Dorsch, S.J. Huber, K. Mimasu and J.M. No, *Echoes of the Electroweak Phase Transition: Discovering a second Higgs doublet through $A_0 \to ZH_0$*, *Phys. Rev. Lett.* **113** (2014) 211802 [arXiv:1405.5537] [INSPIRE].

[29] N. Chen, C. Du, Y. Fang and L.-C. Lü, *LHC Searches for The Heavy Higgs Boson via Two B Jets plus Diphoton*, *Phys. Rev.* **D 89** (2014) 115006 [arXiv:1312.7212] [INSPIRE].

[30] N. Chen, J. Li, Y. Liu and Z. Liu, *LHC searches for the CP-odd Higgs by the jet substructure analysis*, *Phys. Rev.* **D 91** (2015) 075002 [arXiv:1410.4447] [INSPIRE].

[31] R. Enberg, W. Klemm, S. Moretti, S. Munir and G. Wouda, *Charged Higgs boson in the $W^{\pm}$ Higgs channel at the Large Hadron Collider*, *Nucl. Phys.* **B 893** (2015) 420 [arXiv:1412.5814] [INSPIRE].

[32] CMS collaboration, *Search for a pseudoscalar boson A decaying into a Z and an h boson in the llbb final state*, CMS-PAS-HIG-14-011 (2014).

[33] ATLAS collaboration, *Search for a CP-odd Higgs boson decaying to Zh in pp collisions at $\sqrt{s} = 8$ TeV with the ATLAS detector*, *Phys. Lett.* **B 744** (2015) 163 [arXiv:1502.04478] [INSPIRE].

[34] CMS collaboration, *2HDM scenario, H to hh and A to Zh*, CMS-PAS-HIG-13-025 (2013).

[35] F. Mahmoudi and O. Stal, *Flavor constraints on the two-Higgs-doublet model with general Yukawa couplings*, *Phys. Rev.* **D 81** (2010) 035016 [arXiv:0907.1791] [INSPIRE].

[36] M. Misiak et al., *Updated NNLO QCD predictions for the weak radiative B-meson decays*, *Phys. Rev. Lett.* **114** (2015) 221801 [arXiv:1503.01789] [INSPIRE].

[37] B. Coleppa, F. Kling and S. Su, *Constraining Type II 2HDM in Light of LHC Higgs Searches*, *JHEP* **01** (2014) 161 [arXiv:1305.0002] [INSPIRE].

[38] C.D. Froggatt, R.G. Moorhouse and I.G. Knowles, *Leading radiative corrections in two scalar doublet models*, *Phys. Rev.* **D 45** (1992) 2471 [INSPIRE].

[39] C.D. Froggatt, R.G. Moorhouse and I.G. Knowles, *Two scalar doublet models with softly broken symmetries*, *Nucl. Phys.* **B 386** (1992) 63 [INSPIRE].

[40] A. Pomarol and R. Vega, *Constraints on CP-violation in the Higgs sector from the rho parameter*, *Nucl. Phys.* **B 413** (1994) 3 [hep-ph/9305272] [INSPIRE].

[41] A. Wahab El Kaffas, P. Osland and O.M. Ogreid, *Constraining the Two-Higgs-Doublet-Model parameter space*, *Phys. Rev.* **D 76** (2007) 095001 [arXiv:0706.2997] [INSPIRE].

[42] H.E. Haber and D. O'Neil, *Basis-independent methods for the two-Higgs-doublet model III: The CP-conserving limit, custodial symmetry and the oblique parameters S, T, U*, *Phys. Rev.* **D 83** (2011) 055017 [arXiv:1011.6188] [INSPIRE].

[43] T. Han, T. Li, S. Su and L.-T. Wang, *Non-Decoupling MSSM Higgs Sector and Light Superpartners*, *JHEP* **11** (2013) 053 [arXiv:1306.3229] [INSPIRE].

[44] D. Eriksson, J. Rathsman and O. Stal, *2HDMC: Two-Higgs-Doublet Model Calculator Physics and Manual*, *Comput. Phys. Commun.* **181** (2010) 189 [arXiv:0902.0851] [INSPIRE].

JHEP11(2015)051

[45] J.F. Gunion, H.E. Haber, G.L. Kane and S. Dawson, *The Higgs Hunter's Guide*, *Front. Phys.* **80** (2000) 1 [INSPIRE].

[46] LHC Higgs Cross section Working Group collaboration, J.R. Andersen et al., *Handbook of LHC Higgs Cross sections: 3. Higgs Properties*, arXiv:1307.1347 [INSPIRE].

[47] N.D. Christensen, T. Han, Z. Liu and S. Su, *Low-Mass Higgs Bosons in the NMSSM and Their LHC Implications*, *JHEP* **08** (2013) 019 [arXiv:1303.2113] [INSPIRE].

[48] M. Drees, M. Guchait and D.P. Roy, *Signature of charged to neutral Higgs boson decay at the LHC in SUSY models*, *Phys. Lett.* **B 471** (1999) 39 [hep-ph/9909266] [INSPIRE].

[49] Particle Data Group collaboration, J. Beringer et al., *Review of Particle Physics (RPP)*, *Phys. Rev.* **D 86** (2012) 010001 [INSPIRE].

[50] R. Guedes, S. Moretti and R. Santos, *Charged Higgs bosons in single top production at the LHC*, *JHEP* **10** (2012) 119 [arXiv:1207.4071] [INSPIRE].

[51] M. Hashemi, *Single Top Events as a Source of Light Charged Higgs in the Fully Hadronic Final State at LHC*, *JHEP* **05** (2013) 112 [arXiv:1305.2096] [INSPIRE].

[52] M. Hashemi, *Observability of Light Charged Higgs Decay to Muon in Top Quark Pair Events at LHC*, *Eur. Phys. J.* **C 72** (2012) 1994 [arXiv:1109.5356] [INSPIRE].

[53] D. Das, L. Mitzka and W. Porod, *Discovery of Charged Higgs through $\gamma\gamma$ final states*, arXiv:1408.17 c04 [INSPIRE].

[54] N. Kidonakis, *Differential and total cross sections for top pair and single top production*, arXiv:1205.3453 [INSPIRE].

[55] J. Alwall, M. Herquet, F. Maltoni, O. Mattelaer and T. Stelzer, *MadGraph 5: Going Beyond*, *JHEP* **06** (2011) 128 [arXiv:1106.0522] [INSPIRE].

[56] J. Alwall et al., *The automated computation of tree-level and next-to-leading order differential cross sections and their matching to parton shower simulations*, *JHEP* **07** (2014) 079 [arXiv:1405.0301] [INSPIRE].

[57] T. Sjöstrand, S. Mrenna and P.Z. Skands, *PYTHIA 6.4 Physics and Manual*, *JHEP* **05** (2006) 026 [hep-ph/0603175] [INSPIRE].

[58] DELPHES 3 collaboration, J. de Favereau et al., *DELPHES 3: a modular framework for fast simulation of a generic collider experiment*, *JHEP* **02** (2014) 057 [arXiv:1307.6346] [INSPIRE].

[59] A. Avetisyan et al., *Methods and Results for Standard Model Event Generation at $\sqrt{s} = 14$ TeV, 33 TeV and 100 TeV Proton Colliders: A Snowmass Whitepaper*, arXiv:1308.1636 [INSPIRE].

[60] L. Moneta et al., *The RooStats Project*, PoS(ACAT2010)057 [arXiv:1009.1003] [INSPIRE].

[61] RooStats Team collaboration, G. Schott, *RooStats for Searches*, arXiv:1203.1547 [INSPIRE].

[62] http://www-ekp.physik.uni-karlsruhe.de/~ott/theta/theta-auto/.

[63] ATLAS collaboration, *Measurement of the t-channel single top-quark production cross section in pp collisions at $\sqrt{s} = 7$ TeV with the ATLAS detector*, *Phys. Lett.* **B 717** (2013) 330 [arXiv:1205.3130] [INSPIRE].

[64] F. Kling, T. Plehn and M. Takeuchi, *Tagging single Tops*, *Phys. Rev.* **D 86** (2012) 094029 [arXiv:1207.4787] [INSPIRE].

JHEP11(2015)051

Appendix F

Searches for non-SM Heavy Higgses at a 100 TeV pp Collider

The article *Searches for non-SM Heavy Higgses at a 100 TeV pp Collider* has been accepted for publication in the International Journal of Modern Physics A [26].

International Journal of Modern Physics A
Vol. 30, No. 23 (2015) 1544005 (12 pages)

DOI: 10.1142/S0217751X15440054

Searches for non-SM heavy Higgses at a 100 TeV *pp* collider

Jan Hajer,[*,†,‖] Ahmed Ismail,[‡,§,**] Felix Kling,[¶,††]
Ying-Ying Li,[*,‡‡] Tao Liu[*,§§] and Shufang Su[¶,¶¶]

[*] *Department of Physics,*
The Hong Kong University of Science and Technology,
Hong Kong S.A.R., Hong Kong
[†] *Jockey Club Institute for Advanced Study,*
The Hong Kong University of Science and Technology,
Hong Kong S.A.R., Hong Kong
[‡] *Department of Physics, University of Illinois,*
Chicago, IL 60607, USA
[§] *High Energy Physics Division, Argonne National Laboratory,*
Argonne, IL 60439, USA
[¶] *Department of Physics, University of Arizona,*
Tucson, AZ 85721, USA
[‖] *jan.hajer@ust.hk*
[**] *aismail@anl.gov*
[††] *kling@email.arizona.edu*
[‡‡] *ylict@connect.ust.hk*
[§§] *taoliu@ust.hk*
[¶¶] *shufang@email.arizona.edu*

Published 18 August 2015

In this write-up, we summarize the production of non-SM Higgses in the Type II Two Higgs Doublet Model at a 100 TeV *pp* collider, as well as their decays. We present the reach for $pp \to bbH^0/A \to bbtt$, $bb\tau\tau$ as well as $pp \to tbH^\pm \to tbtb$, $tb\tau\nu$ at the 100 TeV *pp* collider and outline the possible search channels via Higgs exotic decays. We point out that a combination of these conventional channels potentially yields full coverage for $\tan\beta$ and pushes the exclusion limits from the $\mathcal{O}(1)$ TeV at the LHC to the $\mathcal{O}(10)$ TeV at a 100 TeV *pp* collider, whereas the exotic decays of a heavy Higgs into two light Higgses or one light Higgs plus one SM gauge boson provide alternative discovery channels.

1. Introduction

The discovery of the Standard Model (SM)-like Higgs boson at the Large Hadron Collider (LHC) is one of the greatest triumphs in particle physics.[1–4] Stabilization of the observed Higgs mass of 126 GeV, however, provides strong motivation of physics beyond the SM. In addition, there are puzzles facing particle physics which can not be explained in the SM, for example, the particle candidate for dark

matter or the generation of neutrino mass. Solutions to those problems typically lead to models with an extended Higgs sector. Well known examples include the Minimal Supersymmetric Standard Model (MSSM),[5–7] Next-to-Minimal Supersymmetric Standard Model (NMSSM),[8,9] and Two Higgs Doublet Models (2HDM),[10–13] etc. In addition to a SM-like Higgs boson in these models, the low energy spectrum typically includes extra neutral CP-even and CP-odd Higgses, as well as charged ones.

The discovery of the non-SM Higgses would provide unambiguous evidence for new physics beyond the SM. The search for these extra Higgses, however, is typically challenging at the LHC. For the extra neutral Higgses, most of the current searches at the LHC focus on the conventional Higgs search channels of WW, ZZ, $\gamma\gamma$, $\tau\tau$ and bb channel.[14–20] The production of the extra Higgses is usually suppressed compared to that of the SM Higgs, either due to its larger mass or its suppressed couplings to the SM particles. The decay of the heavy neutral Higgses to the WW and ZZ is absent for the CP-odd Higgs, and could be highly suppressed for the non-SM like CP-even Higgs. The decay modes of $\tau\tau$ or bb suffer from either suppressed signal or large SM backgrounds, and are therefore only relevant for regions of the parameter space with an enhanced bb or $\tau\tau$ coupling. The search for the charged Higgs at the LHC is even more difficult. For $m_{H^\pm} > m_t$, the cross section for the dominant production channel of $tbH^\pm$ is typically small. The dominant decay mode $H^\pm \to tb$ is hard to identify given the large tt and $ttbb$ background, while the subdominant decay of $H^\pm \to \tau\nu$ has suppressed branching fraction. In the MSSM, even at the end of the LHC running, there is a "wedge region" in the $m_A - \tan\beta$ plane for $\tan\beta \sim 7$ and $m_A \gtrsim 300$ GeV in which only the SM-like Higgs can be covered at the LHC. Similarly, the reach for the non-SM Higgses is limited in models with an extended Higgs sector.

In addition to their decays to the SM particles, non-SM Higgses can decay via exotic modes, i.e., heavier Higgs decays into two light Higgses, or one light Higgs plus one SM gauge boson. Examples include $H^0 \to H^+H^-$, $H^0 \to AA$, $H^0 \to AZ$, $A \to H^\pm W^\mp$, and $H^\pm \to AW$, etc. These channels typically dominate once they are kinematically open. The current limits on the beyond the SM Higgs searches are therefore weakened, given the suppressed decay branching fractions into SM final states. Furthermore, these additional decay modes could provide new search channels for the non-SM Higgs, complementary to the conventional search modes. Recent study on exotic Higgs decays can be found in Refs. 21–32. Latest searches from ATLAS and CMS have shown certain sensitivity in $A/H \to HZ/AZ$ channel.[33–36]

A 100 TeV pp collider offers great opportunity for probing non-SM Higgses. The production cross sections can be enhanced by about a factor of 30–50 for gluon fusion and bb associated production, and about a factor of 90 for the charged Higgs for Higgs mass of about 500 GeV, and even more for heavier Higgses. In the new mass domain accessible to the machine, the decays of $H^0/A \to tt$ and $H^\pm \to tb$ are easily allowed kinematically. In the former case, the branching fraction

becomes sizable for intermediate $\tan\beta$ and dominant for low $\tan\beta$. The channels of $pp \to ttH^0/A$, bbH^0/A with $H^0/A \to \tau\tau$, bb, tt potentially provide full coverage of the $\tan\beta$ domain. In the latter case, $H^\pm \to tb$ becomes dominant over the whole $\tan\beta$ domain if exotic decay modes are not present. New kinematics of these signal events at a 100 TeV pp collider also bring new handles. For example, the top quark appearing in the decay could be highly boosted. Looking into its internal structure (though a finer granularity of both ECAL and HCAL is typically required) or requiring an extremely hard lepton in top decays can efficiently suppress the relevant backgrounds. In addition, exotic Higgs decays can provide alternative search channels at the 100 TeV pp collider when the conventional decays are suppressed.

In this paper, we summarize the production and decay of heavy non-SM Higgses at a 100 TeV pp collider, and highlight the main search channels for H^0, A^0 and $H^\pm$ and its reach potential. Note that while it is a viable possibility for the light CP-even Higgs h^0 being non-SM like, and the heavy CP-even Higgs H^0 being SM-like (the so-called H^0-125 case with $\sin(\beta-\alpha) \sim 0$),[37] in this paper we focus on the conventional case of h^0 being the SM-like Higgs of 125 GeV with a heavy non-SM H^0. For simplicity, the results presented in the following sections are for the alignment limit of $\cos(\beta-\alpha) = 0$, even though regions of $\cos(\beta-\alpha)$ away from zero can still be accommodated by the current experimental Higgs search results.[37]

The paper is organized as follows. In Sec. 2, we briefly introduce the Type II 2HDM with its particle content and relevant couplings. In Sec. 3, we present the dominant production cross sections for H^0, A^0 and $H^\pm$ at the 100 TeV pp collider. In Sec. 4, we discuss the decay modes for heavy Higgses. In Sec. 5, we present the reach for heavy Higgses at a 100 TeV pp collider using the conventional decay modes into SM fermions. In Sec. 6, we discuss the prospect for heavy Higgs discovery via exotic decay modes to light Higgses or one light Higgs plus a SM gauge boson. In Sec. 7, we conclude.

2. Type II 2HDM

In the 2HDM,[a] we introduce two SU(2) doublets Φ_i, $i = 1, 2$:

$$\Phi_i = \begin{pmatrix} \phi_i^+ \\ (v_i + \phi_i^0 + iG_i)/\sqrt{2} \end{pmatrix}, \tag{1}$$

where v_1 and v_2 are the vacuum expectation values of the neutral components which satisfy the relation: $v = \sqrt{v_1^2 + v_2^2} = 246$ GeV after electroweak symmetry breaking. Assuming a discrete $\mathcal{Z}_2$ symmetry imposed on the Lagrangian, we are left with six free parameters, which can be chosen as four Higgs masses (m_h, m_{H^0}, m_A, $m_{H^\pm}$), the mixing angle α between the two CP-even Higgses, and the ratio of the two vacuum expectation values, $\tan\beta = v_2/v_1$. In the case in which a soft breaking of the $\mathcal{Z}_2$ symmetry is allowed, there is an additional parameter m_{12}^2.

[a]For more details about the 2HDM, see Ref. 10.

The mass eigenstates contain a pair of CP-even Higgses: h^0, H^0, one CP-odd Higgs A and a pair of charged Higgses $H^\pm$:

$$\begin{pmatrix} H^0 \\ h^0 \end{pmatrix} = \begin{pmatrix} \cos\alpha & \sin\alpha \\ -\sin\alpha & \cos\alpha \end{pmatrix} \begin{pmatrix} \phi_1^0 \\ \phi_2^0 \end{pmatrix}, \quad \begin{aligned} A &= -G_1 \sin\beta + G_2 \cos\beta\,, \\ H^\pm &= -\phi_1^\pm \sin\beta + \phi_2^\pm \cos\beta\,. \end{aligned} \tag{2}$$

Two types of couplings that are of particular interest are the couplings of a Higgs to two gauge bosons, as well as the couplings of a SM gauge boson to a pair of Higgses. Both are determined by the gauge coupling structure and the mixing angles. The H^0VV and h^0VV couplings are:[38]

$$g_{H^0VV} = \frac{m_V^2}{v}\cos(\beta-\alpha)\,, \quad g_{h^0VV} = \frac{m_V^2}{v}\sin(\beta-\alpha)\,. \tag{3}$$

The couplings for a SM gauge boson with a pair of Higgses are:[38]

$$\begin{aligned} g_{AH^0Z} &= -\frac{g\sin(\beta-\alpha)}{2\cos\theta_w}(p_{H^0}-p_A)^\mu\,, \\ g_{Ah^0Z} &= \frac{g\cos(\beta-\alpha)}{2\cos\theta_w}(p_{h^0}-p_A)^\mu\,, \end{aligned} \tag{4}$$

$$\begin{aligned} g_{H^\pm H^0W^\mp} &= \frac{g\sin(\beta-\alpha)}{2}(p_{H^0}-p_{H^\pm})^\mu\,, \\ g_{H^\pm h^0W^\mp} &= \frac{g\cos(\beta-\alpha)}{2}(p_{h^0}-p_{H^\pm})^\mu\,, \end{aligned} \tag{5}$$

$$g_{H^\pm AW^\mp} = \frac{g}{2}(p_A-p_{H^\pm})^\mu\,, \tag{6}$$

with g being the SU(2) coupling, θ_w being the Weinberg angle and p_μ being the incoming momentum of the corresponding particle. Note that A and $H^\pm$ always couple to the non-SM-like Higgs more strongly, while the $H^\pm AW^\mp$ coupling is independent of the mixing parameters.

In the Type II 2HDM, one Higgs doublet Φ_1 provides masses for the down-type quarks and charged leptons, while the other Higgs doublet Φ_2 provides masses for the up-type quarks. The couplings of the CP-even Higgses h^0, H^0 and the CP-odd Higgs A to the SM gauge bosons and fermions are scaled by a factor ξ relative to the SM value, as presented in Table 1.

Table 1. The multiplicative factors ξ by which the couplings of the CP-even Higgses and the CP-odd Higgs to the gauge bosons and fermions scale with respect to the SM value. The superscripts u, d, l and VV refer to the up-type quarks, down-type quarks, leptons, and WW/ZZ respectively.

$\xi_{h^0}^{VV}$	$\sin(\beta-\alpha)$	$\xi_{H^0}^{VV}$	$\cos(\beta-\alpha)$	ξ_A^{VV}	0
$\xi_{h^0}^{u}$	$\cos\alpha/\sin\beta$	$\xi_{H^0}^{u}$	$\sin\alpha/\sin\beta$	ξ_A^{u}	$\cot\beta$
$\xi_{h^0}^{d,l}$	$-\sin\alpha/\cos\beta$	$\xi_{H^0}^{d,l}$	$\cos\alpha/\cos\beta$	$\xi_A^{d,l}$	$\tan\beta$

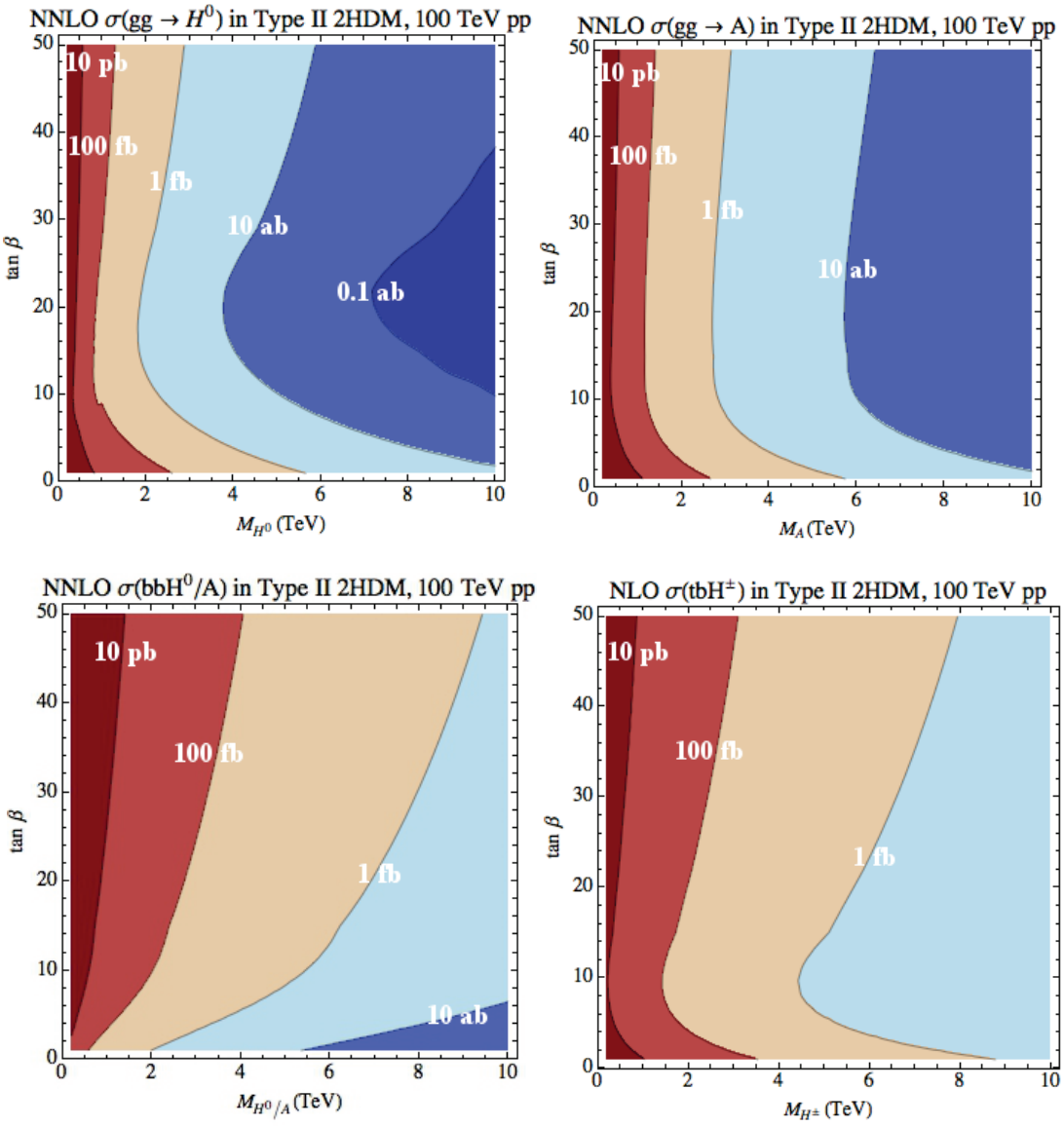

Fig. 1. Dominant production cross sections for non-SM like Higgses in the type II 2HDM at the 100 TeV pp collider: NNLO cross section for $gg \to H^0$ or A (top left and top right panel, calculated using HIGLU[39] with the NNPDF2.3 parton distribution functions[40]), NNLO cross section for bottom-associated production bbH^0/A (lower left panel, calculated using SusHi.[41–43] bbH^0 and bbA cross sections are the same in the alignment limit), NLO cross section for $tbH^\pm$ (lower right panel, calculated in Prospino[44,45]).

In addition, the $H^\pm tb$ coupling is

$$g_{H^\pm tb} = \frac{g}{2\sqrt{2}m_W}\left[(m_b \tan\beta + m_t \cot\beta) \pm (m_b \tan\beta - m_t \cot\beta)\gamma_5\right], \qquad (7)$$

which is enhanced at both small and large $\tan\beta$. The $H^\pm\tau\nu$ has similar enhancement at large $\tan\beta$ as well.

3. Production Cross Sections

The dominant production processes for the neutral Higgses are gluon fusion $gg \to H^0/A$ with dominant top and bottom (for large $\tan\beta$) loops, as well as bbH^0/A associated production. ttH^0/A associated production could be important as well.[46] The dominant production process for the charged Higgses is $tbH^\pm$ associated production. Production cross sections at 100 TeV pp collider for A^0, H^0 and $H^\pm$ are shown in Fig. 1. For H^0, we have assumed the alignment limit of $\cos(\beta-\alpha)=0$ in which the light CP-even Higgs is the SM-like one, and the couplings of the heavy CP-even Higgs H^0 to the SM particles is the same in amplitude as that of the CP-odd Higgs A, but differs in the relative sign of the couplings to the up type quarks comparing to that of the down type quarks. For charged Higgs production, corrections from resumming top logarithms may play a role at 100 TeV,[47,48] but are not expected to significantly affect the general features of the results.[48,49] For neutral Higgses, gluon fusion production and ttH^0/A dominates at low $\tan\beta$ [46] while bbH^0/A associated production dominates at large $\tan\beta$. The $tbH^\pm$ production cross section gets enhanced at both small and large $\tan\beta$.

Comparing to the 14 TeV LHC, the production rates can be enhanced by about a factor of 30–50 for gluon fusion and bb associated production, and about a factor of 90 for the charged Higgs for Higgs mass if about 500 GeV, and even more for heavier Higgses, resulting in great discovery potential for heavy Higgses at a 100 TeV pp colliders.

4. Heavy Higgs Decays

Conventional decay modes for heavy Higgses are $H^0 \to tt/bb/\tau\tau/WW/ZZ/\gamma\gamma$, $A \to tt/bb/\tau\tau$ and $H^\pm \to tb/\tau\nu/cs$. Note that for h^0 being SM-like, H^0 decays to WW and ZZ are highly suppressed given that $\cos(\beta-\alpha)\sim 0$ is preferred. The branching fractions for a heavy H^0, A, and $H^\pm$ are shown in the dashed curves in Fig. 2, assuming exotic decay modes are kinematically forbidden.

Five main exotic decay categories for Higgses of the Type II 2HDM are shown in Table 2. Once these decay modes are kinematically open, they typically dominate over the conventional decay channels, as shown in Fig. 2 for H^0 (left panel),

Table 2. Exotic Decay modes for Higgses in the 2HDM. H in column two refers to any of the neutral Higgs h^0, H^0 or A.

	Decay	Final states	Channels
Neutral Higgs H^0, A	HH type	$(bb/\tau\tau/WW/ZZ/\gamma\gamma)(bb/\tau\tau/WW/ZZ/\gamma\gamma)$	$H^0 \to AA, \ldots$
	HZ type	$(\ell\ell/qq/\nu\nu)(bb/\tau\tau/WW/ZZ/\gamma\gamma)$	$H^0 \to AZ$, $A \to H^0 Z, \ldots$
	H^+H^- type	$(tb/\tau\nu/cs)(tb/\tau\nu/cs)$	$H^0 \to H^+H^-, \ldots$
	$H^\pm W^\mp$ type	$(\ell\nu/qq')(tb/\tau\nu/cs)$	$H^0/A \to H^\pm W^\mp, \ldots$
Charged Higgs	$HW^\pm$ type	$(\ell\nu/qq')(bb/\tau\tau/WW/ZZ/\gamma\gamma)$	$H^\pm \to H^0 W$, $AW, \ldots$

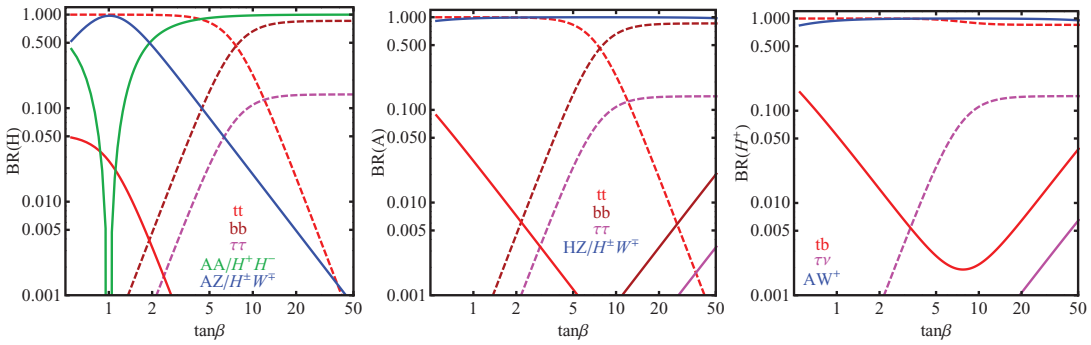

Fig. 2. Branching fractions for H^0 (left panel), A (middle panel) and $H^\pm$ (right panel). The parent and daughter Higgs masses are chosen to be 2 TeV and 800 GeV, respectively. Note that in the $H^0(A)$ decay, we have assumed either light A (H^0) *or* light $H^\pm$, but not both. Dashed curves are the branching fractions when exotic decay modes are kinematically forbidden. All decay branching fractions are calculated using the program 2HDMC.[50]

Table 3. Main conventional search channels for non-SM Higgses to cover various $\tan\beta$ regions[51] at a 100 TeV pp collider.

	$\tan\beta$	Channels
Neutral Higgs H^0, A	High	$pp \to bbH^0/A \to bb\tau\tau, bbbb$
	Intermediate	$pp \to bbH^0/A \to bbtt$
	Low	$pp \to H^0/A \to tt$, $pp \to ttH^0/A \to tttt$
Charged Higgs $H^\pm$	High	$pp \to tbH^\pm \to tbtb, tb\tau\nu_\tau$
	Low	$pp \to tbH^\pm \to tbtb$

A (middle panels), and $H^\pm$ (right panel). Note that in the alignment limit of $\cos(\beta-\alpha)=0$, the branching fraction of $H^0 \to h^0h^0$ is zero. The branching fractions for heavy A are similar to those of H^0, except that the decay modes of H^0H^0 and H^+H^- are absent.

Note that the current experimental searches for the non-SM Higgs always assume the absence of exotic decay modes. Once there are light Higgs states such that these exotic modes are kinematically open, the current search bounds can be greatly relaxed.[22,24,26]

5. Conventional Search Channels

At a 100 TeV pp collider, new mass domains for both neutral and charged Higgs bosons become accessible, given the enhanced production cross sections and the dominance of decays to final states with top quarks (at small $\tan\beta$ for neutral Higgses and at both small and large $\tan\beta$ for charged Higgses), as well as novel kinematic features of the decay products. Combining production processes and decay channels, the main search channels to cover various $\tan\beta$ regions are summarized in Table 3.

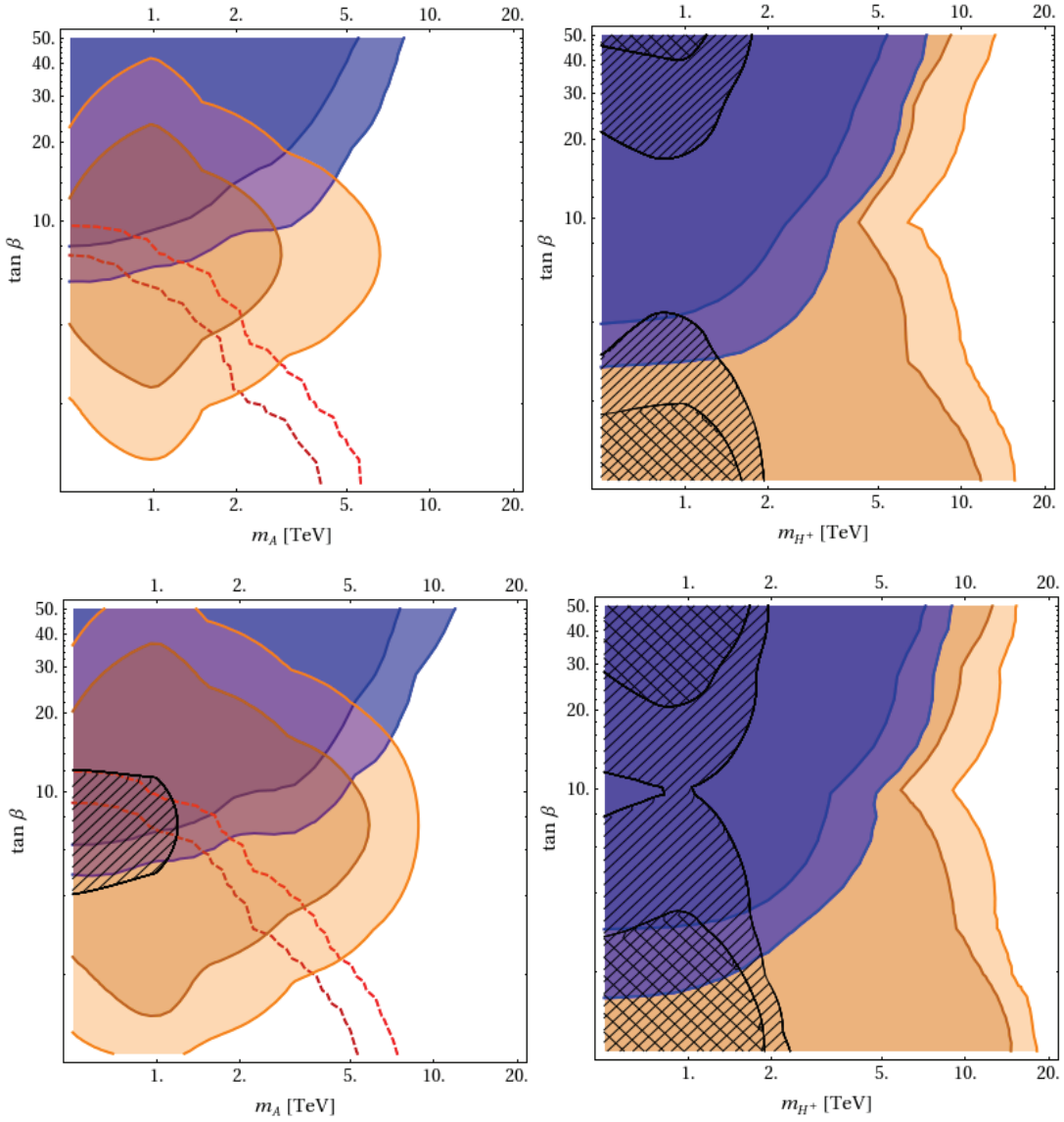

Fig. 3. Discovery reaches and exclusion limits for the MSSM Higgs bosons at a 100 TeV pp collider.[51] The two regions with the same color and different opacities are excluded by assuming a luminosity of 3 ab^{-1}, and 30 ab^{-1}, respectively. Left: neutral Higgs bosons (H^0/A). The blue and orange regions are excluded by the channels $pp \to bbH^0/A \to bb\tau_h\tau_l$, $pp \to bbH^0/A \to bbt_ht_l$ and $pp \to H^0/A \to t_ht_l$, respectively. Right: charged Higgs bosons ($H^\pm$). The blue and orange regions are excluded by the channels $pp \to tbH^\pm \to tb\tau_h\nu_\tau$ and $pp \to tbH^\pm \to t_hbt_lb$, respectively. The cross-hatched and diagonally hatched regions are the predicted discovery contours (or exclusion contours) for associated Higgs production at the LHC for 0.3 ab^{-1}, and 3 ab^{-1}, respectively.

The top quarks from the heavy Higgs can decay either hadronically or leptonically. The hard leptons produced from top decay products, together with the boosted top jets, can efficiently suppress the backgrounds, including the irreducible backgrounds of tt and $ttbb$. For final states with taus, either large transverse mass for the signal events or hard leptons from tau decays can efficiently distinguish the

signal and backgrounds. The choices made in the illustrative analyses below (see caption of Fig. 3) also benefit the reconstruction of the heavy Higgs resonance. In addition, the large rapidity of the two non-top b-jets in $pp \to bbH^0/A \to bbtt$ and $pp \to tbH^\pm \to tbtb$ can be used to further suppress the backgrounds; this kinematic feature has not been applied for the H^0/A and $H^\pm$ searches at the LHC.

To fully utilize the kinematic features of the signal events, a Boosted Decision Tree method may be used to search for heavy Higgses decaying to semileptonic tops or taus.[51] The 5σ discovery reaches and 95% C.L. exclusion limits yielded by these channels are presented in Fig. 3, with various luminosities (3 ab^{-1}, and 30 ab^{-1}) and an ATLAS-type detector assumed. The exclusion limits for both the neutral and charged Higgs bosons are pushed from the $\mathcal{O}(1)$ TeV scale at the LHC to the $\mathcal{O}(10)$ TeV scale at a 100 TeV pp collider for almost the whole range of $\tan\beta$ (except the low $\tan\beta$ region for the neutral Higgs, which potentially can be covered by the channel $pp \to ttH^0/A \to tttt$ [46]). In particular, the wedge region for the neutral Higgs searches ($\tan\beta \sim 7$) and the low $\tan\beta$ region for the charged Higgs searches are fully covered by the channels $pp \to bbH^0/A \to bbtt$ and $pp \to tbH^\pm \to tbtb$, respectively.

6. Exotic Search Channels

Other than decays into conventional searches channels as mentioned in Sec. 5, exotic Higgs decays to final states with two light Higgses or one Higgs plus one SM gauge boson provide complementary search channels. Here, we list such exotic Higgs decays and consider potential search strategies.

- ***$H^0 \to AA$***

With one final state Higgs decay via bb, and the other decay via $\gamma\gamma$, the $bb\gamma\gamma$ channel has been shown to be sensitive to the di-Higgs final states,[52] in particular, with resonance enhancement of the production cross section. Final states involve taus might also be useful in probing this decay. Associated production with bb can enhance the reach further at large $\tan\beta$.

- ***$H^0 \to AZ$ or $A \to H^0Z$***

With $Z \to \ell\ell$ and $H^0/A \to bb, \tau\tau$, the final states of $bb\ell\ell$, $\tau\tau\ell\ell$ can be obtained with gluon fusion production, or in the bb associated production with two additional b jets.[21–23] Recent searches from ATLAS and CMS have shown certain sensitivity in this channel.[33–36] In parameter regions where $\mathrm{Br}(A \to H^0Z) \times \mathrm{Br}(H^0 \to ZZ)$ is not completely suppressed, ZZZ final states with two Z decaying leptonically and one Z decaying hadronically can also be useful.[22] Other channels with top final states could be explored as well.

- $\boldsymbol{H^0 \to H^+H^-}$

With both $H^\pm$ decaying via $\tau\nu$ final states, the signal of $\tau\tau\nu\nu$ can be separated from the SM W^+W^- background since the charged tau decay product in the signal typically has a hard spectrum compared to that of the background.[26] Utilizing the top identification strategy as mentioned in Sec. 5, $ttbb$ or $tb\tau\nu$ final states could also be useful.

- $\boldsymbol{H^0/A \to H^\pm W^\mp}$

Similar to the H^+H^- case, $H^\pm \to \tau\nu, tb$ and $W \to \ell\nu$ with $\ell\tau\nu\bar{\nu}$ or $tb\ell\nu$ could be used to search for $H^0/A \to H^\pm W^\mp$. Note that for the CP-even Higgs H^0, the branching fraction of $H^0 \to H^\pm W^\mp$ is mostly suppressed comparing to $H^0 \to H^+H^-$ as long as the latter process is kinematically open and not accidentally suppressed (see Fig. 2).[26] However, for the CP-odd Higgs A, this is the only decay channel with a charged Higgs in the decay products.

- $\boldsymbol{H^\pm \to H^0W, AW}$

This is the only exotic decay channel for the charged Higgs in the 2HDM. Given the associated production of $tbH^\pm$, and the decay of H^0, A into the bb or $\tau\tau$ channel, $\tau\tau bbWW$ or $bbbbWW$ can be used to probe this channel.[24] $H^0/A \to t\bar{t}$ could also be used given the boosted top in the high energy environment.

7. Conclusion

Discovery of the non-SM Higgs bosons in an extended Higgs sector would provide clear evidence for new physics beyond the SM. At the 14 TeV LHC, the conventional search channels for neutral and charged Higgses leave a wedge region open around intermediate $\tan\beta \sim 7$ and $m_A \gtrsim 300$ GeV in which only the SM Higgs is detected. Exotic decays of heavy Higgses into two light Higgses or one light Higgs and one SM gauge boson provide complementary search channels once they are kinematically open.

A 100 TeV pp collider offers great discovery potential for non-SM heavy Higgses. In this write-up, we summarized the reach at the 100 TeV pp collider for conventional search modes, in particular, via the $H^0/A \to t\bar{t}$ and $H^\pm \to tb$ channels. Potentially, the whole range of $\tan\beta$ can be probed for masses up to about 10 TeV when various channels are combined. We also outline the possible search channels for exotic decays when the branching fractions for conventional channels are suppressed. Combinations of those channels can greatly extend the reach of the non-SM Higgs at a 100 TeV pp collider.

Acknowledgments

We would like to thank Tilman Plehn for fruitful discussion. A. I. is supported by the Department of Energy under Grant DE-AC02-06CH11357 and DE-FG02-12ER41811. F. K. and S. S. are supported by the Department of Energy under

Grant DE-FG02-13ER41976. T. L. and J. S. are supported by fund at the Hong Kong University of Science and Technology. Y. L. is supported by the the Hong Kong PhD Fellowship Scheme (HKPFS) issued by the Research Grants Council (RGC) of Hong Kong. Y. L., T. L. and S. S. also would like to acknowledge the hospitality of the Jockey Club Institute for Advanced Study, HKUST, where part of this work was completed.

References

1. ATLAS Collab. (G. Aad *et al.*), *Phys. Lett. B* **716**, 1 (2012), arXiv:1207.7214.
2. ATLAS Collab. (G. Aad *et al.*), Tech. Rep. ATLAS-CONF-2013-034, CERN, Geneva (2013).
3. CMS Collab. (S. Chatrchyan *et al.*), *Phys. Lett. B* **716**, 30 (2012), arXiv:1207.7235.
4. CMS Collab. (S. Chatrchyan *et al.*), Tech. Rep. CMS-PAS-HIG-13-005, CERN, Geneva (2013).
5. H. P. Nilles, *Phys. Rept.* **110**, 1 (1984).
6. H. E. Haber and G. L. Kane, *Phys. Rept.* **117**, 75 (1985).
7. R. Barbieri, *Riv. Nuovo Cimento* **11**(4), 1 (1988).
8. J. R. Ellis, J. Gunion, H. E. Haber, L. Roszkowski and F. Zwirner, *Phys. Rev. D* **39**, 844 (1989).
9. M. Drees, *Int. J. Mod. Phys. A* **4**, 3635 (1989).
10. G. Branco *et al.*, *Phys. Rept.* **516**, 1 (2012), arXiv:1106.0034.
11. H. Haber, G. L. Kane and T. Sterling, *Nucl. Phys. B* **161**, 493 (1979).
12. L. J. Hall and M. B. Wise, *Nucl. Phys. B* **187**, 397 (1981).
13. J. F. Donoghue and L. F. Li, *Phys. Rev. D* **19**, 945 (1979).
14. ATLAS Collab. (G. Aad *et al.*), *J. High Energy Phys.* **1411**, 056 (2014), arXiv:1409.6064.
15. CMS Collab., Search for charged Higgs bosons with the H^+ to tau nu decay channel in the fully hadronic final state at $\sqrt{s = 8}$ TeV, CMS-PAS-HIG-14-020 (2014).
16. CMS Collab. (S. Chatrchyan *et al.*), *Phys. Lett. B* **722**, 207 (2013), arXiv:1302.2892.
17. ATLAS Collab. (G. Aad *et al.*), Tech. Rep. ATLAS-CONF-2013-027, CERN, Geneva (2013).
18. CMS Collab. (V. Khachatryan *et al.*), *Phys. Rev. D* **90**, 112013 (2014), arXiv:1410.2751.
19. G. Aad *et al.*, Tech. Rep. ATLAS-CONF-2013-090, CERN, Geneva (2013).
20. CMS Collab. (S. Chatrchyan *et al.*), Tech. Rep. CMS-PAS-HIG-13-021, CERN, Geneva (2013).
21. B. Coleppa, F. Kling and S. Su, arXiv:1308.6201.
22. B. Coleppa, F. Kling and S. Su, *J. High Energy Phys.* **1409**, 161 (2014), arXiv:1404.1922.
23. E. Brownson *et al.*, arXiv:1308.6334.
24. B. Coleppa, F. Kling and S. Su, *J. High Energy Phys.* **1412**, 148 (2014), arXiv:1408.4119.
25. F. Kling, A. Pyarelal and S. Su, arXiv:1504.06624 [hep-ph].
26. T. Li and S. Su, arXiv:1504.04381 [hep-ph].
27. U. Maitra, B. Mukhopadhyaya, S. Nandi, S. K. Rai and A. Shivaji, *Phys. Rev. D* **89**, 055024 (2014), arXiv:1401.1775.
28. L. Basso *et al.*, *J. High Energy Phys.* **1211**, 011 (2012), arXiv:1205.6569.

29. R. Dermisek, J. P. Hall, E. Lunghi and S. Shin, *J. High Energy Phys.* **1404**, 140 (2014), arXiv:1311.7208.
30. B. Mohn, N. Gollub and K. A. Assamagan, Tech. Rep. ATL-PHYS-PUB-2005-017; ATL-COM-PHYS-2005-021; CERN-ATL-COM-PHYS-2005-021, CERN, Geneva (2005).
31. K. Assamagan, *Acta Phys. Pol. B* **31**, 881 (2000).
32. K. A. Assamagan, Y. Coadou and A. Deandrea, *Eur. Phys. J. Direct C* **4**, 9 (2002), arXiv:hep-ph/0203121.
33. CMS Collab., Tech. Rep. CMS-PAS-HIG-14-011, CERN, Geneva (2014), https://cds.cern.ch/record/1969698.
34. CMS Collab., Tech. Rep. CMS-PAS-HIG-13-025, CERN, Geneva (2013), https://cds.cern.ch/record/1637776.
35. ATLAS Collab. (G. Aad *et al.*), *Phys. Lett. B* **744**, 163 (2015), arXiv:1502.04478.
36. CMS Collab., Tech. Rep. CMS-PAS-HIG-15-001, CERN, Geneva (2015), https://cds.cern.ch/record/2014119.
37. B. Coleppa, F. Kling and S. Su, *J. High Energy Phys.* **1401**, 161 (2014), arXiv:1305.0002.
38. J. F. Gunion, H. E. Haber, G. L. Kane and S. Dawson, *Front. Phys.* **80**, 1 (2000).
39. M. Spira, arXiv:hep-ph/9510347.
40. R. D. Ball *et al.*, *Nucl. Phys. B* **867**, 244 (2013), arXiv:1207.1303.
41. R. V. Harlander, S. Liebler and H. Mantler, *Comput. Phys. Commun.* **184**, 1605 (2013), arXiv:1212.3249.
42. R. V. Harlander and W. B. Kilgore, *Phys. Rev. D* **68**, 013001 (2003), arXiv:hep-ph/0304035.
43. R. V. Harlander and W. B. Kilgore, *Phys. Rev. Lett.* **88**, 201801 (2002), arXiv:hep-ph/0201206.
44. T. Plehn, *Phys. Rev. D* **67**, 014018 (2003), arXiv:hep-ph/0206121.
45. W. Beenakker, R. Hopker and M.Spira, arXiv:hep-ph/9611232.
46. N. Craig, J. Hajer, Y.-Y. Li, T. Liu and H. Zhang, to appear.
47. T. Han, J. Sayre and S. Westhoff, arXiv:1411.2588.
48. S. Dawson, A. Ismail and I. Low, *Phys. Rev. D* **90**, 014005 (2014), arXiv:1405.6211.
49. M. Flechl, R. Klees, M. Kramer, M. Spira and M. Ubiali, arXiv:1409.5615.
50. D. Eriksson, J. Rathsman and O. Stal, *Comput. Phys. Commun.* **181**, 189 (2010), arXiv:0902.0851.
51. J. Hajer, Y.-Y. Li, T. Liu and J. F. H. Shiu, arXiv:1504.07617.
52. U. Baur, T. Plehn and D. L. Rainwater, *Phys. Rev. D* **69**, 053004 (2004), arXiv:hep-ph/0310056.